# *A faint galaxy redshift survey and implications for cosmology*

Thomas James Broadhurst

# A FAINT GALAXY REDSHIFT SURVEY AND IMPLICATIONS FOR COSMOLOGY

by

Thomas James Broadhurst B.Sc.



A Thesis
Submitted to the University of Durham
for the Degree of
Doctor of Philosophy

ABSTRACT

A new faint galaxy redshift survey has been constructed using the fibre optic coupler at the Anglo-Australian Observatory. Intermediate dispersion spectra with resolution $\sim$ 4 Å have been gathered for over 200 field galaxies selected in apparent magnitude slices between $20.0 < b_J < 21.5$ in 5 high latitude fields. Redshift completeness is 85% and the mean redshift agrees well from field to field.

Models for the prediction of faint galaxy distributions are constructed from a bright galaxy redshift survey (Durham/Anglo-Australian Redshift Survey) and show that although the slope of the galaxy number-magnitude count relation is considerably steeper than no-evolution predictions at $b_J \sim 21$, the redshift range observed is similar to that expected for a non-evolving population. If our fields are representative, luminosity evolution can only be occurring in low luminosity galaxies to $z < 0.5$.

The faint spectra reveal strong evidence for enhanced star formation in a large proportion of the galaxies beyond $z \sim 0.1$ which cannot be explained in terms of colour or aperture selection-effects. We suggest that it is these star-forming galaxies which represent the excess in the galaxy counts, at least in the range $b_J < 22$.

The colour and absorption line features of the stronger emission line galaxies can only be reproduced with models incorporating strong short-lived bursts of star formation which temporarily brighten these otherwise low-luminosity systems. We are able to reproduce these observations with a physical 'burst' model in which only galaxies at the faint end of the luminosity function significantly evolve via short ($10^8$yrs) bursts of star formation.

These results are supported by model comparison with very faint colour distributions. We find good agreement with the no-evolution model in the range $b_J - R_f > 1.6$, indicating a minimum of evolution of bright early type galaxies. The excess number count is clearly concentrated blueward of this, and consistent with the expectation of the burst model.

Clustering on small scales, estimated via the 2-point spatial correlation function agrees fairly well with local results, but evidence for a very large

scale periodicity may be indicated by combining this survey with others in the dir ection of the Galactic poles.

To my parents

*'The greatest riddle of cosmology may well be that the universe is, in a sense, creative'*

*Karl Popper, The Self and Its Brain*

Contents.

# PREFACE

This work was carried out between 1985 and 1988 under the supervision of Professor Richard Ellis, at the Department of Physics at the University of Durham.

Some of the work was carried out in collaboration with Richard Ellis and Tom Shanks but the majority is the authors own work. No part of the above thesis has been submitted previously for a degree to Durham or any other University. Certain results have appeared in the following papers:

Broadhurst, T.J., Ellis, R.S. and Shanks, T., 1988 *Mon. Not. R. astr. Soc.*, 235,827

Broadhurst, T.J., Ellis, R.S. and Shanks, T., 1987 In:*High Redshift and Primeval Galaxies, Third IAP Astrophysics Conference*, p231 eds Bergeron J., (Frontieres, Paris)

Broadhurst, T.J. and Salucci P., 1989 In:*Epoch of Galaxy Formation*, p359 eds: Frenk C.S., Ellis R.S, Shanks T., Peacock J., In Press.

# Chapter 1.

# INTRODUCTION

The history of the material content of the universe is unfolding on the sky. Unlike the story of biological evolution which is selectively and indirectly recorded, the finite speed of light and presently vast event horizon allow us to look back in time and witness the process of cosmic evolution.

Cosmology from extragalactic observation is unfortunately a new discipline, based on only 60 years of observational work. Our present knowledge of evolutionary processes is sketchy, lacking large systematic studies of ordinary galaxies at earlier epochs. Here we are limited by our own evolution - most cosmologists are living, and we might expect future observations spanning a much larger baseline in time, to follow evolutionary changes over cosmologically interesting timescales. It is reasonable to suppose, for example, that the present expansion rate and universal geometry will be determined by 'watching' the expansion. With present technology however, a baseline of $\sim 10^4$ years is required to provide useful constraints in this way.

To date we have taken up little of the cosmological information potentially available through observation. We have as yet, no direct observations of the epoch of first star formation and consequently little understanding of the way galaxies formed. We cannot even be sure of how this process may best be observed, since redshift is a strong function of time at early epochs, so that the bright ultra-violet emission from young stars, might appear, for example, at very much longer wavelengths.

Also of great importance to our understanding of the 'initial conditions' of the Hot Big Bang model, are observations of the dynamical evolution of matter and the distribution of galaxies on large scales. We have very little 3 dimensional information on galaxy clustering over large scales and cannot, at present, convincingly discriminate a wide range of proposed cosmogonies.

The work presented in this Thesis surveys galaxies to a significant fraction of the Hubble time, with data obtained to the current limits of spectroscopic and photometric techniques. Thus we are able to examine the evolution of the general galaxy population over recent epochs. In addition the redshift information obtained allows us to investigate the galaxy distribution to depths



much greater than possible from earlier galaxy redshift surveys.

## 1.1 The Cosmological Model

We are fortunate to have at least a clear consensus on the cosmological framework in which we should work, and throughout this Thesis we assume the standard Hot Big Bang model described by the Friedmann equations.

The Friedmann equations are a convenient description of the Robertson-Walker metric which assumes the simple case of a homogeneous and isotropic distribution of matter with dynamics described by General Relativity. (This model is referred throughout as the FRW cosmology.)

These assumptions it appears, are not demanded by the theory of General Relativity (see Peebles 1980), which allows many other forms for the metric. However strong support for large scale homogeneity and isotropy is implied by the accurate isotropy of the Microwave Background which is observed to be smooth to at least 1 part in $10^5$ (Uson and Wilkinson 1984). In fact this is very much more accurate than could be expected even in the FRW cosmology, because at the surface of last scattering, when matter decoupled from radiation, the causal horizon (assuming no subsequent reionisation), had a scale corresponding to an angular size of only 2 degrees. On larger angular scales we would simply expect unrelated background temperatures, and recourse must be made to 'initial conditions' which contrive to set up the distribution of matter with very precise homogeneity.

An explanation of this 'horizon problem' has been suggested from recent advances in particle physics. It has been proposed that symmetry breaking at high temperatures, expected in some classes of Grand Unified Theories (Guth 1981, Linde 1986), may result in a short period of exponential inflation at very early times, so that at recombination the causal horizon of the standard FRW cosmology encompasses a volume very much smaller than that within the horizon of an expanded region connected prior to inflation.

Invoking inflation tidies up another observational difficulty for the FRW model known as the 'fine tuning problem', namely that measures of the mean mass density indicate $\Omega_o \sim 0.1$ (defined as the present ratio of the mass density to that required for closure), which is within only one order of magnitude of the critical value for closure at present, and following the Friedmann equations would be very much closer to the critical value at earlier times. Inflation will smooth

the metric so that the curvature, if not initially flat, will become arbitrarily so. This implies $\Omega = 1.0$ very precisely (in the case of a negligible cosmological constant) and although at face value measurements indicate a slightly lower value this may be understood if the extra mass implied to achieve closure is dark and distributed more smoothly than the luminous galaxies.

## 1.2 Theories of Galaxy Formation

Any sensible cosmogonic scenario may be described as a theory of galaxy formation, since the growth of structure in such a model must result in a plausible explanation for the formation of the galaxies which are, we know, the principle luminous constituents of Universe. There are however, at least two fundamental difficulties for any such model even if we accept the above metric. Firstly galaxies cannot form simply from random fluctuations in the early universe, initial conditions must be specified. The growth of linear perturbations by gravitational instability in the FRW cosmology is insufficient to achieve galaxy mass overdensities from simple Poisson fluctuations (Bonner 1957), since until the horizon is of galaxy scale no growth of perturbations destined to become galaxies can take place. If we invoke 'initial conditions' to put in place these fluctuations over the horizon, then we can always choose a time early enough to introduce them so that galaxies may result.

Inflation can come to the rescue here too, providing primordial perturbations in the mass distribution at early times resulting from quantum fluctuations in the scaler field associated with the symmetry breaking (Peebles 1984). Note that the question of initial conditions still remains, since inflation itself is only possible under certain conditions, and many forms of inflation have been proposed, reflecting our ignorance of very high energy physics.

Also of fundamental importance to theories of galaxy formation, is the nature of the dark material which is observed to dominate the dynamics of spiral galaxies and clusters. Recent work on the dynamical implications of various possibilities for the form of this stuff (White *et al* 1983, Davis *et al* 1985) have shown that, in the context of the FRW model, with standard linear theory based on simple initial conditions, it is the nature of this material which largely determines the overall distribution of galaxies. Of Principal importance is the thermal velocity of the dark matter relative to the expansion rate, at the time when the horizon is galaxy sized, which determines whether galaxies

collapse before or after clusters. For example, at this time, in the case of a light (but massive) neutrino, the particles are relativistic and 'free stream' from overdensities within the horizon, smoothing away galaxy sized fluctuations. This process does not occur at later times when the neutrinos become non-relativistic, and so structure on sufficiently large scales survives this process. With neutrinos of mass 30eV, the earliest bound units are predicted to be of super cluster mass and subsequent dissipative fragmentation is presumed to lead to galaxies.

In contrast galaxies form directly from the initial perturbation spectrum if the dark matter is cold (candidates include photinos and axions (see Ellis 1986 for a review). The particles are massive enough to be non-relativistic and small scale perturbations of the dark survive and grow, and into which baryons subsequently collapse after recombination forming galaxies (Blumental *et al* 1984).

The cold dark matter model, set up in the manner of Davis *et al* (1985), has been shown to be successful in reproducing the small scale clustering and the internal dynamical properties of galaxies but is less successful at large scales. This model is detailed further in subsequent Chapters, in discussion with conclusions presented in this work.

Models in which Baryons alone are responsible for the dark matter are not favoured. This is because early thermodynamical evolution is constrained to produce a mass density of baryons which is less than inflationary value - based on the observed abundances of $^4$He and D (see Pagel 1986). More importantly an open baryon dominated universe will produce anisotropies in the Microwave Background which are in excess of the current upper limits (Wilson and Silk 1981), although assuming isocurvature rather than adiabatic fluctuation minimises this problem (Efstathiou and Bond 1987, Peebles 1987).

## 1.3 Statistical Studies of Faint Galaxies

The work presented in this thesis continues the statistical studies of galaxies based on deep photographic plates which, over the last decade, have provided much basic information on the evolution and structure of the Universe. Large samples of accurately measured magnitudes and positions of faint galaxies are now routinely obtained and studied in their own right, but in addition are the essential data base from which to select galaxies for redshift survey work.

Most of the work presented in this Thesis is concerned with galaxy spectral

evolution, and is motivated by the expectation that the integrated spectrum of stars, making up the optical light from a galaxy, will evolve over time. Stars evolve in luminosity and colour along tracks in the Hertzsprung-Russell diagram, so trivially we must expect galaxies to evolve. In detail however, we cannot make confident predictions for the form this evolution might take, since, although stellar evolution rests on well understood physics, little is known of the basic process of the star formation. The formation of stars involves many non-linear components such as cloud collapse, and is an open system susceptible to unpredictable environmental effects, including the ionising radiation and winds of young stars, spiral density waves and galaxy gravitational interactions. It is also clear that different star formation histories are appropriate to the range of galaxy types - early type galaxies have little gas and few if any young stars, whereas late types are busy with star formation activity.

An empirical approach to the study of evolution can be made by directly observing galaxies at earlier times. Brown and Tinsley (1974), demonstrated that the number-counts of galaxies to the limit of 4 meter class telescopes could be sensitive to the effects of evolution, if the integrated star formation rate of the galaxy population was significantly higher in the past.

This form of evolution is expected to be most obvious at blue and ultra-violet wavelengths where the effects of young stars is strongest, and indeed the B passband 4m prime focus photographic counts of Kron 1978, and Peterson *et al* 1979, showed an excess over the predictions of non evolving count models. These observations spawned an industry of modelling based on stellar synthesis techniques and further deep observations, from which, it was hoped, the effects of evolution would be easily understood in terms of simple parameterisations of star formation. However, even within these restricted assumptions the observed number counts and colours allow a range of widely different description for evolution, and it has been the hope of workers in this field that faint redshift surveys would considerably limit these possibilities by 'de-projecting' the faint galaxy counts (see Tinsley 1977, Koo 1981, and Ellis 1982).

## 1.4 Thesis Outline

The redshift survey presented in Chapter 3 is the first attempt to survey in a systematic way the redshifts of faint galaxies, and forms the centerpiece of this work. The galaxies selected for the survey represent simply a subset of the galaxies identified on deep photographic plates. Sample selection is by apparent magnitude and non-stellar appearance only, and is faint enough, to probe the galaxy number-magnitude count excess. This survey provides redshifts of the general galaxy population which are fifty times fainter than similar redshift surveys attempted in the past and a large depth and lookback time are achieved.

In Chapter 2 we set out the ground work for analysing the faint redshift survey. A model is constructed based on the previous Durham bright galaxy survey of Peterson *et al* (1986), and against which the faint galaxy distributions can be compared. Meaningful interpretations of faint galaxy properties are not possible without such a model, since the faint galaxy distributions comprise all galaxy types spanning a huge range in luminosity.

We first compare this model with the new deep number-counts and colour distributions from the CCD photometry of Metcalfe *et al* (1987). These data extend 2 magnitudes fainter than the current photographic photometry and allow firmer constraints to be placed on the traditional models of evolution. In Chapter 2 we show the difficulty of reproducing the power law behaviour of the counts in B, to the limit of this data, with the traditional evolutionary models, and additionally we argue that a significant component of these counts do not show any evidence for significant colour evolution to the faintest limit.

New conclusions regarding galaxy evolution follow from the analysis of the redshift distribution presented in Chapter 3, which indicates that only low luminosity galaxies are allowed to evolve significantly over the redshifts sampled. We strongly constrain the evolution of bright galaxies to a minimum time variation, consistent with constant star formation rates in the range $z < 0.5$.

In Chapter 4 we probe evolution further, using information from the spectral properties of the faint sample. Comparing the redshift survey spectra with the brighter Durham redshift survey, we find a trend to stronger emission lines in the faint survey. Also in Chapter 4 we examine the faint survey spectra by comparison with the predictions of a stellar synthesis code, which

has been extended to include intermediate resolution stellar spectra. Evidence for stronger rates of star formation in some of the galaxies is evident from the continuum shape, emission and absorption line features indicating that objects with temporarily high star formation rates account for as many as 30% of the galaxies sampled.

In chapter 5 we construct a new model of evolution based on a common occurrence of short 'bursts' of star formation at earlier times. Short bursts of star formation, we show, may enhance a galaxies' luminosity considerably, even if only a small fraction of a galaxies mass is involved. This effect allows the appearance of a population of blue emission line galaxies to appear in the counts, which would otherwise lie beneath the magnitude limit at a given redshift. In this way we are able to account for the observed number-count excess and faint colour distributions.

The faint redshift survey has the additional advantage of providing information on large scale structure by virtue of its depth. In Chapter 6 we examine the distribution of galaxies on both small and large scales making use of the 2 point spatial correlation function. Reasonable agreement with local redshift survey studies is found at small scales, however on large scales we find tentative evidence of a regular periodicity in the galaxy distribution in the direction of the Galactic poles.

# Chapter 2.

# FAINT GALAXY COUNTS, COLOURS AND MODELS

## 2.1 Introduction.

Galaxy number counts have been pursued with renewed enthusiasm over the last decade with the availability of improved photographic emulsions, and the development of automated plate scanning methods. These technical advances have inspired a number of large area sky surveys and helped us to realise the wealth of clustering and evolutionary information contained on deep photographic plates.

The number-magnitude counts and colour distributions of large samples of galaxies can be obtained from such work, but are not easy to interpret since, the galaxies sampled span a large range in luminosity and thus cover a range of redshifts. Predictions of their colour distributions are complicated by this spread in redshift and the intrinsic variation of colour along the Hubble sequence.

To cope with these considerations, when analysing faint galaxy samples we construct a model for calculating number-magnitude, colour and redshift distributions. This model is based on local galaxy properties and set in the standard Friedmann cosmology. The resultant predictions form a benchmark against which faint observations can be examined since, this comparison tests the 'null' hypothesis that galaxies today share the same photometric properties as those sampled at earlier times.

We find that the number magnitude counts cannot be reproduced at faint magnitudes, the observed count lies well in excess of the model prediction for the B passband, in agreement with previous work in this field. The effects of evolution are then examined, but unlike other authors we do not favour descriptions of evolution in which star formation, integrated over the general population, has been much higher in the past. We base this conclusion on model comparisons with newly available deep CCD photometry which show the counts in B to extend as a steep power law for at least 2 magnitudes fainter than the photographic work, but with an unevolved red component.

Finally we point the way to the study of deep , redshift surveys as a means of unravelling the complexities of the counts - the subject of subsequent Chapters.

## 2.2 Number Counts: General Properties

The simplest and well-known prediction for the form of the number counts, is that they should increase with apparent magnitude, m, as $10^{0.6m}$ for the case of a static Euclidean geometry, independent of the galaxy properties. However the standard Friedmann models the expansion and geometry produce a shallower rate of increase of counts with apparent magnitude, and count predictions must take account of differences in properties between galaxy populations. These complications are now outlined.

### 2.2.1 Effects of Redshift

Expansion results in redshifting of a galaxies' spectrum, allowing light from shorter wavelengths to enter the passband of interest and 'stretching' the spectrum, over a given bandwidth, by a factor (1+z). Since the observers passband has a fixed transmission function this stretching in wavelength means the passband represents an increasingly narrow range of wavelength with increasing source redshift. Thus for example in the case of a flat spectrum yielding a lower photon count than in the restframe. An additional reduction in photons results from the relativistic effect of a reduced rate of arrival of photons received from a given redshift, by an another factor of (1+z). The redshifting of shorter wavelength light into the fixed passband means that we must know the spectral energy distribution for the source populations. This is an important consideration in modelling the counts since the shape of a spectrum varies with galaxy colour, being most important for early type systems where the UV flux falls off steeply shortward of optical wavelengths.

The above effects can have a significant effect on the apparent magnitude of an object, and are passband dependent, almost always combining to lower the apparent magnitude with respect to the restframe. Only in the case of the very bluest systems can the steep rise in the spectral energy distribution to shorter wavelengths offset the other two effects. The effects of redshift are given by 'k correction' which is expressed in terms of magnitudes and usually written as (Oke and Sandage 1968),

$$k(z) = 2.5\log(1+z) + 2.5\log\frac{\int_0^\infty I(\lambda)T_r(\lambda)d\lambda}{\int_0^\infty I(\frac{\lambda}{(1+z)})T_r(\lambda)d\lambda} \quad (2.1)$$

Where $F(\lambda)$ is the rest frame spectral energy distribution, and $T_r(\lambda)$ the transmission function for the filter of interest. Note that this is not really a correction at all, but the expected consequence of redshift on a galaxies' spectral energy distribution. The time dilation factor note, is usually included in the distance-luminosity relation (see 2.2 for definition).

### 2.2.2 Selection Functions

The sampling of galaxies with redshift in an apparent magnitude limited sample, is heavily biassed to the bright end of the luminosity function and centered on the characteristic absolute magnitude, $M^*$, where the luminosity function turns over to a steep power law at brighter magnitudes. This behaviour is due to the form of the galaxy luminosity function and the shape of the volume available for sampling objects, and means that the majority of objects sampled are found at $z^*$; the redshift corresponding to $M^*$. In turn,$M^*$ corresponds to the apparent magnitude limit of the sample since the number of galaxies rises steeply with apparent magnitude since, that the majority of galaxies are sampled against the upper apparent magnitude limit, so that this limit approximately determines the depth to which a $M^*$ galaxy is seen.

The luminosity function expressed as a logarithm of the differential space density of galaxies per unit absolute magnitude, shows a break from a steep power law for $M < M^*$, to a much shallow increase with absolute magnitude at lower luminosities, $M > M^*$. For an apparent magnitude limited sample the volumes in which the faint end can be sampled are relatively small compared to brighter magnitudes, and the contribution to the count falls off rapidly below $z^*$. Conversely, for redshifts greater than $z^*$, the objects sampled are from the steeply declining bright end of the luminosity function, which falls off more steeply than the increase in the available volume. These effects result in a bell shaped redshift distribution, or selection function, for an apparent magnitude limited sample which is centered on $M^*$ of the luminosity function.

With this selection function the form of low luminosity end of the luminosity function will always be much less well determined, using redshift information,

than at $M^*$ since the fraction of such systems drops off rapidly at the low redshift range of such a sample - point we examine in greater detail in §2.9.

## 2.3 The No-Evolution Model

As demonstrated above given the significant differential effects of redshift on different classes of galaxies, meaningful discussion of galaxy counts at faint magnitudes is only achieved by comparison with the predictions for the form of N(m) based on models which extrapolate, to fainter magnitudes, the properties of representative local galaxy samples. Here we discuss the construction and requirements of such a model for comparison with faint distributions.

This model is based on galaxy properties which are observed to small fractions of the Hubble time (local galaxies), and model predictions to much larger fractions of the Hubble time assume these properties to be time independent and is thus termed the 'no-evolution' model. This model then, acts as a benchmark against which the counts are compared and against which galaxy evolution can be judged.

The method of construction of a model for predicting faint galaxy distributions has been outlined by many authors (Tinsley 1977,1980, Bruzual and Kron 1980, Koo 1981, Ellis 1982, King and Ellis 1985, Shanks *et al* 1984). Here we establish, using local galaxy data, the properties of the present day galaxy galaxy population discussed above, required by the model. We go on then to discuss the sensitivity of the faint galaxy magnitude colour and redshift distributions to uncertainties in these properties and compare our predictions with the available data.

Since the $k$ corrections are described in terms of polynomials, analytical descriptions of the counts are not readily obtainable, and deep field galaxy count models are always calculated numerically.

Operationally the prescription is to calculate at the luminosity distance for a given redshift the $d_L$, taking the standard friedmann expressions, for the case of the cosmological constant set to zero, this is given by (Weinberg 15.3.24 p485),

$$d_L = \frac{1}{H_o q_o^2}(zq_o + (q_o - 1)(-1 + \sqrt{2q_o z + 1})) \qquad (2.2)$$

where $H_o$ and $q_o$ are Hubbles constant and the deceleration parameter, respectively. The differential volume-redshift relation for this cosmological model,

$dV(z)$, is given by,

$$\frac{dV(z)}{dz}dz = \frac{cd_L^2}{H_o(1+z)^3}dz \tag{2.3}$$

The number of objects per increment in redshift and apparent magnitude can now be calculated,

$$\frac{dN(m,z)_i}{dmdz}dmdz = (\Phi(M+dM)_i - \Phi(M)_i)\frac{dV(z)}{dz}dmdz \tag{2.4}$$

where $\Phi(M)_i$ is the luminosity function for the i$^{th}$ class of galaxy at absolute magnitudes corresponding to apparent magnitude, $m$, related by the usual expression,

$$M = m - 5\log d_L - 25 - k(z)_i \tag{2.5}$$

where $k(z)_i$ is the $k$ correction for the i$^{th}$ class. The apparent magnitude distribution, i.e. the differential number magnitude count, summed over all classes is then,

$$\frac{dN(m)}{dm} = \sum_i \int_o^{z_{max}} \frac{dN(m,z)}{dmdz}dz \tag{2.6}$$

where the maximum redshift $z_{max}$, is the redshift above which contribution from counts goes to zero. Similarly the differential redshift distribution is given by the integral over apparent magnitude,

$$\frac{dN(z)}{dz} = \sum_i \int_o^{m_{lim}} \frac{dN(m,z)}{dmdz}dm \tag{2.7}$$

Thus magnitude limited data makes for a very straightforward approach: we can directly calculate the faint galaxy distributions for apparent magnitude limited data from the volume limited properties i.e. the luminosity functions of each class of galaxy.

In fact to set up the model this calculation must be preformed in reverse, since we are required to establish the luminosity functions and the relative space densities of the various galaxy classes by making use of magnitude limited samples. We can in principle achieve a unique fit (subject to observational uncertainty) from apparent magnitude limited samples of galaxies classified,

by type and/or restframe colour, with complete redshift information for an apparent magnitude limited sample. The redshift and galaxy class calculation of the absolute magnitudes via equation 2.5 (assuming that the redshift is dominated by the Hubble flow), which after correction for volume allows the luminosity function to be established (see Efstathiou *et al* 1988 for discussion the various methods). Here however we adopt a standard form for the luminosity function (see below) and correct this for volume and then compared with the distribution of absolute magnitudes to determine, in the case of a Schecter luminosity function (Schecter 1976), the characteristic parameters $M^*$ and $\alpha$ of each galaxy class. Finally the space densities of each class, or 'mix', are established by comparison with the observed proportions of each type in the magnitude limited sample (note any bright magnitude limited sample can in principle be used since redshift data is not required for this stage), by running the model with the absolute mix set initially arbitrarily, and taking note of the predicted apparent mix to the magnitude limit of the observations then adjusting the absolute mix to reproduce the observations.

Finally the absolute normalisation of the models requires only the observed number of objects at a given (bright) apparent magnitude, and this is best done as we show below using all the available bright field counts, given the observed large field to field variance in the counts.

### 2.3.1 $k$ Corrections and Passbands

We use the $k$-corrections summarised by King and Ellis (1985) which rely primarily on the optical spectrophotometry of Wells (collated and tabulated by Pence 1976) for the various types. The B passband $k$ corrections, for $z < 0.8$, can be applied with confidence and are sufficient to cover the redshift range of counts to the limits of the count data, assuming no evolution (demonstrated below). In $r_F$, the uncertainties in the $k$ corrections are pushed to much higher redshifts, and are much less important.

Above $z \sim 0.8$ and to a maximum of z=1.5 the $k$ corrections are based on satellite broad band UV data and these have become the standard data for count models by virtue of the paucity of observations in UV (see King and Ellis 1985 for a discussion). However as we show below such high redshifts are not expected to be sampled by the counts without strong evolution, and then the correction is dominated by evolution, and in the case of standard luminosity

evolution, are supplied by the evolutionary stellar synthesis codes. So with evolution the high redshift uncertainties in predicting the B counts reflect the uncertainties in the evolutionary models.

The k corrections as a function of type are listed in Table 2.1 for the passbands of interest here. These passbands are termed $b_J$ and $r_F$ bands ($\lambda_{eff}$ = 4800Å and 7000Å respectively) and based on the Kodak IIIa emulsions which represent the best currently available for astronomical photometry. These emulsions are fine grained and provide sufficient resolution for identifying Hubble type to B=17 on Schmidt type telescope plates (Peterson *et al* (1986)) and also permit star galaxy separation to be carried to to B$\sim$ 23 on 4m telescope prime focus plates (Shanks *et al* (1984), both essential to studies of the counts. IIIaJ has the additional advantage of being capable of full hypersensitisation resulting in a detected quantum efficiency of typically 2%. For further discussion of these points see Cannon 1984.

Table 2.1

| Galaxy Type | $k(z)$ for $b_J$ | $k(z)$ for $r_F$ | Colour ($b_J$-$r_F$) | Absolute Mix |
|---|---|---|---|---|
| E/S0 | $4.139z + 0.446z^2$ | $1.36z + 1.07z^2$ | 1.51 | 0.24 |
| Sab | $3.446z - 0.556z^2$ | $1.499z + 0.376z^2$ | 1.41 | 0.19 |
| Sbc | $2.347z + 0.075z^2$ | $0.400z + 0.711z^2$ | 0.99 | 0.23 |
| Scd | $1.948z - 0.225z^2$ | $0.169z + 0.616z^2$ | 0.86 | 0.17 |
| Sdm | $1.218z - 0.238z^2$ | $0.053z + 0.784z^2$ | 0.76 | 0.17 |

### 2.3.2 Cosmological Parameters.

The predicted counts are not dependent on $H_o$. The absolute number number of galaxies is not required by the count models since we use the observed luminosity function which scales as $H_o^{-3}$, which cancels out since the volumes sampled are proportional to $H_o^3$.

The uncertainty in curvature (determined by $q_o$ and $\Lambda$) has an important effect on the counts through the distance-luminosity and volume-redshift relations of equations 2.2 and 2.3. Considering the case of $\Lambda = 0$, the volume is strongly dependent on $q_o$. For an object of given apparent magnitude, the distance at which it is observed for a given redshift, is smaller for a larger $q_o$ since, the larger the deceleration the greater is the redshift induced. For greater $q_o$, this effect allows an object of given luminosity to be observed to a higher redshift.

However, this smaller distance means that the volume available for sampling to a given redshift is smaller. In fact these dependencies work in opposite directions for number-magnitude counts and cancel to first order (Brown and Tinsley 1974), so that geometrical tests of curvature from counts alone, for the interesting range of $q_o$, require great depths, - a point first noted by Sandage (1961).

Thus for the purposes of these models the present large uncertainty in cosmological parameters are not important. However, $H_o$ and $q_o$ do enter into the discussion of evolutionary models, through the time-redshift relation (see later).

## 2.4 Local Galaxy Redshift Surveys.

As established above, in order to predict galaxy counts we require magnitude limited data and redshift information, i.e. a redshift survey. The redshift provides the relative distances required to construct the luminosity functions. In addition, galaxy morphology and/or restframe colour must also be determined since as we shall show there is a clear trend of characteristic magnitude with galaxy class, being lowest for bluer and generally later type systems.

We make use of a previous Durham redshift survey, the Durham/Anglo-Australian redshift survey (DARS), Peterson*et al* (1986), which is magnitude limited to $b_J = 16.75$ from UKSTU Schmidt plate material. This redshift survey totals 340 objects for which accurate redshifts and $b_J$ magnitudes have been determined. The survey samples randomly selected areas over five well separated high galactic latitude–southern hemisphere fields–(for–details–of–the survey strategy and selection see Peterson *et al* 1986).

Foremost, the DARS provides a reliable estimate of the field luminosity function and its variation with Hubble type or $b_J$-$K$ colour. In addition to this Morphological types have been reliably determined for the majority of galaxies in this sample. In addition optical-infrared colours ($b_J$ - $K$) are also available for a subsample of $\sim$ 200 galaxies randomly selected from DARS, (see Mobasher *et al* 1987), which provides an independent check of the model based on Hubble type.

Other bright magnitude limited surveys also exist from which other authors have constructed local galaxy properties. (see Efstathiou *et al* 1988 for a comparison of luminosity functions for the available bright galaxy redshift

surveys). However, DARS has a number of important advantages which make it particularly suitable for our purposes. The survey magnitudes are in the same passband ($b_J$) as the deep galaxy counts and redshift distributions that we will be comparing with later, so no corrections for passband differences are required. These corrections are often large and have a colour dependence making comparisons of photometry between differing photometric systems potentially subject to systematic errors. Secondly DARS has a greater mean depth than comparable surveys and so suffers less from any contamination by local superclustering.

To estimate the luminosity functions, we divide the DARS survey into three type groupings E/S0, Sa through Sbc, and Sc through Im, apply the $k$ correction appropriate to each type and hence determine the absolute magnitude distribution $N(M_{b_J})$ for each group. Following the technique described in Ellis (1982), we parameterise these distributions in terms of those expected for a Schechter (1976) function with a faint end slope, $\alpha = -1.25$, found for the entire survey (Bean 1983, and consistent with Efstathiou *et al* 1988) determining $M^*$ from a minimum $\chi^2$ fit. The trend towards fainter characteristic absolute magnitudes for later types is evident in the results summarised in Table 2.2.

Table 2.2: 'No-Evolution Parameters' ($H_0 = 50$)

| Galaxy Type | $M^*_{b_J}$ | # | Model Predictions |
|---|---|---|---|
| E/S0 | -21.6 | 97 | $\overline{z}(20.5 < b_J < 21) = 0.22$ |
| Sab-Sbc | -21.15 | 117 | $\gamma(20 < b_J < 24) = 0.32$ |
| Sc-IM | -20.85 | 46 | |
| B − K Limits | $M^*_{b_J}$ | # | Model Predictions |
| > 3.65 | -21.39 | 74 | $\overline{z}(20.5 < b_J < 21) = 0.215$ |
| 2.9-3.65 | -21.24 | 61 | $\gamma(20 < b_J < 24) = 0.32$ |
| < 2.9 | -20.52 | 32 | |

Figure 2.1 shows the comparison of the absolute magnitude distributions for the type groupings listed above and the best fit $M^*$ for $\alpha = -1.25$, demonstrating the trend to lower luminosities for later types and the good fit of the Schechter function for the two earliest type groups. The latest types

are not so well fitted here, the distribution of absolute magnitude being much flatter for the data, this group however, represents only a small fraction of the observed sample. Later we explore the effect of varying the luminosity function parameters of the late type galaxies to explore the possible effects of uncertainty at the faint end of the luminosity function on the predictions for faint galaxy distributions.

The relative proportions of each galaxy type (or mix) are then determined as described above (§ 2.3) producing relative space densities of the galaxy type classes and listed in Table 2.1. These are not normalised using DARS since the overall normalisation remains quite uncertain, with the DARS volume density $\sim 40\%$ lower than most other luminosity function estimates (Efstathiou *et al* 1988). Deeeper photometry photometry of 14 Schmidt fields (Stevenson *et al* 1985) also confirms this deficiency. The origin of the DARS deficiency witnessed in each of the 5 well-calibrated distributed fields remains obscure presumably relating to the effects of large scale structure. Fortunately, we are principally interested in the count slope and this, together with the form of the predicted faint redshift distributions (see later), are independent of the normalisation, provided the galaxy properties within the DARS are representative of regions of more typical number densities, see 2.7.2 for further discussion.

As a check on the stability of our models we can redetermine the luminosity function and mix for the subset of DARS with $b_J - K$ colours. Dividing this sample into 3 colour classes in $b_J - K$ we determine the luminosity function of each class in the manner described above. Figure 2.2 shows the best fit Schechter function fits against this data. Comparison with Figure 2.1 demonstrated again that the lowest luminosity class is not well fitted in this way. The bluest objects having a flatter absolute magnitude distribution than the redder classes, and thus a somewhat steeper faint end luminosity function. Poor statistics here prevent us from defining the luminosity function from this data but as noted above for the late type subsample this group of objects represents only a small fraction of the total sample and unless the luminosity function extends to substantially fainter magnitudes with a slope very much steeper than that of the brighter redder galaxy groups, then we need not worry about this class of objects. These points are taken up again in detail later (see Chapter 2.9 and Chapter 3.14).

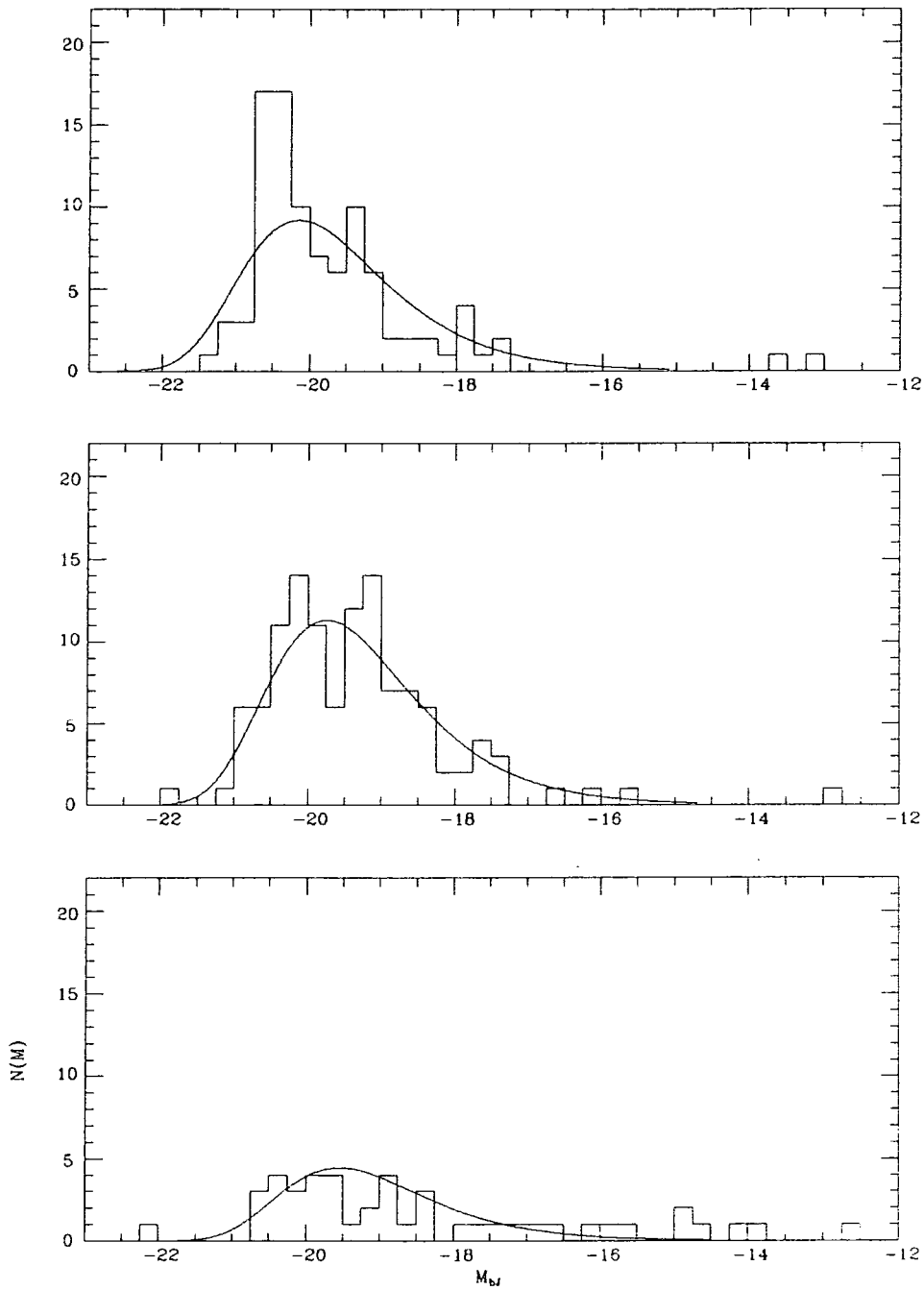


**Figure 2.1. Absolute magnitude distributions for DARS divided by type into E/S0 types (top), Sa-Sbc (middle), Sc-Im bottom. Comparison with best fitting Schecter functions are shown for $\alpha = -1.25$,($H_o = 100 Kms^{-1}Mpc^{-1}$)**

Table 2.2 shows the comparison of this method with the models based on morphological types. Very little difference is found in predictions of the

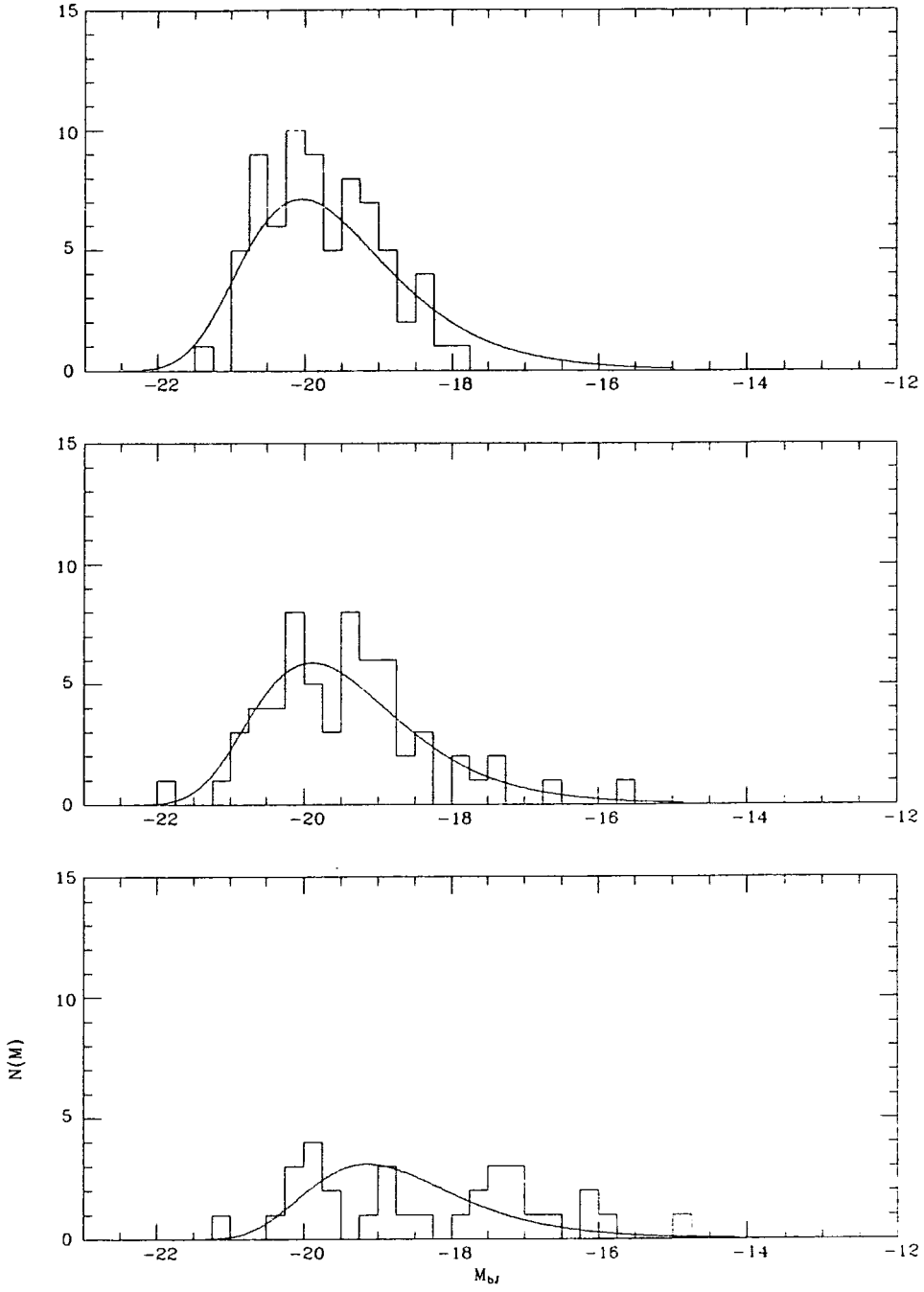


**Figure 2.2. Absolute magnitude distributions for DARS divided by colour, into (top), $b_J - K > 3.65$ $2.9 < b_J - K > 3.65$ (middle), and $b_J - K < 2.95$ (bottom). Comparison with best fitting Schecter functions are shown for $\alpha = -1.25$ ($H_o = 100 Kms^{-1}Mpc^{-1}$**

faint differential count slope, $\gamma$, and mean redshift at $b_J = 21$ (see Chapter 3), between these two different methods of parameterising local galaxy properties.

This agreement is very encouraging and we conclude that we have constructed representative no-evolution models which on which we may confidently explore the predicted faint galaxy distribution to faint magnitudes.

We now go on to describe the range and quality available faint galaxy photometry and the sensitivity of the B and R passbands to differing galaxy properties.

## 2.5 Model Predictions and the Counts

Here we discuss the predicted counts from the no-evolution model, to the faint magnitudes of interest here, and examine the claim for evolution by comparing with count and colour information for magnitude limited counts and colour distributions selected in both the $b_J$ and $r_F$ passbands.

## 2.6 Deep Galaxy Photometry

Counts have concentrated in the main on B band, which has been established over the last 10 years to be the most important in this respect, with its low sky background for this passband and sensitivity to the luminous young stars produced during star formation. The early deep photographic work of Kron (1978) and Peterson *et al* (1979), established 4m prime focus photography coupled with machine measured magnitudes as a powerful approach to deep photometry. This experimental work was complemented by the early modelling of Tinsley (1980) using the local galaxy properties from a bright galaxy redshift survey of Kirshner *et al* (1978), and various possibilities for the evolution of the Hubble sequence, based on stelar synthesis codes. This approach has been improved upon with the work of the Durham group. The DARS redshift survey, described above, is more extensive and better controlled than that of Kirshner *et al*, and selected in the same magnitude system as the deep 4m counts, allowing more rigorous modelling. The count analysis by King and Ellis (1985), included the DARS survey properties, improved satelite UV spectral energy distributions, and the previously unexplored evolutionary effects of spiral bulge evolution. Koo (1986) has also reapraised the counts by extending observations to the U and I passbands. In addition Koo made use of the improved stellar synthesis code constructed by Bruzual (1983) and extended Tinsleys approach to evolution with multi-colour distributions.

Recently the deep CCD work of Metcalfe *et al 1987* and Tyson (1987) has pushed the limiting B magnitude over 2 magnitudes fainter than the deep photographic work, and it is this data on which we concentrate now, since it provides a new challenge to the models.

Counts note, are usually determined in either Kron magnitudes or isophotal magnitude systems. The isophotal magnitude scheme of Peterson *et al* (1979), Shanks (1984), and Metcalfe (1987) are magnitudes determined to a faint limiting isophotes, usually down to $\sim 1\%$ of sky brightness or $26.^m5 arcsec^{-2}$. This surface brightness is $\sim 4$ magnitudes below the typical galaxy central surface brightness, and are claimed on basis of rigorous testing (Ellis 1982, Shanks 1984) that magnitudes traced to this level represent total magnitudes. Kron has also claimed that magnitudes measured in his system of image extrapolation measure effectively total magnitudes (Kron 1982), and Ellis and Koo (see Ellis 1987) have shown close agreement between counts measured in these two systems for the same photographic material (for further discussion see 2.7.4).

### 2.6.1 Count-Model Comparison

The clear result to emerge from the early work described above, is that the observed counts are very much in excess of no-evolution model for $B > 20$. Comparison of the no-evolution model constructed in this work is made with a range of reliable $b_J$ counts and presented in Figure 2.3. We normalise our model to large sample of Schmidt counts of Stevenson *et al* 1986, at 18th magnitude for the reasons given in §2.3.

The counts from both Schmidt and 4m plates, show that whilst sizeable fluctuations in absolute numbers are found between these different fields, the differential counts are well fitted by a single valued slope for magnitudes fainter at $b_J < 20$. The slope determined for the magnitude range $20 < b_J < 23$ is $\gamma = dlogN/dm = 0.43 \pm 0.02$ (Ellis 1987) and the deeper CCD photometry (Metcalfe *et al* 1987, Tyson 1988) show a very similar slope extending to at least $b_J \sim 25$. Figure 2.3 shows that the the predicted counts fall short of those observed by a factor of $\sim 1.5$ at $b_J = 21.5$, and by $b_J = 24$ this rises to $\sim 3$.

Importantly, the no-evolution model predicts a continued flattening of the count slope with apparent magnitude, an effect due directly to redshift dimming (the $k$ correction), so that the predicted slope in the range $20 < b_J < 24$ has

an average value of $\gamma = 0.34$, considerably lower than observed in Figure 2.3. This result is independent of the normalisation and has stimulated much work on galaxy evolution (described below).

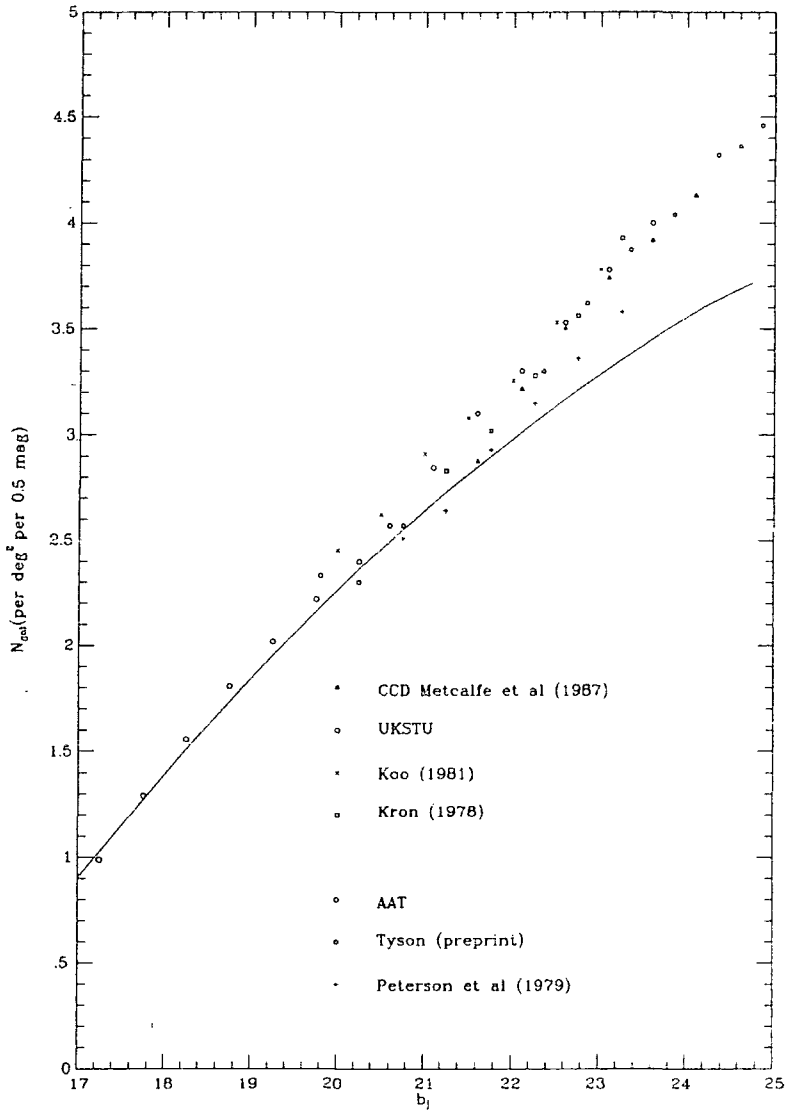


**Figure 2.3. $b_J$ counts combining most of the available 4m data and the brighter UKSTU Schmidt data, and the very deep CCD photometry of Metcalfe *et al.* Plotted for comparison is the no-evolution model derived from DARS.**

### 2.6.2 Faint Colour Distributions

More detail on this count discrepancy is provided by the colour distributions at faint magnitudes. The data of Metcalfe *et al 1987* provide accurately determined $b_J$-$r_F$ colours complete to $b_J = 24$ ($\sigma \sim 0.^m1$ at $b_J = 24$). The no-evolution model can be readily extended to predict colour distributions to this depth, by including the observed mean colour as a function of type (listed in Table 2.1). Since the relationship between type and colour has a well known 'cosmic' dispersion (see, for example, Stavely-Smith *et al* 1987), a small amount of smoothing is introduced in the models so that the mean colour separation between types is roughly twice the gaussian dispersion of the colour smoothing window ($\sigma \sim 0.2$). This procedure is checked later against the distribution of $b_J - r_F$ at bright magnitudes (§2.7.2) and ensures that there is no unphysical irregular structure in the predicted colour distributions.

Predictions for $b_J$ selected $b_J - r_F$ colour distributions are made for data in the form presented by Metcalfe *et al*, shown in Figure 2.4. This comparison is remarkably revealing, and suggests that the count excess is concentrated at blue colours, with a red tail which matches well the no-evolution model. It has been recognised from earlier photographic work that the colour distributions to faint magnitudes in B-R show a tendency to bluer mean colours with increasing apparent magnitude (Koo 1982,1986, Shanks *et al* 1984), but colours determined from photography at faint magnitudes are notoriously difficult to measure and become very unreliable beyond $b_J = 23$. The CCD colours are certainly more reliable, based on linear intensity measurements, and taken at face value imply little colour evolution of early type galaxies with the count excess restricted to $b_J - r_F < 1.6$.

### 2.6.3 R Selected Faint Photometry

Count and colours selected in R complement the work in B but have not been pursued with the same enthusiasm. R counts are more dominated by early type galaxies and are much less sensitive than B to intrinsically blue systems. The previous work of Shanks *et al* 1984 and Koo 1986, show to a much flatter count slope in this passband than B, more consistent with the no-evolution models. Published R band counts to the deepest presently available limits are plotted in Figure 2.5 for $r_F$, with appropriate colour equations from Metcalfe (private communication). Included are the CCD counts of Metcalfe *et al* and

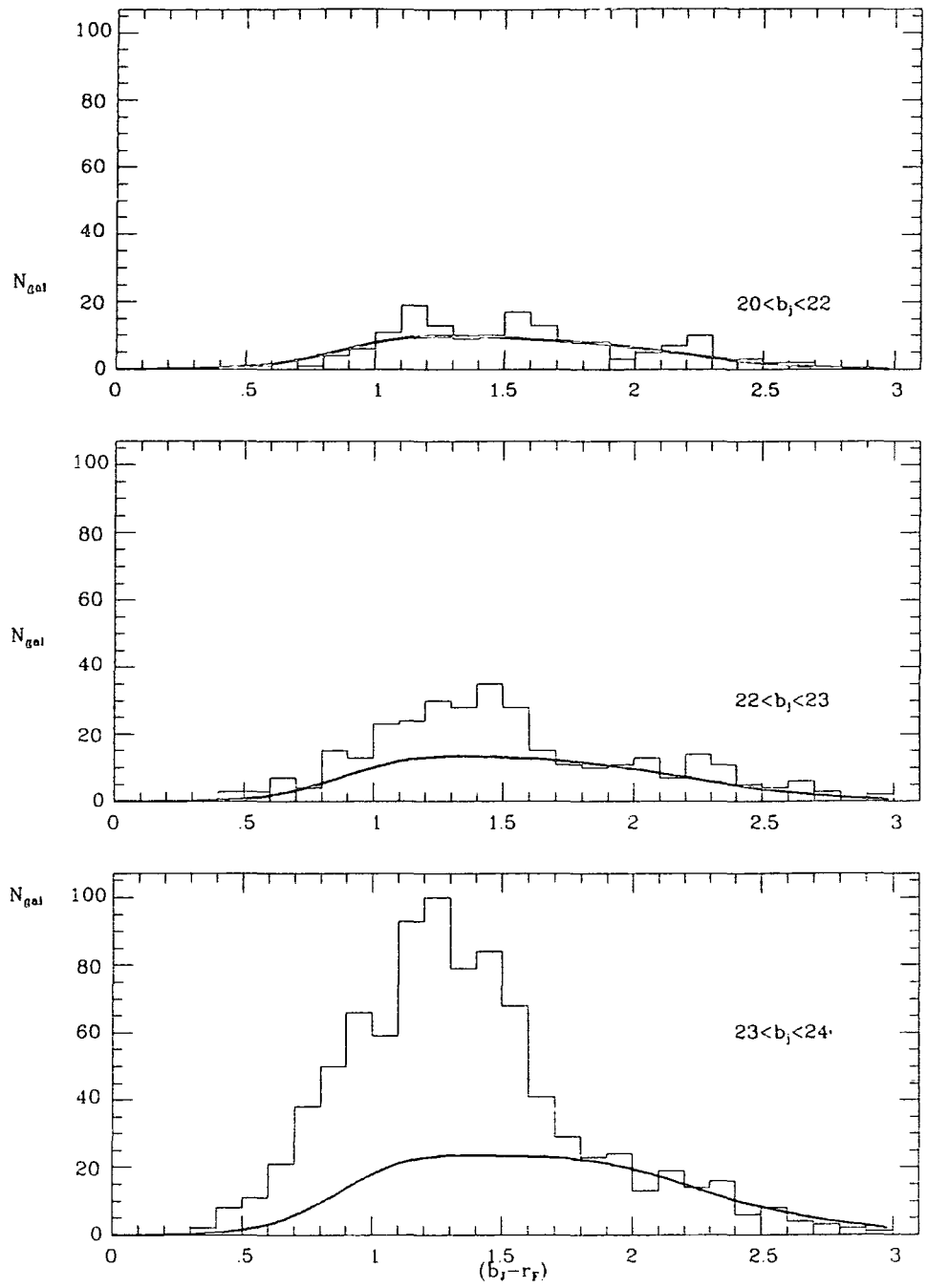


**Figure 2.4. $b_J$ selected $b_J$-$r_F$ colour distributions of Metcalfe *et al* and the no-evolution model**

the Durham photographic counts of Shanks *et al* (1984) which consist of a UKSTU bright Schmidt field to $r_F < 18.5$ and a deep 4m AAT prime focus plate to $r_F < 22$, at the south galactic pole and similar 4m data of Koo (1986)

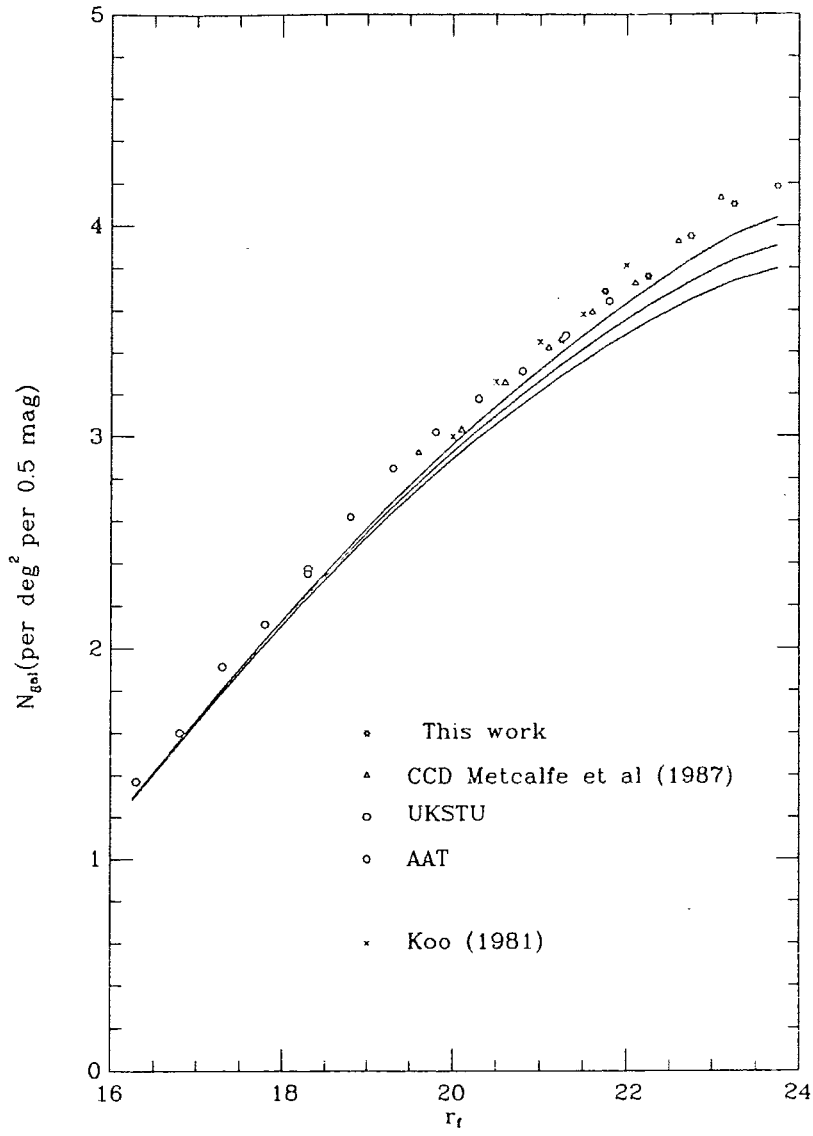


**Figure 2.5. Red counts in $r_F$, also plotted are no-evolution models showing the sensitivity of R selected deep counts to $q_o$. $q_o$ = 0.05,0.5 and 1.0 are shown, the count increases with decreasing $q_o$.**

at the North Galactic Pole.

In addition, plotted here are points referring to this work, this data consists of a small number of deep CCD R fields (10) of total area 0.06 deg$^{-2}$ (cf Metcalfe *et al* with 12 fields covering a total 0.07 deg$^{-2}$) which have been imaged to the deep limit of $r_F < 24$. This photometry is part of other work not discussed in this Thesis (Alington-Smith *et al*, in preparation), taken as offset frames for determining background distributions to high redshift radio

selected groups. The photometry was carried out at the 4m at KPNO on a high quality tectronix chip with the Mould filter system with exposures of 600s and offset by 10 arcmin north and south of the radio source (3C and 4C sources at $z \sim 0.4$), and are mostly at high galactic latitiudes ($b^{II} > 60^{o}$). The data are accurately zero pointed but are aperture measurements, however, at faint magnitudes these most probably represent near total magnitudes since the aperture used is generous 3.65 arcsec diameter and typical faint object lies well within this. A transform from Mould to photographic $r_F$ was made via Johnson system (Metcalfe private communications), and as can seen these counts are consistent in slope and amplitude with the other data shown here.

In order to make predictions for this passband we ideally require luminosity functions obtained in R, however these are not available and we make the reasonable assumption that subtracting the mean $b_J - r_F$ colour for each galaxy type we can transform from $b_J$ to $r_F$. The $k$ corrections for $r_F$, must of course be calculated, this is done as above using Pence's spectra and rely on only the well determined optical spectral energy distributions to the redshifts of interest $z < 1$.

Unlike the B counts, in R the predicted count does have a significant dependency on $q_o$ which is significant for the interpretation of the count at the faintest limits $r_F > 21$ (a point noted by Shanks *et al* 1984). The effect of larger $q_o$ is to diminish the expected count (for the reasons given in §2.3.2), and in Figure 2.5, we plot $r_F$ counts against 3 models with $q_o$ of 0.05 (highest count),0.5 and 1.0 (lowest count). Note the normalisation is carried through from $b_J$, and appears to be 20% to low with respect to the bright count shown here, however this count represents only one field and so we may expect a discrepancy of this order.

The counts in $r_F$ show a clear excess with respect to the model. As in B the model falls away with respect to counts at faint magnitudes, for all reasonable values of $q_o$. The observed count slope is reasonably fit by a single slope $\gamma_{r_F} = 0.32$ for $r_F > 19$, compared with a a model prediction which has an average slope of 0.28.

A smaller value of $q_o$ gives the best fit to the counts, however since the counts are discrepant in $b_J$ then we may expect that the $r_F$ count should also reflect this excess, and so these counts cannot be taken as an argument for

a low value of $q_o$, but more reasonably for a higher $q_o$, with some effect of evolution, as we go on to show. This point is emphasised by the lack of a turn over in the $r_F$ counts to the faintest limits, indicating that a no-evolution model even with very small $q_o$ will not provide a reasonable match at fainter limits. The reason for this sensitivity of the $r_F$ counts to $q_o$, lies in the greater depths of objects selected at faint magnitudes in $r_F$, a result of the generally higher continuum flux at longer wavelengths, relative to B, for most galaxy types. Further insight into these points is provided by the colour distributions selected in $r_F$ below.

### 2.6.4 $r_F$ selected $b_J - r_F$ colours

We now model the $r_F$ selected $b_J - r_F$ colour distribution of Metcalfe *et al.* to examine the count excess in $r_F$ directly. Figure 2.6 shows the no-evolution model prediction to the deepest $r_F$ limit for which the colours are complete ($q_o = 0.5$ is assumed) and we find the same qualitative behaviour as for $b_J$. The data show an excess over the model restricted to $b_J - r_F < 1.6$, which rises with increasing apparent magnitude with respect to the no-evolution model, but note the fractional excess above the no-evolution model is lower in this passband.

The no-evolution model is again a good fit to the red tail of the colour distribution. Note however the sharp fall off in the reddest objects at the faintest magnitude slice, this results from an incompleteness which is expected. since objects with $b_J - r_F > 2.5$ and $r_F > 22.5$ will lie below $b_J$=25; the blue limiting magnitude for this data.

Note that $q_o = 0.5$ provides the best fit in the above colour comparison predictions. However, there are a number of possible systematic problems in modelling in $r_F$, most importantly we do not have $r_F$ determined luminosity functions. In addition the well known colour-luminosity relation for early type objects must have an effect at some level. We claim, based on this colour data, only that the sensitivity of the faint colour distribution to the interesting range of $q_o$ may be significantly greater than the effect of colour evolution of early type galaxies.

With redshift information for these red objects, deeper CCD colours and better determined local $r_F$ luminosity function, we will be able to place stronger constraints on $q_o$ with this approach.

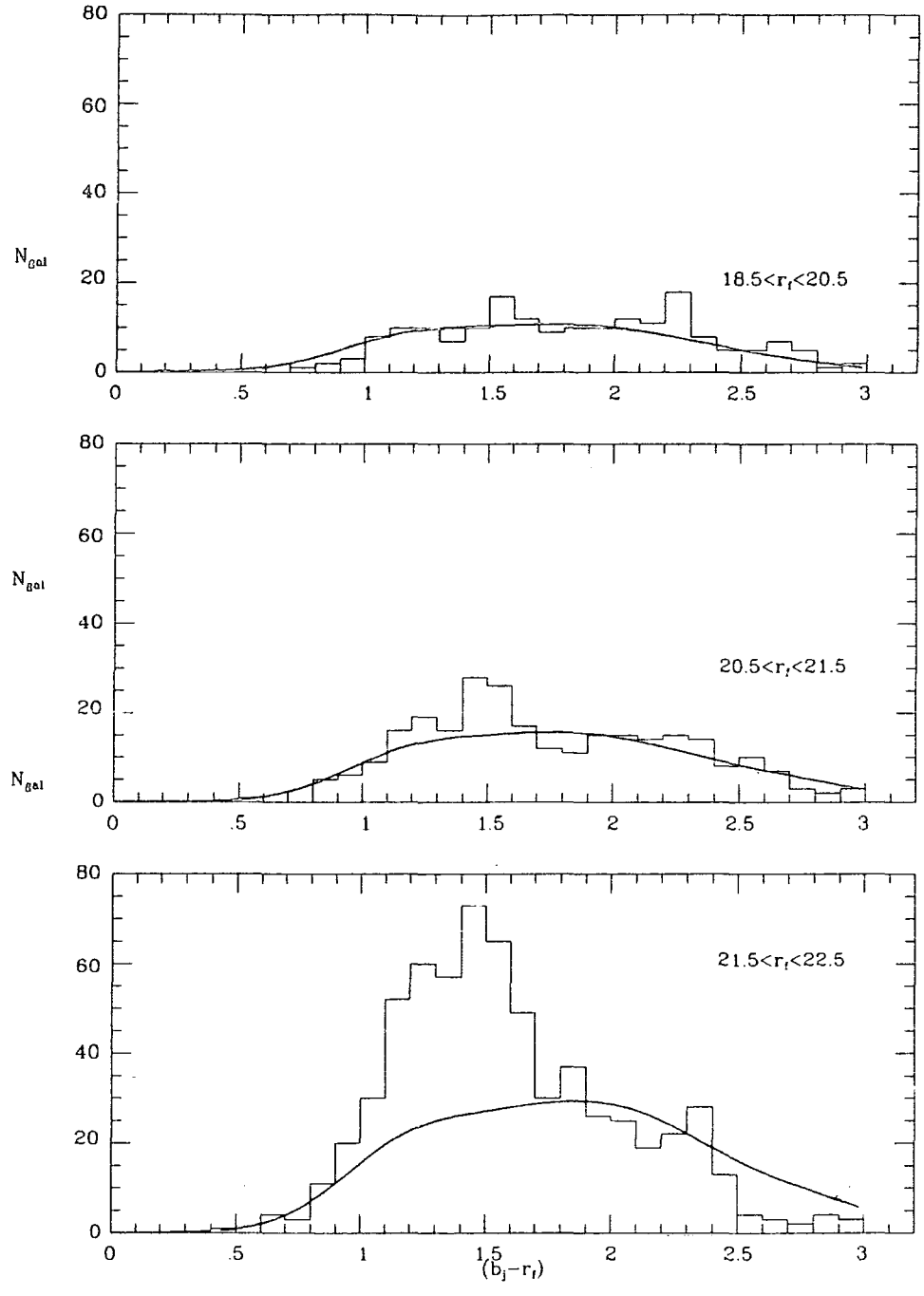


**Figure 2.6. As Figure 2.4 but for the colours are selected in $r_F$**

## 2.7 Model Uncertainties

Here we examine possible sources of systematic error in the parameterisation of the models and and examine to what extent we may change our above

conclusions. Note the no-evolution model is constructed in a similar fashion to most previous work and the predictions are similar to those published by King and Ellis (1985) and Shanks *et al* (1984), differing only in the precise parameterisation of local galaxy properties.

### 2.7.1 Luminosity Functions

The fits to the luminosity functions are not unique, $M^*$ and $\alpha$ of the Schecter function are strongly correlated, and thus changing $\alpha$ will alter the count predictions. However excluding the latest types the maximum allowable changes result in only marginal count differences. Taking the $1\sigma$ error ellipse calculated by Efstathiou *et al* (1988), we may choose $\alpha$ as low as $-0.9$ which leads to a decrease in $M^*$ by a maximum of $-0.^m5$. This would result, for example, in a predicted mean count slope in the range $20 < b_J < 23$ of $\gamma = 0.32$ compared with $\gamma = 0.34$ of our adopted model. Thus the likely uncertainty in the choice of Schecter function is small compared to the count excess.

### 2.7.2 Mix of Types and Normalisation

The relative fractions of the various Galaxy types is important in determining the net effect of $k$ corrections, for example underestimating the contribution of late/blue galaxies will result in a larger predicted mean depth and a flatter count slope, since as established above, these systems have generally smaller $k$ corrections and lower luminosities.

The fields making up the DARS survey, on which we base our mix, have a low overall count which compared to bright count average of Stevenson *et al* (1985) DARS is $\sim$ 40% lower, to survey limit of $b_J$=16.75. and comparison with the luminosity functions derived from other local redshift surveys (Efstathiou *et al* 1988) confirms this.

This discrepancy may relate to large scale clustering however, we may test the appropriateness of the DARS mix by comparing the model prediction with colour distributions at bright magnitudes, for fields which have more representative counts. The bright galaxy counts of Stevenson (1986), show that the brightest reliably determined count is at $b_J$=18, and in Figure 2.8 we compare the model prediction with the colour distribution of the SGP field for the range $17.5 < b_J < 18.5$. The requires a small amount of smoothing to simulate the effect of random error on the magnitudes, and to overcome the

discreteness of the model. Here we smooth the prediction with use a gaussian of $\sigma = 0.^m2$ which this has little effect on the form distribution. The observations are very well fitted, indicating our mix is well determined from the DARS data and that no significant systematic effect here from field variations in clustering.

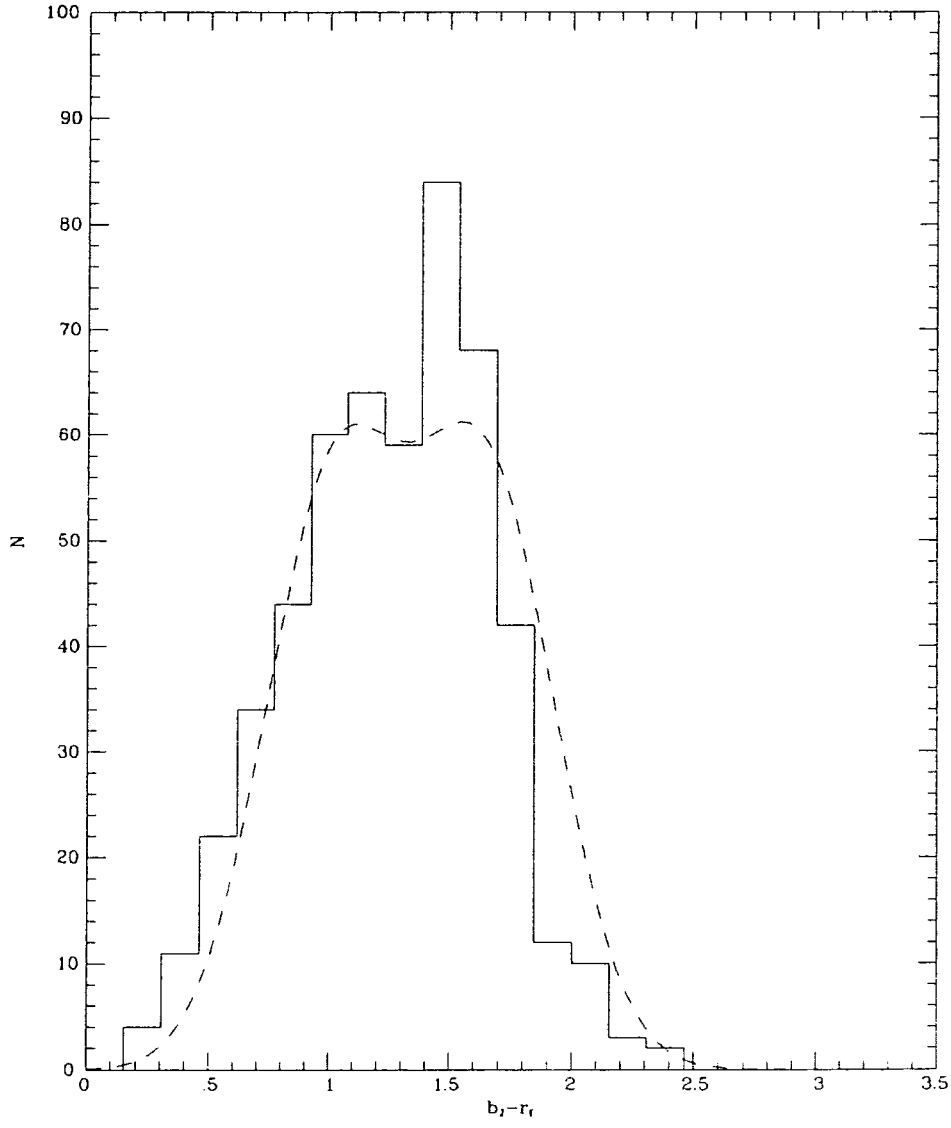


**Figure 2.8. Bright $b_J$-$r_F$ colours $17.5 < b_J < 18.5$, and the no-evolution model prediction (normalised to stevenson *et al*)**

### 2.7.3 Reddening

Another possible source of systematic error in the number counts are the effects of internal and galactic extinction. In this work however, reddening cancels to first order for the following reasons. Firstly the fields used for the both deep counts and the bright galaxy redshift surveys ( on which the count models are based), are at high galactic latitudes. In fact the deep 4m fields are in some cases a subset of the area of the Schmidt field used at bright magnitudes. To first order then any galactic reddening will be not effect the counts since it will effect the bright and faint data equally; the count model based on the bright limited data will then be applicable for predicting the deep data, assuming extinction is smooth over angular scales of a few $deg^2$. More importantly working at high galactic latitudes minimises the effect of galactic extinction.

Internal extinction is also of little concern since galaxy inclination to the line of sight, is distributed in the same way independent of apparent magnitude, and is thus affects the bright redshift survey and the faints counts equally, i.e. we are comparing like with like no correction is applied. Note differential effects resulting from the increased redshift of the faint data may have a small effect. Extinction is more important at short wavelengths and the mean redshift is expected to increase with apparent magnitude, making the deeper data on average redder - assuming no-evolution. This is also true of any reddening dependency on type, since the largest internal extinction is likely to be most important for later type, objects, which are favoured at higher redshift because of their small $k$ corrections.

These effects are differential and in any case work in the opposite direction of the count excess, which we know from the observations presented above, becomes increasingly bluer with apparent magnitude. Thus invoking significant internal reddening will make the count excess even greater.

Finally the spectra used by Pence (see above) to determine the $k$ correction as a function of type and adopted here, are not corrected for reddening but again the observations are mostly a fairly high latitude and barring small scale structure in galactic redding the observations cancel out to first order.

Here we conclude that the effects of extinction are at most second order effects that mean if anything we may have *underestimated* the faint count, in

the opposite sense to the count discrepancy.

### 2.7.4 Systematics and Total Magnitudes

The source of potentially the largest systematic error in all of this type of work is the possibility of hidden selection effects resulting from the difficulty of measuring magnitudes at low surface brightnesses, and indeed the difficulty in even detecting objects for which the central surface brightness which is small compared with the sky. This point has been made by Disney 1976, and Disney and Phillipps (1983), and explored in detail by the early count models of the Durham group (Ellis *et al* 1977).

CCD data allows in principle magnitudes to be estimated to much smaller fractions of the sky background, since CCDs do not suffer the saturation effects of photographic emulsions longer exposures are allowed producing a better determined background count. Metcalfe *et al* (1987) work with a surface brightness limit of only 0.2% of sky, and the close agreement of his counts to the mean photographic count demonstrates that isophotal effects on magnitude estimates for the majority of objects sampled are not a source of serious concern. In any case the effect on the observed count slope would most likely be to flatten it with increasing magnitude, since surface brightness suffers a factor of $(1+z)^{-4}$ relativistic dimming, Ellis *et al* (1977) show that effect if important may manifest itself as a sharp turnover in the observed counts at faint apparent magnitudes. Importantly however, model predictions compare like with like, since the bright galaxies which are used to construct the models and the faint galaxies with which they are compared, cover a very narrow range of central surface brightnesses, centered on $b_j = 20.^m \text{arcsec}^{-2}$, which is fully 2.5 magnitudes above the sky surface brightness in $b_J$. Examples of objects with very much lower central surface brightness have been found (Davies *et al* (1988), such objects would not be included in the models and equally, would not be sampled at faint magnitudes.

## 2.8 Luminosity, Colour and Density Evolution

In this section we address evolution in the context of stellar synthesis codes and by assuming simple parametric forms for the time variation of the star formation history. This approach to modelling the effects of evolution was pioneered by Tinsley (1977). Bruzual (1983) has improved on this technique by developing a versatile model of spectral evolution which incorporated a more accurate stellar synthesis code. Below in an analysis of the effects of evolution on the faint galaxy distributions, we make use of Bruzuals' latest code.

Evolution and the effect on galaxy counts has been traditionally addressed in the context of such stellar synthesis codes, however the exhaustive work of many authors the last 10 years (see reviews by Tinsley 1980, Ellis 1982,1988) have led to few clear constraints on the history of star formation for the general galaxy population. The difficulty in interpreting the counts in terms of these evolutionary models, is the number of star formation parameters which must be specified in order to begin to compare with observations, and because the form of the counts does little to distinguish the wide range of possibilities open to such models. With the more accurate and deeper new CCD data however, it is possible to do much better, and in this section we concentrate on simple model comparisons against this data and derive some firmer constraints for the evolution of the general galaxy population.

The major uncertainty in describing evolution is that little is understood about the history of star formation and its variation with Hubble type, or equivalently present day colour, so that necessarily simple parameterisations of this history have to be adopted. Crude constraints may be derived from model comparison with the present day range of colour along the Hubble sequence. This comparison has been studied in detail for the UBV passbands (Tinsley 1968, Huchra 1977, Larson and Tinsley 1978) with the clear and uncontrovertial result that the ratio of the present star formation to the past average varies along the $U-B$ - $B-V$ colour locus, being smallest for the bluest/latest objects, with early high rates of star formation required to reproduce the colours of the reddest (E/S0) systems. However it is only possible to set limits on the ratio of the present rate of star formation rate to the past average, as a function of present day colour, and not to produce interesting constraints on the history and timescale of star formation. The present day range in colours

may for example, be reproduced by assuming an exponential decline in the star formation rate, in which the e-folding time is varied to generate the present range of galaxy colours. This parameterisation of star formation is termed a '$\mu$' model in Bruzuals' notation, and where $\mu$ is defined as the fraction of mass converted to stars in the first Gyr. Equally, we may adopt a history in which strong initial star formation is followed by continuous constant star formation for which the relative fractions of mass involved in the two phases of star formation are varied so that the bluest objects have negligible initial star formation, and the reddest have only the early phase - termed the 'c' model by Bruzual.

These parameterisation are very different but nevertheless reproduce the observed present day range of colours for standard sequence galaxies. In addition this comparison will not distinguish between different initial mass function; the Salpeter form (Salpeter 1955) or Miller-Scalo (Miller and Scalo 1979) give similar results. The range of colour is also insensitive to the age of galaxies in the usual range of uncertainty (6-16 Gyrs). This is because colour is a slowly varying function of time resulting, for early type systems, from the gradual burning down of the main sequence and in the case of late type galaxies the slow build up of long lived low luminosity stars - produced during the more continuous star formation, has only a small effect on the colour evolution.

A second major uncertainty is the conversion of evolutionary changes, which are modelled as spectral changes with time, to an evolution with redshift. The changes in luminosity are strongly dependent on the available lookback time and thus to the values of $H_o$ and $q_o$ and the epoch of formation. The steepest evolution produced with smaller lookback times - or larger $H_o$, for a given choice of $q_o$. In practice the procedure for obtaining luminosity or colour evolution with redshift, is to calculate from the ages of the set of spectra generated by the code, the redshift of each spectrum appropriate to the cosmological parameters adopted, and then to convolve the spectra with the passbands of interest using these redshifts. Finally the evolution is calculated via the apparent magnitude-redshift relation (equation 2.3) for the same cosmology.

Related to this problem is the redshift of first star formation. Choosing redshifts above 5 for the onset of star formation effectively hides any luminous early stage from the B band since by this redshift the Lyman limit is redshifted

into the B band and little flux is emitted by a thermal spectrum shortward of the this cutoff (912Å). Hence any high luminosity generated by initially strong star formation is only important for the counts if it takes place at $z < 5$.

The effect on the counts for these forms of evolution can be significant and dependent on the choice of star formation history, as realised by Tinsley (1968). Most generally this is because with increased star formation in the past a higher luminosity is produced so that to a given flux limit, galaxies are sampled to greater depth and thus over a larger volume, resulting in an increased galaxy count to this limit.

### 2.8.1 Luminosity Evolution and Count Models

In all this modelling we limit ourselves to the Miller-Scalo IMF, but as noted above in terms of luminosity and colour evolution any standard IMF would do equally well. The limitations of these models have been thoroughly discussed by other authors (see King and Ellis 1985 and Koo (1986) for recent reviews), and stem from our ignorance of the process of star formation. For example, the IMF derived for our local neighborhood may not universal and time independent as we must assume. Additionally the stellar library on which the spectral evolution is modelled includes only local stars which are of solar metallicity. However we are able to reproduce in detail the optical spectral properties of galaxies with these codes (see chapter 4.5) giving us confidence that these effects are not important at the level of this work. Furthermore since we are principally interested accounting for the excess of 'blue' objects, we are then concerned mainly with a limited range of stars, namely A and F types, so that for our purposes the shape of the IMF is not important.

We start by considering the simplest case of the 'c' model discussed above. This model may be appropriate for early type systems (E/S0) which in general show no significant present star formation activity. An initial short burst of star formation ($\leq$ 1Gyr) with no subsequent star formation, is typically chosen as a reasonable star formation history for these systems (Tinsley 1980, Bruzual 1983). Here we apply this equally to the entire E/S0 luminosity function, and to keep modelling straightforward we leave the remaining types unevolved.

Figure 2.9 shows that a significant hump-like count excess can result (first discussed by Tinsley 1980) for this case, providing that the initial phase of star formation continues to $z < 5$. This hump is in effect the luminosity

function of the early type galaxies shifted brightward by several magnitudes, and broadened by the range of redshift over which this star formation covers. This hump feature is more pronounced if the initial star formation is of shorter duration and for higher values of $H_o$ and $q_o$. For the case of $z_f > 5$ the effect on the counts of this star formation history, is negligible (compare with the no-evolution model in Figure 2.9) as expected from the above discussion. The observed counts do not show an excess of this form, they are well fitted by a single slope for $b_J > 20$ to the present faint limit of $b_J \sim 25$, and this may simply indicate that this mode of star formation is either inappropriate, or took place at $z > 5$.

Interestingly the early 4m photographic counts of Kron 1978, did seem to show a hump feature and were interpreted initially by Tinsley in favour of the above model, however subsequent reanalysis of this plate by Koo (1982) showed a smoother rise in the counts and in addition incompleteness at faint magnitudes certainly contributed to a flattening of slope conspiring to produce an acceptable agreement with the initial burst models. However, this early conclusion led to optimism that redshift data as bright as $b_J \sim 20$ would reveal in the counts, a population of high redshift 'primeval galaxies' - galaxies undergoing initially high rates of star formation. Subsequent searches for such systems to much greater depths have not to date revealed any convincing candidates (see Koo 1986 for a review of these efforts), (and a point we address in Chapter 3 with deep redshift survey data), indicating very clearly that 'c' type models with a low redshift of first star formation are strongly ruled out in their simplest form.

A more successful approach to modelling evo lution is via the more smoothly varying star formation histories characterised by the $\mu$ models. Large $\mu$ ($\mu > 0.5$) will reasonably reproduce the present day optical colours of an early type galaxy, and give rise to smoother changes of luminosity with time. Figure 2.10 shows the change in the count slope for a range of such models applied only to E/S0 types for a range of cosmological parameters.

The effect on the counts is now much less significant and relatively unaffected by $z_f$ (here fixed at 10) and $q_o$. However the predicted slope is not a power law having a lower mean slope than observed, and clearly a greater excess is also required. Note the effect on the counts is greatest for $\mu = 0.5$, and the cases of $\mu = 0.3$ and 0.7 are very similar. In the case of $\mu > 0.5$ a

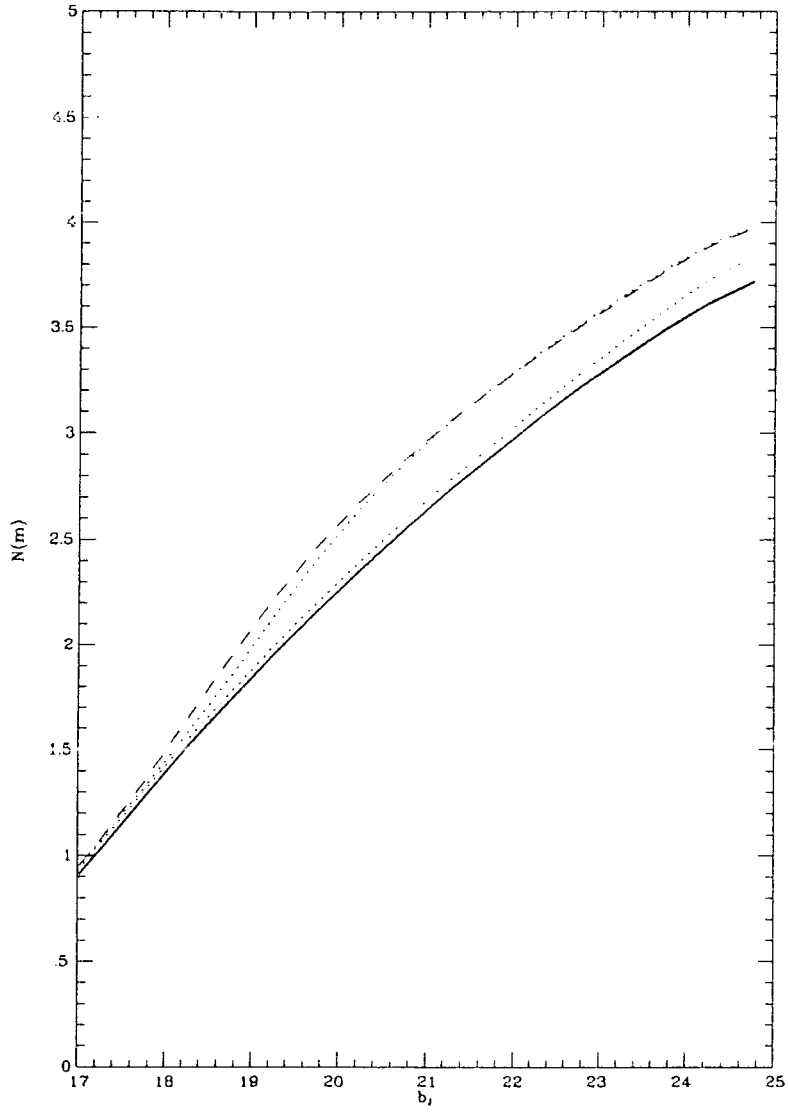


**Figure 2.9. c-model predicted counts for applied to E/S0 systems. Dashed curve refers to $H_o = 75$, and dotted curves are for $H_o = 50$ with $z_f = 5$ (upper curve) and $z_f$=20 (lower curve). Shown for comparison is the no-evolution model, heavy curve.**

higher rate of change of star formation takes place earlier and results in lower luminosities to the depths sampled by the counts than the case of $\mu = 0.5$. With $\mu < 0.5$ a lesser evolutionary effect results since the gradient of evolution is smaller; $\mu = 0$ note corresponds to a constant star formation rate with time and so has virtually no effect on the counts.

The remaining types are now included in this model to increase the excess

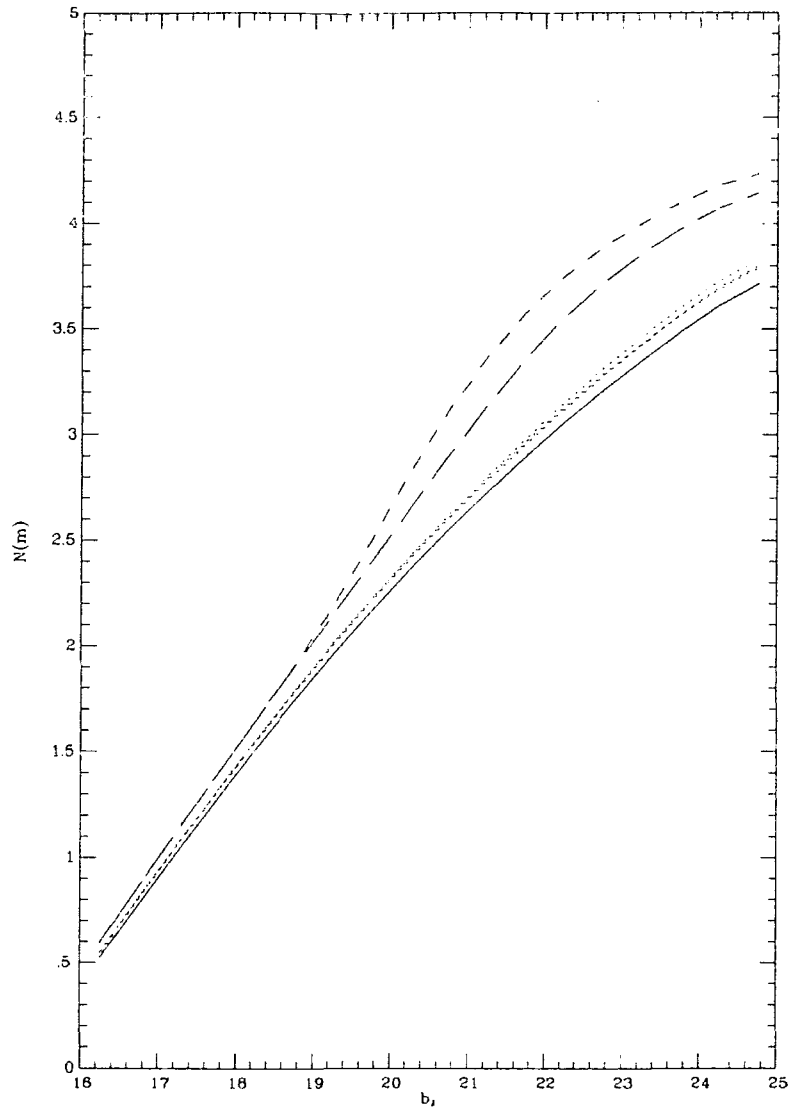


**Figure 2.10.** $\mu$ **models predictions for** $b_J$**. Solid line:no evolution model, dotted lines** $\mu = 0.5$ **model for E§0 types only** ($H_o = 50$ **(lower) and 75 (upper). Long dashed curve:** $\mu = 0.5$ **for all types, short dashed is combined** $\mu$ **model (see text for details).**

for which $\mu < 0.5$ is implied by the present colours. However, much lower $\mu$ models appropriate to later spiral types are of lesser effect. This is demonstrated in Figure 2.10 the steep $\mu = 0.5$ model applied to the earlier types, and $\mu = 0.3$ to the later types gives approximately the right excess but the count slope falls off for $b_J > 23$, also shown is $\mu = 0.5$ applied to all types, which gives too large an excess with a more pronounced turn over at $b_J > 23$. Better

fits can be achieved with a lot more 'fiddling'. Other authors have achieved a smoother predicted slope and a better fit to the counts with these models but only by incorporating asynchronous evolution, i.e. choosing a range of ages for different Hubble types (Tinsley 1980, Koo 1981). King and Ellis (1985) also achieve a reasonable fit by Mixing together the exponetially declining models with an early type 'c' model applied to spiral bulges. Importantly however, this modelling extends only to the photographic limit of $b_J \sim 23$, and beyond this such models must show a turn over in the predicted count slope since they are 'tuned' to reproduce these observations. Sustaining a monotonically rising slope is very difficult with these models but required by the deeper CCD data as discussed above.

The only reliable test of smoothly evolving luminosity evolution models, is through the redshift distribution. If the count excess results from the greater depth afforded by increases in luminosity, this will manifest itself in the distribution of redshifts sampled at a given apparent magnitude. Compared with the no-evolution expectation a redshift distribution with this form of evolution will be skewed to higher redshifts. Redshift data has long been recognised as a clear goal of deep survey work, (see Tinsley 1977 for early discussion of importance of redshift distributions) and the subject of the next chapter.

### 2.8.2 Evolution and Colours

The faint CCD colour distributions discussed earlier present a much greater challenge to the traditional luminosity evolution models than the counts. As demonstrated above little or colour evolution is indicated by the data redward of $b_J - r_F = 1.6$, to as faint at $b_J = 24$ - corresponding to redshifts of $\sim$ 0.4–0.8 (without evolution). The count excess lies instead at the blue end of the observed colour distributions, and this poses a serious problem for the models, since the significant amounts of luminosity evolution required in these traditional models to reproduce the counts are accompanied by bluer colours. Figure 2.11 shows the colour distribution for the combination $\mu$ model described above which shows a lack of objects predicted to have red colours ($b_J - r_F > 1.6$). We conclude that whatever the form of luminosity evolution applied, if large changes in star formation rates are invoked in order to explain the count excess, the predicted distribution will not extend to the red colours observed at faint magnitudes.

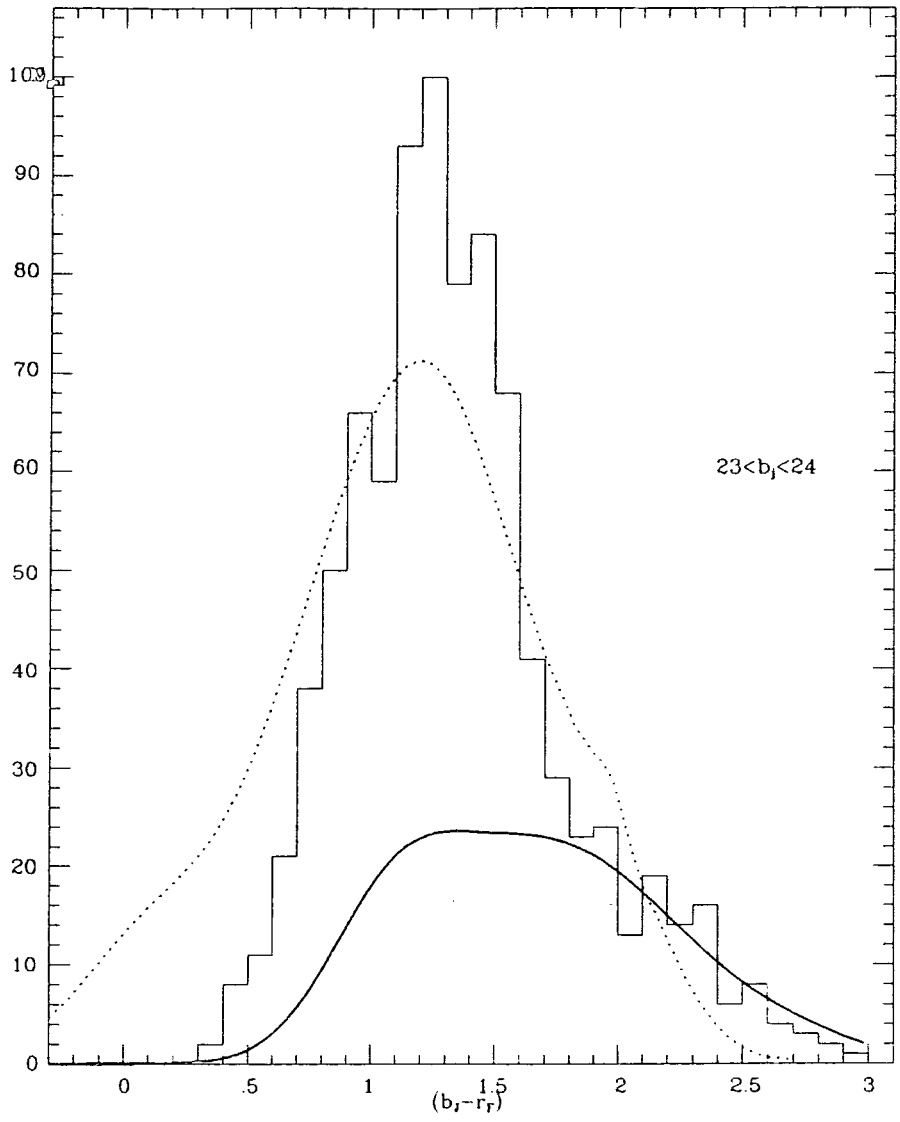


**Figure 2.11. Combined $\mu$ model prediction (normalised):dotted curve no-evolution model: solid line (data as for Figure 2.8)**

However since we must expect high star formation rates for early type systems given their present day red colours we may be forced to conclude that this early strong star formation is hidden either by dust or takes place above z$\sim$ 5, in which case no significant evolution in the colours will be observed. This of course leaves the problem of generating the count excess since as demonstrated little effect on the counts will be produced.

### 2.8.3 Dynamical Evolution

Not discussed so far is the possibility of dynamical evolution. Koo recognised (Koo 1986) that a steep increase in the number density of objects with lookback time, can be made to reproduce the counts in $b_J$. Renewed interest in the possibility of dynamical evolution has been generated by the detailed N-body simulation of White *et al* (1987) for the canonical Cold Dark Matter (CDM) cosmogony (Davis *et al* 1985). In this model, strong evolution in galaxy number density is expected to result from the effects of merging of the initial sub-galactic stellar systems, in the first few Gyrs.

In this model we may get around the problem of the hump count excess generated by late epoch of galaxy formation (a low redshift of formation is expected for CDM), since initial high rates of star formation would take place in the sub-units, and thus be of lower luminosity than for the same amount of star formation concentrated in a single conglomerate. These high redshift smaller systems could then form a substantial part of the blue galaxy excess, at magnitudes faint enough to avoid detection in primeval galaxy searches (see Baron and White 1987, Silk and Szalay 1987). The red tail would then simply represent the much lower redshift count component, formed from the subsequent merging of the systems for which no significant star forming activity remains. As we go on to show in subsequent chapters we prefer much lower redshifts for the blue excess and to $b_J < 22$ at least this process cannot be important.

More generally we can say that dynamical evolution far from producing a count excess at earlier times may help to reconcile the observed lack of evidence for any postulated *late* redshift of first star formation ($z_f < 5$). Since at a given apparent magnitude, a galaxy of given luminosity can always be subdivided such that the resulting parts are of low enough luminosity to fall beneath the detection threshold. In this way, by invoking suitable dynamical evolution, a feature in the counts due to a late epoch of first star formation can be avoided.

### 2.8.4 Summary

The conventional explanation for the steep slope of the blue number magnitude counts is that at least some subset of the galaxies were more luminous in the past. This can be understood via one of two pictures. Either main sequence brightening occurs in passively evolving systems, such as in Bruzual's

(1983) c-models. Here the detectability of such evolution depends critically on the value for $z_f$, becoming harder for early formation eras. Alternatively, star formation may be extended in duration but gradually declining with time (Bruzual's $\mu$ models) and although the evolution seen has a similar origin, the amount expected depends on the form of the star formation history.

Clearly the precise way in which evolution is modelled affects any $N(m)$ prediction. The c-models with strong initial bursts at a fixed epoch of formation, $z_f$, and no subsequent star formation at later times, produce *humps* in the number counts. If $z_f$ is low ($< 5$), these humps would lie within the observable range and as such this model is difficult to reconcile with the uniform slope of the counts to very faint magnitudes. If the hump is shifted outside the observable magnitude range by making $z_f$ large, then the c-models produce no significant excess of galaxies at intermediate magnitudes. (This is in contrast to the situation in early type galaxies at very high redshift, where the passive evolution associated with the c-models *does* differ from the no-evolution case). In short, c-models with a single epoch of galaxy formation applying to *all* galaxies can be ruled out by the counts alone without significant extinction or dynamical evolution.

It is possible to do better with $\mu$ models although a turn over in the predicted counts at $b_J < 23$ is a feature of these models, clearly however there is a wider scope for the form of smoothly evolving star formation histories than explored here. Of great interest is apparent the lack of colour evolution at the red end of the observed colour distribution at faint magnitudes, this is not expected since, significant colour evolution with this form of star formation results from the relatively large changes in star formation rates appropriate to present day E/S0 and early type spirals.

## 2.9 Count Models and Dwarf Galaxies

The luminosity function, determined from bright field galaxy surveys, is poorly constrained at magnitudes fainter than $M_{b_J} = -17$ (Efstathiou *et al* 1988, Phillipps & Shanks, 1987) because the volumes available for sampling intrinsically faint galaxies in surveys such as DARS - limited at $b_J = 17$ - are small and may not contain representative numbers. A larger than expected contribution from such galaxies might explain both the steep count slope and the absence of a high redshift tail. The steep slope arises naturally because,

by virtue of its proximity, such a population would not be subject to redshift dimming and would maintain a Euclidean $10^{0.6m}$ slope to faint magnitudes.

The changes in the space density of sub-luminous galaxies required to fit the counts are very large. We find, for example, that if we invoke a new late-type dwarf population whose luminosity function has a standard form ($\alpha$ = -1.25) but with a characteristic magnitude, $M^*_J$ = -17.0, i.e. 4 magnitudes fainter than that of the standard mix, the space density of these galaxies must be 20 times that of the entire bright galaxy population in order to reproduce the observed count slope in the range $20 < b_J < 24$. Such a model, whilst extreme, is not significantly ruled out by the observed number of dwarf galaxies sampled in the brighter DARS survey.

The addition of a dwarf population does then provide a viable alternative no-evolution model and whilst one might argue about the precise way in which any dwarf population is incorporated, it is clear that any additional population of local objects invoked to constitute the count excess and if of later types, may help understand the blue colours of the excess. This model is very easily tested with faint redshift information since there should appear a large low redshift component in the distribution of redshifts for $b_J > 20$.

## 2.10 Conclusions

We have constructed and carefully tested galaxy number count models which we conclude are accurate descriptions of the local galaxy populations. These models are based on $b_J$ photometry and are ideal for comparison with the deep counts, which are mostly observed in the same passband.

We have compared the predictions of a range of different models with available deep field galaxy photometry and conclude the following,

i) The counts in $b_J$ show a count excess which rises rapidly with increasing apparent magnitude against the no-evolution prediction. The faint colour distributions of Metcalfe *et al* show this excess to be blue, restricted to $b_J$-$r_F < 1.6$. 'c' type models with a late epoch of star formation are not supported by the form of the counts since a hump-like excess is expected unlike the power law behaviour observed.

ii) A red tail to the faint colour distribution is observed which shows a remarkable consistency with the no-evolution expectation, indicating very directly that little or no evolution of redder systems has taken place. This

result favours a model in which the star formation in early type systems ceased at very early times so that colour evolution is then minimal. In this case a high redshift of first star formation ($z > 5$) or some form of dynamical evolution may be required. This lack of colour evolution argues strongly against earlier interpretation of the count excess in terms of traditional luminosity evolution models which favour more continuous star formation histories, but for which significant colour evolution of early type galaxies is required.

iii) The above conclusions are supported in $r_F$; the excess to the faint $r_F$ limit is fractionally smaller and shows an excess over the no-evolution model only for colours blueward of $b_J - r_F \sim 1.6$.

iv) Non-evolving non-standard models are allowed by the present uncertainty in the faint end of the galaxy luminosity function, these models are rather ad-hoc and require a large population of low luminosity systems to lie just beneath the present limits on the local faint end luminosity function.

These conclusions span a wide range of possibilities for the interpretation of the excess faint count. Convincing tests await observations of the redshift distribution of apparent magnitude limited samples for $b_J > 20$. Luminosity evolution if it is to be significant in accounting for the count excess will show a clear trend to higher mean redshifts with respect to the no-evolution model, and in the case of a large low luminosity population a large low redshift excess would be found.

The remaining chapters are devoted to the study of faint galaxy redshift and spectral data, which together with the photometric data described here imply a very different model from those discussed above.

# Chapter 3.

# THE DURHAM/AAT FAINT GALAXY SAMPLE.

## 3.1 Introduction.

The discussion of count models in Chapter 2 has pointed to the need to obtain redshifts for faint magnitude limited samples of galaxies. In particular redshift surveys selected in the B, are identified as essential data for understanding the count excess observed in this passband.

By $b_J = 21$ the counts are at least 30% in excess of our standard no-evolution model and reliable redshifts may be obtained to this depth with the FOCAP fibre system on the Anglo-Australian telescope (AAT).

## 3.2 Selection of Redshift Survey Galaxies.

Multi-object spectroscopy must be employed in order to minimise demands on telescope time and so selection of objects is made within a magnitude-limited *slice* rather than all galaxies brighter than some limit, this allows one to sample the maximum number of redshifts near the faint limit of the survey where the count excess is greatest. Practicalities of observing time and instrumentation led us to adopt a magnitude range of $20 < b_J < 21.5$, as a reasonable compromise between the desire to go as faint as possible yet gather a large enough sample of galaxies; from previous local redshift surveys $\sim$ Few $\times 10^2$ objects has been found to give reasonable information on the present day galaxy luminosity function (Efstathiou *et al* 1988).

Previous high redshift cluster studies ($z\sim 0.3$) show satisfactory spectra for line identification can be obtained to $b_J = 21.5$ on the AAT at 4 Å resolution using the Image Photon Counting System (IPCS) in under a night's exposure (see Sharples *et al* 1985), to obtain a similar signal to noise (S/N) we initially adopted $\sim 25,000s$ as a reasonable expectation of the exposure time required for each sample of galaxies comprising a faint field survey.

The field centres for the survey were chosen randomly from a variety of high latitude deep areas available to the Durham group in its various photometric programmes according to the scheduling of the spectroscopic telescope time. In each of 5 fields, galaxies were selected on the basis of apparent magnitude and

non-stellar profile from measuring machine scans of the photographic material. The procedures for galaxy photometry and star/galaxy separation have been discussed at length in the early Durham number count papers, Peterson *et al*, 1979, Shanks *et al* 1984), but we briefly summarise the techniques here.

For three fields, prime focus $b_J$ AAT plates were available and photometry was possible to an isophote of 1 - 2% of the night sky brightness, typically a surface brightness of $\mu = 26$ $b_J$ magnitudes arcsec$^{-2}$. Galaxies in these fields were selected from 10 - 20 by 20 arcmin areas in the magnitude range $20.5 < b_J < 21.5$. Two additional Schmidt fields were photometered in the slightly brighter range $20.0 < b_J < 21.0$. Although the isophote was somewhat brighter, 25 $b_J$ magnitudes arcsec$^{-2}$, detailed work (Shanks *et al*) has shown the magnitudes at these limits are not seriously affected by small changes in the limiting isophote. In each field, the photometric calibration is based on CCD photometry of stars and galaxies taken under good conditions (see above references).

Star/galaxy separation may be confidently achieved at these magnitudes applying algorithms defined in the earlier Durham papers, but each spectroscopic target was visually checked and a small number of misclassifications, merged objects and plate defects were rejected. We chose not to determine how many (if any) of the objects with stellar profiles might be compact galaxies. To do this would have doubled the spectroscopic time required since *all* stellar objects would have to be surveyed as well; furthermore, from the spectroscopic survey of Morton *et al* (1985) to B = 20, there seems no indication that an extragalactic population is hiding in the stellar component (apart from QSOs and the associated narrow lined objects commonly found with the UVX technique however these have low sky density to $b_J = 21$ they represent less than 1% of the total number of images identified as galaxies to this limit (Boyle 1986).

Finally, since our multiple-object technique cannot accept object pairs closer than 18 arcsec, in a small number of close pairs only one object was chosen. These manual deletions to the otherwise machine-generated catalogue affected at most 5% of the sample. The precise field areas and sample sizes are given in Table 3.1 along with the name of each field, to which we will refer to from now on. Note the differences in sampling rate and field area reflect the large count variance discussed in Chapter 2.6.1 and Chapter 6.8. For example

both the SGP and the 197 fields are sampled fully and cover the magnitude range but the 197 field covers twice the area of the SGP field, with half the number of available targets.

Table 3.1 Survey setup parameters and field properties.

| R.A. | Dec | Field | Magnitude Limits ($b_J$) | Field Area | Exposure Time | Sampling Rate | Completeness | $\Delta\bar{z}$ |
|---|---|---|---|---|---|---|---|---|
| 005436 | -275450 | SGP | 20.5–21.5 | 22.8′ × 9.5′ | 29,300s | 1/1 | 59/70 | .225 |
| 015930 | -495959 | 197 | 20.5–21.5 | 20.0′ × 20.0′ | 25,800s | 1/1 | 31/38 | .249 |
| 220303 | -185442 | MT | 20.5–21.35 | 20.0′ × 20.0′ | 13,500s | 1/2 | 30/35 | .235 |
| 205556 | -252554 | 529 | 20.0–21.0 | 24.6′ × 11.2′ | 22,500s | 1/3 | 35/41 | .209 |
| 035458 | -310237 | 419 | 20.0–21.0 | 22.4′ × 22.4′ | 16,000s | 1/3 | 32/36 | .193 |

Altogether a total of 230 galaxies were chosen in the magnitude range $20< b_J <21.5$ from the 5 fields. The sampling rates vary from field to field due to the number available in the required magnitude range. The catalogue of spectroscopic targets is a strictly apparent magnitude limited.

## 3.3 Observations

Spectroscopic observations were made using the *FOCAP* fibre-optic multi-object coupler at the AAT (see Gray 1986, Ellis and Parry 1987 for technical details). At the AAT Cassegrain focus, 50 fibres of diameter 2.6 arcsec were fed to the RGO spectrograph equipped with a 66 Å /mm grating and the IPCS as a detector. For 3 of a total of 5 runs a further 50 fibres were also fed to the low dispersion Faint Object Red Spectrograph (FORS), a fixed format high throughput collimatorless spectrograph with a GEC CCD detector inside an evacuated Schmidt camera. In each case 6 of the 50 fibres were dedicated to recording sky spectra; the sky positions were determined from the absence of objects to $b_J = 24.5$ on the prime focus plates and to $b_J = 22$ on the Schmidt plates.

The IPCS data cover the wavelength range 3850 - 6100 Å at 4 Å resolution and the FORS data 5000 - 10,000 Å at 15 Å resolution. The bulk of the redshifts were measured using the IPCS data where the targets were strictly controlled according to the magnitude limit. The FORS data is of such low resolution that only strong features can be seen and for that reason, the FORS

galaxy samples were not so carefully selected. To begin with, the FORS samples were simply a different random subset of the $b_J$-selected catalogue, but as IPCS redshifts became available through on-line data reduction, we transferred some of the successful IPCS targets to FORS for confirmatory exposures.

The wavelength range used for the IPCS observations 3850 - 6050 Å samples the distinctive spectral features, [OII] 3727 Å and Ca II H and K 3933, 3968 Å over the interval $0 < z < 0.6$, ideal for examining most models likely to explain the number counts. Although FORS did not generate a large redshift list, the additional wavelength coverage does allow us to constrain the possibility that a number of high redshift ($z > 0.6$) galaxies may be present in the samples (see later).

Long exposures of 15000 to 30000s were made on each field according to the magnitude limit and observing conditions (see Table 3.1). Blank sky offset and calibration lamp exposures were taken at intervals of 3000 sec, the former to measure hour angle variations in the fibre-fibre response. Spectrophotometric standards were taken through individual fibres and relative spectrophotometry is discussed in §6).

These observing techniques are now well established for faint spectroscopy with this system and with software developed John Lucey for reducing this data (Carter and Lucey 1988) allowed rapid preliminary reductions to be carried out during runs so that decisions on objects that needed further exposure and those for which redshifts had been acquired already could be made easily, this allowed for higher redshift completeness and a larger overall data set, thus maximising the available observing time.

Note from a total of 10 nights of dark time allocated to the project during August and November 1985 and August 1986, only 6 were clear.

## 3.4 Data Reduction

Within the magnitude range of the survey the typical ratio of object count/sky is 0.1-0.25 and hence careful sky subtraction is essential. The method of sky subtraction and fibre transmission calibration for this setup is well-established (Sharples *et al* 1985, Ellis and Parry 1987). Briefly, the reduction of IPCS data requires corrections for 2D 'S' distortion of the spectra, introduced by the detector. Each spectrum recor ded is 'followed' both spatially and in

wavelength, and the success of the fit checked visually allowing adjustments to the order of polynomial fit and centroiding if necessary. Once the set of spectra comprising one exposure has been successfully followed in this way the spatial sections making up an individual spectrum are collapsed resulting in spectra which are one dimensional only. The spectra comprising each object set, arc lamp and offset sky exposures were extracted in this way.

Linear wavelength calibration (scrunching) was carried out using the FIGARO software. This requires first the identification of known arc features in the arc spectra taken between object exposures. In general, 20 or so spectral lines are identified and their wavelengths are used to construct a polynomial for calibration. This is then applied to each set of object and arc extracted spectra produced above resulting by applying a 2D linear calibration of the arc spectra to the object spectrum. The accuracy of the calibration for individual spectra comprising the 2D arc exposure is typically 0.15Årms or 0.05pixels, i.e. much smaller than the resolution of the spectrograph (4Å). Fibres with anomalously low transmission or spectra suffering the largest 'S' distortion (those objects at the ends of slit) fare a little worse $\sim$ 0.3Å, but by interpolation of the calibration along the slit, from object to object the calibration of poor fibres can be improved.

The object, arc and offset sky exposures are reduced in this way and the final output comprises a 3D data set of multiple exposures of individual objects which are recorded as one of fifty spectra on each 2D exposure, these are the survey objects and blank sky recordings. Sandwiched between are the offset sky exposures which are used to evaluate relative fibre transmission. An individual object may be recorded over many nights at different positions along the slit and through different fibres, these positions are recorded and the entire set of observations may be reduced to the final sky subtracted object spectra in one further set of transformations using software developed by the author. In this process sky subtraction was carried out for the IPCS data with run weighting, following the method described by Robertson (1986) and was applied to the IPCS data. This allows for variations in object/sky count resulting from changes in observing conditions, zenith distance field guiding accuracy and idiosyncrasies of the fibre system (see below). The optimal method of run weighting for the IPCS data is straightforward in the case of detectors without

readout noise, and is given by,

$$I_{\mathrm{tot}_j} = \frac{1}{\sum_{i=1}^{n_r} W_i} \sum_{i=1}^{n_r} W_i I_{ij}$$

where,

$$W_i = \sum_j \frac{I_{\mathrm{obj}_j}}{I_{\mathrm{obj}_j} + I_{\mathrm{sky}_j}}$$

i, denotes run number and j, spectral element, $W_i$, are the run weights and $I_{\mathrm{tot}_j}$, is $j^{th}$ element of the resulting coadded spectrum which are calculated here using the entire spectrum, excluding only the very ends where sky subtraction is unreliable so that, $\lambda_0 = 4000\mathring{A}$ and $\lambda_f = 5800\mathring{A}$. Note that estimation of run weights as a function of wavelength is more desirable but for the low count levels obtained per run this cannot be defined with enough precision.

Figure 3.1, demonstrates the importance of run weighting for a sample of spectra from a number of 1500s exposures, these objects are both faint and show object-to-sky ratios which vary considerably from run to run, the resulting spectra are displayed for both objects with and without run weighting, note that for object 1 weighting proves crucial to the identification of a redshift.

## 3.5 Sky Subtraction Precision

One of the limitations of fibres with FORS arises from the fact that the sky spectrum is highly structured, thus a 1 % sky subtraction precision is still inadequate for absorption line work when the features overlap the night sky OH emission bands. Together with the lower spectral resolution and slight undersampling, this explains the poor success rate of the red FORS data. Figure 3.2 shows the effect of the night sky emission lines on restricting redshift survey work in the near infrared, smooth sky background below 6500Å contrasts with the bright and irregular features at larger wavelengths.

An important question to address is the precision to which sky subtraction can be achieved with fibre optic couplers. The sky spectrum is recorded using 6 fibres spaced evenly along the entrance slit of the spectrograph. The combined sky spectrum for each field run when subtracted from the individual sky fibres thus gives an indication of the sky subtraction precision achieved. The nightly *rms* residual is only 1.2 % of sky and only marginally above the photon noise

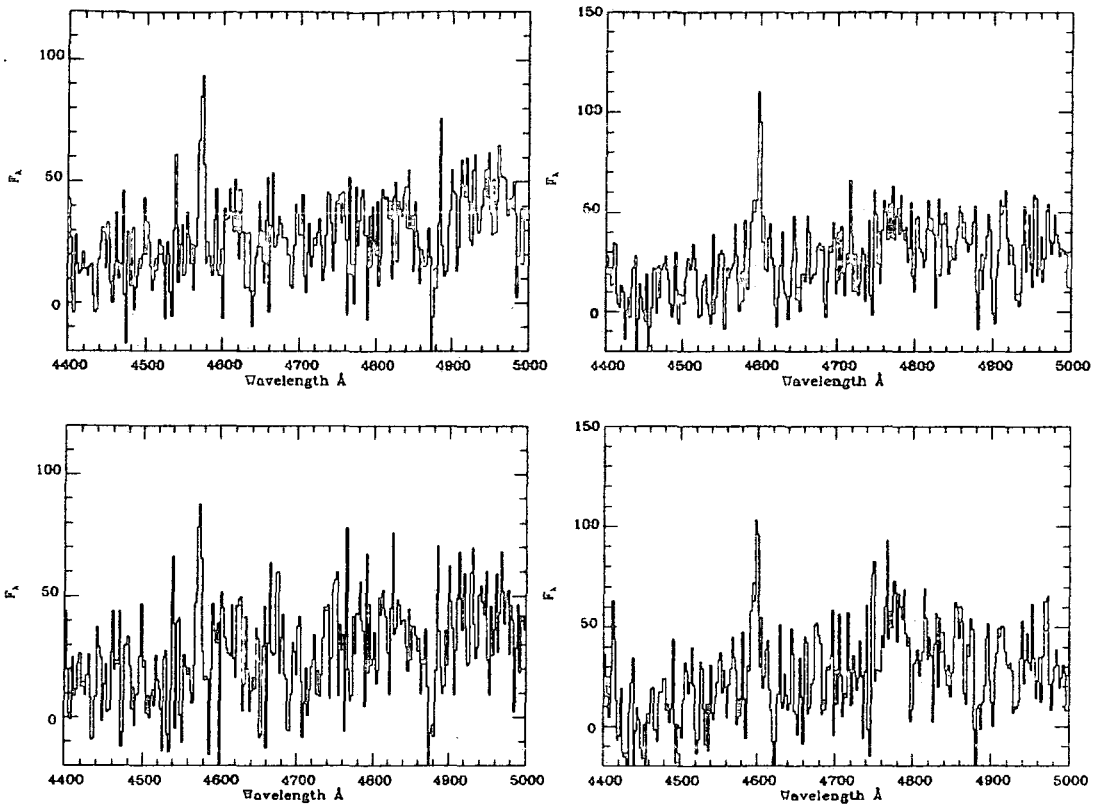


**Figure 3.1** Spectra with (top) and without (bottom) run weighting, note improvement in signal to noise by run weighting.

expectation. Figure 3.3 shows that there is no trend in the sky residual with fibre number, an observation of crucial importance for the measurement of spectral features and equivalent widths (see Chapter 4 for full discussion).

## 3.6 Redshift Determination and Measurement

Once sky subtracted and flux calibrated, redshifts were measured by line fitting techniques for the emission line spectra and via cross-correlation with co-added nearby and intermediate redshift cluster galaxy templates. A template constructed of 12 post-star-burst galaxies identified in AC103 proved to be very useful for corroborating emission line redshifts where Balmer absorption features are present. This template and a red galaxy template also constructed from the AC103 cluster extends in wavelength into the restframe near-UV, allowing a greater wavelength matching of the survey galaxies than for the standard low redshift velocity templates.

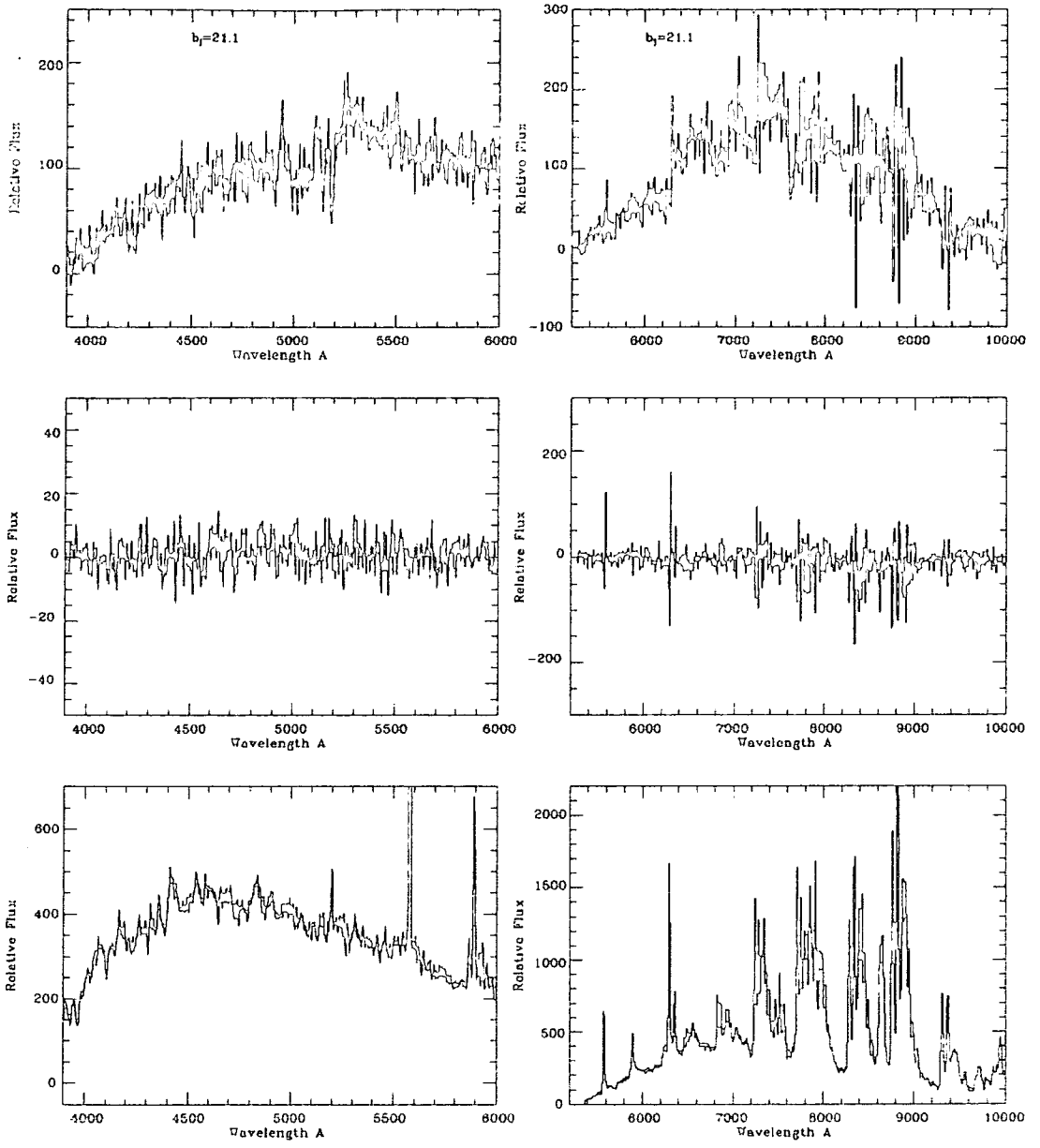


**Figure 3.2** Comparison of sky subtraction with IPCS (left column) and FORS (right column). Bottom compares sky spectra (note fierce emission line bands in FORS spectrum) center and top show sky subtraction from sky and object spectra respectively, note the large residuals above 7000Åin the FORS spectrum.

The range in spectral type of objects observed covers galaxies with both identifiable emission and absorption features and those for which only emission or absorption lines are visible. In a small number of cases, $< 15\%$, the quality of the spectrum is such that only one emission feature is visible. The

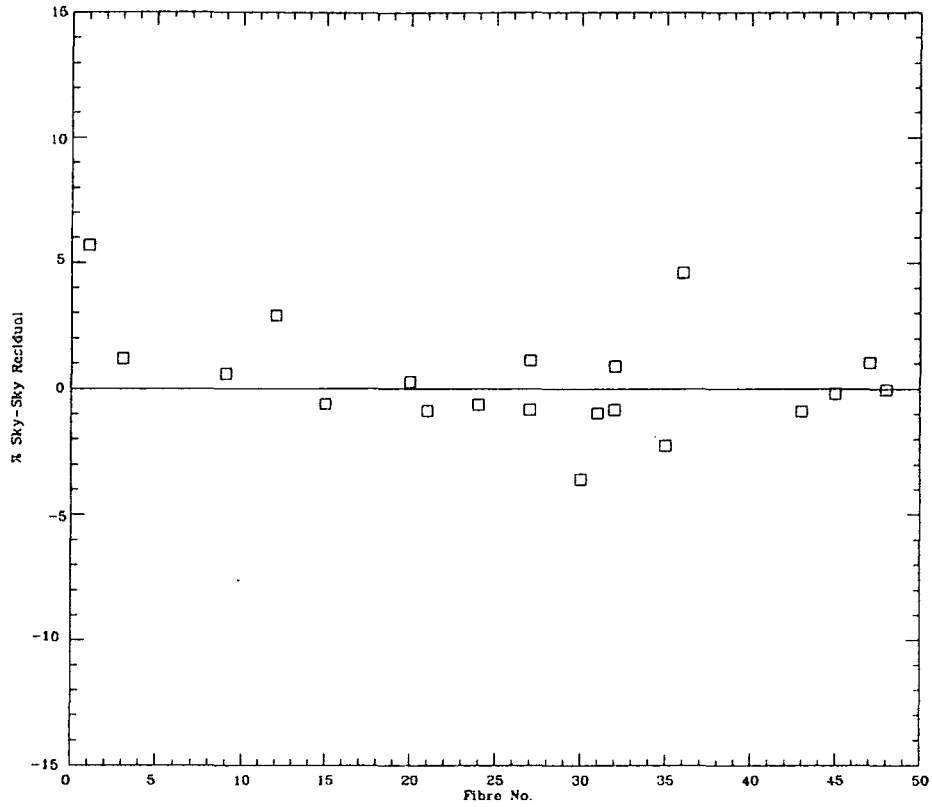


**Figure 3.3** Sky-sky residual totalled along each sky dedicated spectrum for 1 nights exposure, as a function of fibre number.

identification of this line is taken in all these cases to be [OII]3727Å. This is a safe procedure if the line lies below the restframe wavelength of $H\beta$ at 4861Å, since no other line is so prominent in ordinary galaxy spectra.

The majority of galaxies (75%) have both an emission and absorption line redshift which makes the redshift unambiguous. Smaller fractions of the total sample are identified from emission and absorption lines only. The absorption line redshifts are identified from the Calcium H and K pair at 3968,3963Å respectively, this double feature is easily identified in early type spectra, and is in any case often supported by the presence of the G band feature at 4304Å. Objects with visible emission lines comprise 85% of the total sample and of these 40% have more than 1 emission line feature making their redshifts secure, and 80% have a confirming absorption line redshift.

In cases of only one emission line, the redshift ambiguity can be examined

by coadding sets of spectra to look for confirmatory features. Figure 3.4 shows 2 spectra constructed by coadding 5 single emission line only objects for which the line lies at wavelengths greater than restframe $H\beta$, in the first case we obtain redshifts assuming $H\beta$ and secondly assuming the line is [OII]3727Å. Spectrum 2 reveals the high order Balmer absorption features as expected if the spectral feature is indeed [OII]3727Å, and for spectrum 1 no tendency to bring out the [OIII]4959,5007Å doublet is found, indicating that the emission line is correctly identified as [OII]3727Å and do not form a redshift distribution which is discontinuous with the majority of objects as would otherwise be the case.

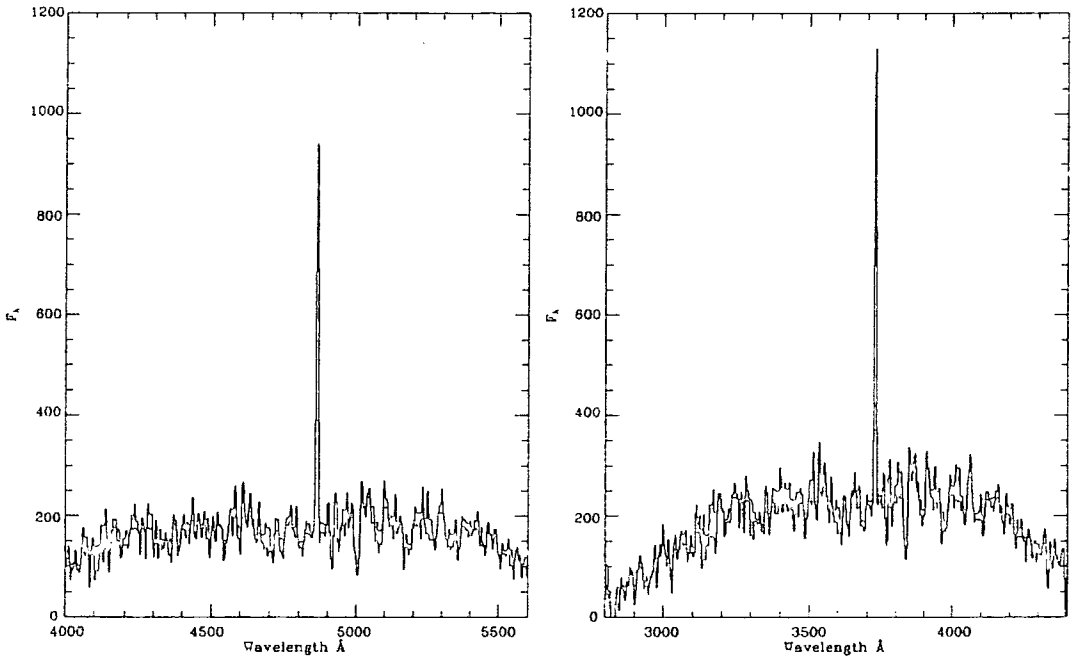


**Figure 3.4** Left panel; Restframe coadded spectrum assuming emission feature is $H\beta$4861Å. Right panel; same, assuming emission feature is [OII]3727Å, note appearance of higher order balmer series in the range 3700Å-4000Å.

Note these Balmer absorption features in these strong single lined objects are weak features because of infilling by HII recombination emission lines, (see Chapter 4) and it is not surprising that the S/N of this work does not bring these features out in individual spectra.

An estimate of the redshift accuracy can be made by comparing emission and absorption line redshifts for those objects with both measurements. Figure 3.5 shows this comparison as a function of the cross correlation parameter r (see Tonry and Davis 1978, for definition). The variance is very small, $135 kms^{-1}$ (1 channel), and is constant with r indicating no important systematic effects with the suitability of the template to the object spectrum; lower r values and systematic velocity errors may result from both poorer S/N and/or object-template mismatching.

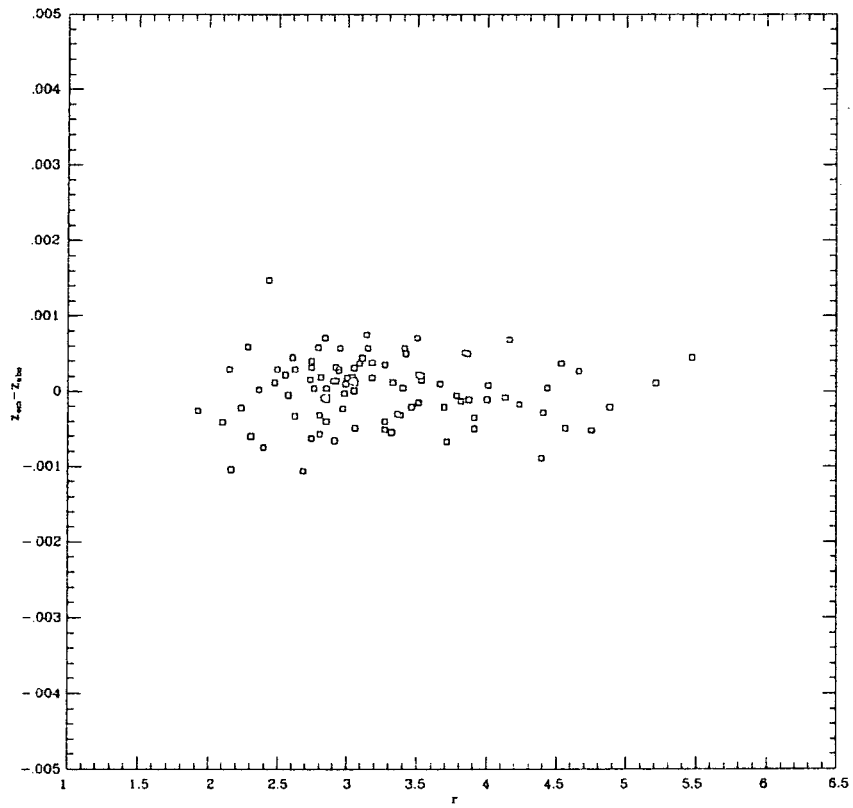


**Figure 3.5** Internal velocity errors from emission and absorption line redshift difference as a function of the cross-correlation parameter, r,

## 3.7 Drawbacks of the Fibre System

The FOCAP system, although remarkable in its ability to permit new areas of study, has a number of weaknesses which limit the scope of faint spectroscopy.

The main problem, in terms of our ability to obtain redshift completeness, is the large variation in sensitivity of the spectrograph along the slit. This is a spectrograph design problem and produces as much a 40% vignetting at the edges of the slit (low and high fibre numbers) relative to the center. Since no preference for apparent magnitude of a galaxy was made when positioning objects along the slit for observation, vignetting has the effect of producing the poorest spectra for faint objects observed at the ends of the slit. This is the principle reason why our data is not fully complete and the result of this effect is to produce a weak trend of incompleteness with apparent magnitude. Note also that there are a number of fibres in each bundle which have low response as a result of end damage, and this exaggerates further the above trend of incompleteness with apparent magnitude.

Two further problems exist in producing quality data at low object to sky ratios for this system. Firstly a background of scattered light is present across the detector producing as much as 15% of the sky count in the center of the detector and falling to lower levels on all sides. Since sky subtraction done by subtracting off the sum of these spectra then the effect of a varying scattered light to true sky background along of this form is to produce a trend such that the subtraction is rather too large at at the ends of the slit and underestimated in the center. However this background is vignetted like the unscattered data and neatly cancels for fibres midway between the slit ends and the center, leaving sky residual of $\sim 1\%$ with a small trend to larger residuals at the slit ends and for low transmission fibres (see Figure 3.3).

Large variations in object to sky count ratio are found for some objects in the sample and although run weighting will minimise the effect on the resultant spectral quality, such large variations will effect the completeness rate. The origin of this effect is most probably fibre wobble at the junction between the fibre ferrule and the aperture plate, which is clearly important in the resultant quality of a small number of objects for which the fibre may be inadequately secured during observation.

### 3.7.1 Evaluation of Completeness

Completeness is clearly an important factor in ensuring the redshift distribution, $N(z)$, is representative of the magnitude-limited sample and as outlined above a number of subtle effects make the evaluation of this a complex problem however we are fortunate that completeness in redshift achieved with the IPCS data is very high for all fields, ranging from 82 to 89 %, and for the magnitude range $20.5 < b_J < 21$, is very high at 90%. Of a total of 230 spectra acquired with the IPCS, redshifts were successfully secured for 187, and note that a few stellar spectra and spectra through defective fibres have been removed. The objects for which a redshift could *not* be assigned are those for which the observed photon count is demonstrably smaller as a result mainly of the object position on the detector which suffers from vignetting of up to 40% at the slit edge. Consequently, there is only a very weak dependence of completeness and apparent magnitude, shown in Table 3.2. This is also demonstrated in Figure 3.6 which shows the completeness versus magnitude for individual fields.

| $m_{b_j}$ | No. of fields | Completeness | $\overline{z}$ |
|---|---|---|---|
| 20.0-20.5 | 2 | 29/32 | 0.188 |
| 20.5-21.0 | 5 | 97/108 | 0.225±0.015 |
| 21.0-21.5 | 3 | 61/80 | 0.235 |

**Table 3.2** Completeness and mean redshift as a function of apparent magnitude

The importance of this result is that we can be confident that the overall reason for incompleteness is simply the low photon count and consequently we are not loosing a particular class of objects in our sample, for example a very high redshift or spectrally peculiar component.

As remarked above, the available redshift window for the frequently seen [OII] 3727 Å is $0 < z < 0.6$. However, the redshifts observed all lie below $z = 0.47$. Although our completeness varies from field to field, the mean redshift and range in redshifts are very similar. It is therefore unlikely that the objects without redshift lie beyond the observable redshift window. The spectral coverage of FORS complements that of the IPCS in this respect and we are thus able to extend the search for emission line objects to $z < 1.0$; however,

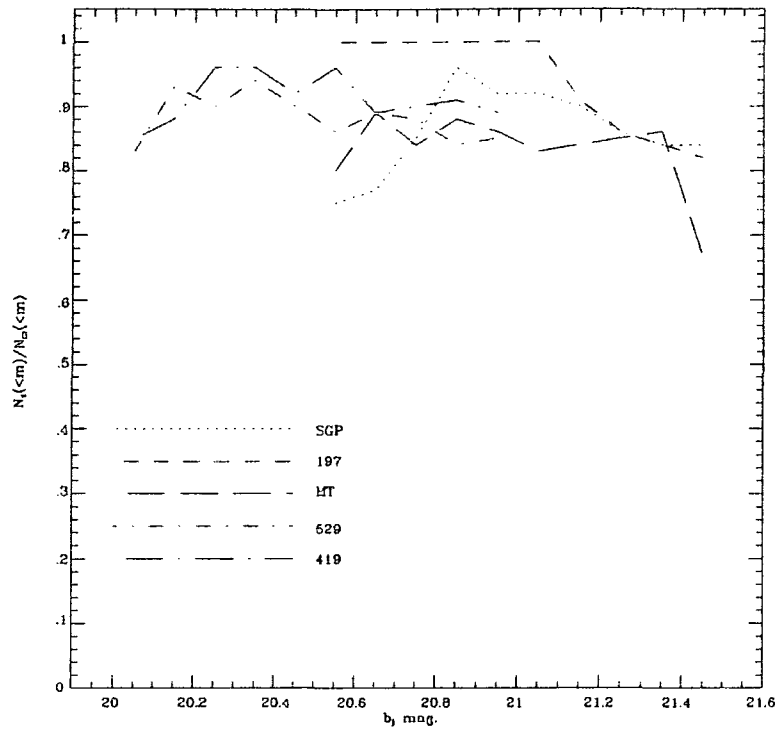


**Figure 3.6** Completeness rate for all fields as a function of apparent magnitude, completeness displayed here is defined as the total fraction of objects with successful redshifts down to the limiting apparent magnitude (ordinate).

no high redshift galaxies were found (although some confirmatory [O III] and H$\alpha$ emission in lower redshift galaxies were noted). In fact the redshift range derived from the sparse FORS data (30 galaxies) is very similar to that seen in the IPCS data. We thus conclude that the present level of completeness is sufficient for defining the redshift distribution of field galaxies in the magnitude range observed, and in any case we we restrict most of our analysis to to range 20.5-21.0 for which the incompleteness is very small; 11 failures from 108 galaxies.

## 3.8 The Catalogue

The final redshift measurements are listed in an appendix to this thesis (Appendix I). For each field we list the galaxy ID regardless of whether a redshift was eventually determined. The astrometric position in 1950.0 coordinates is

accurate to $< 0.5$ arcsec precision rms. In the case of the emission and/or absorption redshift, these are uncorrected for any local motions. The final column lists the rest-frame equivalent width, $W_\lambda$, for the [O II] 3727 Å emission line (see discussion in § 6.1). Those objects determined to be stars are included in the catalogue for completeness but are eliminated from the analysis henceforth. The columns are from left to right:

1 &2: Object position Right ascension and Declination, these are accurate to less than 1 second of arc.

3 : Apparent magnitude in the $b_j$ system and accurate to $0.^m15$

4 &5 Emission and absorption line redshifts (see above for discussion of accuracy)

6 : r factor, strength of absorption line cross correlation.

7 : Equivalent width of [OII]3727Åemission line, (see Chapter 4).

In Appendix II we show all the IPCS spectra of the galaxies which comprise the survey, in order of their entry identification number in the redshift catalogue (column 1). A small sample are shown here in Figure 3.7, to illustrate the range in spectral types with redshift.

## 3.9 Results.

In this section the redshift data are combined to form a redshift distribution, N(z), and comparison of this observed redshift distribution is made with the predictions of the models discussed in Chapter 2. These predictions are for magnitude limited data and thus it is necessary to weight model redshift distributions according to the relative fractions of the data which are sampled between magnitude limits chosen for each field, these are detailed in Table 3.1.

### 3.9.1 The Observed Redshift Distribution

The redshift distribution presented in Figure 3.8 is coadded from all survey fields and weighted by the inverse ratio of the number of galaxies observed per field to the average of all fields, this ensures the resultant distribution is not biassed by the clustering of individual fields and must be more representative of the true redshift distribution. Note that typical velocity errors on individual redshift measurements are very small ($\delta z/z = 10^{-4}$ see Figure 3.5) at the

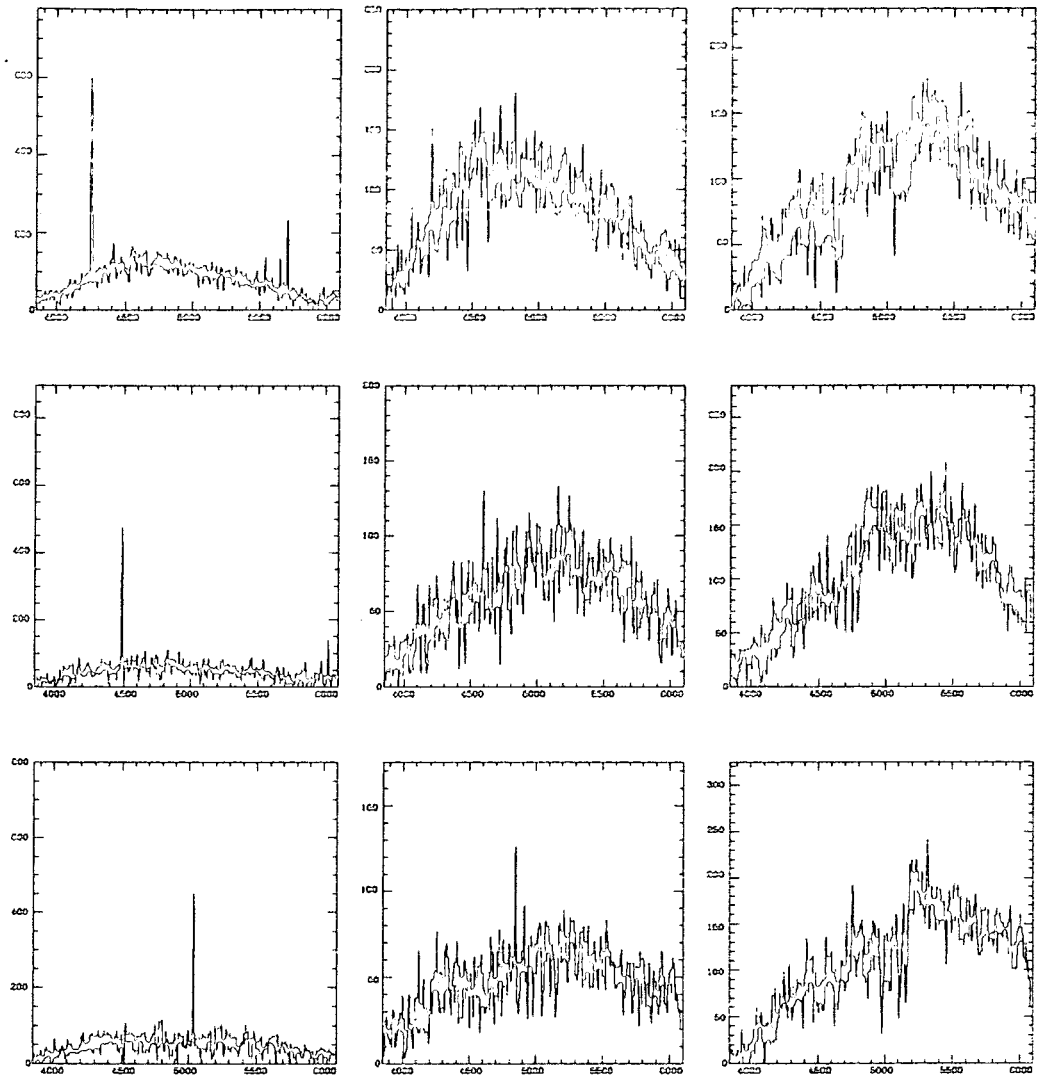

**Figure 3.7** Spectral types covered by data; redshift range increases from top to bottom of each column (inset top right), and spectral types range from emission line only (lefthand column), emission and absorption (center column) and absorption line only (righthand column).Line identifications are indicated.

resolution of this work and so do not affect the gross properties of the distribution considered here.

This distribution is relatively smooth, as expected for a well-defined selection function based on a galaxy luminosity function which is not discontinuous. However, the distribution within each field shows obvious clustering in redshift space and considerable variation in structure is apparent from field to field (see

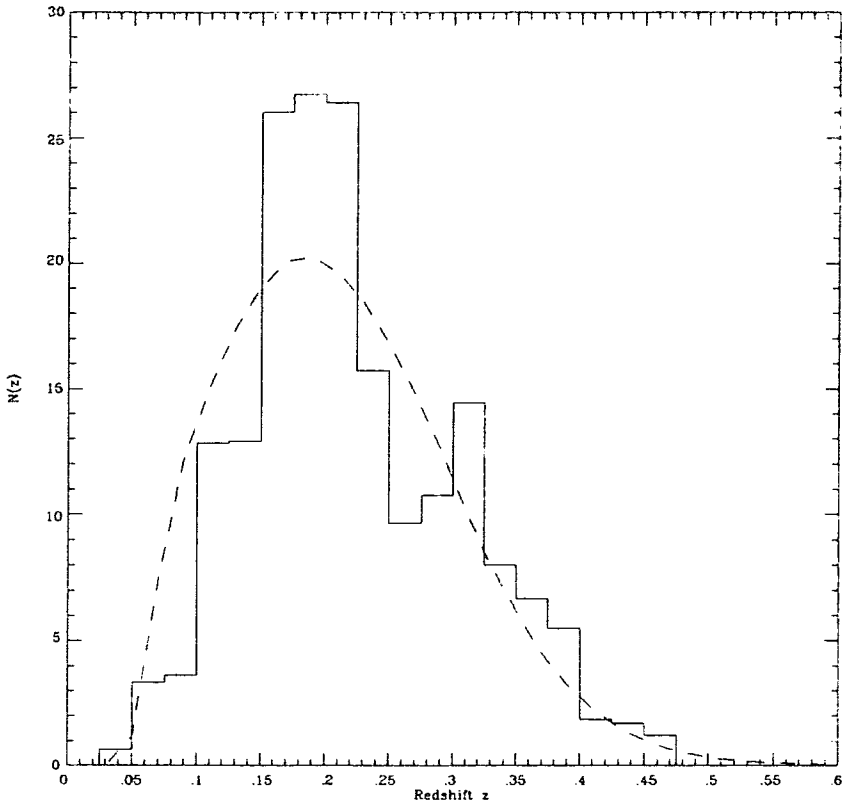


**Figure 3.8** Resultant field number weighted observed redshift distribution (histogrammed in bins of $\Delta z = 0.025$ compared with the normalised No-evolution expectation.

Chapter 6) and this emphasises the importance of sampling many independent fields; the true redshift distribution is clearly better estimated from small samples drawn from a number of fields rather that concentrating the data in only one field.

Table 3.1 shows the mean redshift for each field note that fields with matched magnitude limits have similar means. This may be expected since, as is evident from the coadded distribution, the majority of objects are most readily sampled in a rather narrow redshift range which is symmetric about the mean, and so to first order the mean is not very sensitive to the fluctuations in the redshift distribution caused by galaxy clustering. Conversely the number of galaxies sampled per field from a narrow distribution is sensitive to the clustering and this is apparent from a comparison of the extreme fields SGP and 197; these fields have high and low counts with respect to the mean for

$b_J > 20$ and the differences in clustering at redshifts $z = 0.2$ may be responsible for their anomalous counts over the full magnitude range available on these plates.

The relationship between count variance, clustering and the selection function are discussed further in Chapter 6.

Note that the majority of objects sampled at $z \sim 0.2$ which corresponds to $M^*$ of the Schecter function, this is a natural feature of a magnitude limited sample, resulting from the combination of the form of the luminosity function and the volume sampled. The volume increases rapidly with increasing redshift but the luminosity function falls off steeply at luminosities greater than the break in the luminosity function $< M^*$, this produces a fall off in the redshift distribution at $z > 0.3$ for the apparent magnitude limits of this sample. Conversely at low redshifts, $z < 0.1$, the volume available for sampling galaxies at luminosities below the break in the luminosity function falls off more quickly than can be compensated for by the larger space density of galaxies at lower luminosities. The net effect is that redshift distributions selected by apparent magnitude are most sensitive to objects at the break or $M^*$ of the luminosity function. This effect is further exaggerated in this data set since by z=0.2 the $k$ corrections of early and late type galaxies cancel the differences in $M^*$ between these types; an early type galaxy has a $k$ correction of 0.8 magnitudes with respect to a late type but the difference in $M^*$ is also of this amount but in the opposite sense.

## 3.10 'No-Evolution' model

When comparing model redshift distributions with data we normalise to the numbers of objects observed in the survey, both because of the uncertainty in space density referred to in Chapter 2.7, which results from the observed large count variance at bright magnitudes, and the similarly large scatter in the faint counts, from which the survey samples are derived.

The average count from the presently photometered 4m prime-focus plates and the extensive CCD data now available indicates the the averaged excess is in the range 20-50% of the no-evolution prediction at $b_J \sim 21$, if the models are normalised to the bright count as described in Chapter 2.7.

given this uncertainy we Normalise the predicted redshift distributions to

the observations for convenience. In the normalised 'No-Evolution' model good agreement is found with the observed redshift distribution. The fit to the distribution for $z > 0.3$ is of particular interest since here the effect of pure luminosity evolution should be strongest (see below), but the agreement with the standard 'No-evolution' model indicates directly that little if any evolution of the bright end of the luminosity function can have taken place to $z < 0.5$.

This result is very surprising because, as emphasised in Chapter 2.3 the 'No-evolution' model fails to account for the $N(m)$ count slope in the range 20 $< b_J <$ 24, and yet, as we show later the width of the field galaxy luminosity function implies that a spectroscopic survey to $b_j = 21.5$ contains valuable information on the origin of the steep count slope to much fainter magnitudes; for example the luminosity function at z=0.35 is observed at $b_J = 21.5$ in this sample, corresponds to a faint absolute magnitude of $M_{b_J} = -21.5$ for galaxies of average type Sbc, and if we could sample the luminosity function only 1.5 magnitudes fainter at this redshift i.e.to $M_{b_J} = -20$ this would take us to $b_J = 23$ where we know that the count excess is much higher, a factor 3-5, and yet *no evolution of the bright end of luminosity function is found at this redshift.*

It seems inconceivable, given the discussion above and in Chapter 2.3, that any no evolution model could be adjusted to meet this challenge: the count slope in $b_J$ from our no-evolution model is $\gamma = 0.34 \pm 0.02$ at the depth of this survey, and we conclude the evolution present in the redshift data *lies in the same redshift range as those objects represented in the local field survey.*

To check that the survey is sufficiently large to provide a well-determined redshift distribution, listed in Table 3.2 are the mean redshift, $\overline{z}$, for 3 successive magnitude intervals of width $0^m5$. The trend found between $\overline{z}$ and the increasing apparent magnitude interval is well-behaved. Whilst the actual mean value at a given magnitude is clearly model dependent, the derivative is less so, an increase in mean redshift with increasing apparent magnitude is predicted for all models considered in Chapter 2, non-evolving or evolving.

Furthermore, the error estimate, derived from the field-to-field scatter in $\overline{z}$, for the interval $20.5 < b_J < 21$ common to all fields (see Table 3.2), gives a confident indication of the representative nature of the redshift distributions observed, for this magnitude range the mean and the error on the mean are

found to be $\overline{z} = 0.22 \pm 0.015$.

## 3.11 Luminosity Evolution

Here we reconsider the effects of luminosity evolution, however it is clear at the outset from the above discussion of the redshift distribution that luminosity evolution in the context of Bruzual's models cannot have been significant for bright galaxies.

As demonstrated in Chapter 2.8 the precise way in which this form of evolution is modelled affects any $N(z)$ prediction that we can compare with our survey, but only if star formation rates have smoothly evolved so that they were much higher in the past for the majority of galaxies can we reasonably expect to account for the count discrepancy in $b_J$. To keep the question of what star formation history to apply and the consequences for N(z) straightforward, we quantify the fraction of the total galaxy population for which strong evolution must be applied to reproduce the steep count slope in the $b_J$ passband, and ask whether the $N(z)$ relation implied is consistent with the new observations. A $\mu = 0.5$ model reproduces well the present day spectrum of an E/S0 galaxy type (Bruzual 1983), and thus represents strong and extended evolution for which present day star formation rate which is negligible. The present day spectrum produced by a c model is very similar to a high $\mu$ model at optical wavelengths, for the same age but, as shown in Chapter 2.8 the c-model in its simplest and intended form cannot reproduce the steep count slope.

Table 3.3 compares the predictions of the $\mu = 0.5$ model with the data. The mean redshift, $\overline{z}$, for the magnitude range $20.5 < b_J < 21$ is calculated, where our data is most complete, along with the slope of the differential number magnitude counts, $\gamma$, in the magnitude range $20 < b_J < 24$.

From this comparison it is clear that it is not possible to produce a steep and single valued count slope for an evolutionary model where one subset of the galaxy population follows a Bruzual $\mu$ model. Even in the extreme case where all galaxies follow one $\mu$ model the luminosity evolution produced is large but a corresponding high redshift tail is expected in $N(z)$. A count slope marginally consistent with the data can be produced if *all* galaxies follow a 16 Gyr $\mu = 0.5$ model. Quite apart from being unphysical, given the observed range in colour for the Hubble sequence, this model is easily ruled out by the observed

| Luminosity Evolution | Types Applied | $\gamma(20 < b_J < 24)$ | $\overline{z}(20.5 < b_J < 21)$ |
|---|---|---|---|
| $\mu = .5$ model | E/S0 | 0.329 | 0.225 |
| | E/SO-Sbc | 0.375 | 0.246 |
| | ALL | 0.419 | 0.272 |
| Faint Pop. Model | | $\gamma(20 < b_J < 24)$ | $\overline{z}(20.5 < b_J < 21)$ |
| | | 0.44 | 0.17 |
| Data | | $\gamma(20 < b_J < 23)$ | $\overline{z}(20.5 < b_J < 21)$ |
| | | 0.43±0.02 | 0.225±0.015 |

**Table 3.3** Model predictions for comparison with observed mean redshift and count slope (see text).

redshift distribution.

The failure of this form of evolution is demonstrated most clearly in Figure 3.9, where due allowance has been made for the different magnitude limits of each field. It is immediately apparent that the predicted N(z) is strongly ruled out by the observations since, the luminosity evolution required in order to achieve the required count slope has a strong effect on the redshift distribution especially at higher redshifts, which is not observed. The lack of movement of the high redshift tail demonstrated by the excellent fit to the 'no-evolution' model underlines this point and indicates that luminosity evolution for the majority of bright galaxies has been negligible to $z < 0.5$, and that a new evolutionary process must be invoked such that the count excess is concentrated not at the high redshift end as for pure luminosity evolution discussed here, but must be spread evenly over redshift which implies a differential form of evolution. Before alternative forms of evolution are discussed the observed lack of evolution at the bright end of the luminosity function is examined more rigorously in terms of the standard stellar synthesis codes.

### 3.11.1 Minimum Evolution

Since of course stellar evolution must take place in any system of stars (with at least one member!) then we must attempt to understand the above lack of significant luminosity evolution.

In Chapter 2.8 it was demonstrated that in the early stages of star

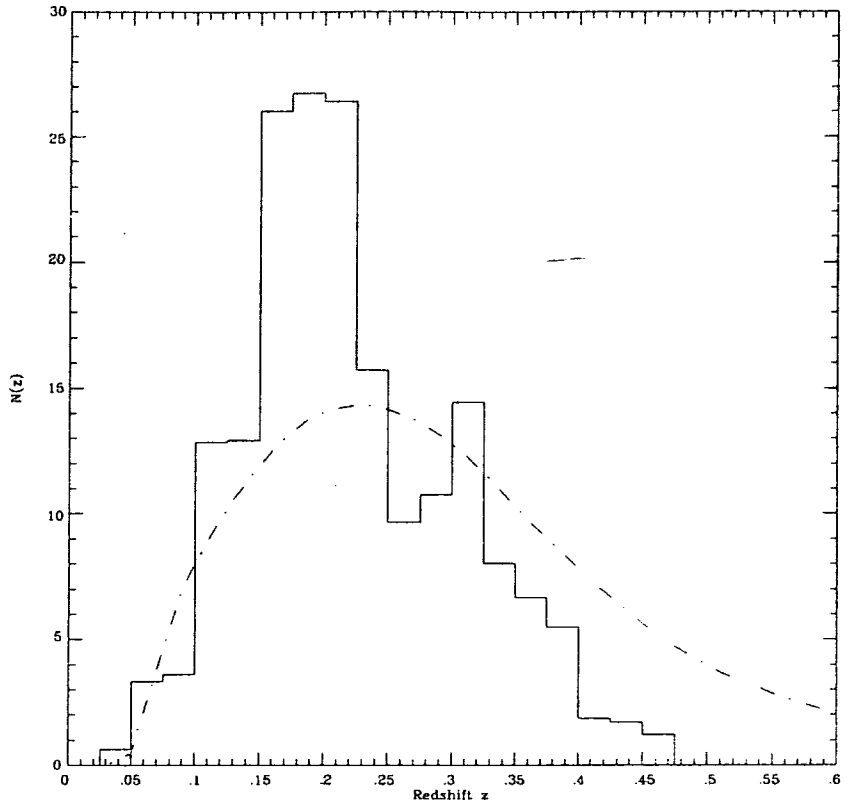


**Figure 3.9** Observed redshift distribution as in Figure 3.8, compared with strong luminosity evolution model (normalised) which fits the count slope. Note absence of a high redshift tail to the data.

formation in early type components large increases in luminosity are expected particularly at short wavelengths, but that these changes need have no significant effect on the counts in the B passband, for example objects may be hidden at high redshift ($z_f > 5$), obscured by dust or initially such stellar systems may be of low mass (see Chapter 2.3 for a full discussion).

However we also require that the effect of evolution be small for early type spirals, the present day colours of which require a higher star formation rate in the past. Experimenting with different evolutionary histories within the framework of of the Bruzual models, it can be readily established that minimum changes in luminosity with lookback time are achieved for the case of a constant star formation rate at all times.

The evolution chosen comprises both a c-model for E/S0 systems and

extended constant star formation for all later types are calculated here for a range of cosmological parameters. The c model is applied such that stars are formed in a dynamical timescale (0.1 Gyrs) at high redshift ($z > 5$), and constant star formation is allowed to proceed for a time dependent on the cosmology chosen such that 5% gas remains at the present day, typical of local bright spirals (Stavely-Smith *et al* 1988).

Table 3.4 shows this form of evolution for different values of $H_o$ representing the extreme cases of large and small lookback times, note $q_0$ and $z_f$ fixed at 0.5 and 10 respectively.

| $H_0$ | $q_0$ | $z_f$ | $\Delta\overline{z}(21.5 < bj < 20.0)$ | $\Delta\overline{\gamma}(24.0 < bj < 20.0)$ |
|---|---|---|---|---|
| 50 | 0.5 | 10 | .006 | .009 |
| 75 | 0.5 | 10 | .009 | .015 |
| 100 | 0.5 | 10 | .009 | .017 |

**Table 3.4** Minimum Evolution models

This model produces very little effect on either the count slope or redshift distribution, with largest effect for case 3 naturally, which has the shortest lookback time. Thus it is reasonable to suppose little evolution of the bright end of the luminosity fuction may take place if the general population follows such a model, and so be consistent with the form of the high redshift tail. However the question of evolution remains since, within our sample evolution must manifest itself as the counts are well in excess of our standard no-evolution model at these magnitudes.

The implication for bright spiral galaxies, at least, is that their evolution is consistent with a constant rate of star formation to much earlier times and before additional forms of evolution are explored, other evidence for constant star formation is discussed further.

## 3.12 Discussion

Other observational support for constant star formation histories is evident from measurements of both past and present star formation for local samples of galaxies, and from other deep redshift survey work, these observation are now discussed in detail.

### 3.12.1 Local Evidence for Constant Rates of Star Formation

Extensive local extragalactic surveys point to steady star formation histories for the full range of spiral galaxies over recent times. The principle method employed is to measure the present rate of star formation via integrated $H\alpha 6563\AA$ recombination emission and compare this with a past rate determined from an broadband magnitude which is converted to a star formation via a suitable stellar synthesis code and represents an average past rate over the life time of stars which contribute to the flux in the passband of interest.

Gallagher *et al* (1984) have applied this crude technique to a sample of local late type (Sbc-Scd) and dwarf galaxies selected in B for which they conclude that form the majority of these systems a near constant star formation history.

This result however, depends on the lifetimes of the majority stellar types which contribute to the B luminosity, and in Chapter 4 the possible insensitivity of this approach to short term bursts of star formation is pointed out.

Kennicut (1984), has also determined instantaneous star formation rates using the recombination emission line approach but rely on UBV colours to establish the past star formation history, and is better able to define the past star formation history. Kennicut concludes that the majority of spirals, of Hubble type Sa to Sc, have undergone a constant disk star formation history over the last few Gyrs.

The implication of this work is that ordinary bright disk galaxies have undergone a constant star formation for the last 1 or 2 Gyrs in agreement with our findings regarding the bright end of the luminosity function. This picture is complicated by the need to reproduce the redder colours of early type galaxies but this can be produced as in the 'minimum' evolution model discussed above with an early high rate of star formation.

Further discussion of local extragalactic observations of star formation rates present and past is left to Chapter 4, however it may be concluded here that

constant star formation rates may be most naturally expected for disk systems, and thus it may not be surprising that little if any pure luminosity evolution has been found at faint magnitudes.

### 3.12.2 Other Deep Redshift Data

Complementing the deep redshift survey work of ordinary optically selected galaxies is the deep redshift survey of Koo and collaborators, this work is ongoing and the various results that have been presented in a preliminary form by Koo over the last 3 years are discussed.

The objects of Koo's survey have been selected in Krons' F passband (Koo 1981) ($\lambda_{eff} = 6100\AA$), which is redder than $b_J$ used here, for which the observed count discrepancy is lower making evolution more difficult to sample. Some of this data is gathered at fainter magnitudes than the work presented here (Koo quotes 22.5 (Koo 1987) as the equivalent limiting magnitude in B), but to date completeness has not been reached to this limit. Koo's survey has other important differences it samples only 2 fields compared with 5 here, making the definition of the selection function less certain for his data, but the sample has one third more objects in total for which broad band colour information is available, allowing for a wider range of evolutionary tests.

The main result of Koo's survey is the same as that presented here that the redshift distribution is consistent with only a very small amount of luminosity evolution but that the data do show a significant excess of blue strong emission galaxies (Koo 1987) in agreement with the conclusions of Chapter 4.

The redshift distributions for all (incomplete) data are presented by Koo (1987), these also show very pronounced clustering, confirming the result found in this survey that field to field variations in structure are very pronounced.

Unfortunately modelling of Koo's data is not possible without full details of the magnitude limits of the various sub-samples that comprise his survey since they are as yet unpublished. However the approach he takes in constructing non-evolving and evolving models are not dissimilar to those of Chapter 2, and thus we may be confident of his conclusion of little luminosity evolution.

An examination by Bruzual of the colour redshift distribution for Koo's survey (Bruzual 1986) also shows evidence for little or no evolution within the framework of the Bruzual models. A red envelope for the colour distribution can be defined over all redshifts and shows that systems as red as present day early

type galaxies are found to the highest redshifts observed ($z < 0.55$). Bruzual makes the claim that evolution must have proceeded at a rate very much slower than the early expectations which were based only on the B count excess. (see Tinsley 1977, Bruzual and kron 1981 for pre-redshift survey, colour-redshift discussion), and in agreement with the results of Chapter 2 which extend to fainter magnitudes.

This trend of little colour evolution for early type objects is found to extend to higher redshifts in the small colour selected survey of Hamilton (1986). Here examples of red selected early type galaxies with no significant colour evolution are found at all redshifts to $z < 0.8$.

## 3.13 Luminosity Evolution:Conclusions

The clear conclusion is that standard models for luminosity evolution cannot simultaneously fit the observed $N(m)$ or $N(z)$. From the counts alone it appears that there is considerable difficulty in retaining a single slope over such a wide magnitude range, but the determining factor is the absence of any high redshift tail in our survey which would be expected from the effects of overall luminosity evolution, whether it be in a subset or in the entire field population observed.

Luminosity evolution in the conventional form discussed in earlier work must therefore have had only a small effect on the photometric properties of galaxies with $z < 0.5$. This suggests that the redshift of galaxy formation is high for any population obeying the c-type models, and that a large proportion of the population might be displaying a fairly constant star formation rate with look-back time.

The major new conclusion from the redshift survey, however, is that at least one extra evolutionary process needs to be invoked to explain the observed redshift and count distributions at the faint limits of this data.

Before discussing other forms of evolution we readdress the problem of the faint end of the luminosity function since a dense dwarf population can offer a non evolving alternative to the interpretation of the counts and which is easily addressed with faint redshift survey data.

### 3.13.1 Low Luminosity Population model

This model is presented in Chapter 2.9 as an alternative to the strongly evolving models and must be taken as a serious alternative, since local field magnitude limited redshift surveys sample relatively few low luminosity systems (see §3.2), potentially producing a misrepresentative no-evolution model which will not predict a steep sloped count excess. Figure 3.10 shows the redshift distribution predicted by the model of Chapter 2.9 which successfully reproduces the count slope in $b_J$, (Table 3.3 lists the mean redshift and count slope in the magnitude ranges of interest) but results in a major distortion of the redshift distribution. This model is also clearly ruled out as an explanation for the count excess, the data much better fit the no-evolution model at the low redshifts of interest, where the effects of such a population would be evident. This indicates straightforwardly that models based on local surveys are not estimating the luminosity function incorrectly at the faint end and that dwarfs are not a significant contribution to the excess count.

Whilst one might argue about the precise way in which this population is incorporated, it is clear that any additional population of local objects invoked to constitute 30% of the galaxies at $b_J \sim 21$, must add a major low z tail which can be ruled out by our survey.

In fact one can turn the question around and ask what limits our faint survey places on the space density of low luminosity galaxies in the *field* environment. Firstly, it is important to recognise that the measuring machines used to construct the photometric galaxy catalogue (on which our survey is based) operates at a threshold of between 25.5 and 26.5 $b_J$ magnitudes arcsec$^{-2}$, thus dwarfs of exceptionally low surface brightnesses are unlikely to be recognised (Chapter 2.7.4). Nonetheless, this surface brightness limit would be sufficient to identify most catalogued dwarfs in the Virgo and Fornax clusters (Phillipps *et al* 1988). The absence of any galaxies in our survey with $z < 0.03$ is consistent with a luminosity function extrapolated from that determined for bright galaxies - in contrast to the conclusions derived in the Virgo and Fornax clusters.

### 3.13.2 Evolution in the Faint End Slope

The above evolutionary models are examples of pure luminosity evolution and fail to achieve a satisfactory fit to both N(m) and N(z) since this form of

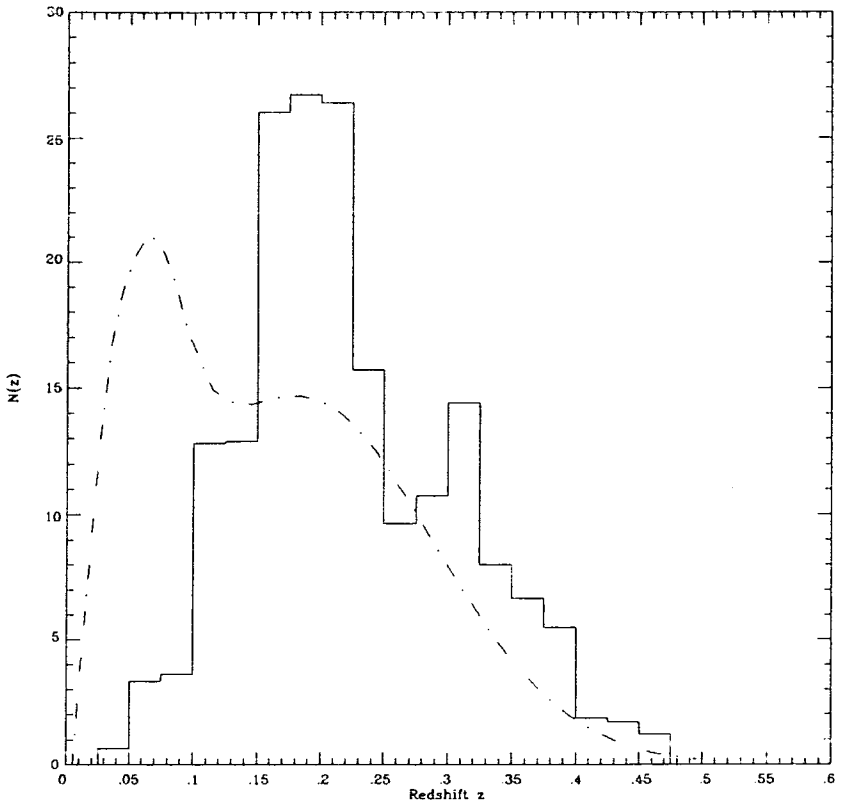


**Figure 3.10** Observed redshift distribution as in Figure 3.8, compared with a No-evolution non-standard low-luminosity model.

evolution is independent of luminosity so that the bright end of the luminosity function necessarily evolves. To get around this problem differential evolution is required, and here we explore the simplest empirical evolution of the luminosity function which can be made consistent with the count slope and redshift distribution.

It is possible to generate a steep $N(m)$ slope without significantly evolving the brightest galaxies by simply increasing the slope of the faint end of the luminosity function with redshift i.e. the only galaxies which we allow to evolve are the precursors of todays intrinsically faint galaxies. This ensures a low mean redshift with respect to pure luminosity evolution, since although the faint end of the luminosity function forms an increasingly important contribution to the *counts* at fainter magnitudes, with little change in the bright end. Here we will regard the model as a completely empirical form of *luminosity-dependent*

evolution, deferring a discussion of any physical significance until Chapter 5.

An excellent fit to the data is obtained from the simple relationship that the number of galaxies in any given absolute magnitude bin of $0.^m02$, $N(M)$, evolves with redshift (for the range $z < 1$) such that,

$$\log \Phi(M)_z = \log \Phi(M)_{z=0} + (0.1z + 0.2z^2) \log \left( \frac{\Phi(M)}{\Phi(M_0)} \right)_{z=0}$$

where $\Phi(M_0)_{z=0} = 10^{-7}\mathrm{Mpc}^{-3}0.^m02^{-1}$galaxies, and $M_0 = -23$ is the bright end limit of the luminosity function.

Figure 3.11 shows the evolution of the luminosity function for the range of observable magnitudes for this case. Note that the low luminosity limit at a given redshift is determined by the maximum luminosity distance observable for an apparent magnitude limit of $b_J = 25.0$.

A count slope of $\gamma = 0.43$ for $b_J > 20.0$ is obtained in this way, with a mean redshift of $\bar{z} = 0.22$ in the range $20.5 < b_J < 21.0$, in agreement with the data. The resulting redshift distribution is presented in Figure 3.12.

Whilst the range is accurately matched by the data, the distribution is not particularly well fitted, there being an excess of galaxies observed with z $\sim$ 0.2. However, examining the redshift distributions for each field it is apparent that this excess is mostly due to clustering effects within one field (SGP) and as noted earlier the *range and mean redshift* of each field to be largely insensitive to clustering whereas the *distribution* is strongly affected by variations in the numbers of clusters sampled per field at the peak of the selection function, a point returned to in Chapter 6.

### 3.13.3 Conclusions

We have obtained a redshift sample which is large enough and with a high level of completeness, so that popular models for the count discrepancy in the B passband can be examined.

Our main result is that whilst the slope of the number magnitude counts at our spectroscopic limiting magnitude argues for an excess of faint blue galaxies, yet the form of the redshift distribution is in agreement with the no-evolution prediction. This allows us to infer the following:

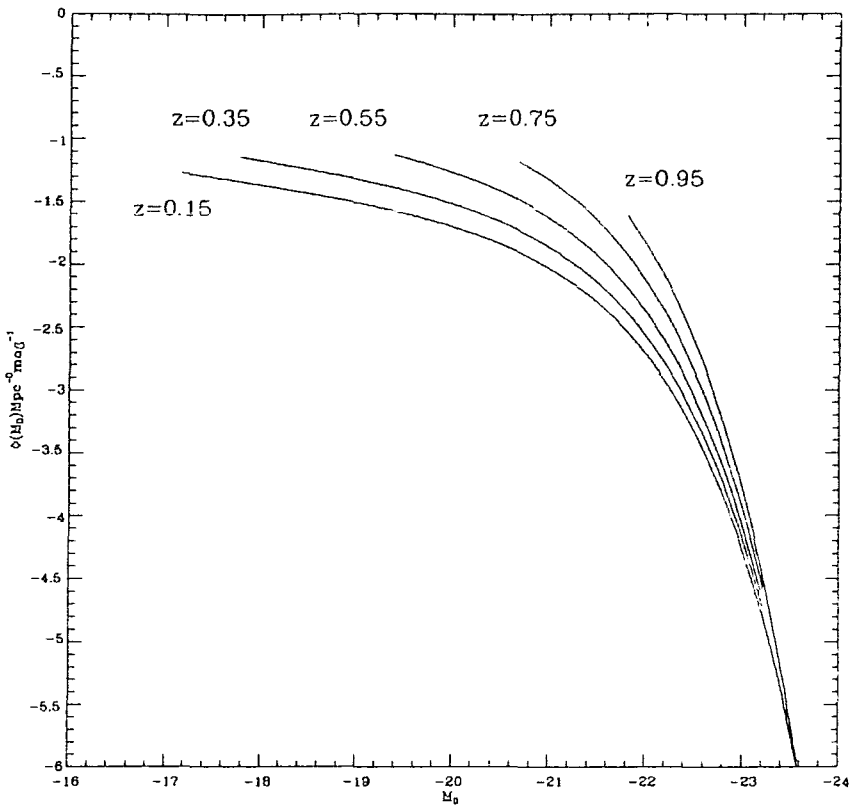


**Figure 3.11** Evolution of the Luminosity Function according to the empirical model described above. Note the low luminosity cut off at a given redshift corresponds to the faint apparent magnitude limit of $b_j = 25.0$ for that redshift, which is the limit of the application of this model since $b_j = 25.0$ is the faintest reliable limit of currently available photometry.

1. Luminosity evolution for galaxies at the bright end of the luminosity function must have been very small over the redshift interval $0 < z < 0.5$ and thus the popular luminosity evolution models based on stellar synthesis codes are restricted to those models producing only a minimal effect on bright galaxies, and thus this form of evolution is *not* the principle reason why the slope of the blue number magnitude counts is steep at $b_J > 20^m0$.
2. Models invoking a substantial population of intrinsically faint field galaxies are also ruled out by the redshift distribution and thus non-evolving non-standard models cannot provide the count excess.
3. The observations are consistent with a simple evolutionary steepening of the luminosity function with redshift. This may be interpreted as a luminosity dependent luminosity evolution.

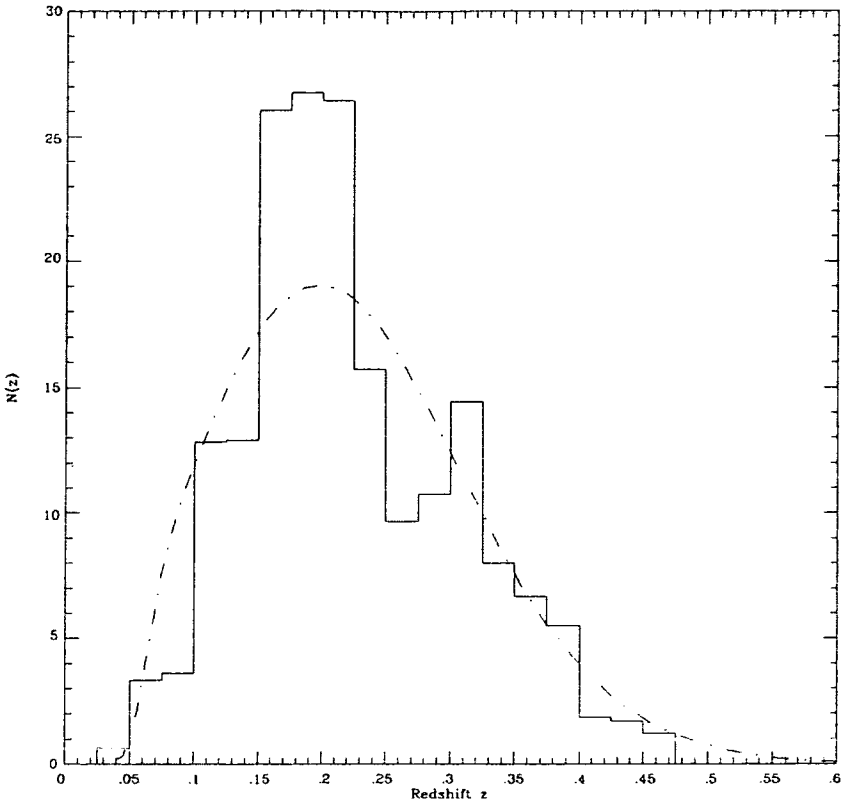


**Figure 3.12** Observed redshift distribution as in figure 3.8, compared with an empirical model of evolution (described in the text)

# Chapter 4.

# SPECTRAL ANALYSES AND EVOLUTION.

## 4.1 Introduction.

In Chapter 3 we showed that luminosity evolution over the entire luminosity function, required by the standard evolutionary models discussed in Chapter 2, is not supported by the faint survey redshift distribution. We find no evidence for an extended high redshift tail to this distribution, indicating that for the bright end of the luminosity function, no significant evolution of star formation activity has taken place to at least $z \sim 0.5$. This result is suprising in view of the evolution implied by the steep count slope and blueing trend found for faint galaxy samples (see Chapter 2), since the redshift survey is simply a subsample of this photometric data. In this Chapter we look carefully at the faint survey spectra for evidence of the increased star formation activity, by comparing the faint survey spectra with both local galaxy samples (e.g. DARS), and with model spectra, generated from a stellar synthesis code.

Spectral information for field samples at faint magnitudes has, to date, consisted of only broad band colours. Such data is of limited value unless colours can be connected to redshifts, although some useful evolutionary constraints are possible with the deep colour distributions examined in Chapter 2. However, our faint redshift survey is rich in spectral detail and provides not only a statistical description of the general star formation history via the redshift distribution, but allows a direct description of star formation rates from comparison of spectral features sensitive to star formation with modelled spectra.

By coadding subsamples of spectra, detailed spectra can be built up, bringing out weak spectral features such as Balmer emission and absorption lines, useful in establishing star formation rates. Individually, most spectra show the prominant emission line feature [OII]3727Å, indicating ongoing star formation, and the distribution of the equivalent width of this line is compared with local data to look for possible evolutionary effects.

## 4.2 Observed Equivalent Widths of [OII]3727

For both the local DARS and the faint redshift survey the observed redshift distribution is such that for each sample the prominent emission line [OII]3727Å falls within the spectral range of the data, and we are able to measure accurately the equivalent width of this line for all objects in each survey. In fact of all the spectral features present in these surveys [OII]3727Å is the strongest and often the only feature which is measurable with any degree of precision.

Unfortunately the strength of this feature (unlike the Hydrogen recombination series is also present during star formation), cannot be directly related the rate of star formation, since it is sensitive to metallicity and temperature (see later §4.5). Nevertheless a comparison of the distribution of the equivalent width of this line between these two surveys provides, in principle, a measure of the relative importance of star formation between the surveys and therefore a useful empirical test for evolution.

### 4.2.1 Line Measurements and Errors

The equivalent width of this feature, $W_\lambda$[OII]3727Å , is measured for all faint survey galaxies with redshifts, using a SPICA routine (EWIDTH). This is a semi-interactive routine which allows the user to define the continuum in a window either side of the emission line. The continuum under the line is estimated by interpolation after $2\sigma$ clipping of discrepant continuum points, and the resulting equivalent width is then corrected by $1/(1+z)$ to its restframe value.

Uncertainty on this measurement results from a combination of both random and systematic error on the line and continuum measurements and in the subtraction of sky background. Also systematic effects may result from the presence of other spectral features in the wavelength range covered by the line and the adjacent continuum.

The error on sky subtraction is discussed in Chapter 3.5, and has an rms error of $\sim 1\%$, averaged along a fibre and for the duration of a run. Examining individual sky fibres the sky subtraction (defined by 6 fibres distributed evenly along the slit of the spectragraph) appears to be random, and thus if the window widths for calculating the equivalent widths cover a sizable fraction of the spectrum ( typically $\sim$20% is chosen ), then the sky subtraction error will

be small $\sim$ 2%. The ratio of mean continuum object to sky count is 0.2-0.4 so the 2% error on the sky subtraction translates into an error on the mean continuum level of between 6% and 10%. If we define $\delta_o$ as the fractional error sky subtraction, the fractional error on $W_\lambda$ is then given by,

$$\frac{\Delta W}{W_\lambda} = \frac{\delta_o}{1 \pm \delta_o} \tag{4.1}$$

(note the sign of the term in the denominator is in the opposite direction of the size of the error in equivalent width, being largest in the case of an overestimated sky and resulting in a larger equivalent width). Thus random errors in sky subtraction which skews the distribution in equivalent width to a higher mean value by a factor, $1 + \delta_s/1 - \delta_s$, the error being greater if sky subtraction is overestimated. However in the worst case (the lowest object to sky ratio), the error on the equivalent width due to sky subtraction is only 10% (skewed by only 20%) and for typical case only 6%, corresponding to 1Å for the mean survey equivalent width of 20Å.

Uncertainty in the definition of the continuum may provide an larger source of error. The fractional error here is largest for smaller equivalent widths and given by,

$$\frac{\Delta W}{W_\lambda} = \frac{\delta_c}{1 \pm \delta_c}(1 + R) \tag{4.2}$$

where $\delta_c$ is the fractional error in the continuum, and R the ratio of continuum to line fluxes averaged over the emission feature. The fractional error, at a given line width, is larger for a low continuum count. In the worst case of only a $2\sigma$ peak emission line strength (this is established by comparison with the noisiest confidently eye detected features, but note the significance is higher than the simple formal error estimate, based on the continuum noise, since for identification, a line must show itself as an excess over the continuum for at least 3 spectral increments), eqation 4.2 becomes,

$$\frac{\Delta W}{W_\lambda} = \frac{1}{\sqrt{nm} \pm 1}\left(1 + \sqrt{n}/2\right) \tag{4.3}$$

where $m$ is the number of spectral increments over which the continuum is defined which is typically $\sim$ 200 channels, and $n$ for the worst case, is a

continuum count of $\sim 30$ per channel, giving a fractional error of 15%. This for a typical continnum strength and for $W_\lambda = 20\AA$, is only 6%.

Random errors due to continuum definition and sky subtraction are then at most $\sim$ 25% and more typically only 10%, or 2Å for a typical measurement.

However, in any equivalent width measurement, potentially the most worrying source of error is in the intrinsic structure of the spectrum itself, since this may result in a systematic error on the continuum level estimated beneath the line. [OII]3727Å lies in a reasonably well behaved part of a galaxy spectrum, only the very highest Balmer absorption features are present close to the line, which are generally very weak (see Figures 4.9 and 4.10). Fortunately empirical estimates of this error have been calculated for this line from similar data. The large program of cluster spectroscopy of Couch & Sharples (1987) uses the same instrumental setup as the faint survey at the same resolution and continuum signal-to-noise. They find that in their observed range 5Å<$W_\lambda$[OII]3727Å<40Å the systematic error decreases from 50% at 5Å, to 15% at 20Å, for typical cases, in agreement with the above discussion and indicating only small systematic effects.

Thus we conclude that errors are generally of the order of a few Angstroms over the full range of observed equivalent widths. The fractional error is greatest at small eqivalent widths and a lower limit of 5Å should really be placed on this measurement for spectra of typical quality - below this the error on the equivalent width is of order the measurement. As we show below we are most interested in the strong lined objects ($> 20\AA$) for which the equivalent width measurements are typically only in error by 10-10% or $\sim 2\AA$, and quite adequate for our purposes.

## 4.3 Results

The rest-frame equivalent width distribution of [OII]3727Å for the faint survey and DARS are shown in Figure 4.1. In both cases the distributions are complete including objects with no detectable emission, negative values note, are assigned to zero.

It is immediately apparent from Figure 4.1 that objects with strong [OII]3727Å are much more numerous in the faint survey, the distribution being much flatter and extending over a larger range in $W_\lambda$ than DARS. The fraction of galaxies with $W_\lambda > 20\AA$ rises from 15% at $b_J < 16.5$ to 55% at $b_J \sim$

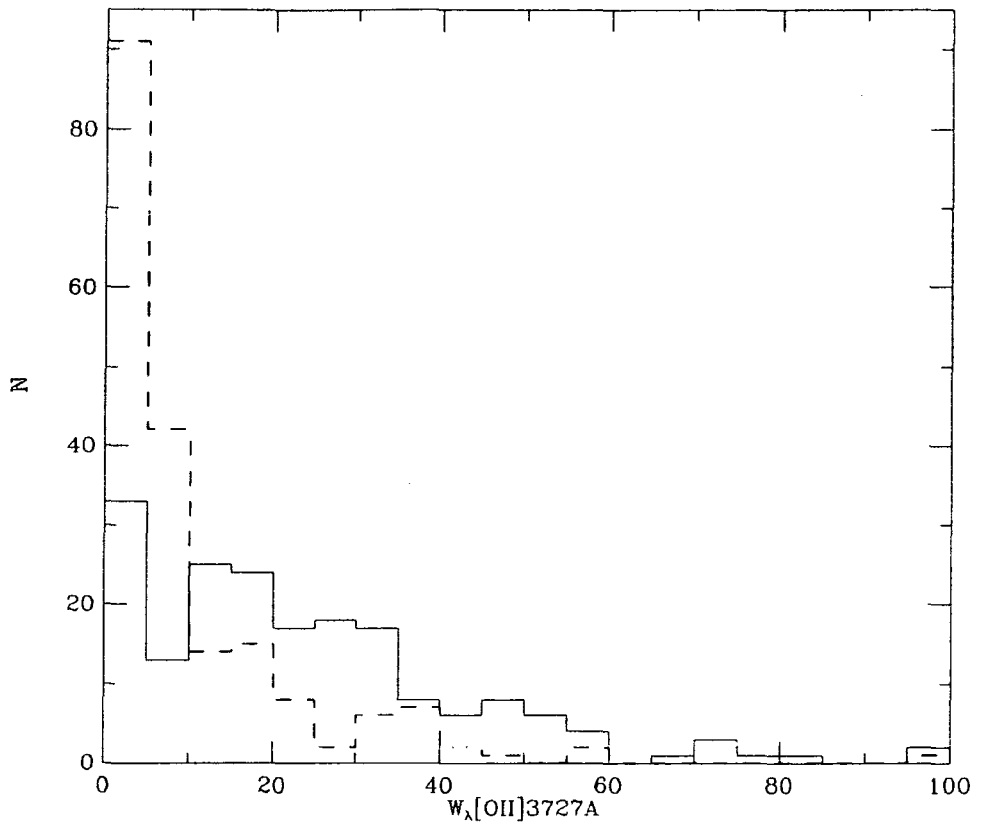


**Figure 4.1 Comparison of equivalent width distributions of [OII]3727Å, for the faint survey (solid) and DARS (dashed).**

21, however, before we can talk about this large difference between surveys in terms of any trend to increased star formation at faint magnitudes, the role of selection selection effects must be explored.

### 4.3.1 Selection Effects

Two obvious selection effects may result from differences in the method of observation and the depths between these surveys. Firstly the size and shape of the aperture used in the spectroscopy are different. The fibre observations of the faint survey were made with a circular aperture with a diameter of 2.67 arcsec, but for DARS a long slit was employed and the spectrum coadded over an aperture of $4 \times 20$ arcsec.

However, the projected physical size that these apertures cover is in fact quite similar at the respective mean depths of each survey. The physical

aperture at the mean redshift of DARS, $\overline{z} = 0.05$ has dimensions $4 \times 21h^{-1}$ Kpc, and for the faint survey the fibre covers a diameter at $\overline{z} = 0.22$ of $12h^{-1}$Kpc. The ratio of areas is then 1.33, with DARS covering the larger area indicating that if anything, the faint survey may be less sensitive to the spectral contribution from emission lines.

Infact, the range in $W_\lambda$ found for the DARS sample is very similar to that seen in background field galaxies of the local sample of Dressler and Gunn's (1983). They chose a large circular aperture of diameter 29 $h^{-1}$ kpc to obtain spectra integrated over the whole galaxy. This indicates that for DARS, the emission line contribution to the galaxy spectrum is not underestimated. Thus we conclude that the equivalent width estimates for DARS and the faint survey can be compared without the need for any significant correction for aperture differences.

The Second effect results from differences in the rest-frame wavelength sampled at the mean survey depth of these two surveys. The faint survey samples further towards the ultraviolet than DARS ($\lambda_{eff} \sim 3700$ Å c.f. 4200 Å ) and hence the relative difference in k corrections between star forming and quiescent systems will reveal a greater number of the former in the faint survey.

This effect can be quantified in the case of 'no-evolution', using the faint count models and assuming a simple correlation between $W_\lambda$[OII]3727Å and type. For example, by identifying objects of $W_\lambda > 20$ Å as predominantly late types, the no-evolution model predicts that the observed ratio of late types to earlier types will only increase by a factor of 1.6 between the bright and faint redshift surveys. The increase observed is, however, far greater and amounts to a factor $\sim$5 in the proportion of galaxies with $W_\lambda > 20$, and $\sim 7$ for $W_\lambda > 30$.

It is possible to model the expected changes in the equivalent width distribution between surveys more exactly by incorporating into the count models, discussed in Chapter 2, the dependency of the equivalent width of [OII]3727Å on galaxy colour. This can be established using a subsample of DARS with both equivalent width and colour measurements.

A clear trend of equivalent width of this line with $b_J - K$ colour, for the sample of Mobasher *et al* (1988), is found combining all the standard types, see Figure 4.2a. Figure 4.2a shows the clear trend to larger equivalent widths with bluer colour for standard sequence galaxies, this is naturally expected

and reflecting the full range of star formation rates. By comparison the morphologically peculiar class which shows a different behaviour (see Figure 4.2b), this is discussed in Chapter 4.6.

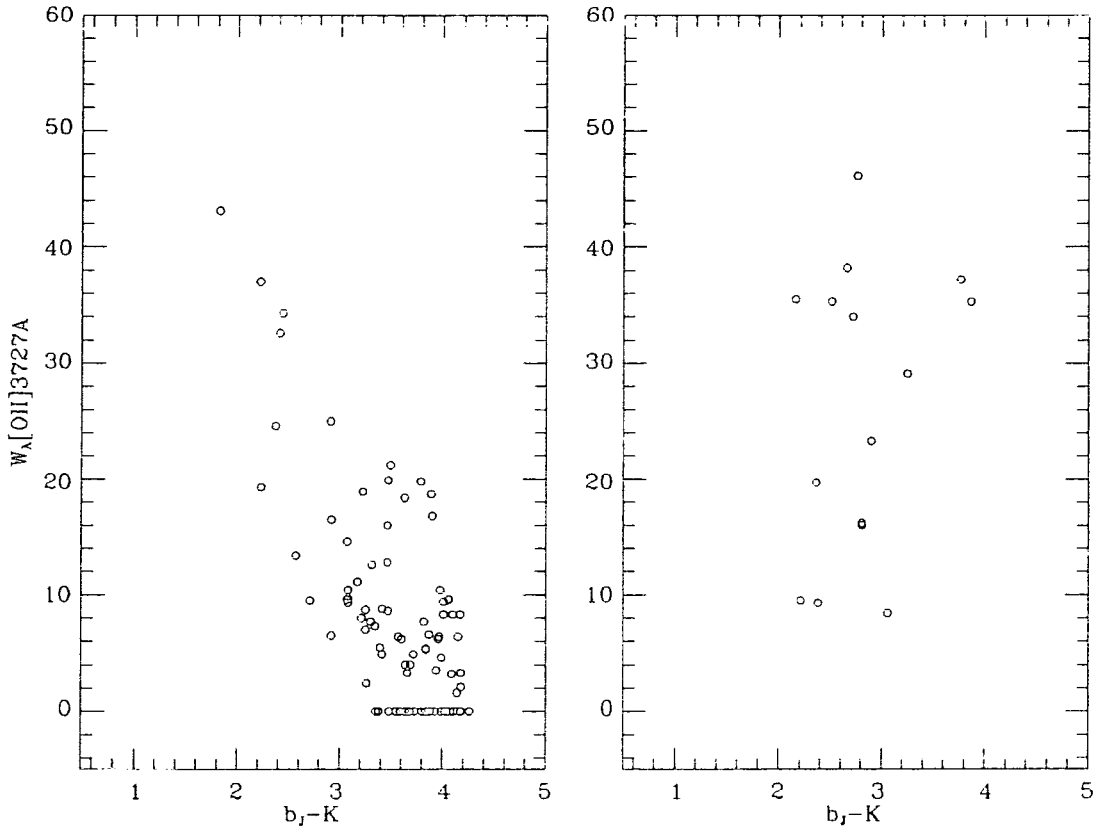


**Figure 4.2 $b_J - K$ vs. $W_\lambda$[OII]3727Å for the DARS survey. The lefthand panel a) shows the distribution for galaxies classified on the Hubble sequence E-Sdm/Irr, and b) on right for object classified as peculiar or for which no standard classification was possible.**

Using Figures 4.2a and 4.2b, and the $b_J$-K count model discussed in chapter 2.4, the equivalent width distribution to $b_J < 16.5$ is constructed. We include the scatter in this relation, using a Gaussian distribution of colour class in the $b_J - K$ count model. Note that since the equivalent width of an emission line cannot be less than zero (by definition), the Gaussian chosen to match the scatter for the reddest objects is not symmetrical. The model predicted distribution for the DARS sample distribution of this subsample (109 objects) is very good, so too is that for the larger sample of galaxies from DARS with

a measured equivalent width, shown in Figure 4.3.

At fainter magnitudes the no-evolution model prediction for the distribution of $W_\lambda$, is found to flatten only slowly with increasing apparent magnitude and for the magnitude range of the faint redshift survey this effect is insignificant compared to the observed change in the distribution, this is demonstrated in Figure 4.3. The model predicts an increase in the ratio of objects predicted to lie above 20Å of only 1.8 at $b_J \sim 21$ which is in agreement with the cruder prediction based on morphological argument above, but falls well short of the factor 5 observed.

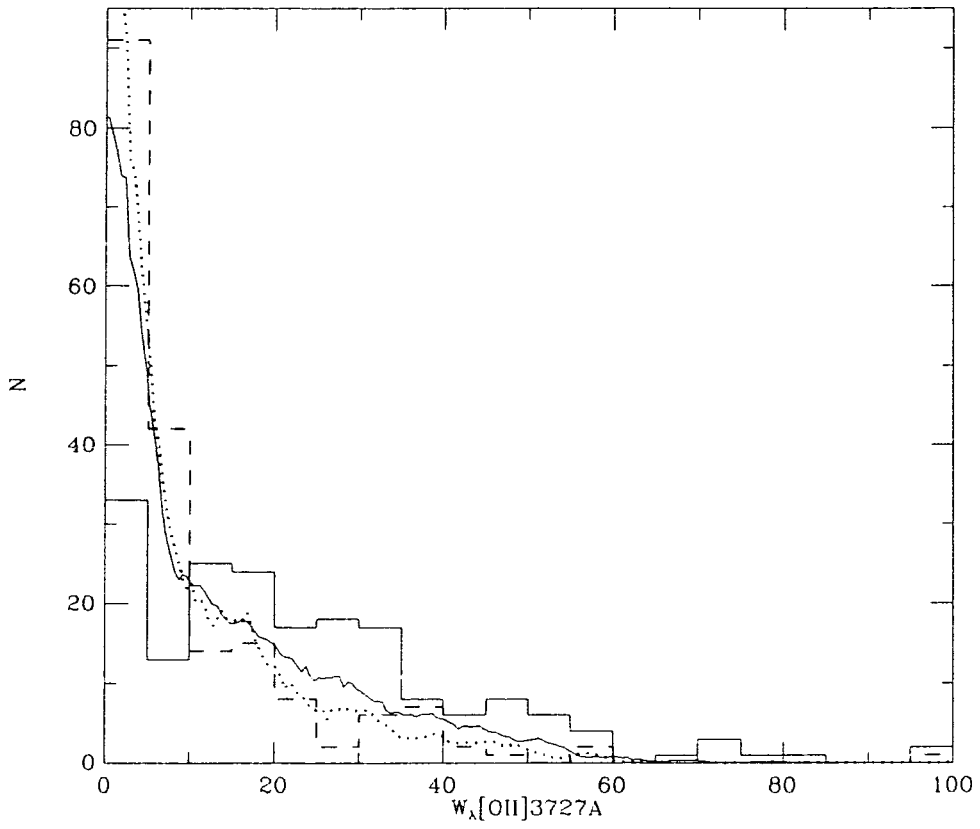


**Figure 4.3. Comparison of equivalent width distributions of [OII]3727Å, for the faint survey and DARS, with modelled curves. The dotted curve refers to DARS and the solid curve is the model prediction for the faint survey, to be compared with the solid histogram.**

In summary, therefore, we conclude that the observed equivalent width distribution $21 < b_J < 21.5$ of the faint survey is a poor match to the predictions

based on DARS, and that the selection effects discussed above, resulting from differences in aperture size and rest wavelength coverage between these two surveys, at most account for a small fraction of the observed difference between the two distributions in Figure 4.1.

Importantly there is a consistency between the fraction of faint survey galaxies whose $W_\lambda$ lies in excess of the local distribution and the count excess at $b_J \sim 21$ - 21.5 c.f. (see the no evolution prediction of chapter 2.5). In addition, since the galaxies with $W_\lambda > 20$ Å are generally the bluest systems, by virtue of their strong star formation, it follows that the same galaxies could be responsible for the bluing in the colour distributions at faint magnitudes, described in Chapter 2.6.

### 4.3.2 Other Correlations With $W_\lambda$[OII]3727

The distributions of redshift and magnitude as a function of equivalent width of [OII]3727Å within the faint survey are now examined, in order to learn more about the luminosities of the strong lined objects and their relationship with the evolution implied by the count slope and redshift distribution.

The redshift distributions of strong and weak lined objects are shown in Figure 4.4. Objects with $W_\lambda$ [OII]3727Å>30Å clearly lie in a lower redshift range than for the remainder of objects. The contribution to the redshift distribution above $z = 0.25$ shows a marked decline of objects with $W_\lambda > 30$Å, and for $z < 0.15$, objects with $W_\lambda > 20$Å comprise 80% of the survey.

This difference in redshift distribution between strong and weak lined objects is also apparent from the application of a KS test to the distributions divided at 20Å, revealing the very significant result, that these distributions sample the same parent population at only the 1% level. This trend is also illustrated in Figure 4.5. Here the mean redshifts at a function of $W_\lambda[OII]$ is presented in bins containing equal numbers, showing a clear trend to lower redshifts at large equivalent widths. Interestingly the peak in this distribution at z=0.25 corresponds to $\sim$ 15Å which is typical of normal mid sequence spirals (see § 4.6), these systems have a smaller $k$ correction than earlier types of lower equivalent width but which have the brightest restframe luminosities, and the shallower depth of the weaker lined objects may reflect the differential effect of the $k$ correction .

A direct test of the importance of this strong lined population to the

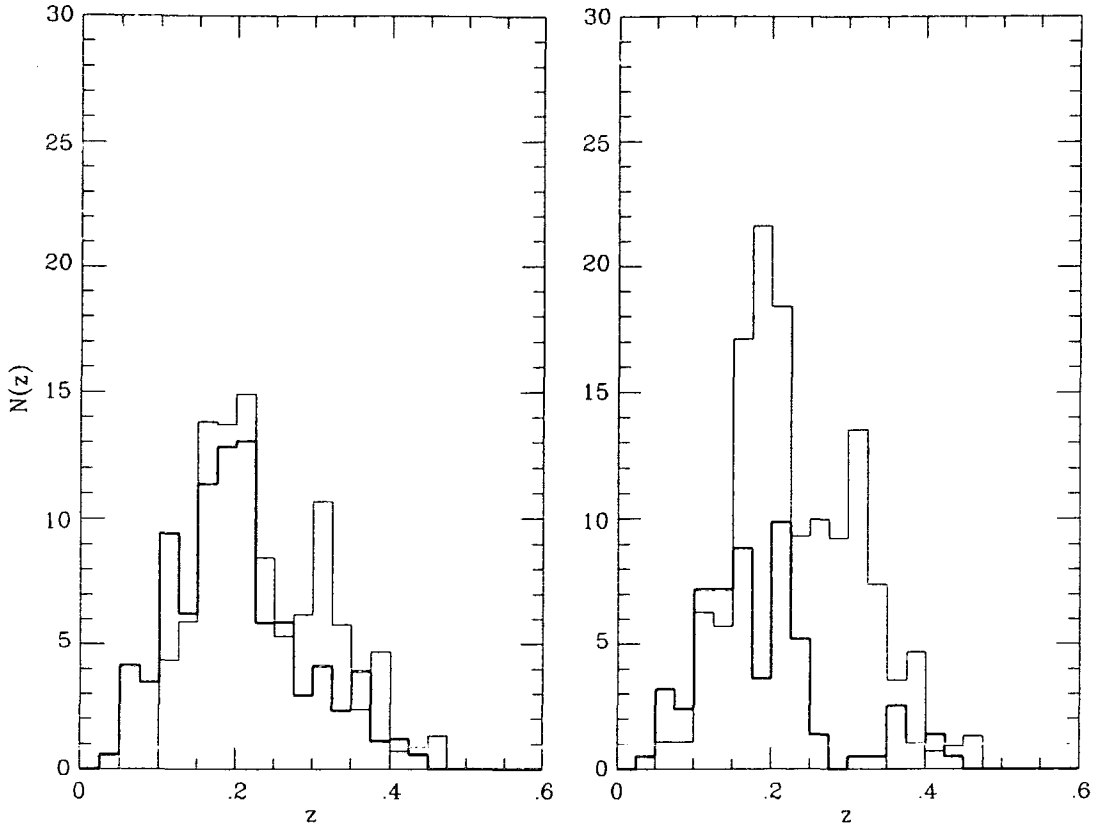


**Figure 4.4 a) Shows a comparison of the faint survey redshift distribution divided at $W_\lambda[OII]3727\AA = 20\AA$, the heavy line referring to objects with $W_\lambda > 20\AA$, b) likewise, for with the division at $W_\lambda = 30\AA$.**

$b_J$ counts can be made by examining the differential number count slope, $\gamma$, as a function of $W_\lambda$. This is calculated for each field by dividing the sample into $0^m5$ bins for two ranges of equivalent width split at$W_\lambda[OII] = 20\AA$. This produces two samples of roughly equal numbers, over the five separate fields of the survey. The count slope is related to the ratio of objects sampled in the faint and bright magnitude bins, $n_2$ and $n_1$ respectively, via

$$\gamma = \frac{1}{\Delta m} log(\frac{n_2}{n_1}) \tag{4.4}$$

(where $\Delta m$ is the bin width), we find $\gamma = 0.61 \pm 0.2$ for $W_\lambda > 20$ Å and $\gamma = 0.18 \pm 0.1$ for $W_\lambda < 20\AA$, with errors determined from field to field variations. This diffence in count slope indicates in a direct way that the strong line galaxies may be responsible for steeping the $N(m)$ slope, since not

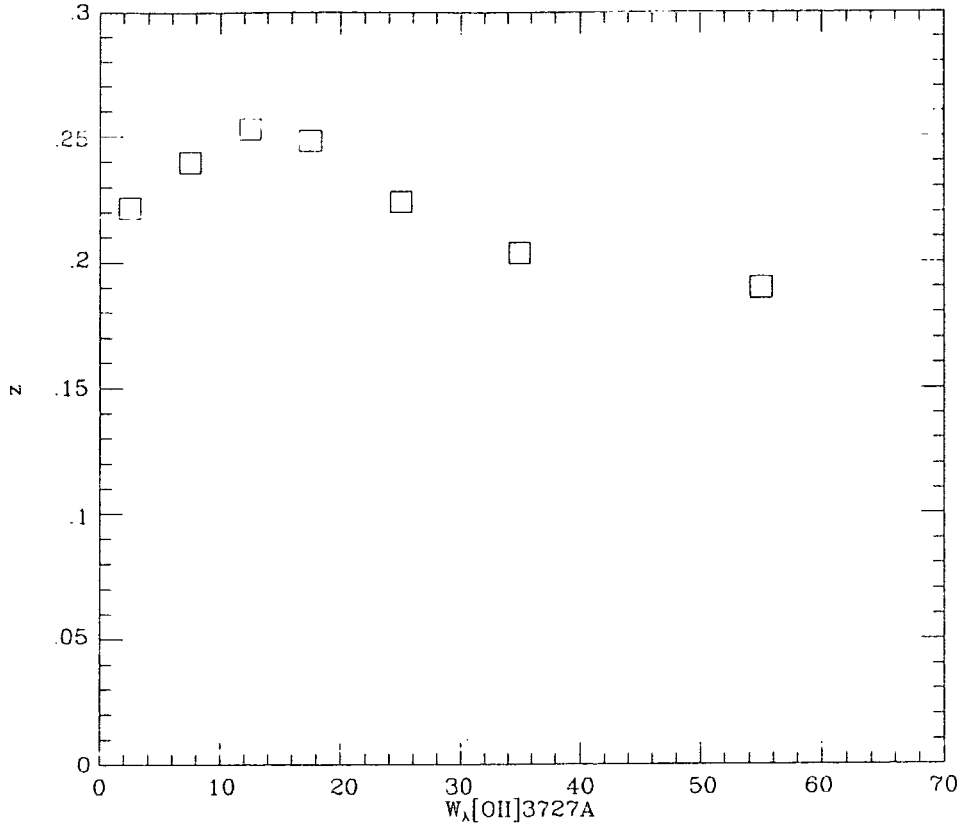


**Figure 4.5** Trend of mean redshift with equivalent width, points denote the centers of bins divided so that approximately equal numbers of objects are sampled in each bin.

only is their count slope consistent with a Euclidean value they are comparable in number with the weaker lined objects, and must therefore have a steepening effect on the counts.

We can conclude from this section that these correlation suggest a straightforward explanation; the excess in the counts at $b_J \sim 21$ can be identified with the star forming strong emission line galaxies, implying strong evolution in star formation activity by $z \sim 0.2$.

Further insight into the nature of this form of evolution is now presented via more detailed modelling of spectral properties of the survey spectra.

## 4.4 Models for the Emission Line Galaxy Spectra

Detailed modelling of galaxy spectra is a straightforward extension of the stellar synthesis codes used thus far to determine coarse spectral properties such as colours and luminosities. The code of Bruzual has been extended by Couch and Sharples to generate galaxy spectra, using a library of main sequence stars observed by Jocoby *et al* (1984). These spectra were observed at the $4\AA$ resolution on an IPCS detector, and are therefore ideal for comparison with the faint redshift survey. The method of inclusion of spectra from this catalogue is detailed by Couch and Sharples (1987).

Spectral features in the galaxy spectra, at optical wavelengths, which are sensitive to changes in star formation have been identified by many authors. It is these features which we attempt to reproduce here by experimenting with a variety of star formation histories for comparison with coadded spectra from the faint redshift survey. Of principle interest are the Hydrogen Balmer emission and absorption lines, these are present in all galaxy spectra with ongoing or recent star formation. Stars predominantly of A type have both strong high order Balmer absorption line spectra and may also dominate the spectrum in the restframe blue and near UV, for galaxies with high rates of star formation. Ongoing star formation also generates Balmer emission lines, these are recombination lines resulting from Hydrogen ionised by Lyman continuum photons produced by O and early B type stars (Osterbrock 1974).

These emission lines tend to 'fill in' the Balmer absorption lines and at the resolution and signal to noise of this work we are not able to distinguish these from each other. To resolve this difficulty the amount of line infilling is estimated assuming the emission to be characteristic of a typical HII region. Couch and Sharples (1987) include such an HII spectrum in their code by calculating the number of Lyman continuum photons generated from the hot stars and converting this to an emission line flux at $H_\beta 4681\AA$The HII emission line spectrum is then scaled by adjusting the relative strength of other emission lines to $H_\beta$. The resulting emission is then added to the model generated absorption line spectrum. This procedure allows theoretical predictions of a galaxy spectrum at any time for the adopted star formation parameters.

Line infilling of balmer line features is only important during star formation since it results from stars whose lifetimes are typically very short ($< 10^6 yrs$),

and is strongest for the low order lines, given by the relative probabilities of recombination (see Osterbrock 1974 for a full discussion of the emission line properties of HII regions). In contrast the Balmer absorption lines are most prominent at lower orders and may persist after star formation has ceased until the A and F stars have burned off the main sequence ($\sim$ 1Gyr). These spectral properties and also the properties of other emission and absorption features for a variety of star formation histories are now demonstrated by comparison of the model generated predictions against spectral data from the faint redshift survey.

## 4.5 Spectral Modelling for the Faint Redshift Survey

It is not well established that fibre data is suitable for determining accurate relative fluxes, and so here we take only our best data, for which we are confident that the observations were made under photometric conditions, and check this by subjecting the data to some tests.

Spectral standards (standard white dwarfs stars) were taken at the beginning and end of each run through a fibre at the centre of the RGO spectrograph slit with which the data was fluxed. Here we concentrate on one field (field 419, see Table 3.1 for details of this field), of 40 objects where we are most confident of accurate fluxing. The faint redshift survey data was gathered principally for redshift identification and not for examining detailed spectral features, however by coadding the data, spectra covering a wide range of spectral classes can be produced, with continuum signal-to-noise high enough to be of use in examining the weak features of interest.

We divide up and coadd the spectra according to to equivalent width of [OII]3727Å, in ranges corresponding to cases of interest. In fact by selecting galaxies with $W_\lambda \sim 0$, we can check the accuracy of the calibration. These are the reddest spectra in the sample and we expect these red galaxies not to show significant differences in the continuum shape with respect to the present day spectral energy distribution of a typical early type galaxy (see Chapter 2.8 and 3.12 for a discussion of the rate of colour evolution in early type systems. A number of rich cluster studies have shown the early type galaxy colour magnitude sequence not to show signs of significant evoloution to redshifts as high as z=0.5 (Ellis 1987), consistent with the predictions of the Bruzual code for the case of systems which have not undergone significant star formation for

several Gyrs (Bruzual 1983).

Figure 4.6 shows the agreement between the mean spectrum of 5 galaxies chosen as described above, (these objects cover a redshift range $0.2 < z < 0.3$), and compared with Pence's averaged local early type spectral energy distribution (Pence 1976). The agreement is better than $\pm$ 5% over the wavelength range of interest, see Figure 4.6, thus confirming the accuracy of our relative flux calibration.

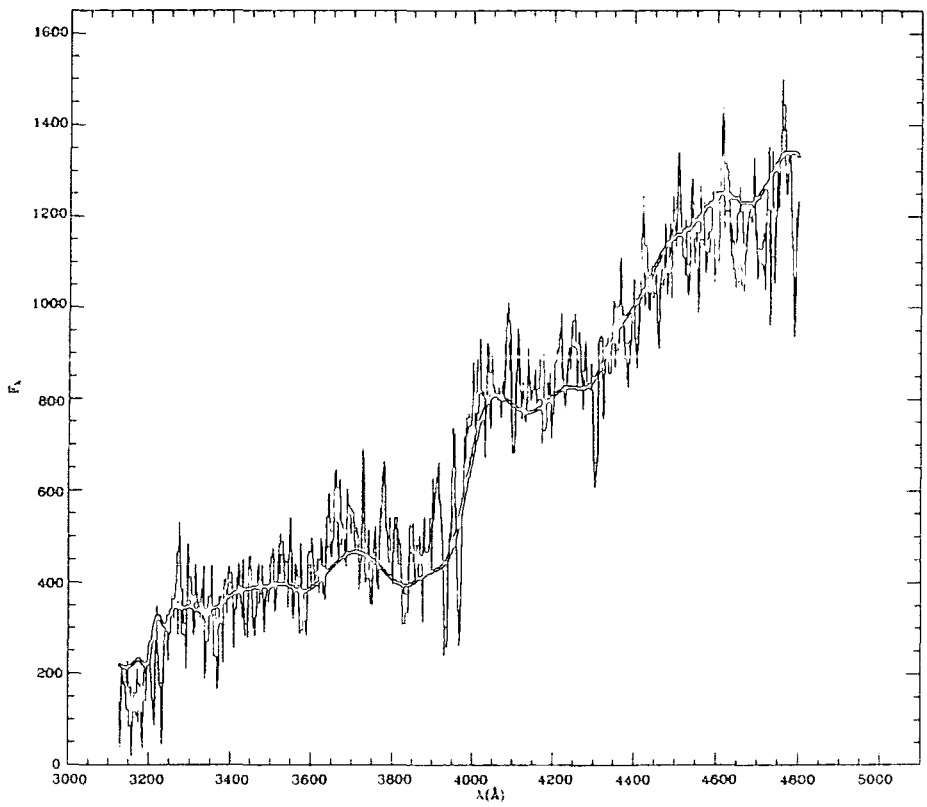


**Figure 4.6. Comparison of the coadded spectrum of galaxies selected to have $W_\lambda$[OII]3727Å = 0, and Pence's spectral energy distribution for an early type galaxy.**

For interest and to demonstrate the small effect of evolution for early type spectra and the important information contained in absorption line features we compare this observed spectrum (spectrum 1) with the predicted spectrum of a c-model (see Chapter 2.8 for definition), from the modified high resolution code, at 6Gyrs and 12Gyrs. This comparison is shown in Figure 4.7 and we

normalise to the data over a wide central wavelength range. An excellent fit to both the continuum and absorption line features is produced by both model spectra, i.e. over this large age range. Of principle interest are the Ca H and K absorbtion lines at 3968Åand 3963Å, which are accurately reproduced. The models (normalised) are distinguishable only by the differences in flux at the short wavelength range, which is marginally greater for the younger, 6Gyr, model.

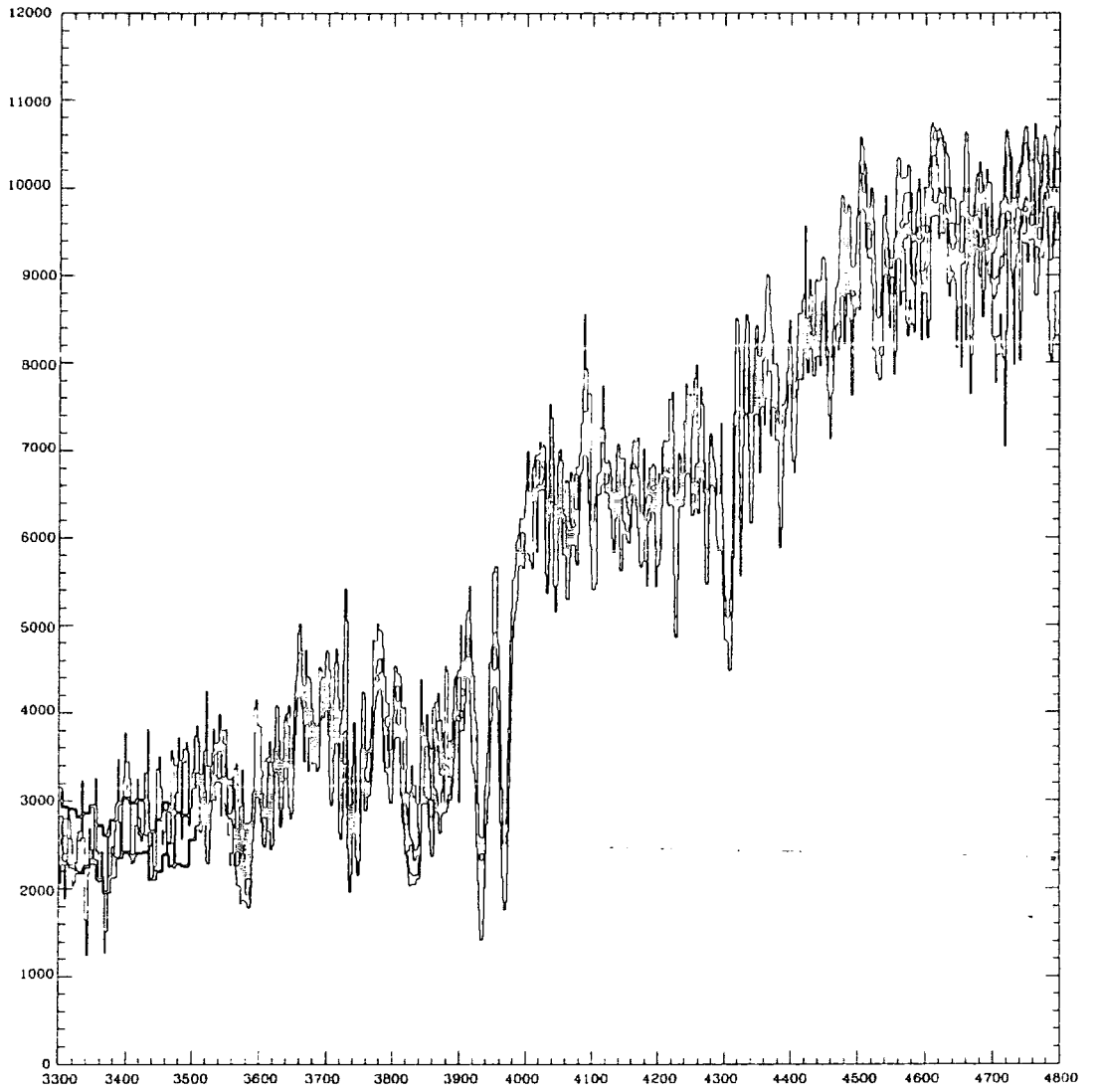


**Figure 4.7 Comparison of the coadded spectrum of galaxies selected to have $W_\lambda$[OII]3727Å= 0 (spectrum 1), and 'C-model' generated spectra for 6 Gyrs and 12Gyrs (solid curves).**

In summary, these galaxies which have a mean redshift of $\bar{z} = 0.25$ are indstinguishable from present day E/SO's. The addition of even a small amount of ongoing or recent star formation will reverse the the ratio of K to H over spectrum 1, resulting from additional absorption by $H\epsilon 3970$Å which is almost coincident in wavelength with Ca H and is thus a sensitive indicator of star formation. This change in line ratio found within the group selected in range $5\text{Å} < W_\lambda < 15\text{Å}$ (spectrum 2) and plotted in figure 4.8. Comparison with spectrum 1, shows this spectrum to have a flatter continuum and the Balmer absorbtion line series, of course the presence of [OII]3727Åemission also indicates that star formation is ongoing.

A fuller discussion of the models is required to interpret the spectra of objects with higher rates of star formation, since in detail the strength of the predicted emission lines depends sensitively on the choice of the IMF at high masses and the amount of extinction of the short wavelngth photons generated by the massive stars. Note though, the discussion that follows does not bear on the *continuum* modelling, which in the wavelength range of the observations is dominated by stars less massive than those principally responsible for the HII emission lines.

The observed Balmer emission line strengths are determined by the IMF at the high mass end ($> 10m_\odot$) and by the amount of extinction of Lyman continuum photons by dust local to the star forming regions. The degree of extinction will depend on the geometry of the star-dust distribution (see Rowan-Robinson and Crawford 1988), but may be crudely determined empirically from the spectra as outlined below.

Throughout this work we assume a Miller Scalo IMF (Miller and Scalo 1979), and we adopt a high mass cut off at $20M_\odot$, the Lyman continuum photon flux is then determined by the star formation rate and calculated as described by Couch and Sharples.

The fraction of the Lyman continuum flux, generated by massive stars, absorbed by the dust has to be specified, and it is clear that even very ordinary spiral galaxies can be luminous in the far infrared (Saunders *et al* 1988 in preparation), implying significant amounts of extinction at short wavelengths. Some constraint on the amount of extinction can be obtained by examining the Balmer emission and absorption line features of the modelled spectra. Since

the Balmer line emission is strongest for lower order transitions, the degree of infilling of the corresponding absorption line features is differential with order being smaller for higher order lines and more dominated by emission at longer wavelengths. We can take advantage of this in the models so that for the various star formation histories of interest, we first arrive at a suitable fit to the overall continuum shape and then adjust the emission line spectrum to acheive consistency with the Balmer absorption line and emission line strengths.

For the flattest continuum spectra objects Lyman continuum extinction is certainly required but with little reddening at optical wavelengths. For objects with small $W_\lambda$ this proceeedure is not required as no visible emission line infilling is found. Note that the IMF upper limit of $20M_\odot$ is almost certainly on the low side so that greater extinction may be required. Absorption by a factor of $\sim 3$ of Lyman continuum photons is consistent with comparisons covering all star forming spectral types found here based on $H_\gamma$ and $H_\beta$ features. Note that [OII]3727Å although very sensitive to the presence of star formation is not of use in this way, this feature is very sensitive to metallicity and nebular temperature. Observations of local extragalactic HII regions, in fact, show a large variation of this line with respect to $H_\beta$ (McCall *et al* 1985, Gallager and Hunter 1986) and we find in all cases [OII]3727Å is underestimated by the models, indicating that the HII spectrum used in the code may not be representative of the degree of ionisation displayed by our faint survey emission line galaxies.

Returning to the constraints on star formation histories provided by the models, we model spectrum 2 most successfully by a simple constant star formation rate with initial early star formation (1Gyr burst) consuming half the mass. Note the duration and variation in rate of this earlier star formation is not important in determining the spectrum only the fractional conversion to stars, The parameterisation of the early star formation is chosen only for convenience, a suitable $\mu$ model (see Chapter 2.8 for definition) could be found. The resultant spectrum observed the range of ages from 6-12 Gyrs show an excellent fit to the observations see Figure 4.8a. The rest frame colour model colour is B-V is $\sim$ 0.6-0.75, (depending on age) which is typical of a mid sequence spiral and such objects are expected to to be sampled in this redshift survey. The emission line strength note has been reduced by 3 so not to

produce any effect, the low order Balmer absorption lines, but the absorption in this case may of course may be greater.

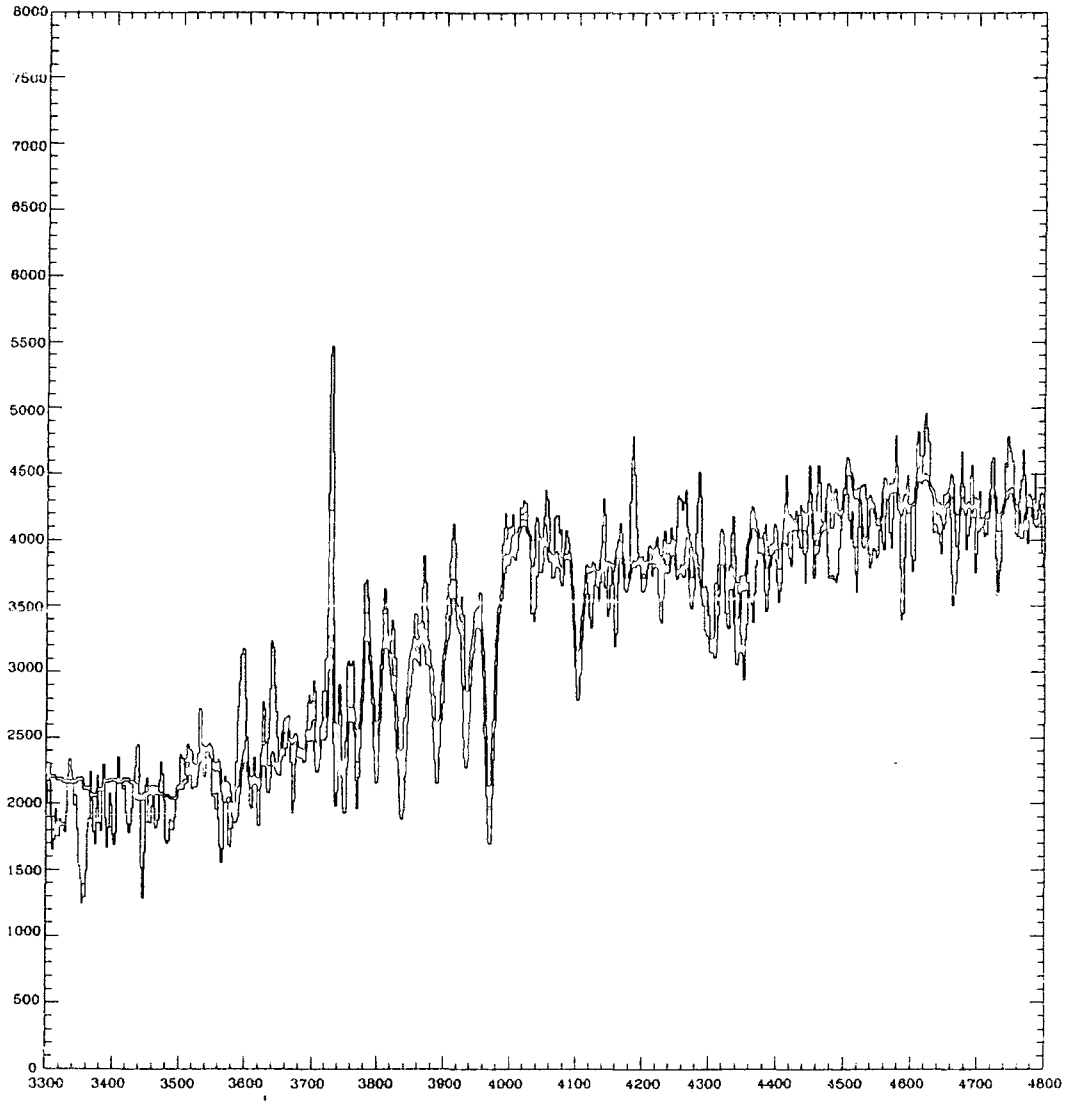


**Figure 4.8a Comparison of the coadded spectrum of galaxies selected in the range $5 < W_\lambda[OII] < 15$ (spectrum 2), with model generated spectra with half the available mass consumed over the first Gyr and subsequent star formation which has been constant for 6 Gyrs (solid curve) and 12 Gyrs (dotted curve).**

An extended c-model corresponds to constant star formation with no early enhanced rate is shown for compari son with spectrun 2 in Figure 4.8b, this model has B-V$\sim$ 0.45 – 0.55 (depending on age) which is typical of a late type

spiral. The fit here is not good, the continuum is too blue and the predicted Ca H to K ratio is too large, with noticeable infilling at $H\delta$ and lower order. The extended c-model represents the bluest spectrum that it is possible to generate for star formation which does not *decrease* with lookback time and so represents a 'benchmark' so that observed spectra which are bluer than will require non-standard star formation histories, as we shall discuss below.

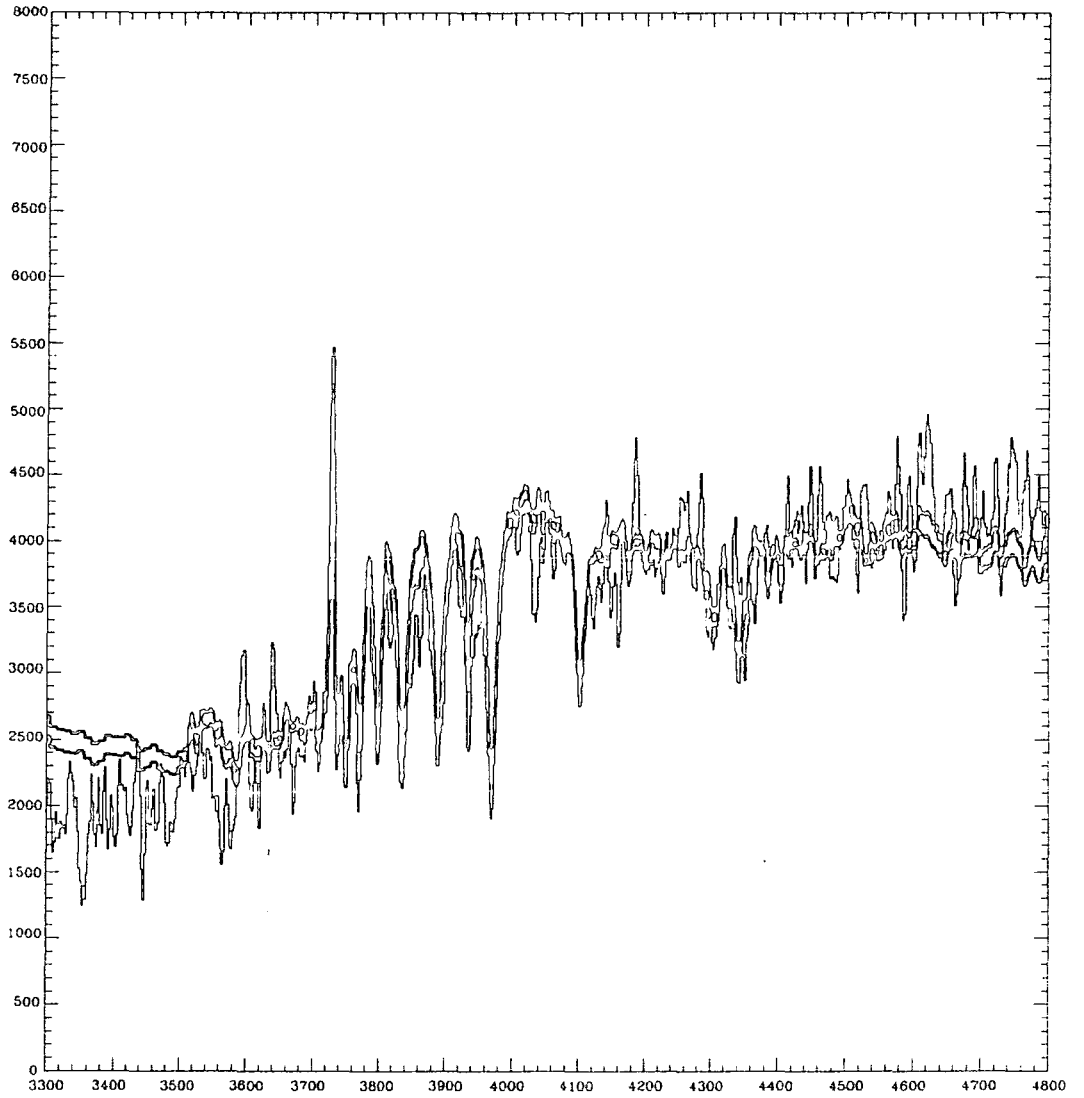


**Figure 4.8b Comparison of the coadded spectrum of galaxies selected in the range $5 < W_\lambda[OII] < 15$, with model generated spectra with star formation which has been constant for for 6 Gyrs (solid curve) and 12 Gyrs (dotted curve).**

In the higher range $20 < W_\lambda < 35\AA$ (spectrum 3) we first compare the coadded spectrum with the successfull fit for spectrum 2 (Figure 4.9a), to examine trends in spectral features. Very obviously the strength of [OII]3727Å has increased (by definition) and the continuum is bluer, indicating a trend to bluer colours at higher equivalent widths as may be expected (see Figure 4.2).

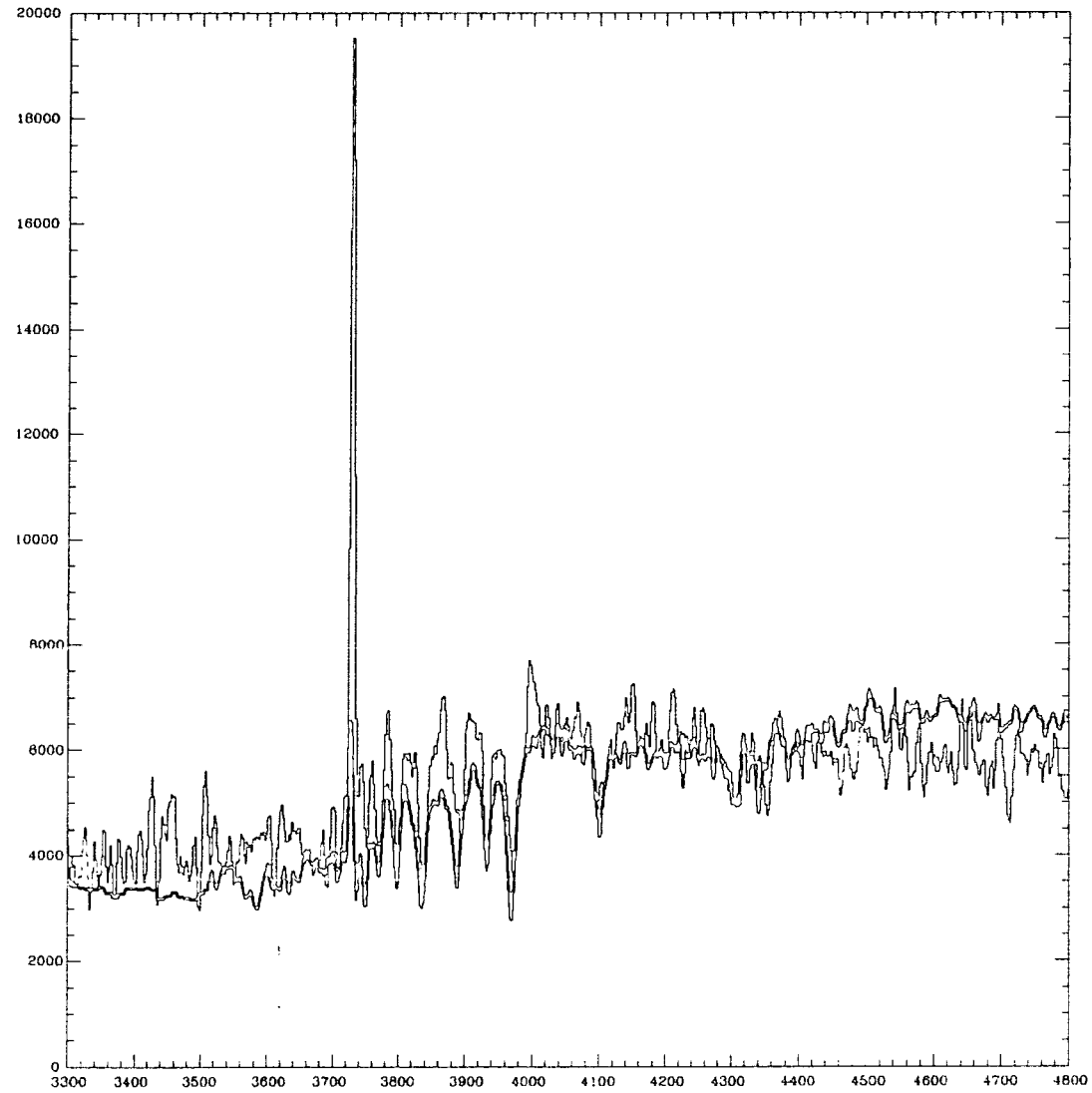


**Figure 4.9a Comparison of the coadded spectrum of galaxies selected in the range $20 < W_\lambda[OII]3727\AA < 35$ (Spectrum 3), with model generated spectra with the modelled constant star formation (12Gyrs) and initial burst consuming 50% gas.**

Importantly Ca H is of the same depth as Ca K indicating that infilling

by ongoing star formation is taking place and making shallower all the lower order Balmer lines as observed. However to reproduce spectrum 3 we cannot simply invoke a lower extinction to produce more line filling, we require a higher mean starformation rate to generate a bluer spectrum. Comparison with the 'benchmark' extended c-model, shows that a higher star formation rate, although better reproducing the Balmer features and continuum slope cannot reproduce the K feature (Figure 4.9b). It maybe that this coadded spectrum covers too large a range of star formation histories for model comparison to be meaningful, or that a suitable addition of low and high starformation components will work. A spectrum dominated by a very high rate of star formation compared to the extended c-model is not tenable however, producing negligible Ca K and too blue being dominated by A stars and for which Ca K is a weak feature.

More promising fits to spectrum 3 are produced by a combination of high and low star formation rate components, so that each has some effect on the spectrum in this wavelength range. Such a model we term a burst model, since there is a temporary increase in star formation rate in this case. What is required in order to help reproduce this spectrum is a burst strength large enough to have a significant bluing effect but not so strong that it washes out the older features. Some improvement can be achieved by for example adding a weak 2% burst of 0.2Gyrs duration to a system with 25% mass undergoing long term constant star formation (i.e. a 75% c-model plus 25% constant star formation for 16Gyrs), however given the possibility of large systematic problems associated with interpreting a coadded spectrum which may not represent a homogeneous spectral class, we will not persue this approach further until more data allow a finer division by spectral type in this equivalent width range.

Of much greater interest are spectra at the largest $W_\lambda$. Spectrum 4 covers the range $W_\lambda > 35$ which comprises $\sim$ 20% of all objects in the survey. Within the subsample examined here are 6 objects all of which have very flat spectra. We exclude from our coadded spectrum one object since its emission line properties are unusual with respect to the rest. This object has prominent Ne[III]3869Å, indicative of a high nebular temperature, inclusion would confuse the emission to extinction relationship.

Firstly comparison with the extended 'c' model (described above) is shown

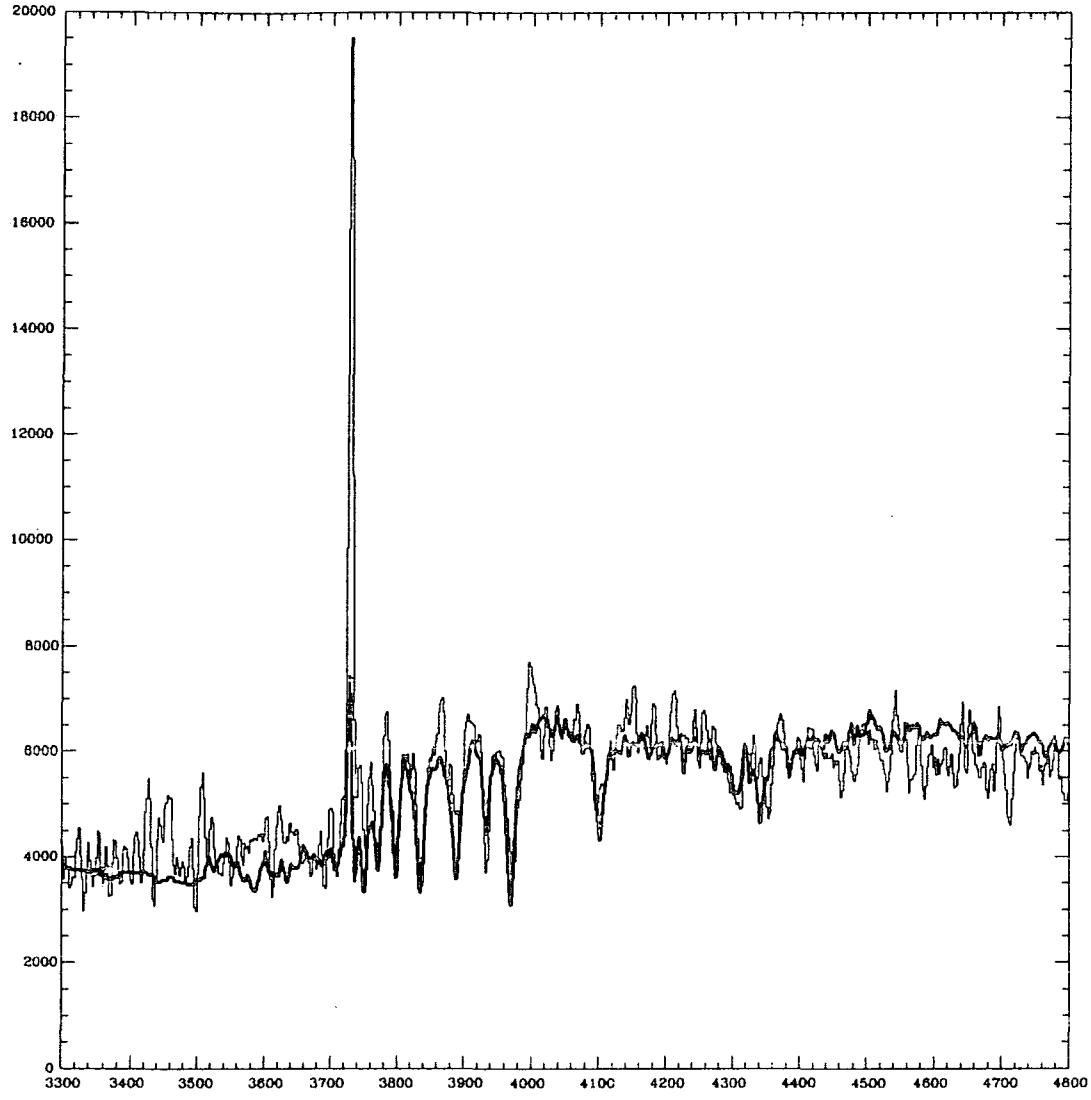


**Figure 4.9b Comparison of the coadded spectrum of galaxies selected in the range $20 < W_\lambda[OII]3727\AA < 35$ (Spectrum 3), with model generated spectra with star formation which has been constant for 12 Gyrs.**

in Figure 4.10a, clearly this class of object are undergoing very strong star formation the spectrum is much bluer than this model with very prominent [OII]3737Å, and much shallower Balmer features with emission at $H_\gamma$, and very weak Ca K.

This class of galaxy clearly do not fall on the standard spiral star formation sequence, and in order to reprduce such a flat continuum a star formation rate higher than this extended 'c' model ($> 5M_\odot yr^{-1}$) is required. A very good fit

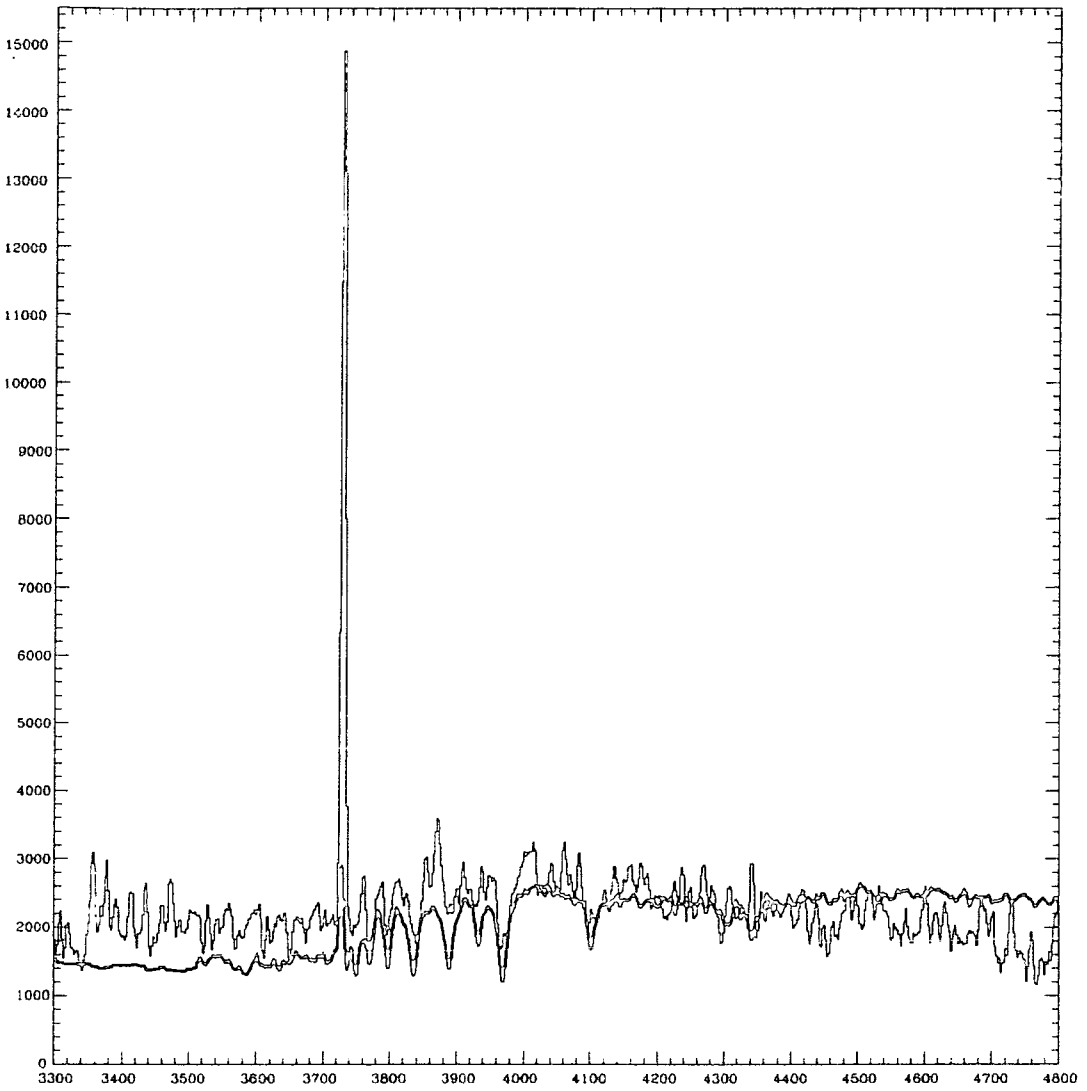


**Figure 4.10a Comparison of the coadded spectrum of galaxies selected in the range $35 < W_\lambda[OII]3727\AA$ (Spectrum 4), with an extended 'C' model viewed at 12Gyrs.**

can be produced by adding a short 0.2Gyr burst to the extended 'c' model and viewed at 0.2Gyrs corresponding to peak luminosity, see Figure 4.10b. The star formation rate is a factor 5 increased above the underlying rate in this case, with a corresponding restframe colour, B-V=0.39. Note that we choose to view the effect of a burst at peak luminosity since the probability of inclusion within the survey is greatest at this time. Peak luminosity always corresponds to the time just before star formation is stopped (see Chapter 5 for discussion).

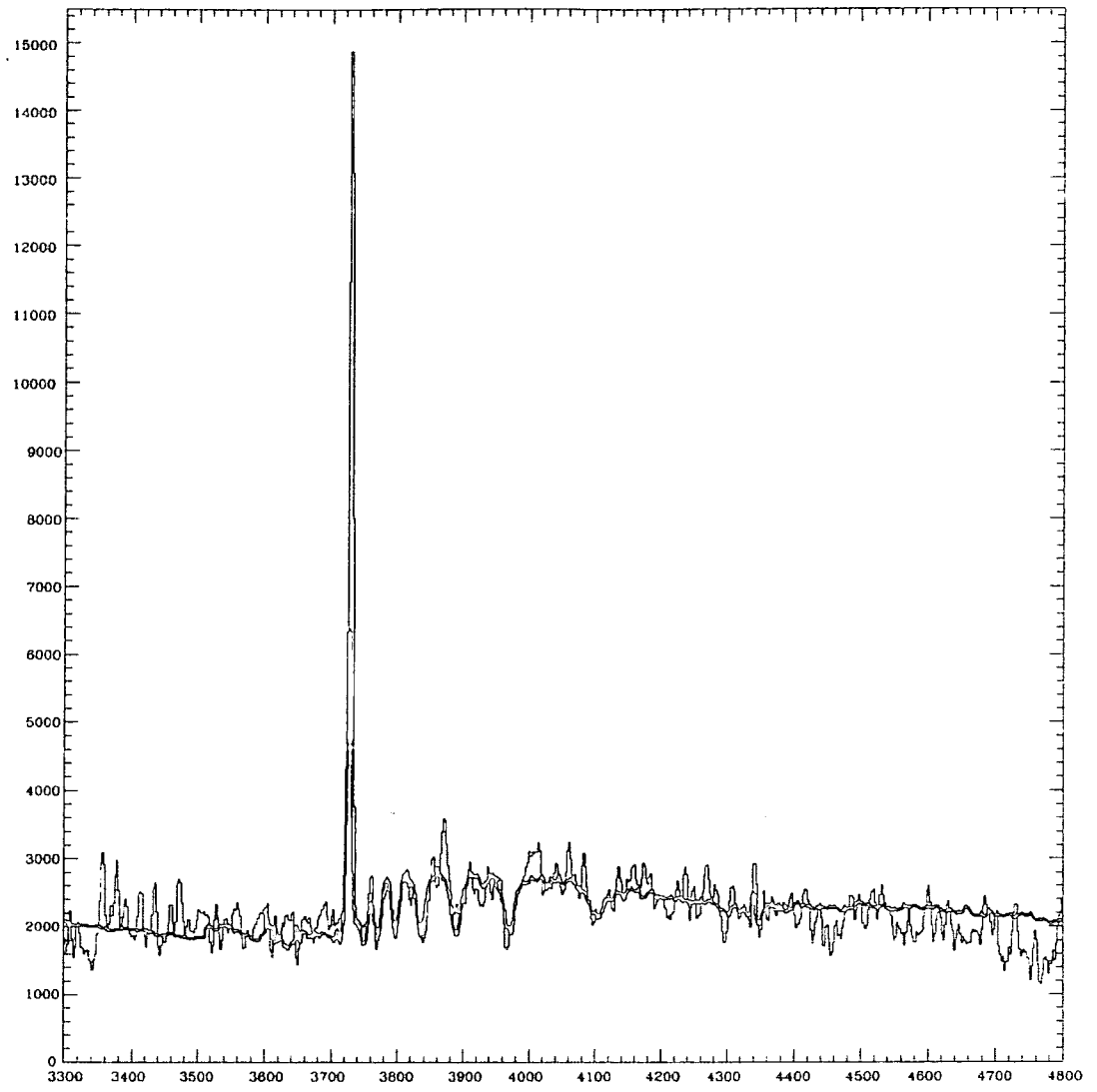


**Figure 4.10b Comparison of the coadded spectrum of galaxies selected in the range $35 < W_\lambda[OII]3727\AA$ (Spectrum 4), with a burst model consisting of an underlying extended c-model and a burst of duration 0.2 Gyrs of 3% mass.**

This model does not provide the only reasonable fit to spectrum 4. somewhat stronger bursts can be tolerated, for example a 0.1Gyr burst consuming 5% mass, added to an underlying old population (c-model) can successfully reproduce the spectral shape but with some evidence for a stronger contribution from the underlying spectrum may be suggested in order to pull down the continuum shortward of 4000Å (see Figure 4.10c). In this case the B-V colour at peak burst luminosity is 0.32 with a star formation rate of $50 M_\odot yr^{-1}$ and



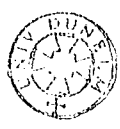

the light shortward of ~5000Å is completely dominated by the burst (the old stellar component here is very cool). Note that since a burst which dominates the light completely does provide at least a reasonable fit we may speculate that this spectrum may argue for no underlying stellar component however, the restframe colour implied for this burst would be only $B - V = 0.13$ after 0.2 Gyrs, and would be too blue for the observed colour distributions at faint magnitudes. We return to this point in Chapter 5.

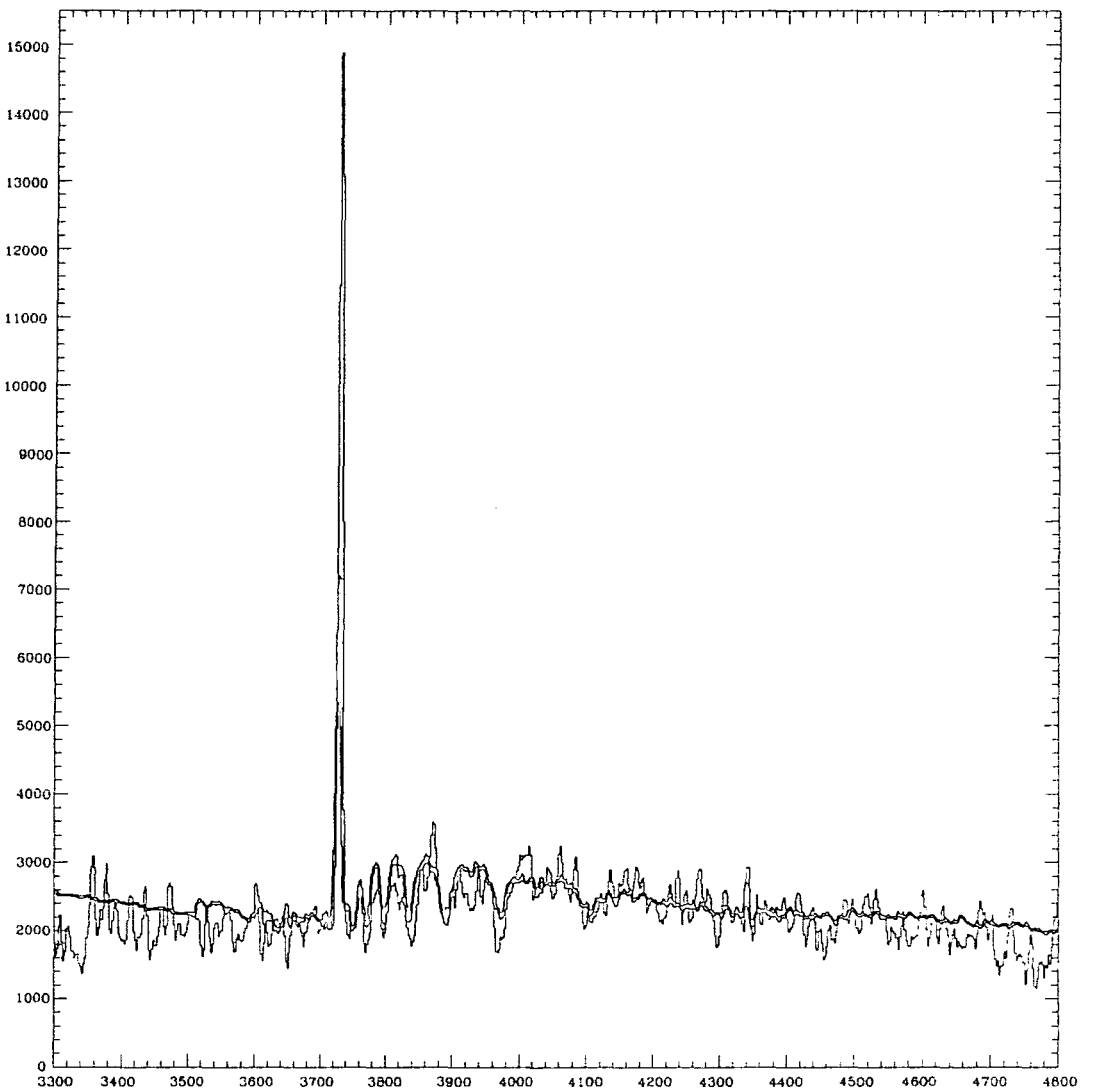


**Figure 4.10c Comparison of the coadded spectrum of galaxies selected in the range $35 < W_\lambda[OII]3727\AA$ (Spectrum 4), with a burst model consisting of an underlying C model and a burst of duration 0.1 Gyrs of 5% mass.**

Clearly then spectrum 4 demonstrates the need for a temporarily high starformation rate in this strong lined subset of our survey. A longer period of enhanced star formation is not favoured since this leads to a redder spectrum with deeper Balmer absorption lines for bursts durations longer than the lifetime of A stars ($\sim$ 0.5Gyrs).

Note also that whilst we have not complicated the problem by including the effects of reddening at optical wavelengths, reddening in strong star forming regions may be significant, in the case of Markarian or local HII galaxies which may be typical of this class, the reddening is observed to be small typically $E(B-V) \sim 0.2$ (Huchra 1977). Larger extinctions have been observed in other cases from detailed spatial studies within the central 'cores' of strong star forming systems (see Rowan-Robinson 1988), but we in the *luminosity weighted mean reddening* will imply a lower extinction by a factor depending on the spatial distribution of reddening.

### 4.5.1 Bursts and Faint Galaxy Distributions

The bursts described above clearly have a strong effect on the spectrum of the host galaxy, and here we quantify these effects on an objects $b_J$ magnitude and $b_J - R_F$ colours. Short duration bursts peak in luminosity strongly at the time just prior to the cessation of star formation. If we view the burst model of Figure 4.10c at a lookback time of $\sim$ 3 Gyrs to correspond with the mean redshift of the survey, the change in apparent magnitude after 0.1 Gyr is substantial $\Delta b_J$ = -$2^m$2. Since the survey is magnitude limited, if such bursts are representative, we will preferentially select galaxies at the peak burst luminosity. Substantial changes in colour are also expected during such a burst, after 0.1 Gyrs at $z = 0.2$, $\Delta(b_J - R_F)$ = -1.$^m$5. Note if the duration of the burst is longer and if residual star formation is present in the underlying spectrum as in the model decribed in Figure 4.10b these changes will be much less extreme, at 0.2Gyrs, $\Delta\ b_J$ = -1$^m$3 and $\Delta\ b_J - R_F = -0.8^m0$.

Modelling these changes in a statistical way over the general galaxy population for comparison with our deep photometry is pursued in chapter 5.

### 4.5.2 Summary

We conclude that for spectra with $W_\lambda[OII]3727 < 20\AA$, which is in the range typical of normal spirals, the spectra can be fitted with normal star

formation histories (see spectrum 1 and 2). However the strongest lined 20% of the sample do require high star formation rates, which we fit best with short bursts ($< 0.2$Gyrs) of star formation.

These bursts by virtue of the increase in luminosity and blue colours may have a strong evolutionary effect on the counts at faint magnitudes if as seems likely from the above modelling this form of star formation was more prominant in the past. This finding supports our earlier claim (§4.2) of an evolutionary trend based on the larger fraction of strong lined objects found in the faint redshift survey coampared with DARS.

In the next section we go on to explore what is understood of the extent of this mode of star formation locally and in other deep survey work.

## 4.6 Starbursts and local galaxy samples

### 4.6.1 DARS

We now discuss evidence for starburst activity locally and emphasise the results from DARS in particular. The DARS redshift survey is ideal for comparison with the faint survey, since the two surveys are selected in the same way i.e. magnitude limited in $b_J$, so we can compare the relative contributions of this population between surveys, and make use of the additional morphological and colour information from DARS.

As demonstrated earlier the equivalent width distribution of [OII]3727Å with $b_J - K$ for the morphologically peculiar DARS sample, shows a much larger scatter than the relation defined by the standard types (compare Figures 4.2a and 4.2b). This points to a variation in star formation properties for this sample and is perhaps the expected behaviour of a population of starburst systems: strong interactions, result in distorted optical morphologies of 'peculiar' appearance and are synonymous with enhanced star formation, producing bluer optical colours and stronger emission lines.

In fact the resulting colour and line strength depend on the relative strength of the burst and the stage at which it is observed. This spread in time will result in a large scatter in colour-colour or colour-emission line strength for such samples compared with standard sequence galaxies. These points have been demonstrated by Larson and Tinsley 1978 and Hucra 1977

and we confirm this behaviour in DARS, by comparing the colour-equivalent width distributions of Figure 4.2.

The majority of the peculiar systems in DARS have very blue $b_J-K$ colours and large $W_\lambda[OII]3727\AA$ and comprise 70% of objects with $W_\lambda > 20\AA$; the remainder classified as very late type( Sc-Im ). These objects are concentrated at lower luminosities in DARS, but for the faint survey a large contribution from these systems is found up to and beyond the mean survey redshift, corresponding to $M^*$ of the luminosity function (see Figure 4.4). The distribution of absolute magnitude and $W_\lambda[OII]3727\AA$, for DARS is presented in figure 4.11. This shows clearly that the majority of weak lined objects are sampled near $M^*$ as expected ($W_\lambda[OII]3727\AA < 10\AA$) but that the strongest equivalent widths lie at the lowest absolute magnitudes with some exceptions.

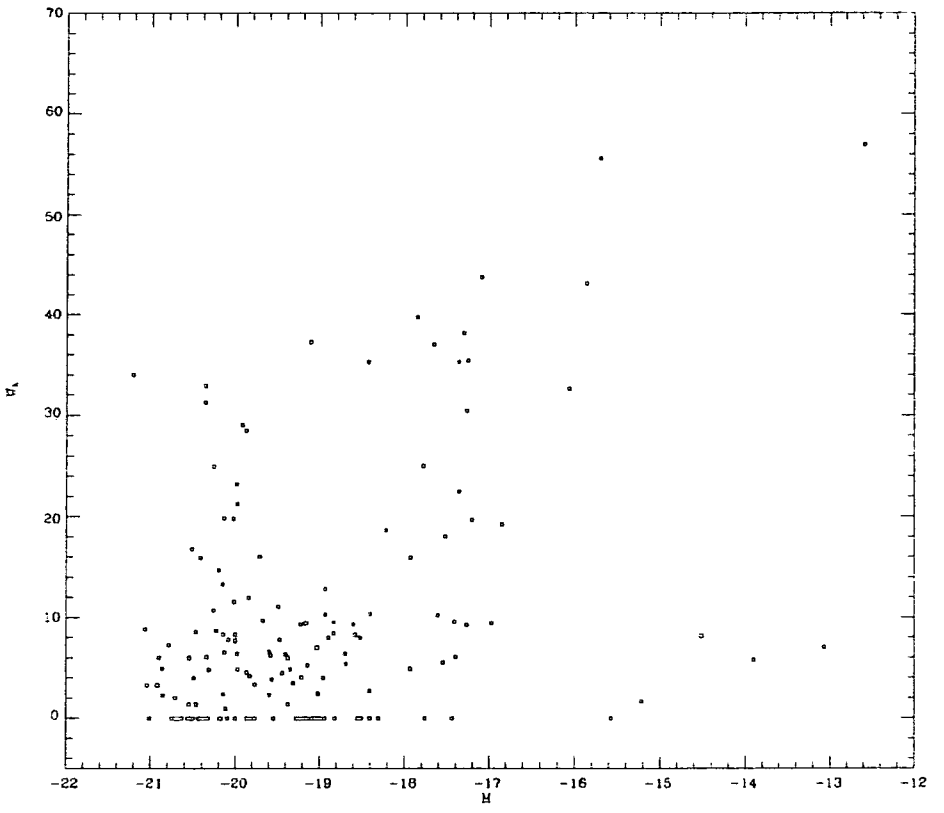


**Figure 4.11 Distribution of $W_\lambda$[OII]3727Å with absolute magnitude for the DARS survey ($H_o = 100km^{-1}Mpc^{-1}$).**

This difference in luminosities between the two surveys for the strong lined objects, may indicate an evolutionary trend in the mean strength of burst, and will be of useful in constraining models for a form of evolution which includes bursts of star formation, discussed in the next chapter.

## 4.7 Evidence for Bursts from other Surveys

There is wealth of evidence for starburst activity in other local samples of galaxies and many authors have identified and quantified the extent and strength of the starburst phenomenon. It has been demonstrated that particularly useful for large statistical studies of this class of objects, are samples selected in the UV and thr far-infrared (FIR). At short optical and UV wavelengths the luminosity from the excess of young stars formed during a burst is preferentially radiated, and absorption of Lyman continuum photons, produced by the most massive stars ($> 10M_{\odot}$) by dust results in subsequent reradiation at FIR wavelengths . This point has been amply demonstrated from follow-up work of IRAS selected galaxy samples (Rowan-Robinson 1988, Leech *et al* 1988). Extragalactic sources selected at 60 microns show, in the main, sources with anomalously high FIR to optical flux ratio's, the FIR spectra of which can be most successfuly modelled by the inclusion of a starburst component (Rowan-Robinson and Crawford 1988).

Of greater interest for our purposes are the effects on optically selected samples of this mode of starformation. As discussed above large changes in luminosity and colour can result from only small amounts of star formation if the timescale over which stars are formed is short. This property of short duration bursts was first examined by Searle *et al* (1973) and later by Larson and Tinsley (1978), to help account for the bluest UBV colours present in optically selected samples. Larson and Tinsley compared the Shapley Ames galaxy sample, with the Arp atlas of mophologically peculiar galaxies. The larger scatter and bluer colours for the Arp objects in the U-B, B-V two-colour distribution they concluded is easily accounted for by incorporating short bursts of star formation ($< 0.2Gys$) onto the colour-colour locus of the normal galaxy sequence. This claim for starburst activity was made in essentially the same way as the earlier work of Searle *et al* (1973) (via stellar synthesis codes and two colour data), but is based on better defined samples and in addition, provides direct morphological evidence of the importance of galaxy interaction as instrumental in the temporary enhancement of star formation, a link now

clearly established in much of this kind of work.

Huchra (1977b) has explored the question of the local blue galaxy populations by including in a UBV analysis modelled Balmer emission line strengths, in much the same way as in the analysis of §4.4. For a mixture of ordinary field and various blue galaxy samples predominantly Markarian objects, he concludes that 'composite' or burst galaxy spectra provide the only reasonable interpretation for the colours and star formation rates implied by the $H_\beta$ emission line strengths, i.e they are not simply young systems.

Extensions of this form of analysis to determine the ratio of the 'instantaneous' star formation rate, derived from hydrogen recombination line strengths, with the time averaged past rate has also been studied as outlined in chapter 3.9. Hunter and Gallagher (1986) have applied this sort of method to a large sample of late type and dwarf galaxy samples and also conclude near constant star formation rates no evidence for strong bursts of star formation. This is a suprising claim for the dwarfs in their survey given the above discussion and in view of the very blue B-V colours and flat strong emission line spectra of a large fraction of their large dwarf galaxy sample. These spectra and colours are very similar, in a large number of cases, to the results of the strong lined spectra presented here in §4.6. However, these authors use the B magnitude to estimate the past average star formation rate - a procedure fairly safe for smooth star formation histories, but in the case of short bursts the B magnitude cannot be used in this way. In §4.5 we demonstrated that large increases in B can take place during a short burst of star formation, accompanied by stronger emission lines. These effects will, under Hunter and Gallager's assumptions, tend to go unrecognised, they may misinterpret such objects as having high star formation rates but steady over a large time. Thus the assertion by these authors that bursting sources are not a significant feature of the local galaxy population may be understood as a deficiency of their technique, particularly as applied to dwarf systems. In fact the conclusion of Thuan for a sample of blue compact dwarf galaxies (Thaun 1988) concludes the opposite, that these systems are undergoing strong bursts and that many examples exist locally.

Local estimates of the space density of the starburst class of object are hard to establish given their rarity, but of great interest for establishing rates of evolution by comparison with the faint survey. The extensive and thorough

survey of local nuclear starburst galaxies of Bolzano (1983) has however, been able to reliably established that this class of object comprise at least 3% of the field galaxy luminosity function to the low luminosity limit of $M_v$=-17.5, consistent with the fraction of anomalous sources observed in DARS.

## 4.8 Evolution and Other Faint Survey Work

In the following discussion we attempt to bring together conclusions regarding evolution from samples other than the optical field galaxy studies of this Thesis. Field counts at faint radio fluxes and deep field far-infrared counts are beginning to provide interesting information on the evolution of field galaxies. Also of great interest is the large body of information regarding evolution at optical wavelengths, from studies of high redshift rich clusters.

### 4.8.1 High Redshift Cluster Photometry and Spectroscopy

The earliest compelling evidence for evolution at optical wavelengths was presented in the broad band photometric work of distant cluster samples presented by Butcher and Oemler 1978. The evidence for evolution rested on a comparison of the colour distributions for these clusters and those expected on the basis of low redshift rich studies (also quantified Butcher and Oemler 1979). Although little evolution was found in the colour of the E/S0 sequence galaxies there appeared a clear excess of bluer systems in the direction of the distant clusters (termed the 'BO' effect). Further large survey photometry of a sample of southern distant clusters by Couch (1985) confirmed this evolutionary excess of objects bluer than the expected E/S0 sequence.

Subsequent spectroscopy has allowed a very clear and suprising interpretation of this excess, as predominantly composed of systems with either evidence of very recent strong star formation or systems undergoing strong star formation. The former have been christened 'E+A' galaxies by Dressler and Gunn (1983), since the combination of an early type galaxy spectrum and an A star component provide an excellent fit to the spectra of this class of object. These systems have no apparent ongoing star formation but have by the presence of A star like spectral features, very obviously been forming stars within $< 0.5$Gyrs (lifetime of an A star). Furthermore the fractional contribution of young stars required imply that prior to the cessation of star formation, the rates required to account for the strength of the Balmer emission features, have been very

high and for this reason these systems have been more popularly dubbed 'post-starburst galaxies' (PSG). PSG's are common to all spectroscopic studies of the distant cluster samples, Dressler (1983,1984) and Lavery and Henry (1986) Sharples *et al* (1985) Couch and Sharples (1987).

The Strong emission line class form a lesser component of the blue galaxy excess, but have been the subject of much study. Lavery and Henry find that for 3 Abell clusters at the relatively low redshift for cluster work of $z \sim 0.2$, a relatively large fraction of the blue strong lined cluster galaxies. Measured $W_\lambda[OII]3727\AA$ for these objects are high in range $30\AA < W_\lambda[OII]3727\AA < 100\AA$, and interestingly comparable in strength and redshift to the strong lined objects of the faint redshift survey. This type of object has also been identified in the very comprehensive spectroscopic survey work of 3 rich southern clusters of Couch and Sharples (1987) at $z = 0.3$. Couch and Sharples present a unifying picture of the the PSG and strong lined objects as the products of starburst activity the presence of strong emission lines or anomalously deep Balmer features depending at which stage during the burst objects are 'caught', a picture supported by the UV-optical photometry of Maclaren *et al* (1987). However the interpretation of the Butcher Oemler effect is complicated by the large variations in fractional blue galaxy content between clusters, which does not have a clear dependence on redshift (Ellis 1987).

Comparison with field galaxy evolution may not be so straight forward, clearly a very much smaller fraction of PSG's are observed in our survey (see Appendix II). One important selection effect that may be of interest in this context is the choice of passband which for the deep cluster spectroscopy discussed above is nearly always R. In §4.5 we demonstrated how the change in magnitude of a burst varies as the burst progresses peaking during the star formation period and falling away quickly once star formation has ceased. The effect produces in larger magnitude change in B relative to R, since B selection is weighted strongly by the large relative increase in luminosity during the star formation period, especially for short bursts, with the result at a given redshift B selected samples will contain a greater ratio of bursting to PSG'S than for R selected samples. In fact for R this ratio will tend to be weighted by *time* rather than luminosity, and in the case of short bursts favours sampling the post burst stage which is of order $\sim$ 0.5Gyrs (Lifetime of A stars) since, the

response of the spectrum to a burst is relatively flatter in this passband.

We may also expect a redshift dependence in selection of this form of evolution since if, as indicated above, bursts are more common for less luminous systems then to the same apparent limiting magnitude clusters sampled at different redshifts will reveal a differing proportion of bursting sources. This redshift dependent selection effect is clearly demonstrated in the faint redshift survey spectra; to the limit $b_J = 21.5$ the fraction of strong lined objects falls off rapidly with redshift beyond $z = 0.2$, and this magnitude represents the current limit of faint object spectroscopy for any deep spectroscopic study.

In addition Maclaren *et al* (1988) has speculated that superimposed on a general pattern of evolution a cluster dependent time clock may operate, presumably connected to the dynamical history of a cluster, which may account for the large scatter the appearence of spectral evolution between clusters, with the possible result of disguising the presumed redshift (time) dependent nature of evolution.

However, despite the apparent lack of homogeneity in cluster samples, bursts of star formation are clearly of importance constituting the majority population responsible for the colour evolution observed for rich cluster samples.

So the idea that *some* galaxies undergo short bursts of star formation is familiar from distant cluster spectroscopic studies and considering the different environments the similarity in the form of evolution implied in both sets of data points clearly to bursts of starformation as a very important evolutionary process.

### 4.8.2 Faint Radio Source Counts

The recent extension of the radio source counts to milli-Jansky and submilli-Jansky levels has revealed an upturn in these counts suggestive of a new population of sources at these faint levels. This upturn is now firmly established for several well separated fields and of the same form at both 21cm (Windhorst 1984, Condon and Mitchell 1984) and 6cm (Fromalont *et al* 1986, Donnelly *et al* 1987). Modelling of the radio source counts has indicated that the excess at these faint flux levels, indicates the presence of a count excess with a Euclidean slope (Condon 1984) which has been variously interpreted, along the same lines as the optical B count excess, and as in the optical, multicolour and redshift information have been most useful in constraining the

possibilities.

A brief history of these developments is sketched below, since it now appears to very closely parallel the course of the interpretations of the counts in B, indeed as we shall show below the starburst evolution presented in this chapter may manifest itself as both the optical B and milli-Jansky radio count excesses.

Without reliable redshift and colour information, initial guesses for the turn up in the counts at these faint flux levels ranged from very strong radio luminosity evolution of ordinary spirals (Condon 1984), presumed related to possible large increases in star formation rate for this population to $z \leq 0.8$. Alternatively Subrahmanya *et al* (1983) speculate that a low redshift low luminosity population will produce a steep count slope (in the same way as the optical dwarf count models discussed in 2.9). The initial follow-up work of optical identification with the deep Westabork field of Windhorst's' thesis (1984) was carried out on 4m prime focus photographic plates in UBFN passbands by Koo *et al* (1985). These plates providing secure source identification for 70% of the sample for $S_\mu > 0.6$mJy) to a limit of $B \sim 23.5$. On the basis of these identifications and the resulting optical colours, the simplest interpretation was that, as expected the majority of sources were red and represented passively evolving 'Standard Candle' elliptical galaxies found at higher radio fluxes. The remaining bluer sample was readily presumed, (in the spirit of the early conclusions for Bruzual models applied to the 3C bright radio sample, see Lilly and Longair 1982), to be the earlier strong star forming counterparts of the red population.

However follow-up spectroscopy to $F < 21$ showed that whilst the reddest objects sampled (to a maximum redshift of $z = 0.6$) did indeed follow a passively evolving bright elliptical galaxy prediction as expected, one third of the sample comprising the objects lying blueward of the elliptical colour-redshift locus lay in the lower redshift range $z < 0.3$. So far from being the high redshift precursors of red elliptical galaxy population, these blue objects form a separate lower redshift population of sources and are responsible for the turn-up in the radio count at milli-Jansky fluxes. Interestingly Koo *et al* note that this blue population is also characterised by peculiar optical morphologies, with examples of high surface brightness-compact objects and interacting or merged sources.

A small number of very low redshift ($z < 0.05$) sources were found at bright magnitudes $F' < 16$ displaying spiral morphology which are an expected minority contribution from local ordinary objects with radio properties typical of normal spirals, which fall into the radio selected sample by virtue of their proximity. These ordinary local objects provide a useful comparison with the majority morphologically peculiar blue sample, since their radio/optical flux ratios may be considered normal, and Koo *et al* calculate this ratio is on average 10 times greater for the majority blue population at $16.5 < F < 21$, indicating unusual radio activity more typical of non-seyfert Markarian or interacting galaxies observed locally (see Beirmann *et al* 1985).

Deep field VLA images and further optical identification extended to deep CCD photometry, have emphasised these results and have clearly demonstrated that the upturn in the radio counts at mJy and sub-mJy levels is the result of intermediate redshift blue sources. Koo *et al* (1986) present an optically complete sample to sub-mJy levels, $S_\mu > 0.1$mJy, and redshifts complete to $R < 20$ (20 sources in total). They conclude that the presence of the same blue population identified at mJy fluxes, but this population is proportionally much greater at sub-mJy levels following the upturn in the souce counts, with redshift range $z < 0.3$. This sample is also characterised peculiar optical morphologies and emission line strengths which are indicative of strong starformation activity.

Thuan and Condon (1987) have obtained deep near infrared photometry for another deep VLA field (Condon and Mitchell 1984) to sub-mJy levels with partial redshift information to $b_J < 21.5$ Again the conclusion of these authors is that the count excess at the sub-mJy level is dominated (almost exclusively) by systems which are are very blue. To $b_j < 21$ a complete optical sample has a mean $b_J - K = 3.8$, with 40% which are very blue; $b_J - K < 3.0$, and can be compared in colour to the optically selected peculiar systems at bright magnitudes from DARS (Figure 4.2b).

Thuan and Condon claim evidence for a starburst population at intermediate redshifts based on these colours and limited emission line data - a result also put forward by Donnelly *et al* (1987) on the basis of radio properties and optical colours. The bluest systems they point out, have the most compact radio sources, and combined with the radio spectral indices found for this population indicate, by comparison with local well studied starburst systems,

that this blue galaxy faint radio are starburst systems and responsible for the evolution implied by the steep radio count slope at sub-mJy levels. Donelly *et al* argue, based on the redshift range of their data ($z\sim 0.25$), strongly against the suggestion of a non evolutionary explanation for this excess.

There is then at sub-mJy levels a striking similarity with our faint redshift survey results, namely that a population exists in both samples of strong star forming objects at the same magnitudes, $b_J < 21.5$, producing an evolutionary excess in both sets of counts.

It is possible to examine this connection further by asking how much of the optical count excess are sources are identified as in the radio to sub-mJy levels. The sample of Thuan and Condon is of particular interest in this respect because identification is carried out on $b_J$ Schmidt plate to $b_J = 21.5$, which is the magnitude limit of our faint redshift survey. Thus the sub-mJy and optical count excesses can be compared very directly. In fact, 45 of 159 images identified in the VLA field to 0.1mJy covering an area, $30' \times 30'$, lie in the range $b_J < 21.5$. The radio count excess in $b_J$ based on Thuan and Condon's data is 180 galaxies $degree^{-2}$, for images down to 0.1mJy with complete optical identification to $b_J < 21.5$. Sources at lower flux levels may of course lie at $b_J < 21.5$ so that this surface density represents a minimum count to this magnitude limit. Some contribution from the passively evolving E/S0 population and from ordinary but local spirals is expected, and from spectroscopy by Koo *et al* (1986) this is estimated as <30%.

The field average integrated optical count to the same limit, $b_J < 21.5$, is $\sim 1400 \pm 200 deg^2$ (see Figure 2.5). Assuming the same percentage error on the optically identified sub-mJy count means that the blue radio count excess represents at least 10%–17% of the total optical counts to this magnitude, i.e. it is consistent with the optical count excess based on the spectroscopic results of this Chapter and the count slope discussion of chapter 2, which is calculated to lie in the range 15%–30% to $b_J < 21.5$

This result of great interest for the interpretation of the optical evolution discussed in this thesis, since it indicates that the starburst galaxy population representing the evolution in the radio at sub-mJy levels are the same class of objects sampled in the optical and responsible for the evolution observed in the faint radio source counts.

This coincidence if confirmed by larger sub-mJy samples, strengthens considerably our conclusions for the nature of the optical evolution. Our result of strong evolution in starburst activity is based essentially on the spectra of the strongest emission line systems sampled in the redshift survey and the requirement of evolution implied by the steep count slope in B. The faint radio source count evolution is also best explained in the same way but is argued *completely idependently*, based on the radio properties: the evidence for starburst activity is based on large radio/optical flux ratios, the steep radio spectra and compact radio morphology of the blue galaxy population.

Finally of direct interest in the context of star burst evolution is the IRAS deep survey (Houck and Hacking 1987) however, the mean apparent magnitude of optically identified images in the deep field FIR images reach only B$\sim$ 18.5 with 90% optical completeness over $6.25 deg^{-2}$. Houck an Hacking claim that evolution may be present to the limit of their deep data, $S_{60\mu} > 50$mJy based on FIR count slope models. At face value, strong evolution is required, and these authors identify starburst galaxies as the obvious candidate for evolution. In any case an evolutionary trend in this population may be expected since good correlation is found between radio-FIR fluxes (de Jong 1985) and we know from the radio source count discussion above that this population are found to show strong evolution (independent of the optical evidence).

Spectroscopic redshift survey or deep radio follow-up work in this area will help reveal the strength and nature of the evolution implied by these IRAS faint source counts, but for now we note an interpretation of these counts in terms of evolution of a starburst population is not unexpected in light of the discussion above.

## 4.9 Summary and Conclusions

The results of this chapter both from a detailed spectroscopic of our faint survey and from comparison of this survey with local and other deep field data has pointed clearly to strong evolution of starburst activity over recent epochs. The evidence for this is now listed,

i) The equivalent width distribution of [OII]3727Å of objects sampled in our faint survey is very extended to high values by comparison with DARS. We conclude that random and systematic sources of error cannot account for this difference, and that more strong emission line objects are sampled at faint

magnitudes than locally.

ii) Detailed spectral modelling of the star formation properties of the faint galaxy sample reveal that at least 20% are undergoing anomalously strong star formation best explained by short duration ($\leq$0.2Gyrs) bursts of starformation in otherwise quiescent stellar populations.

iii) This mode of star formation is locally rare and restricted to very low luminosity galaxies. By $z \sim 0.2$ short duration bursts have an important evolutionary effect, and this form of evolution is consistent with evolution found in other deep survey work. In particular the evolution required by the steep faint radio source counts and redshift distribution has been strongly suggested to result from starburst activity, based on independent radio emission properties.

iv) The effects of even a small burst of star formation (if the burst duration is short), has a large effect on the host galaxy luminosity and colour and must therefore have an important effect on the faint galaxy counts and colour distributions, and may account for the evolution implied by these data.

The last point is fully explored in the next chapter where we go on to develop an evolutionary model for comparison with the faint galaxy photometry and redshift distributions by including recurrent starburst activity in low luminosity systems.

# Chapter 5.

# STARBURST MODELS OF GALAXY EVOLUTION

## 5.1 Introduction.

In the previous two chapters we have presented the need for a new description of galaxy evolution at faint magnitudes. The most popular expectation, namely that evolution of the general galaxy population would result from smoothly declining star formation rates over a Hubble time, has not been supported by the faint redshift survey redshift distribution analysed in Chapter 3.

In Chapter 4 we examined the star formation histories of objects selected in the faint survey, revealing the possibility that short bursts of strong star formation were a common feature of field galaxies by $z = 0.2$. Comparison of the spectral properties of this faint sample with the brighter DARS survey also reveals clear evidence of a strong evolutionary trend for increased star formation at faint magnitudes.

This aim of this chapter is to develop new models for describing the faint galaxy counts colours and redshift distributions, including only starburst activity. Bursts of star formation, if common over recent epochs, will clearly have an important effect on the faint galaxy colours and luminosities, as demonstrated in 4.5, adding an additional blue and luminous population to the counts and colour distributions.

## 5.2 Model Constraints and Requirements

A number of very basic points can be made about the role of bursts in galaxy evolution. From local redshift surveys we know this activity is present for $\sim$5% of the general galaxy population (see discussion in 4.6) and so we may expect this form of activity to be recurrent for a typical burst timescale of $10^8$yrs, since this represents only $\sim 1\%$ of the Hubble time. A burst rate of a few per Hubble time is required on the simplest assumption that these events are shared by the whole galaxy population. Restricting this activity to a subset of the population will push up this rate, and furthermore from the discussion in 4.4 this class of object represent at least 20% of objects sampled in the faint

survey by $z \sim 0.2$. Importantly we may naively expect stronger bursts in the past resulting from the larger available gas content at earlier times, and hence an evolutionary trend.

Unfortunately theoretical work in the area of general star formation has proved fairly fruitless in describing even the simplest cases of star formation (see reviews by Silk (1986), Schramm (1988) for a discussion of the likely physical complexity of this problem), although realistic numerical modelling is now making some progress (Struck-Marcell and Scalo 1987). However, for the purposes of the models presented here we require only a statistical description of this mode of star formation. For this we require knowledge of the time scale characterizing such activity, the star formation rates and initial mass functions and a plausible picture of how these may evolve.

These basic burst properties do have observational constraints both from our analysis of Chapter 4 and from well studies local examples of this phenomenon, these are now detailed:

i) The spectral evidence of chapter 4.4 indicates that burst of star formation are short $\sim 10^8$yrs. This short timescale for star formation has the consequence that even if only small amounts of mass are involved in the burst the light in the UV and B passbands can be totally dominated by the burst (see Chapter 4.5). This is especially true if the underlying galaxy has a cold UV spectrum i.e little or no ongoing star formation and becomes increasingly more important at higher redshift, where the contrast between the burst spectrum and a UV cool underlying spectrum is greatest. For the same mass of gas, longer duration bursts note, are more difficult to detect, resulting in spectra which resemble late type spirals whilst forming stars, with relatively small changes in luminosity and colour compared to a shorter burst.

ii) The observed redshift distribution taken together with the steep count slope imply that evolution must have a differential effect with galaxy luminosity, so that the luminosity function is steeper in the past (see chapter 3.11). In fact we observe the strongest emission line objects to lie in the lower end of the redshift distribution (see figure 4.4) which emphasises that star formation events are more prominent in somewhat lower luminosity galaxies.

iii) The form of the initial mass function (IMF) of strong star forming regions has been the subject of much recent debate. A consensus has developed that standard IMF's are too abundant in low mass stars to support star formation for timescales greater than only $10^7$yrs in many locally well studied examples of this phenomenon, given the available gas supply. Silk (1985) and Larson (1986) argue that star formation may in general be the result of a bimodal IMF, with a high mass mode being dominant during burst star formation. Direct indications that burst mode star formation is restricted to high mass stars only ($>\sim 3M\odot$), comes from UV spectral features and from consideration of the UV spectrum and far infrared luminosities of Markarian type objects (Villefond & Thuan (1983), Augaurde &Lequeux (1985)) and from the distribution of emission over all wavebands from the detailed study of M82 (Rieke *et al.* 1984) Although it may be premature to generalize these results to all starburst activity, we do explore the effects of IMf's with only high mass stars.

Taken together i) and ii) imply a simple evolutionary process in which short bursts of star formation lift the luminosity of a some fraction of galaxies, the quiescent luminosity of which would otherwise lie below the limit of a magnitude selected survey, into the observed sample. This process must go on in such a way such that only systems well below $M^*$ of the luminosity function can host the large changes in magnitude implied by the strongest line spectra. This is a strong constraint on the model, we cannot produce significant numbers of high luminosity burst galaxies or we will be inconsistent with ii) and yet even small bursts on the timescales implied by i) will produce large increases in luminosity. Below we suggest a simple physical model in which we naturally expect such a differential evolution, and we make use of the above observational constraints to parameterise the star formation.

## 5.3 A Quantitative Description of Burst Evolution

In this section we attempt to reproduce the faint survey mean redshift and photometric distributions discussed in Chapter 2, using the above observational constraints and with physical arguments where possible. Comparison with the faint galaxy distributions, principally the redshift distribution of the faint survey and the slope of the observed $b_J$ number counts, we assess for example, how common the bursting phenomenon has to be, and derive crude limits on the

range of star formation properties involved.

It would seem reasonable that only galaxies known to have appreciable gas contents should host bursts and so we restrict this activity to spirals which constitute 70% of the field population (see table 2.1). We assume for simplicity that the dominant evolutionary effect is not an increase in the frequency of burst with lookback time but a trend towards larger bursts in the past. Increasing the frequncy of bursts without changing their strength does not lead to a strong gradient of evolution, whereas a decline in burst strength can achieve a strong effect on the counts, and is naturally understood given the larger fractional gas content available at earlier times.

The first and simplest form of evolution examined is the case of burst star formation of a fixed mass, i.e. independent of galaxy mass, which we then go on to generalize into a more flexible model taking account of the gas available for star formation.

### 5.3.1 Mass Independent Models

As indicated above we require a form of evolution which is differential with galaxy luminosity in order that we do not evolve the bright end of the luminosity function significantly, in line with our conclusion of Chapter 3.11. A strong differential effect would be the natural consequence of bursts of star formation characterised by a narrow dispersion of mass, one might speculate, for example, that a certain 'critical mass' may be required for this mode of star formation.

For example in the case of a fixed mass of stars formed in a burst the the luminosity produced at a given time during a burst, $L_b$, may be large in comparison with the underlying luminosity, $L_g$, being greatest for a small system but can have a negligible effect on the luminosity of a more luminous galaxy. At a given time after the start of a burst, the change in absolute magnitude of a galaxy we denote as $M_{bg}$, which can be linked to $L_b$, and $L_g$, via,

$$\Delta M_{bg} = 2.5 \log (L_b/L_g + 1) \tag{5.1}$$

at an arbitrary reference magnitude, $M_{go}$, (discussed later), we can write down the change in magnitude as a function of galaxy absolute magnitude, $M_g$, as

$$\Delta M_{bg} = 2.5 \log \left( \frac{10^{0.4\Delta M_{bgo}} - 1}{10^{0.4(M_{go} - M_g)}} + 1 \right) \tag{5.2}$$

This dependence of burst strength with absolute magnitude is plotted in Figure 5.1 for a range of $\Delta M_o$, showing clearly that a 'fixed burst' luminosity can produce a large differential effect, even over only a small range in magnitude about $M_{go}$. This model is only one possibility for a differential form of burst strength and host luminosity, and we now outline a more general differential model for which this model is a limiting case.

### 5.3.2 Gas Dependent Models

Linking the total mass of stars formed during a burst to the total gas available for forming stars (we take HI as an indicator of the total gas content), is straigthtforward to model. We assume that the that the star formation rate (SFR) averaged over a burst is simply proportional to the gas content, in other words a given burst consumes a fixed fraction of the available gas.

Furthermore, since lower luminosity (and generally later type, see Table 2.2), galaxies are observed to have typically the largest available gas contents there will clearly be a differential effect of increased burst strength with decreasing host luminosity, as required.

Such a relationship can be parameterised from observation so that the gas content of a galaxy $m_{\rm HI}$ is related to its luminosity, $L_g$, via a relation of the form,

$$L_g \propto {m_{\rm HI}}^{\beta} \tag{5.3}$$

where $L_g$ is measured in the B passband. Observed values of $\beta$ are greater than 1.0 for late type systems (Comte 1985), implying a greater gas mass fraction to B luminosity for lower luminosity galaxies. Unfortunately, appropriate data for the full range of types is not yet available and uncertainties in this correlation from variations with mass/light ratio with galaxy luminosity, suggest that the observations may underestimate the value (Bothun 1984, Salucci, private comm.).

If we assume $SFR \propto m_{HI}$ i.e. taking HI to indicate fractional gas content, this implies, $L_b \propto m_{HI}$, where $L_b$ is the luminosity of the burst componant only, or for a given galaxy mass-to-light ratio we have,

$$L_b \propto L_g^{1/\beta} \tag{5.4}$$

and normalising to galaxy of $M_{g_o}$ as in equation 5.2 we have,

$$\Delta M_{bg} = 2.5 \log \left( \frac{10^{0.4\Delta M_{bg_o}} - 1}{10^{0.4(\frac{\beta-1}{\beta})(M_{g_o} - M_g)}} + 1 \right) \tag{5.5}$$

Note this equation does not depend on the observations referred to above (equation. 5.3), it can be considered as a more general empirical relationship where the choice of $\beta$ simply determines the relative dependance of burst luminosity on galaxy luminosity. This expression has the advantage of being flexible, covering a large and interesting range of possibilities. For example in the case $\beta = 1$, or star formation during the burst proportional to galaxy luminosity, this relation reduces to $\Delta M_{bg} = \Delta M_{bg_o}$ i.e. independent of galaxy absolute magnitude. At the other extreme for large $\beta$, expression 5.5 reduces to 5.2 i.e. burst luminosity independent of galaxy luminosity. This point is demonstrated in Figure 5.1, $\beta = 5$ closely matches case 2 (same $\Delta M_{bg_o}$) of the 'fixed mass' model. The case $\beta \sim 1.5$ also shown, corresponds roughly to the observed variation of gas mass with galaxy luminosity.

In calculating the effects of bursts we must also include the time dependence of the burst luminosity. Denoting the time from the start of the burst, $t_b$, we normalise to $\Delta M_{bg}(t_b)$ at $t_o$, the time corresponding to peak burst luminosity for $M_{bg_o}$. (this time is always just prior to the cessation of star formation), and given by

$$\Delta M_{bg_o}(t_o) = 2.5 \log \left( \frac{10^{0.4\Delta M_{bg_o}} - 1}{L_b(t_o)/L_b(t_b)} + 1 \right) \tag{5.6}$$

which is substituted into equation 5.5, to give the general change in absolute magnitude as a function of time after the burst commences and for arbitrary absolute magnitude. Note the denominator is the ratio of burst luminosity to peak burst luminosity and for this we require the stellar synthesis code to generate the time-dependent restframe spectra of the burst spectrum. This set of spectra are then used to detemine the relative changes in the burst component luminosity, after specifying the star formation parameters of the burst and the transmission curve for the passband of interest.

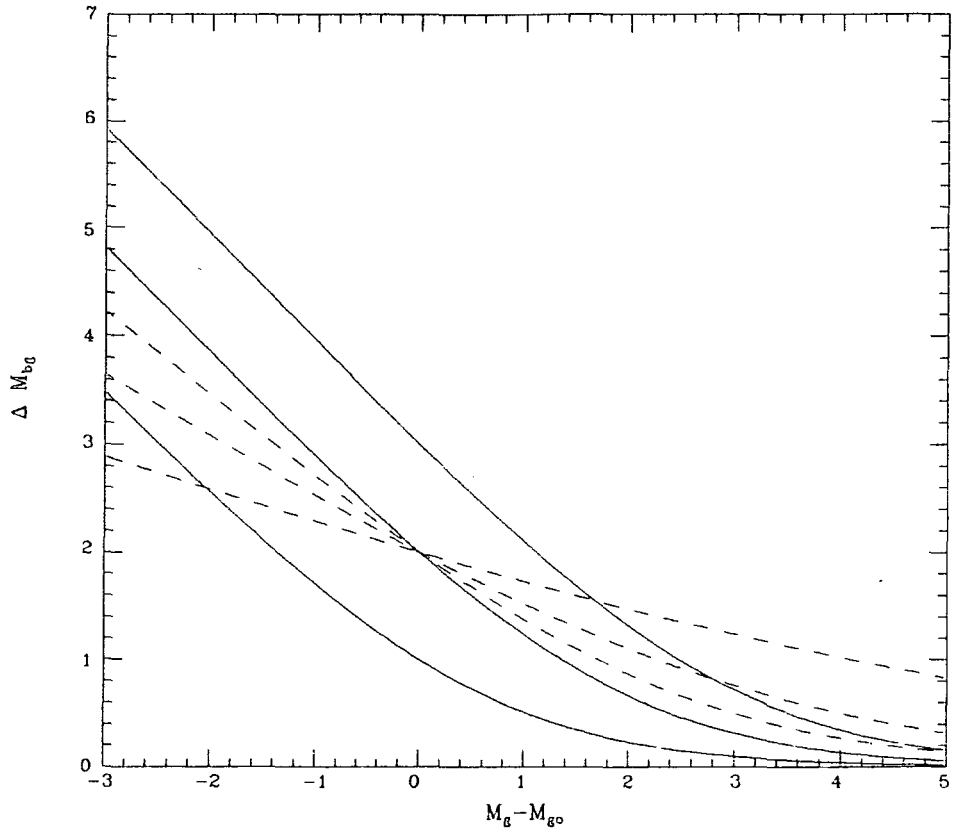


**Figure 5.1. Changes in magnitude with underlying galaxy magnitude, with reference to the normalisation $M_{g_o}$. Solid lines are fixed mass model, for 3 values of $\Delta M_{bg_o}$ of 1,2,3 mag. dashed lines indicate behaviour of gas models for case $\Delta M_{bg_o}$=2.0 and $\beta$=1.5,2.5,5 (increasing gradient)**

The above expressions relate to changes in absolute magnitude, however we are interested in incorporating bursts into predictions for faint galaxy distributions selected by apparent magnitude and we must at this point generalize our discussion of bursts to changes in apparent magnitude. And in so doing, take into account the selection effect that a galaxy undergoing a burst becomes considerably easier to detect with redshift. To account for the effect of redshift we must write down an expression for the $k$ correction of the galaxy plus burst spectrum. This will be dependent on the stength of the burst, the time during the burst at which the object is viewed its redshift and the form of the underlying spectrum.

We calculate the resultant $k$ correction of galaxy spectrum plus burst spectrum in terms of the rest frame change in absolute magnitude, $\Delta M_{bg}$,

starting from the standard definition of the $k$ correction (Oke and Sandage 1968),

$$K(z) = 2.5\log(1+z) + 2.5\log\frac{\int_0^\infty I(\lambda)T_r(\lambda)d\lambda}{\int_0^\infty I(\frac{\lambda}{(1+z)})T_r(\lambda)d\lambda} \tag{5.7}$$

Where $F(\lambda)$ is the rest frame spectral energy distribution, and $T_r(\lambda)$ the transmission function for the filter of interest. $I(\lambda)$, the flux received from a source, can be split into galaxy and burst components, so that,

$$K_{bg}(t_b) = 2.5\log(1+z) + 2.5\log\left(\frac{F_g}{F^o_{bg}(t_b)} + \frac{F_b(t_b)}{F^o_{bg}(t_b)}\right) \tag{5.8}$$

where $t_b$ is the time after the burst commenced (which can be related to redshift via a time-redshift relation) at which the $k$ correction is being calculated, and superscript "$o$" denotes the restframe. The flux ratio's are are simply,

$$F_s = \int_0^\infty I_s(\lambda)T_r(\lambda)d\lambda \tag{5.9}$$

where the subscript, s, denotes either the galaxy, g, or burst, b, contribution as appropriate. Similarly,

$$F^o_{bg}(t_b) = \int_0^\infty I_{bg}(\frac{\lambda}{(1+z)})T_r(\lambda)d\lambda \tag{5.10}$$

Substituting the $k$ corrections for the burst and galaxy spectra, $k_g$, and $k_b$, respectively into expression 5.8 gives

$$k_{bg}(t_b) = 2.5\log(1+z) + 2.5\log\left(\frac{F^o_g(t_b)}{(1+z)F^o_{bg}(t_b)}10^{0.4K_g} + \frac{F^o_b(t_b)}{(1+z)F^o_{bg}(t_b)}10^{0.4K_b(t_b)}\right) \tag{5.11}$$

now from equation 5.6 we have

$$\frac{F^o_g}{F^o_{bg}(t_b)} = 10^{0.4\Delta M_{bg}(t_b)} \tag{5.12}$$

and substituting this into equation 5.8 gives the $k$ correction for the combined burst and galaxy spectra in terms of the $k$ corrections for the burst and galaxy components separately;

$$k_{bg}(t_b) = 2.5 \log \left( \frac{10^{0.4K_g}}{10^{0.4\Delta M_{bg}(t_b)}} + (1 - 10^{-0.4\Delta M_{bg}(t_b)}) 10^{0.4K_b(t_b)} \right) \tag{5.13}$$

Note in the $lim_{\Delta M_{bg}(t_b) \to 0} K_{bg}(t_b) = K_g$ and at the other extreme, for a strong burst, $lim_{\Delta M_{bg}(t_b) \to \infty} K_{bg}(t_b) = K_b(t_b)$, as required.

The general expression for the change in apparent magnitude for a galaxy with a burst, can be simply derived in the same way as for equation 5.6 yielding

$$\Delta m_{bg}(t_b) = 2.5 \log \left( \frac{10^{0.4(\Delta M_{bg}(t_o) + k_g - k_{bg}(t_o))} - 1}{\frac{L_b(t_o)}{L_b(t_b)} 10^{0.4(k_b(t_b) - k_b(t_o))}} + 1 \right) \tag{5.14}$$

So equation 5.5 can be substituted into 5.14 to produce $\Delta m_{bg}(t_b)$, which is the general equation for the effect of a burst on an underlying spectrum, at any time during the burst at any redshift of interest. However, for the case of a system undergoing repeated bursts the combined effect of all previous bursts must be calculated since these bursts may have an effect on the photometric properties over a timescale larger than the time between bursts. This is done simply by coadding, by summing $\Delta m_{bg}(t_b)$ over n bursts at any time, t, representing the age of the system, so that the total change in apparent magnitude is given by,

$$\Delta m_{bg}^{tot}(t_b) = 2.5 \log \sum_{n=1}^{n} \left( \frac{F_{bg}(t_b)}{F_g} \right)_n \tag{5.15}$$

where

$$\frac{F_{bg}(t_b)}{F_g} = 10^{0.4\Delta m_{bg}(t_b)} \tag{5.16}$$

$\Delta m_{bg}^{tot}(t_b)$ is then the evolutionary correction $E_{bg}(t_b)$ or equivalently $E_{bg}(z)$, and fed into the expression relating a galaxies apparent and absolute magnitudes, so that

$$M_{bg} = m_g - 5 \log d_L - 25 - k_g(z) - E_{bg}(z) \tag{5.17}$$

The evolution of $E_{bg}(z)$ must now be parameterised, and for our assumption $SFR \propto m_{HI}$, this can be specified very simply, as we show later.

### 5.3.3 Summary

To summarise, we have outlined an analytical framework with which to calculate the redshift and luminosity dependence of bursts of star formation. This framework requires only the colours and $k$ corrections for the underlying galaxy spectrum and a set of burst spectra which describe the variation of the burst spectrum over time during the star formation and subsequent fainter stages. Furthermore the spectra characterising the burst and the object spectra can be treated completely separately in our formalism, considerably simplifying the process of modelling.

The burst spectra are generated from the Bruzual stelar synthesis code which are calculated for a given set of star formation parameters chosen to characterise the burst (discussed later). The spectra from this 'template burst' are then convolved with the transmission curve for the passband(s) of interest, and the relative luminosity changes with time for the burst are then calculated for inclusion in 5.14. The burst $k$ corrections, $k_b(t_b)$, are then generated by redshifting the set of spectra which describe the burst, using equation 5.7 - for use in equation 5.13. The galaxy $k$ corrections and colours, for the underlying Hubble types, are already established and listed in Table 2.1. All that remains is to specify the normalisation, $\Delta M_{bg_o}$ at $M_{bg_o}$, which is fixed by the Bruzual code once the present day fractional gas consumption for a burst at $M_{bg_o}$, is specified (see later for a fuller discussion) and finally the evolution of burst strengths.

### 5.3.4 Evolution

The importance of linking star formation to gas content is not only the differential effect on the luminosity function that can be achieved in this way, but also because the evolution of this mode of star formation is specified assuming simply that the star formation rate is proportional to gas content.

Below two cases are explored which have very different histories for the evolution of the gas content, and illustrate the plausible scope of descriptions for this form of evolution. These cases represent extremes of evolution in terms of the gas consumption. In the first case a standard initial mass function (IMF)

is adopted for which most mass is locked up on a timescale of order the Hubble time in low mass stars. As an alternative, the case of burst star formation restricted to short lived massive stars is examined, for which the majority of gas may be recycled on a timescale smaller than the time between bursts.

### 5.3.5 Burst Evolution with a Standard IMF

The evolution in the case of a standard IMF is straightforward to calculate. Here we adopt the Miller-Scalo IMF (Miller & Scalo 1979) for which the majority of gas $\sim 80\%$ is locked in stars with large lifetimes ($\sim$ Hubble time) and we can therefore safely ignore the effect of gas recycling as approximately all gas consumed is locked up in long lived low mass stars. In this case an evolutionary trend is produced becuase a fixed fraction of the available gas is locked up in low mass stars with each episode of star formation, leaving a diminished gas content for subsequent bursts. For a given fractional gas consumption per burst, we can constrain the maximum number of bursts by ensuring that the models reproduce the present day gas content and value for the index $\beta$. This form of evolution proceeds more steeply for lower luminosity systems, which helps to achieve a redshift dependent increase in the slope of the luminosity function, as indicated by the faint survey data (see 3.13).

The evolution for this simple case of repeated bursts of fractional gas depletion, $f$, proceeds so that after n, bursts, we have

$$\mathrm{m}'_{HI} = (1-f)^{n}\mathrm{m}^{i}_{HI} \tag{5.18}$$

where $\mathrm{m}^{i}_{HI}$ is the initial gas mass. This depletion results in a corresponding increase in the stellar mass, and a long term increase in the absolute magnitude of the galaxy. i.e. after a burst has died away the resulting luminosity of the galaxy is enhanced by rougly a time independent amount due to the increase in long lived stars. This means that the present day absolute magnitude, $M^{o}_{g}$, of a galaxy maps onto a lower initial luminosity, $M^{i}_{g}$, and this must be accounted for in the models. After a total number of bursts $n_t$ we find that,

$$M^{i}_{g} = M^{o}_{g} - 2.5\log\left(\frac{(1-(1-(1-f)^{n_t}))}{(1-f)^{nt}} R^{o}_{g_o} 10^{0.4\frac{(\beta-1)}{\beta}(M^{o}_{g}-M^{o}_{g_o})}\right) \tag{5.19}$$

Where, $R^o_{g_o}$, is the present day fraction of mass in gas for a galaxy of $M^o_{g_o}$. Note also that this expression is of interest since it provides a constraint on the relationship between the maximum allowable number of bursts and the fractional gas consumption, for a given $\beta$ and $R^o_{g_o}$. For the values $\beta = 1.25$ and present fractional gas to stellar mass ratio 0.1 we have,$f < (1 - 0.2)^{\frac{1}{n_t}}$, which with $f = 0.1$ (10% gas consumption during the burst) allows a maximum of 15 bursts, which drops to only 3 with $f = 0.5$.

The initial peak burst change in magnitude in the restframe can be related to the ratio of the gas content at present to its initial value via,

$$\Delta M^i_{bg_o}(t_b) = 2.5 \log \left( \frac{10^{0.4 \Delta M_{bg_o}(t_b)} - 1}{R^o_{g_o}/R^i_{g_o}} + 1 \right) \tag{5.20}$$

where,

$$R^i_{g_o} = \frac{R^o_{g_o}}{(1-f)^{nt} - (1-(1-f)^{n_t}) R^o_{g_o}} \tag{5.21}$$

so that finally we can now write down the expression for the evolution, i.e. the change in burst strength, which after n (denoted by dash )bursts is given by,

$$\Delta M'_{g_o}(t_b) = 2.5 \log \left( \frac{10^{0.4 \Delta M_{bg_o}(t_b)} - 1}{R^i_{g_o}/R'_{g_o}} + 1 \right) \tag{5.22}$$

and substituting this into 5.14 completely describes the evolution of this model.

This relationship must be rewritten using redshift instead of time as the dependent variable via the time-redshift relation appropriate for the cosmological model chosen. In all this discussion we use $H_o = 75 kms^{-1} Mpc{-}1$ and $q_o = 0.5$. These parameters, in particular $H_o$, determine the duration in redshift of a burst of fixed timescale, and are therefore tied to the the burst rate, this is because the integrated emission over a fixed redshift range, due to a series of bursts is the product of the burst duration and number. This means that if for example, if a lower value of $H_o$ were chosen then a larger number of bursts would be required to give the same amount of evolution by approximately the ratio of this value to 75kms$^{-1}$Mpc$^{-1}$, and so the modelled rates resulting from this analysis can scaled in this way for other values of $H_o$.

A discussion of the operational procedure for including the effects of recurrent bursts into the count models is discussed below, but first we consider

an alternative description for evolution which demonstrates the available latitude of this type of model.

### 5.3.6 Burst Evolution and Suppressed Low Mass Star Formation

Before discussing the results of the above model, we consider the the case of suppressed low mass star formation. This has been suggested both observationaly and physical grounds (see §5.2), and will allow us very much stronger evolution than the above model since much smaller fractions of gas are required to give the same burst luminosities as above.

With this form of evolution we may make a number of simplifying alterations to the above expressions of §5.3 Recycling can be unimportant in this case, for example if we do not form stars of mass less than $3M_{\odot}$, then full recycling after only 0.5Gyrs is now a reasonable approximation. In fact a lower mass limit of $3M_{\odot}$, for the IMF is prefered so that the A type stars are which are responsible for the Balmer features of the burst spectrum of Figure 4.10 are present.

With full recycling equation 5.21 reduces to,

$$R'_g = (1-f)^n R^i_g \tag{5.23}$$

and assuming that the burst converts a fixed fraction of gas to stars, then equation 5.22 becomes,

$$\Delta M'_{g_o} = 2.5 \log \left( \frac{10^{0.4\Delta M_{bg}} - 1}{(1-f)^{-n}} + 1 \right) \tag{5.24}$$

and the evolution in the available gas is now controlled by the underlying passive star formation, which as we argued in 3.11 may proceed at a fairly constant rate via a standard initial mass function for the majority of spirals.

Many other plausible forms for the of evolution might be concieved in which bursts would result. For example, interaction is certainly an important in stimulating some burst activity and if as a result merging of systems is an important dynamical process then additional gas and possibly large changes in the underlying galaxy luminosity may be produced in addition to accompanying bursts, requiring modifications to the above description for evolution. In this case one mi ght expect a general steepening of the luminosity function with

lookback time may result, since statistically the more numerous low luminosity systems may merge with each other more frequently (assuming the simplest case no mass dependency on interaction cross section), diminishing the ratio of low to high luminosity systems over time. Such a complex scenario is not worth investigating until some useful constraints on small scale dynamical evolution become available.

### 5.3.7 The Model Grid

To predict observables such as the mean redshift, $\overline{z}$, and count slope, $\gamma$, we incorporate the above calculations into a framework based on the faint galaxy distribution model described in Chapter 2. Account must be made of the potentially non negligible effects on the photometric properties of a galaxy. of previous bursts, the effects of which may last longer than the interburst period.

A grid of star formation histories is constructed so that at any redshift there are a number of bursts in progress, each at various stages, for galaxies of differing luminosity, so that a smooth array of star formation histories are produced for galaxies of and present day ($z = 0$) luminosity according to the above prescription. This in practice means generating a four dimensional grid such that the change in apparent magnitude with redshift $\Delta m(z)$ is specified as a function of galaxy luminosity for a range of start times (corresponding to the first 'wave' of bursts or $z_{b_o}$'s).

This grid of all possible star formation histories for each form of evolution must then be fed into the number count model as a series of evolutionary corrections so that the faint galaxy distributions can be calculated and normalised to the present day fraction of bursts observed at bright magnitudes.

In order to produce a smooth model we calculate $\Delta m(z)$, for a given underlying galaxy absolute magnitude, by staggering . . the bursts of each run with respect to each other. A grid of burst redshifts is produced in the following way, by first assuming that the evolution of burst rate, N(z) with redshift follows a simple power low form,

$$N(z) = N(o)(1 + z)^{\epsilon} \tag{5.26}$$

we can calculate the redshift of each succesive burst at grid position j, $z_j$,

which is given by

$$z_j = \frac{(1+z)}{N(o)}(F_j + 1)^{1/(1+\epsilon)} - 1 \tag{5.27}$$

where $N_G$ denotes the total number of runs making up the grid, and $F_j$ is simply $(-\ j/N_G)$. This can be generalised to specify the redshift of start of each duty cycle for a given grid array position, $z_{ij}$, and assuming that the burst rate has been constant with time then for the case $q_o = 0.5\ \lambda = 0$ we have a grid of burst start redshifts for $i > 1$,

$$z_{ij} = (1 + z_{i=1,j=N_G})^{-0.5} + (1 + z_{i-1,j})^{-0.5} - 1 \tag{5.28}$$

We run the models to the maximum redshift of interest z=2, and for a total of $n_t$ bursts, adding in the bursts on to this grid according to the star formation parameters and evolution gives us the evolutionary correction of equation 5.17 to produce

$$M_{bg}(z) = m_g - 5\log d_L - 25 - k_g(z) - \Delta m_{bg}^{tot}(z) \tag{5.29}$$

This is done for galaxies of different type with the properties as assigned in the count models and listed Table 2.1. $\Delta m_{bg}^{tot}(t)$ is calculated on a four dimensional grid for each type and as a function of redshift and underlying galaxy absolute magnitude at each grid position.

### 5.3.8 Model Colour Distributions

In addition to the counts the observed colour distribution discussed in Chapter 2 is compared with the model developed here. To acheive this we must first derive relationships for the behaviour of the composite galaxy plus burst spectrum colours. In fact this can be achieved straightforwardly in terms of the burst and galaxy colours separately, with the following expression,

$$(B-R)_{bg}(z) = 2.5\log\left(\frac{10^{0.4(B-R)_g(z)}}{10^{0.4\Delta m_{bg}(z)}} + (1 - 10^{-0.4\Delta m_{bg}(z)})10^{0.4(B-R)_b(z)}\right) \tag{5.30}$$

where $(B-R)_g(z)$, $(B-R)_b(z)$, $(B-R)_{bg}(z)$ are the galaxy burst and resultant B-R colour at a given redshift respectively, and $m_{bg}(z)$ is the change in burst apparent B magnitude for the stage of the burst corresponding to z, as defined above.

Note this expression is of the same form as the expression for the combined $k$ correction of equation 5.13 and behaves in the same way, i.e. for a strong burst or (large change in magnitude) the resultant colour tends to the burst colour, and similarly for the case of a weak burst the colour tends to the colour of the galaxy as required. Note also that this expression reduces to the colour of the galaxy when the burst and object colour are the same, again a necessary requirement. Figure 5.2 demonstrates the dependency of colour on burst strength note that the largest changes in colour for a given change in magnitude, take place in redder systems, and for strong bursts the resultant colour tends to that of the burst.

However since at any redshift the luminosity of any number of subsequent burst may not be negligible, the change in apparent magnitude in the 2 passbands are calculated separately and the resulting colour calculated after the addition of the combined fluxes in each band. The change in magnitude in R, $\Delta m_{bg_R}$ can be related to the change in B (calculated in 5.16), via the expression,

$$\Delta m_{bg_R}(z) = 2.5log\Big(10^{0.4((B-R)_b(z)-(B-R)_g(z))}(10^{0.4\Delta m_{bg_B}(z)}-1)+1\Big) \qquad (5.31)$$

The changes in apparent R magnitude are calculated in this way for all grid points of the burst model, along with the corresponding changes in B. These are then fed into the modified count model as evolutionary terms and the resultant overall colour, $(B-R)^{tot}_{bg}(z)$, is then calculated and given by,

$$(B-R)^{tot}_{bg}(z) = (B-R)_g - (\Delta m^{tot}_{bg_B(z)} - \Delta m^{tot}_{bg_R(z)}) \qquad (5.32)$$

The colour distributions for apparent magnitude limited data in $b_J$ can then be generated and provide an additional comparison with faint data.

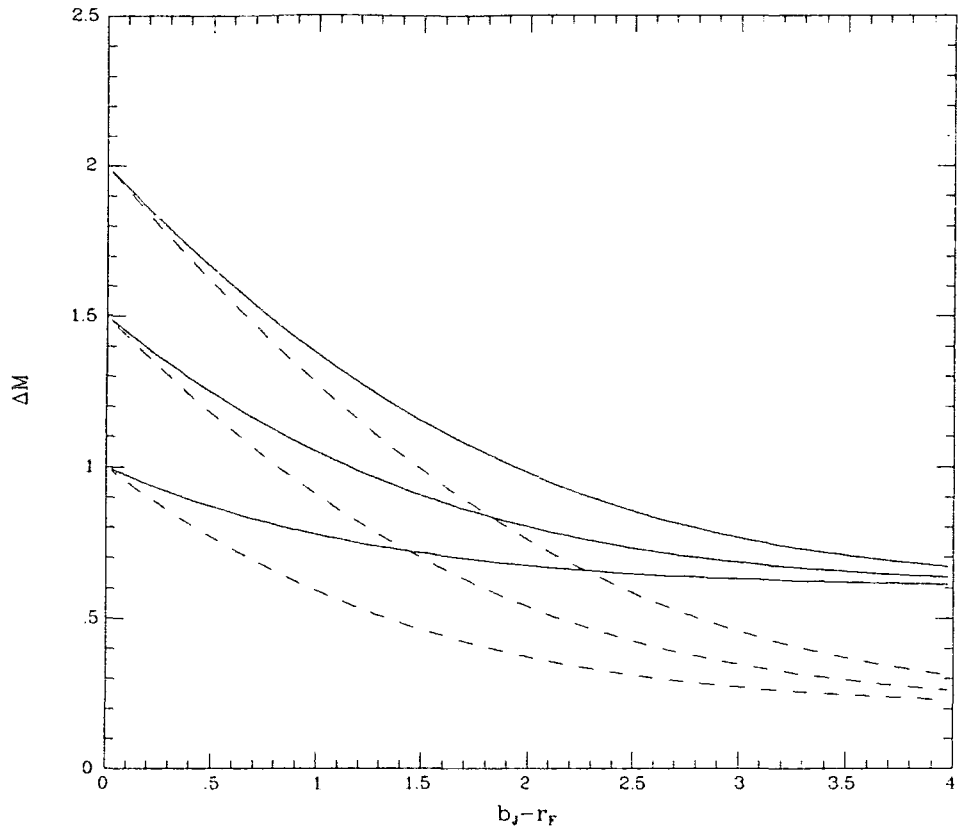


**Figure 5.2. Changes in colour against changes in magnitude, from equation 5.30. The galaxy colours (3 are shown) are given by the values on the y axis for two burst spectrum colours, $b_J - r_f$=0.8 and 0.4, note the largest changes in colour for a given burst strength, $\Delta M_{bg}$, are for bluest burst spectrum and reddest object spectrum.**

### 5.3.9 Summary and Discussion

We have assumed for simplicity that bursts themselves have a narrow range of properties so that only a single template burst was applied to each run of the model. We assume that the star formation rate does not vary during the burst and the IMF is either a standard or truncated Miller-Scalo. and in line with the analysis of 4.5 we set the duration of star formation to 0.1 or 0.2 Gyrs.

We model evolution assuming that the predominant evolutionary effect is an increase in burst strength rather than frequency, related to the increased available gas content, thus we simply set the recurrence timescale to be constant. Below we indicate the total number of bursts in the redshift range $0 < z < 1.0$

by $N_1$ and apply the model only to spiral types (see §5.2)

The calculation of the changes in apparent magnitude should really take into account the variation of M/L and gas content with type, these are not well understood at present, requiring dark matter contributions to the dynamically inferred masses to be accounted for. Broadhurst and Salucci (1989) address the variation of $M/L$ with restframe $B-V$ colour for a sample of local spirals with accurately determined rotation curves. We find that there is a systematic trend of disk $M/L$ with colour so that the bluer galaxies have smaller $M/L$, but the range is only a factor of 5 over all colours and is not be important at the level of this work, since we are concerned only with behaviour averaged over the galaxy population.

The initial mass functions chosen for inclusion in the models represent limiting cases in terms of the evolution of gas content. The standard mass function locks up the majority of mass over a Hubble time, with consequences for the number and strength of bursts allowable given the simple assumption of star formation rates proportional to gas content. In contrast the truncated IMF returns the majority of gas after only 0.5 Gyrs, and allows a larger amount of evolution. However the colours predicted during the luminous stages of the burst (i.e. the time at which bursts will fall most easily into the observed count), are insensitive to the choice of IMF, being dominated mainly by massive stars ($> 2M_{\odot}$).

We have with these models attempted to introduce a dependence of burst strength with galaxy mass by adopting locally determined correlations between star formation rates, HI content and galaxy luminosity with simple descriptions of how these relationships may evolve and below, by comparison with the available faint galaxy distributions, we explore the departures from this model which are required in order to produce a satisfactory fits to the data.

## 5.4 Results

Here we discuss the general behaviour of the above models by comparison firstly with the observed $b_J$ number counts, discussed in Chapter 2.6. The counts maintain a power law slope to the faintest observable limits, $b_J$, with the no-evolution model becoming increasingly discrepant with increasing apparent magnitude. The aim of these models is to close this gap whilst maintaining a low mean redshift consistent with the redshift distribution of the faint redshift

survey. Comparison too with the deep colour distributions allows additional constraints to be placed on these models.

### 5.4.1 Comparison of Model with N(m) and N(z)

The above models are able to produce count slopes in excess of the no-evolution model and mean redshifts which are low with respect to the models of pure luminosity evolution (discussed in 3.13), so long as $\beta > 1.0$ as expected. For the case $\beta = 1.0$ where the bursts are independent of underlying galaxy luminosity, the steepening of the count slope is accompanied by an unwanted increase the mean redshift, and the model time-averaged evolution is equivalent to pure luminosity evolution since the evolution is independent of galaxy luminosity and the luminosity function slides in self similar way to higher luminosities with increasing redshift.

In the simplest model in which we assume only that the burst star formation rate is proportional to available gas content, the choice of burst rate and fractional gas consumption are, as described above, dependent on each other and strongly constrained, limiting considerably the allowable parameter space. However this model, although appealing in its simplicity, has a number of difficulties which make it impossible to simultaneously match N(m) and N(z), at faint magnitudes for the observed value of $\beta = 1.5$. A build up in the luminosity due to long lived stars with successive bursts, tends to flatten the evolutionary gradient in burst strength. More severe however, is the is the shallow differential burst strength with galaxy luminosity (set by $\beta$), which means in order to produce a significant increase in the count slope over the no-evolution model we must set our normalisation high so that bursts are strong even at the bright end of the luminosity function. This results in mean redshifts which are high with respect to the observed value.

Table 5.1 shows quantitatively how this model (model 1) behaves. Increasing the number of bursts note, is offset be the decrease in the allowable fractional gas consumption per burst, with the major effect on the count slope resulting only from changes in the normalisation strength $\Delta M_{bg_o}$. Only marginal increases in the count slope are permissible given the requirement of a $\overline{z} = 0.22 \pm 0.015$ for the faint survey magnitude limits, $20.0 < b_J < 21.5$. As the mean redshift increases, the number of allowable bursts decreases for a given $F$, since the gas consumed can never be more than is allowed by the

total mass of luminous mass of the galaxy given by equation 5.19.

Table 5.1: Burst Model Predictions:Model 1

| $\Delta M_{bg_o}, M_{g_o}$ | Gas Fraction | $N_1$ | $\beta$ | $\gamma(20 < b_J < 24)$ | $\bar{z}(20.5 < b_J < 21)$ |
|---|---|---|---|---|---|
| -1,-19 | 0.15 | 12 | 1.5 | 0.35 | 0.27 |
| -1,-19 | 0.25 | 8 | 1.5 | 0.37 | 0.25 |
| -1,-19 | 0.35 | 6 | 1.5 | 0.39 | 0.25 |
| -1,-20 | 0.35 | 5 | 1.5 | 0.39 | 0.28 |
| -1,-21 | 0.25 | 8 | 1.5 | 0.39 | 0.32 |

Reasonable fits are possible if we relax the constraint on $\beta$ allowing higher values. For example $\beta = 3$ will give a reasonable fit to the counts with a low mean redshift (see Table 5.2, model 2) however we cannot extend this model to low luminosity galaxies ($M > -17$) and follow the model to our redshift limit, since then the changes in magnitude required violate the constraint on the total gas contents. For $b_J > 23$ this model begins to turn over to a lower count slope and the predicted mean redshift is rather larger than our observations suggest. Furthermore the choice of evolution and rate, are at the limits allowed by consideration of the gas content constraint, and for $\beta$ as large as required here, we may be in contradiction with the distributions of gas fractions, given our assumption of star formation rates proportional to gas content. Of course we need not insist on accounting for all observed evolution with a burst model, but it is as we now show feasible to do so with only modest changes to this model.

Table 5.2: Burst Model Predictions: Model 2

| $\Delta M_{bg_o}, M_{g_o}$ | Gas Fraction | $N_1$ | $\beta$ | $\gamma(20 < b_J < 24)$ | $\bar{z}(20.5 < b_J < 21)$ |
|---|---|---|---|---|---|
| -1,-19 | 0.15 | 12 | 2.5 | 0.37 | 0.27 |
| -1,-19 | 0.25 | 8 | 2.5 | 0.38 | 0.24 |
| -1,-19 | 0.25 | 8 | 5 | 0.40 | 0.23 |
| -1,-19 | 0.4 | 8 | 3 | 0.41 | 0.24 |
| -1,-20 | 0.25 | 5 | 5 | 0.42 | 0.28 |

With significant recycling via a truncated IMF, we can transform the burst model, as described in 5.3.7, allowing more evolution at faint magnitudes. This model may in any case, be better motivated by local observations of starburst

systems (see discussion in §5.2).

We choose a model with a Miller-Scalo IMF truncated so that no stars are formed below $3M_{\odot}$. With this IMF we are free to vary $\beta$, $N_1$, $F$ and the normalisation, and it is now possible to produce large amounts of evolution more easily than the above model, since we do not lock up gas for any significant time, and in comparison to the standard Miller-Scalo IMF much smaller amounts of gas are required to achieve the same increases of luminosity.

As above, the burst rate and evolutionary gradient can be varied together to produce an equal effect on $\overline{z}$ and $\gamma$, but in this case too much evolution can be produced producing count excess much in excess of the observed mean count. The best results are again achieved for large $\beta$, ($\beta > 4$), and a normalisation at low enough luminosities, so that that the bright end of the luminosity function does not produce a significant evolutionary contribution, at least not to ($z < 0.5$), as required.

Table 4 lists the range of interesting cases. We find that fractional gas consumption in the range 25-60% with the number of bursts to $z = 1.0$ between 5 and 15 (or a total of 7-20% of the lookback time, with $H_o = 75$ and $q_o = 0.5$) will give a steep power law slope in line with the observed $b_J$ counts, and an observed mean redshift in agreement with our faint redshift survey data. Larger values of $f$, produce an upturn in the count slope, so that it increases with apparent magnitude. Values of $f$, lower than 25% cannot reproduce the count slope even with high burst rates, here the counts turn over at faint magnitudes and the mean redshift is unacceptably high. These points are demonstrated in Figure 5.3 for some of the cases listed in table 5.3, referred to as model 3.

Table 5.3: Burst Model Predictions:Model 3

| $\Delta M_o, M_o$ | Gas Fraction | $N_1$ | $\beta$ | $\gamma(20 < b_J < 24)$ | $\overline{z}(20.5 < b_J < 21)$ |
|---|---|---|---|---|---|
| -1,-19 | 0.15 | 15 | 2.5 | 0.41 | 0.22 |
| -1,-19 | 0.25 | 12 | 5 | 0.43 | 0.21 |
| -1,-19 | 0.35 | 12 | 3 | 0.45 | 0.22 |
| -1,-17 | 0.55 | 15 | 5 | 0.44 | 0.21 |
| -1,-20 | 0.55 | 15 | 5 | 0.47 | 0.22 |
| -1,-21 | 0.45 | 12 | 5 | 0.48 | 0.28 |

The high values of $\beta$ preferred in model 3 represent more the case

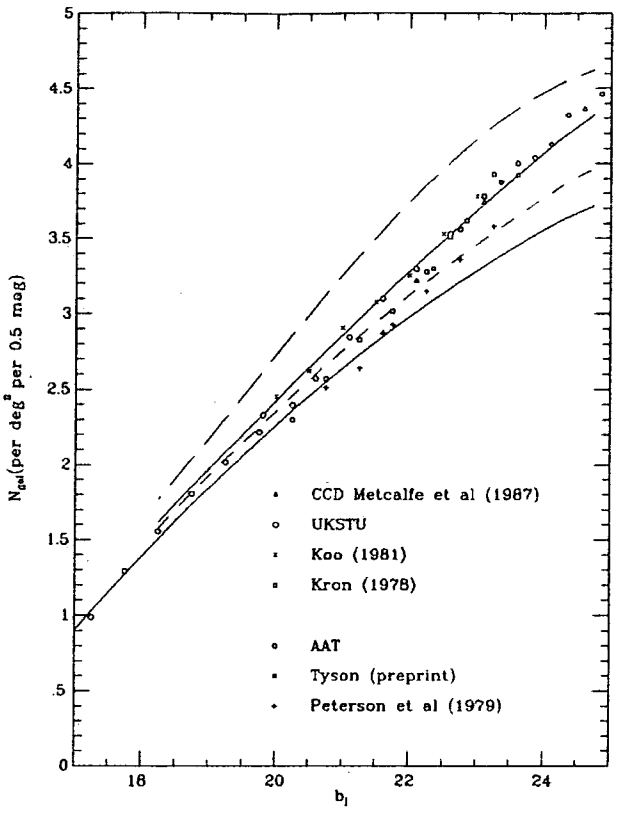


**Figure 5.3. Model counts for cases, 1, 3 and 6 of Table 5.3, plotted against the $b_J$ count data.**

discussed in 5.3 of the fixed luminosity burst or burst 'threshold' model. Of course evolution is required in the strength of the burst and so the 'critical mass' would be a function of redshift, a rather unappealing idea, and instead we may posulate a greater efficiency of star formation in lower luminosity systems for this mode of star formation. Note however if we prefer a lower $\beta$ we can recover our simple assumption of star formation rates proportional to gas content, by restricting this form of evolution to lower luminosity systems. With $\beta = 2$ and a minimum host galaxy absolute magnitude of $-20.0$, we can reproduce the counts with a similar amount of evolution as model 3. This is because for this case, the normalisation is independent of galaxy luminosity, below the threshold value, and contributions to the evolution are now larger for galaxies of higher luminosity, for parameter choices which are similar to model 3 (other than $\beta$).

Interestingly we may speculate that a 'threshold' may be the physical consequence of requiring a minimum gas surface density before a burst can take place, this will evolve brightward with redshift depending on the available gas to galaxy stellar mass. Choosing an absolute magnitude at the threshold at z=0, $M^o_{th}$, it is easy to show that this will evolve such that,

$$M_{th}(z) = M^o_{th} - 2.5(\frac{\beta}{\beta - 1}) \log \left( \frac{10^{\Delta M_{bg_{th}}} - 1}{10^{\Delta M_{bgo}(z)} - 1} \right) \tag{5.33}$$

such a model requires less evolution than model 3 for a given set of parameters, because with increasing redshift the luminosity threshold below which bursts can take place increases, and interesting cases of this model are listed in Table 5.4.

Table 5.4: Burst Model Predictions:Model 4

| $\Delta M_{bg_o}, M_{g_o}$ | $M^o_{g_{th}}$ | Gas Fraction | $N_1$ | $\beta$ | $\gamma$ | $\overline{z}$ |
|---|---|---|---|---|---|---|
| -1,-19 | -21 | 0.15 | 15 | 2.5 | 0.45 | 0.28 |
| -1,-19 | -19 | 0.15 | 15 | 2.5 | 0.40 | 0.22 |
| -1,-19 | -19 | 0.35 | 12 | 2.5 | 0.44 | 0.22 |
| -1,-19 | -19 | 0.35 | 10 | 1.5 | 0.45 | 0.22 |
| -1,-19 | -18 | 0.45 | 15 | 1.5 | 0.42 | 0.21 |
| -1,-19 | -19 | 0.55 | 10 | 1.5 | 0.47 | 0.22 |

This threshold model is also appealing not only for its low values of $\beta$, but because, as shown in Figure 4.4, the redshift distribution of strong lined objects in the faint redshift survey falls off steeply above $\overline{z}$ in the faint survey, indicative of a threshold luminosity for burst events of $\sim M^*$ by $z = 0.2$.

## 5.5 Comparison of Model with Colours

The colour distributions provide a crucial test of these models since we know from Chapter 2.6 that the evolution must be restricted to colours bluer than $b_J - r_f = 1.6$, and at redder colours than this, there is no significant departure from the case of 'no-evolution'.

At the outset we may expect the burst model to produce this effect on the faint colour distributions. The bursts, as demonstrated in Chapter 4.5 are bluest when brightest, and when brightest are most easily observed.

Thus the count excess should be composed in the main of relatively blue objects. We know also from our redshift distribution that the bright end of the luminosity function does not significantly evolve in luminosity to at least $z = 0.5$ consistent with minimum evolution. This passive evolution we know must evolve even more slowly with colour and thus a component of the colour distribution representing the bright end of the luminosity function may show insignificant colour evolution to very faint magnitudes here, and thus explain the red tail in the colour distributions at faint magnitudes. This point was underlined in Chapter 2.6 where we found our no evolution model provided an excellent fit to the observed colours redward of $b_J$-$r_f = 1.6$.

In fact the predicted colours using the best fit parameters of our preferred models (models 3 and 4), are too blue. The peak of the observed $b_J$ selected colour distribution falls at $b_J - r_f \sim 1.2$, (for $23 < b_J < 24$), compared with predictions of $b_J - r_f \sim 0.8$. However, these models are able to reproduce the observed red tail of the colour distribution, as expected. The easiest way to rectify the blue mismmatch is to extend the duration of star formation. The restframe colour of a burst of $10^8$ yrs duration, at peak burst luminosity is $b_J$-$r_f = 0.25$, but with a burst duration of $2 \times 10^8$ yrs this becomes $b_J$-$r_f = 0.46$, with correspondingly larger $k$ corrections. Internal reddening will also achieve the same effect. Using the standard interstellar reddening curve of Whitford (1956), with $E(B-V) = 0.45$ we can bring the predictions of models 3 and 4 into line with the observations although observations of local starburst Markarian objects favour smaller reddening, $E(B-V) \sim 0.2$ (Hucra 1977). We combine the longer duration burst ($2 \times 10^8 yrs$) with the smaller amount of reddening ($E(B-V) = 0.2$) as our favourite model. The best fit model parameters for this case are very similar to those of models 3 and 4 but the burst rates have dropped by a factor of two over the above models to compensate for the longer duration bursts of this model, so that the integrated star formation remains approximately the same. The above corresponding model colour distributions are shown in Figure 5.4 against the very deep CCD colour distributions of Metcalfe et al.(1987) (see Chapter 2 for a discussion of this data), for which reasonable agreement is found in the above models.

We conclude that the colours as may be expected qualitatively reproduce the faint colour distributions but that in detail longer duration bursts and/or

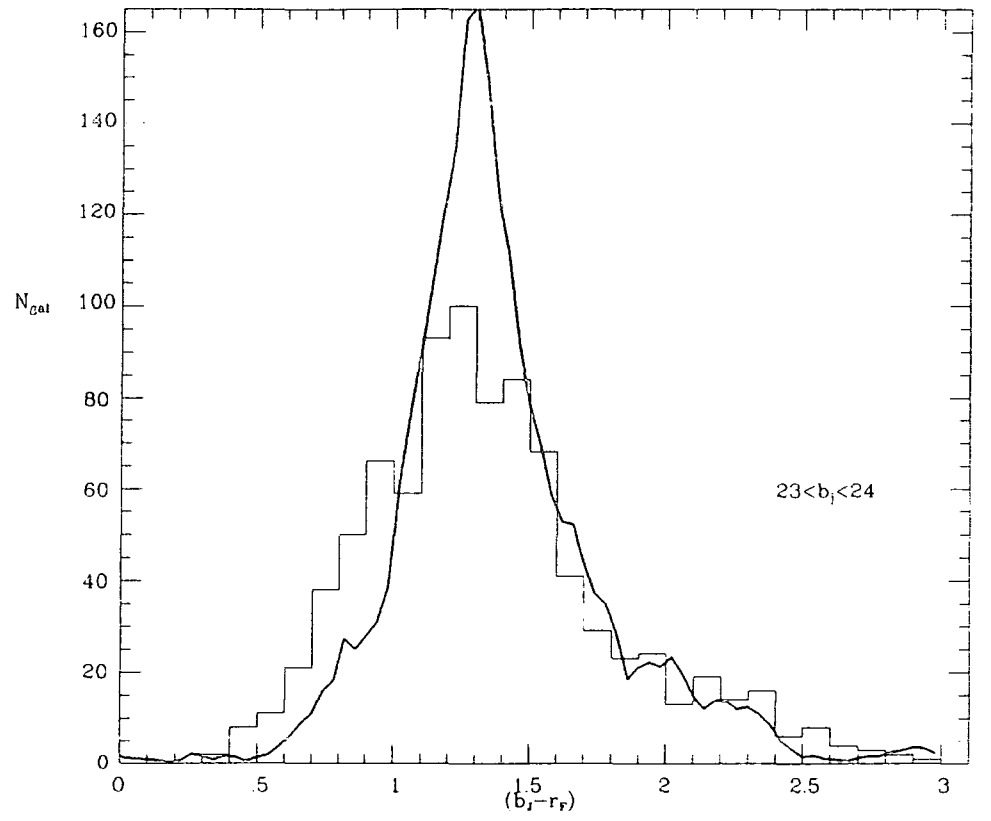


**Figure 5.4. Model colour distributions plotted against the $b_J$ deep CCD data (histogram) for $23 < b_J < 24$. Solid line set up as model 3, case 3 with $2 \times 10^8$ duration bursts and $E(B-V) = 0.25$**

reddening, are required to reproduce the distributions closely. These comparison should really include a dispersion in burst duration and reddening to be realistic, which would produce a larger dispersion in the predicted colour distributions as may be indicated by the data.

Additionally it is important to bear in mind that colour distribution on the choice of definition. Metacalfe *et al* define the R magnitude to a faint limiting magnitude and the area within the limiting isophote found is used to sum the light in B. If however burst light, which is most important in B, is not distributed like the underlying galaxy (most important in R), then this may skew the colour distribution.

## 5.6 Conclusions

The primary conclusion of this chapter is that we can construct simple models which do fit the faint galaxy photometric properties, and simultaneously reproduce the redshift distribution of our faint survey.

All models considered here are able to steepen the count slope significantly with correspond redshift distributions which have a lower mean redshifts with respect to the models of pure luminosity evolution for similar evolutionary count excesses.

In detail however we find that the simplest model for which burst star formation rates are proportional to gas content cannot produce a steep enough count without producing unacceptably high mean redshifts. This problem is partly resolved by relaxing the constraint on the variation of gas fraction with galaxy luminosity.

If we insist on accounting for *all* the evolution seen in the counts via the burst model, then more promising fits are obtained with a truncated initial mass function. This removes the constraints on the evolution imposed by accounting for the gas consumption, and allows a larger rate of evolution.

The deep colours distributions provide additional constraints on these models. We find that the blue excess observed in the colour distributions is best matched by a model which includes either bursts slightly longer than the adopted $10^8$ yrs and/or some internal reddening, otherwise the predicted colours are too blue.

# Chapter 6.

# GALAXY CLUSTERING AND THE FAINT REDSHIFT SURVEY

## 6.1 Introduction.

In this chapter we examine the distribution of galaxies and clusters of galaxies over a range of scales up to $\sim 1000h^{-1}$ Mpc. We concentrate in the main on the faint redshift survey, determining correlation functions on small scales for comparison with the locally determined equivalent measures, and on large scales we include in our analyses other pencil beam surveys and the spatial distribution of Abell clusters.

We find tentative evidence for a very large scale periodicity in the distribution both of galaxies and Abell clusters in the direction of the galactic poles.

## 6.2 Faint Redshift Survey

The faint redshift survey provides information on the spatial distribution of galaxies to $z < 0.45$ or $700h^{-1}$Mpc ($q_o = 0.5$) in 5 well separated fields at high galactic latitudes. This makes the survey useful for examining the galaxy distribution on scales much larger than possible from previous field galaxy redshift surveys. Bright redshift surveys sample depths to $z < 0.1$, with the majority of objects concentrated in the range of redshifts $\Delta z \sim 0.04$. For the faint survey, however, 90% of objects extend over a redshift range $0.1 < z < 0.35$ (see the redshift distribution presented Figure 3.8), which is a 6 fold increase in depth over bright field surveys.

The fields vary slightly in areal coverage and sample galaxies at different rates according to the number of available objects within the magnitude limits of each field and constraints on telescope time (see Table 3.1 for field details). and are typically $\sim 20' \times 20'$ on the sky corresponding to $3h^{-1}$Mpc ($q_o = 0.5$), at the mean survey depth of $z = 0.2$. This width although small compared with the survey depth is, however, much greater than the core radius of a typical rich cluster.

The redshift measurements have an estimated rms error of 135kms$^{-1}$, derived internally from comparison of emission and absorption line measurements

(discussed in Chapter 3.6). Both emission and absorption line redshift measurements proved possible for 75% of the sample, and no trend in the redshift error is found with the cross correlation coefficient, $r$, (see figure 3.5) indicating there are no important systematic errors in the redshift measurements.

This level of redshift accuracy is comparable with much of the bright redshift survey work used for local clustering analyses and corresponds to an uncertainty in distance of only $\sim 1.5h^{-1}$Mpc, which is in any case smaller than the rms peculiar pair velocity dispersion of $\sim 250 - 400kms^{-1}$ determined from virial analysis on scales upto $5h^{-1}$Mpc (Bean *et al*, 1983 Hale-Sutton *et al* 1988). Thus we are able to examine structure on small scales too, which given the mean lookback time of $1.5 - 3h^{-1}$Gyrs, is of interest in the context of dynamical evolution.

Below we present the redshift distributions of the individual fields and discuss the qualitative distributions and then quantify clustering with the 2 point spatial correlation function separately on small ($< 10h^{-1}$Mpc) and large scales ($< 1000h^{-1}$Mpc).

## 6.3 Large Scale Structure

The distribution of galaxies on large scales may directly reflect the initial conditions under which the distribution of matter was arranged. We may expect this because we do not observe peculiar velocities large enough to have significantly rearranged structure on these scales over a Hubble time. Observations of the general local peculiar velocity field may indicate velocities of up to $\sim 500Kms^{-1}$ (Lynden Bell *et al* 1987) corresponding to $\sim 5h^{-1}$Mpc over a Hubble time.

In any case gravitational instability, in the Friedmann model, will produce only linear growth of density perturbations on scales scales $> 10h^{-1}$Mpc, inducing peculiar velocities with respect to the Hubble flow, which grow only slowly with time. Below this scale non-linear growth induces somewhat higher peculiar velocites. Hydrodynamical processes may have a role in redistributing material, however the effect of explosions is limited to scales below 20Mpc or so (Ostriker 1986), although the correspondingly high peculiar velocities may result unless collisional dissipation is important.

On scales greater than $\sim$ 20Mpc we can therefore be very confident that the distribution of galaxies reflects the 'initial conditions', and thus by examining

structure on very large scales we may realistically expect to see the effects, if any, of early physical processes 'written' into the present large scale spatial distribution of galaxies.

The corollory of this is the much asserted claim, that, distinguishing between various cosmogonies is best achieved with information on the galaxy distribution at large scales, and much observational effort has been expended to this end.

### 6.3.1 Observations and Large Scale Structure

The task of observing the galaxy distribution over large scales is a demanding one, requiring large well controlled sample selection with large areal coverage and/or depth, and inevitably data at faint flux levels. In particular, redshift information is very important since it is difficult to be convinced of the reality and spatial extent of claimed 2 dimensional features without spatial information. However in practice we are faced with the situation where we have far more information on the projected galaxy distributions, reflecting the difficulty of obtaining redshift information for large galaxy samples.

Large scale features on the spatial distribution of galaxies are undoubtedly observed. There are claims of linear overdensities of up to $100h^{-1}$Mpc from local galaxy redshift surveys (Chincarini *et al* 1983) and of a filamentary appearance in the all sky Lick catalogue (Moody *et al* 1983). Bridges joining clusters within super cluster complexes have also been noted (Gregory and Thompson 1978, Einasto *et al* 1984, Batuski and Burns 1985)

However assessing the statistical significance of filamentary features has proved difficult (Bhavsar and Ling 1988), and the possible role of selection effects has cast doubt on the reality of some large scale gradients in the Lick counts (Lilje and Efstathiou 1988).

Sheet-like structures are also apparent in the spatial distribution of galaxies, for example Da Costa *et al* (1988), claim such a feature to extend over dimension $10 \times 20 \times 50h^{-3}\mathrm{Mpc}^3$ in an extensive southern sky redshift survey. In addition the presence of an all sky planar structure to at least $30h^{-1}$Mpc, of which the local group is a part, has been identified by de-Vaucoulours (1976) from the spatial distribution of galaxies to at least $3000kms^{-1}$. This large flattened structure has been named the 'super-galactic plane', and may extend radially to at least 10000kms$^{-1}$, to include many well known rich clusters, including

Virgo, Hydra-Centaurus, Perseus, Coma and Abell 1367 clusters (Tully 1986). In an all-sky optical map constructed by Lahav (1986) this feature is clearly apparent as a distinct planar overdensity.

In addition to large overdensities, large volumes devoid of (bright) galaxies have been uncovered in field redshift surveys. The void in the constellation of Bootes of at least $50h^{-1}$Mpc discovered by Kirshner *et al* (1981), is of order the depth of their redshift survey ($100h^{-1}$Mpc) and covers an area of $\sim 1000deg^2$ on the northern sky. A similar void is indicated in the south (Oemler 1986) and in the extensive survey of $\sim 7,000$ galaxies to $B = 15.5$, centered on the NGP, of de Lapperent *et al* (1986), a clear cellular structure in the distribution of galaxies on scales of at least $20h^{-1}$Mpc is apparent.

Statistical and 'botanical' studies of Abell clusters have revealed that that a high degree of clustering amongst rich clusters of galaxies (Hauser and Peebles 1973, Bachall and Soneira 1984a). Claims of super clusters with scales of $\sim$ 100Mpc (Batuski and Burns 1985), and greater, have been made, (Bachall and Soneira 1984b, Tully 1987, Chincarini *et al* (1988).

The number of observed large scale super clusters and voids are presently very uncertain and it is not clear that these observations are difficult to reproduce in the simplest of models for the formation of structure. Detailed N-Body simulations on large scales for the CDM model (White *et al* 1986, are able to reproduce filamentary and void like structures, although the amplitude of correlation function of rich clusters maybe a difficulty for this model, and Bardeen *et al* (1987) have examined the possibility of more power on large scales in this model.

Others have suggested the observed large power in these scales may be suggestive of long range phase correlations in the density distribution (Peebles 1985), and such behaviour is produced in the cosmic string model (Turok 1987).

### 6.3.2 Large Scale Structure and the Faint Redshift Survey

Pencil beam redshift surveys sacrifice areal coverage for depth, and have the potential to intersect structures which are not present in the local galaxy distribution. The distribution of galaxies in the faint survey are shown in the form of one dimensional field redshift distributions presented in Figure 6.1. It can be seen that the distribution of galaxies varies markedly between the individual fields of the survey, with a number of curious features.

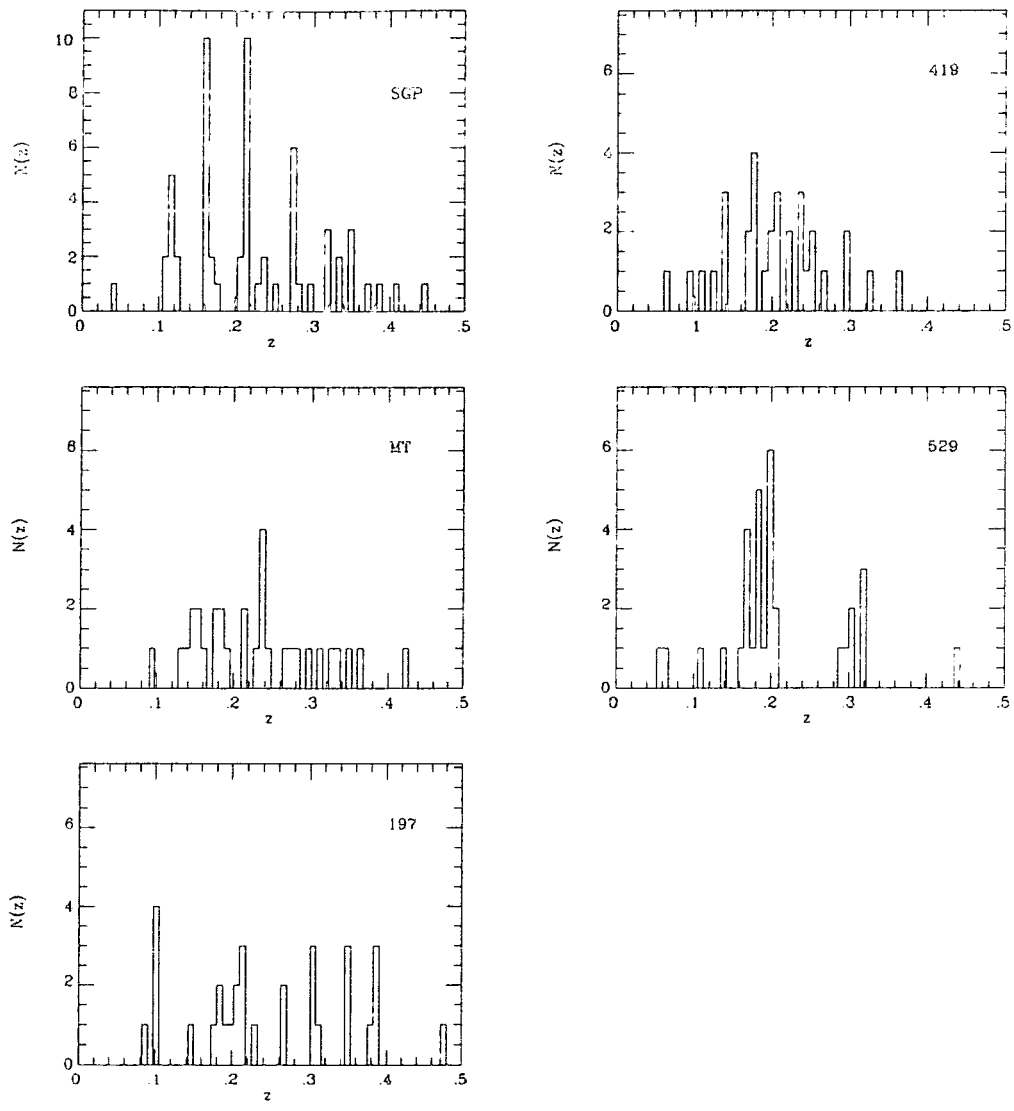


**Figure 6.1. Redshift distributions of the fields comprising the faint redshift survey, field name is indicated top right.**

The SGP field displays sharp overdensities in the redshift distribution separated by lower density regions, with the impression of an apparent periodicity. The spike-like features at z=0.11,0.16,0.23,0.27, contain 80% of all galaxies in the magnitude range for this field ($20.5 < b_J < 21.5$). The numbers sampled in each peak follow the selection function indicating they have similar overdensities and evenly cover the full field area $3 \times 2h^{-1}$Mpc with internal velocity dispersions of of $\sim 700 kms^{-1}$, typical of rich clusters. These peaks are note very evenly

separated by $125h^{-1}$Mpc ($q_o = 0.5$), a point discussed later.

The 529 field also shows interesting structure. No galaxies are sampled in the redshift range $z = 0.2 - 0.3$, or $\sim 250h^{-1}$Mpc ($q_o = 0.5$), and interestingly this gap is adjacent to the largest over-density in the survey (integrating over a scale $100h^{-1}$Mpc). Associations of large underdensities with large over densities have been noted by Bachall and Soniera (1982) who claim the Bootes void is flanked by two very large associations of rich Abell clusters. However since our survey fields are approximately one dimensional care must be taken in the use of the term void as the volume sampled is small compared with the large 3D voids. The most useful quantitative measure of clustering, the 2 point spatial correlation function is now discussed for this survey.

### 6.3.3 Galaxy Correlation Function at Large Scales

Here we assess large scale structure quantitatively via the two point spatial correlation function $\xi(r)$. This statistic is a measure of density fluctuation about a mean density, as a function of galaxy pair separation, $r_{12}$, and can be defined through the joint probability of finding galaxies in volume elements $\delta V_1$ and $\delta V_2$ separated by $r_{12}$, (see Peebles 1980), so that,

$$\delta P(r_{12}) = n^2(1 + \xi(r_{12}))\delta V_1 \delta V_2 \tag{6.1}$$

where, $n$, is the mean space density of objects under study.

On large scales ($> 10h^{-1}$Mpc), the separations are calculated in comoving coordinates, assuming that galaxies participate in the general expansion on these scales (see above discussion).

The method of calculating comoving pair separations has been presented by Osmer (1982), for the case $q_o = 0.5$, and here we outline the general treatment for any $q_o$, and make use of the expression from Weinberg (eqn. 14.2.7 p413), for the transformation of coordinate systems in the Robertson-Walker metric,

$$\mathbb{X}' = \mathbb{X} + \mathrm{a}\Big((1 - K\mathbb{X}^2)^{0.5} - [1 - (1 - K\mathrm{a}^2)^{0.5}]\mathbb{X}.\mathrm{a}/\mathrm{a}^2\Big)$$

where $\mathbb{X}$ is the coordinate vector of one pair member and $\mathbb{X}$' is the resulting vector after transformation by a, K is the curvature term and is 1,0,-1,

depending if, in this metric, the universe is closed, flat or open, respectively. This transformation of coordinates is most easily achieved by converting in Cartesian coordinates so that the pair separation is taken to lie along the z axis,

$$\mathbb{a} = (0, 0, -r_1)$$

$$\mathbb{X} = (r_2 \cos\theta, 0, r_2 \cos\theta)$$

where r, is the comoving coordinate given by

$$r = \frac{zq_0 + (q_0 - 1)(-1 + (2q_0 z + 1)^{0.5})}{H_0 R_0 q_0^2 (1 + z)}$$

and $R_0 = (k/H_0^2(2q_o - 1))^{0.5}$

The magnitude of $\mathbb{X}$', then gives the comoving separation given by,

$$\sin|X'|, q_0 > 0.5$$

$$|X'|, q_0 = 0.5$$

$$\sinh|X'|, q_0 < 0.5$$

The correlation function is generated following the method of Shanks *et al* (1983), in which edge effects are accounted for by simulating the sample selection criteria for large random catalogues and estimated via,

$$\xi(r) = N_{gg}(r)/N_{gr}(r) - 1$$

where $N_{gg}(r)$ is the total galaxy-galaxy pair count at scale, r, and $N_{gr}(r)$ is the galaxy-random pair count, and normalised as described below.

## 6.4 Large Scale Results

The correlation function, coadded over the five fields, is shown in figure 6.2. In Figure 6.2a we show the result of coadding fields weighting by pair counts, and in Figure 6.2b each field is weighted equally. Normalisation of the random pair count is to a global mean count (see below for details). Errors are estimated from field to field uncertainties, unless otherwise indicated. Scales upto $700h^{-1}$Mpc are shown, above this scale their are few pairs in the redshift survey, and the form of the selection function must be well known as each pair member falls in either the high or low redshift tail to the selection function, making the estimate of $N_{gr}$ very uncertain.

The data are binned in constant $\log \Delta(r) = 0.1$, bins and a global normalisation applied. We choose this in preference to field normalisation since, as we discuss later, the count variations between these fields seem to correlate with the form of the redshift distributions, although the contribution to these variations resulting from zero point uncertainties in the photometry, may still be unclear at present (Shanks Private Communication).

The global normalisation is estimated from the mean $b_J$ count of Figure 2.4, and corrections are made to the observed counts for our fields using the sampling rates, magnitude limits and field areas of Table 3.1. We find however, that our correlation functions on large scales are not significantly dependent on the choice of local or global normalisation, but are much more dependent on the method of weighting.

Figure 6.2 shows no significant field weighted correlations on large scales, in that no point lies more than $2\sigma$ from the random expectation. However interestingly the pair weighted correlation function does show peak trough behaviour similar to that of Shanks *et al* (1986).

The advantage of field weighting the correlation functions is that the resultant correlation function is made up of independently estimated and evenly weighted fields, however, in doing this information may be lost since some fields have better estimated correlation functions. The SGP field has the largest number of redshifts but the most unusual clustering properties, and is mainly responsible for the peak-trough behaviour in Figure 6.2b, and thus we present both field and pair weighted estimates of the correlation functions, since this field may not be representative.

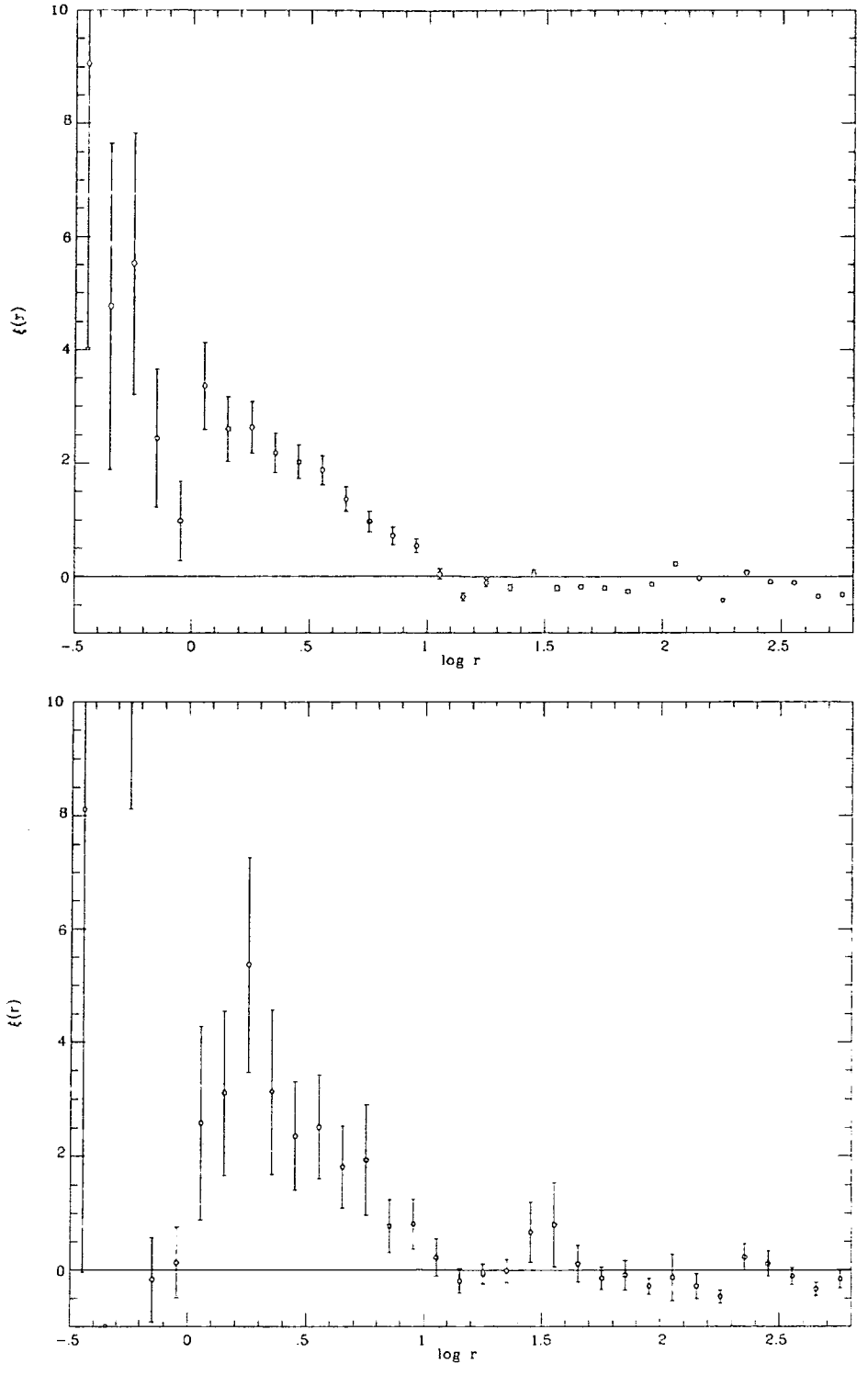


Figure 6.2 Pair weighted (top) and field weighted (bottom) correlation functions for the faint redshift survey.

Logarithmic binning smooths over wide ranges of scales at large pair separations and we choose to bins of $10h^{-1}$Mpc width to give greater spatial resolution on large scales, and now we do seem to find evidence for large scale structure. Figures 6.3 shows the correlation functions binned in this way, note the the anticorrelation centered on $150h^{-1}$Mpc in both plots and a general peak trough like behaviour extending over perhaps $500h^{-1}$Mpc in the pair weighted case. Field weighting results in some cancellation of positive and negative correlations results (indicated by large error bars), and we now look at the fields individually.

A useful representation of the clustering within individual fields is presented in Figure 6.4. Here we plot $N_{dd}$ for each field in linearly separated bins, with the random pair count shown (normalised as above). This representation is equivalent to the correlation function but displays the pair count directly.

For fields 197, MT and 419 the variance in $N_{dd}$ appears to be consistent with poisson noise over all scales, reflecting the smooth redshift distributions for these fields (see Figure 6.1). The SGP and 529 fields, however, behave in a very different way, with very significant features present in the correlation functions at large separations, and note also that these two fields contribute the majority of the small scale pair excess of the correlation function (the first two bins).

The SGP shows a clear periodicity in the correlation function with overdensites separated by anticorrelations, reflecting the periodicity present in the redshift distribution. For this field the amplitude of the positive correlations centered on $125h^{-1}$Mpc and $250h^{-1}$Mpc is very large, this is the consequence of the almost equal spacing of the 4 sharp peaks in the redshift distribution. Interestingly these peaks are separated, in comoving coordinates, to within <10% of a mean separation (for the range $q_o = 0.0$–$1.0$), defined from the 4 prominant overdensities.

The peaks in the autocorrelation functions at separations of $125h^{-1}$Mpc, and $250h^{-1}$Mpc, appear with formal peak significance of $\sim 6\sigma$. Of course we must expect that since galaxies are known to be clustered, it may not be surprising that occasionally a number of clumps is distributed along a line of sight. In which case the pair count will be enhanced by the sum of the product of the number of clump member pairs, thus amplifying the correlation function

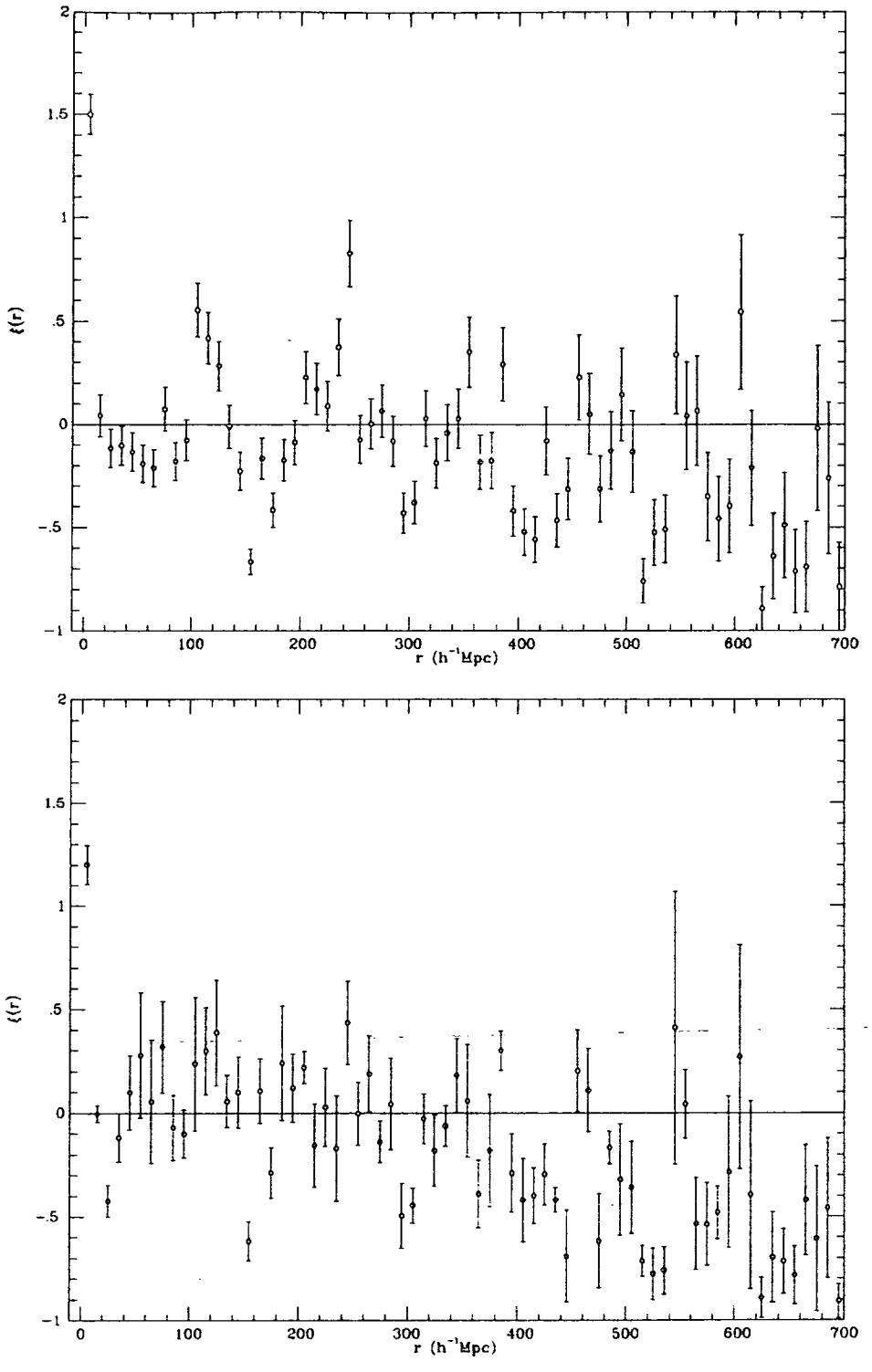


**Figure 6.3 Field weighted (top) and pair weighted (bottom) correlation functions linearly in $10h^{-1}$Mpc bins.**

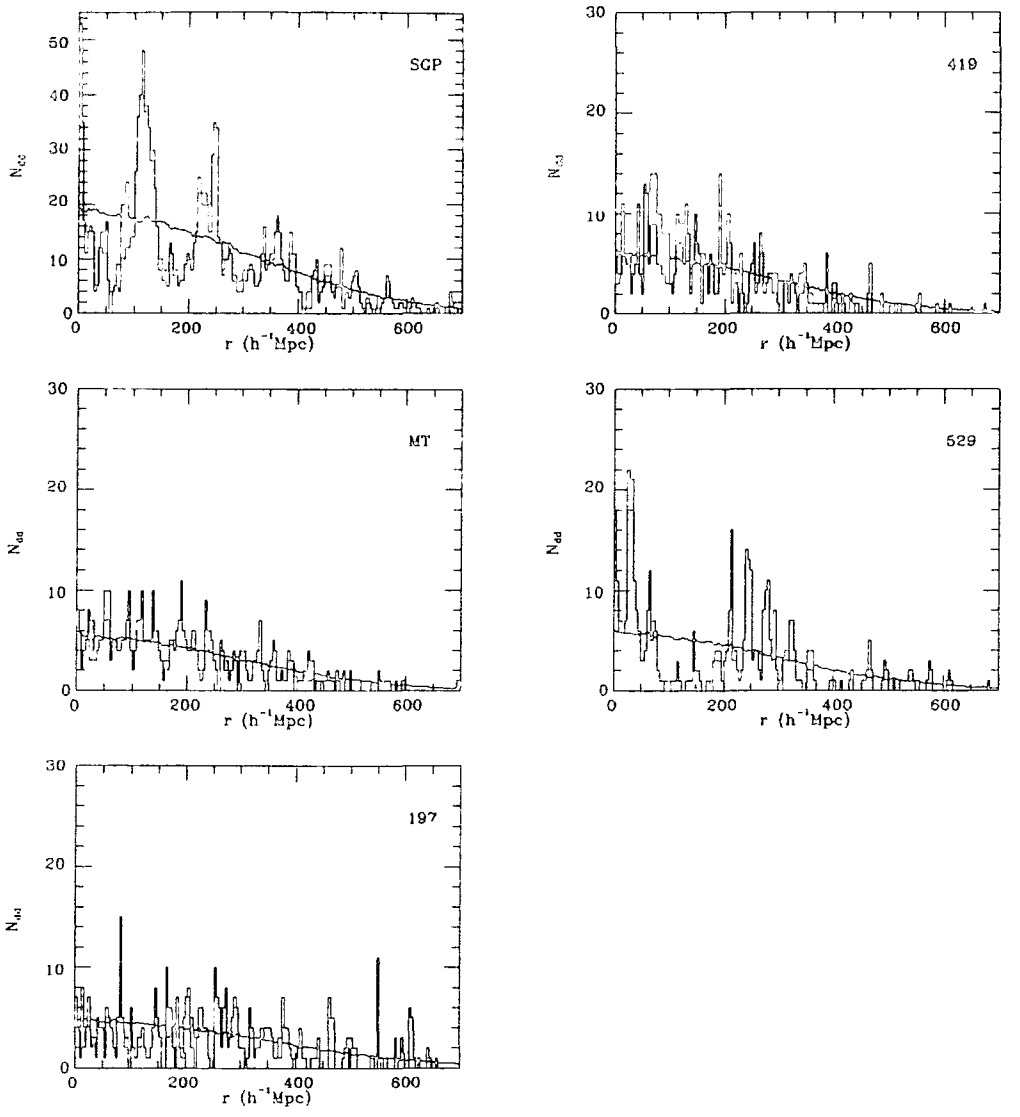


**Figure 6.4 Auto-correlations expressed as pair counts for comparison with the normalised random expectation for the five fields of the survey.**

at the scales corresponding to the inter-clump separations.

However it is perhaps remarkable that the SGP field contains 4 significant over densities and which are so evenly spaced in comoving coordinates, producing a very large excess over random in the pair count at distinct periodic scales. In fact the contribution to the features at 125 and $250h^{-1}$Mpc is from all galaxies in the 4 spike features of the redshift distribution. This behaviour will be returned to later after discussion of the small scale correlations.

## 6.5 Small Scale Structure

This survey by virtue of its large mean depth and velocity accuracy allows an estimation of the correlation function on small scales at an earlier epoch. The mean survey redshift is $z = 0.22$, representing 30% of the lookback time for $q_o = 0.5$ and by comparison with locally determined field galaxy correlations, we may look for any evidence of changes with time, or dynamical evolution. Of course selection effects must be accounted for, in particular the role of spectral evolution. Evolution we have argued, in chapters 4 and 5, produces an excess of star formation in the form of short bursts, consequently if the hosts to such activity are clustered differently from the general population then the correlation function may be affected.

This in principle can be accounted for by removing the strong lined objects, and below we examine separately the small scale correlations for subsets of the faint survey divided according to the equivalent width of [OII]3727Å, (see discussion in Chapter 4.2 of the importance of this feature).

To aid comparison with locally determined galaxy correlation functions the correlation function must be converted from comoving to proper coordinates assuming the 'null' hypothesis of no dynamical evolution on small scales. This can be achieved by simply dividing the amplitude calculated in comoving coordinates by a factor $(1 + z)^{3-\gamma}$ where $\gamma$ is the slope of the correlation function, which we take as the canonical value 1.8 (Groth and Peebles 1977), i.e a difference of 20% in amplitude at the mean redshift of $z = 0.2$.

Figure 6.4 shows the correlation function binned in $\Delta \log r = 0.1 h^{-1}$Mpc in proper coordinates, for individual fields using normalising within fields. The amplitude of the correlation function at small scales is in good agreement with Hale Sutton et al 1988, and this can be seen in Figure 6.4, however, there does appear to be a flattening of the slope for the faint redshift survey sample.

The role of galaxy evolution in altering the observed correlation function can be investigated by dividing the sample by the equivalent width of [OII]3727Å, at 25Å. We find however, (Figure 6.6) no significant difference in the overall shape and amplitude of these correlation functions so the flatter slope of the full sample does not appear to be the result of an increased presence of strong star forming galaxies in the survey with respect to local brighter apparent magnitude limited samples. However the uncertainties on these small samples

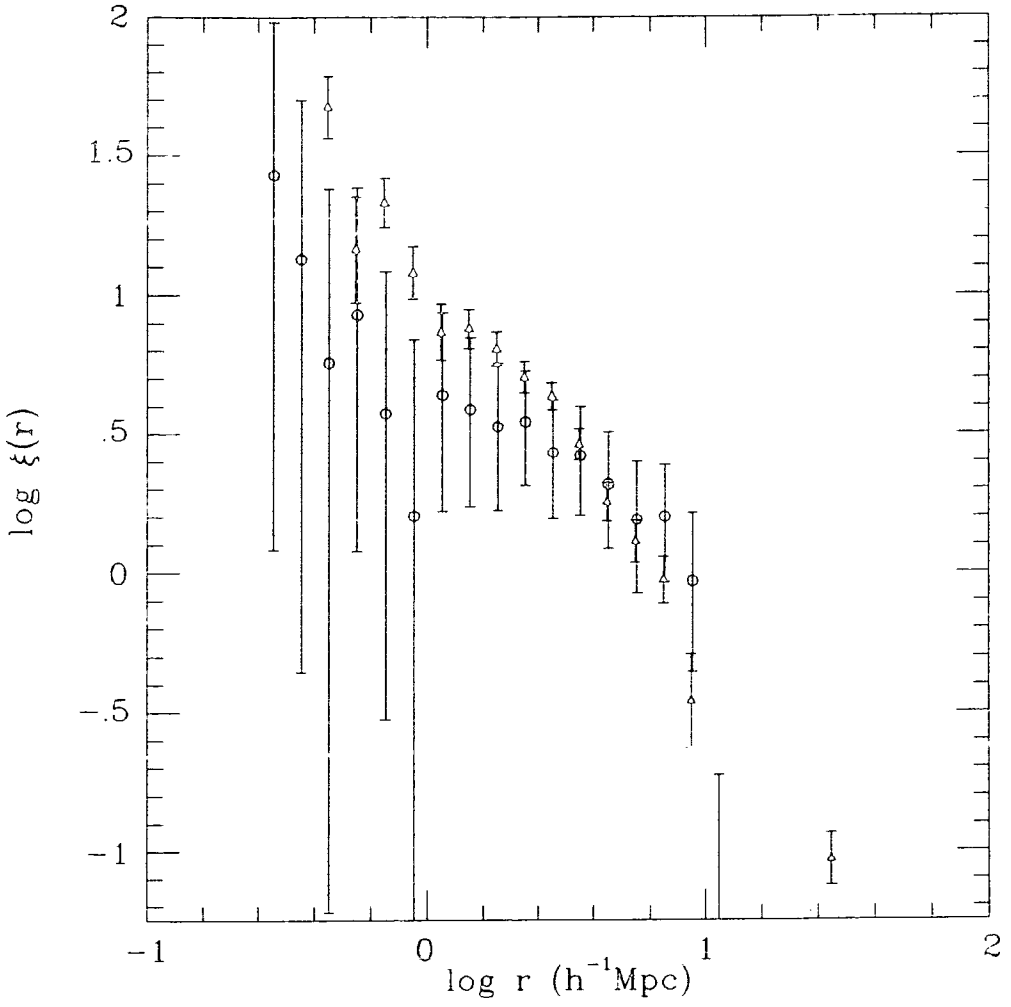


**Figure 6.5 Faint Survey Correlation function at small scales, for the faint redshift survey (open circles), compared with Hale-Sutton (triangles), errors are given by Poisson uncertainty**

are very large and the majority of small scale pair separation are in any case contributed by the SGP and 529 fields, which are unusual fields and so clearly more data are required to assess the role of evolution on the form of $\xi(r)$ at earlier times, before we can be confident of assesing any possible dynamical evolution.

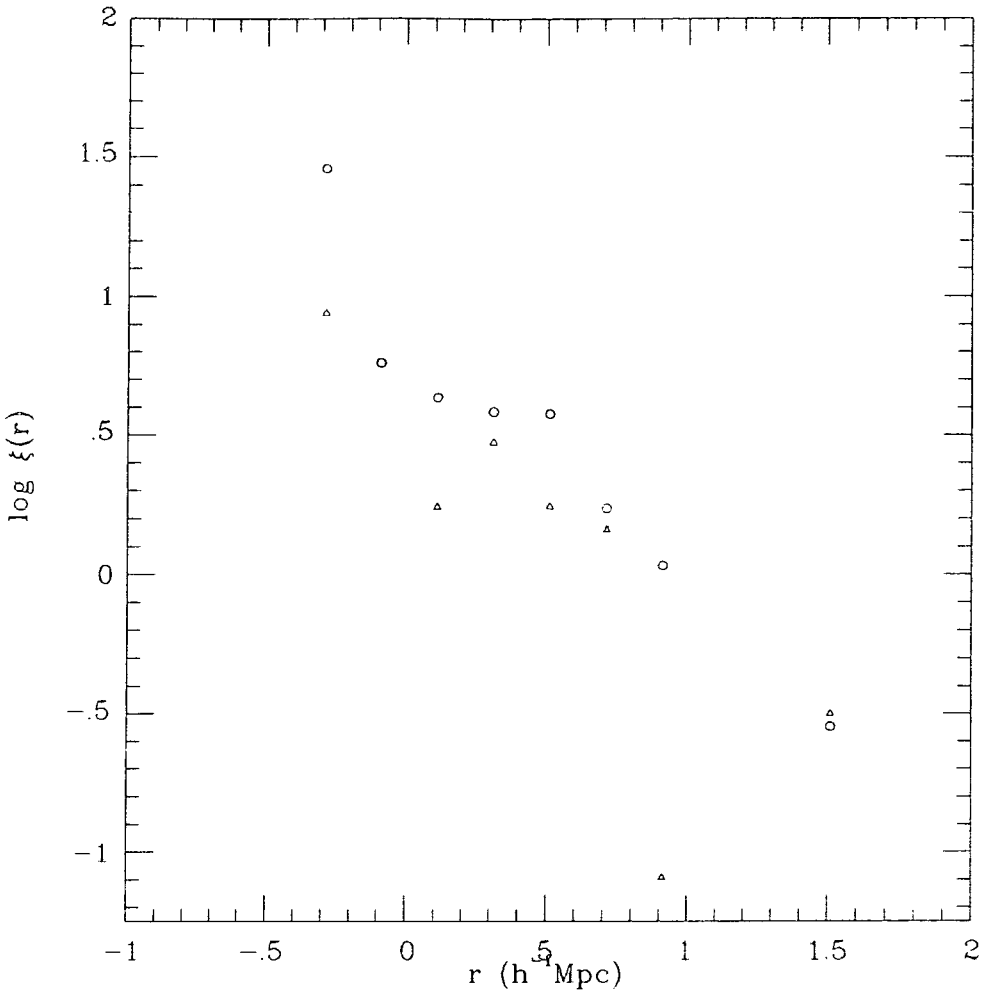


**Figure 6.6 Faint survey correlation function at small scales, for $W_\lambda < 25\AA$ (open circles) and $W_\lambda > 25\AA$ (triangles)**

## 6.6 Other Deep Redshift Surveys on the Galactic Poles

The identification of an apparent periodicity in the distribution of galaxies in the direction of the SGP prompts the question of whether this behaviour is found in other deep fields and in particular along the directions of the Galactic poles, where we have the largest amount of redshift information.

We are fortunate in being able to examine this line of sight in greater detail since the SGP has been studied most intensively. The bright magnitude limited survey DARS (discussed in Chapter 4) covers the redshift range $z < 0.1$ with the peak of the selection function falling at $z \sim 0.05$ - and the AAT plate, (from which the faint survey sample is defined), is central within the Schmidt

plate from which the DARS SGP field was taken, so that the lines of sight of these survey fields differ by only 0.3 degrees.

The redshift distribution of the DARS SGP field is very unsmooth and shows a number of peaks, the strongest of which, after division by the selection function for $b_J < 17$, lie at z=0.02 and 0.06.

The NGP is, for the same reasons as the SGP, a well studied area, and this good fortune means we can add more information about the clustering on the line normal to the plane of the Galaxy. The deep redshift survey of Koo and Kron (see Chapter 3.12 for details), is in the opposite direction (176 degrees away) from the faint survey SGP field and has a similar depth and sky coverage. The magnitude range is not clearly defined and but approximates $B < 22.5$ (Koo 1987). This field has been published in the form of a one dimensional redshift distribution only, in many review articles and these authors have drawn attention to the prominant clustering in the redshift distribution. This field looks remarkably similar to the faint survey SGP field and very unlike their other deep field (see Figure 1 Koo 1986) which is much smoother resembling more the 419, and MT fields of the faint survey.

Figure 6.7 shows this deep NGP field with the faint survey SGP field (normalised to Koo and Krons data), for comparison. The distributions although remarkably similar in that the majority of objects are sampled in sharp and periodic overdensities. The NGP field shows 3 prominent spikes features at z=0.125,0.18 and 0.235 with empty volumes between.

The bright magnitude limited redshift survey of Kirshner *et al* (1981) complements DARS, allowing clustering to be examined in detail in this interesting direction to a depth $z < 0.1$, for which the selection function of Koo and Krons' faint survey is too weak to be useful. The NP5 field of Kirshner *et al* covers 1 degree$^2$, limited to to $B < 16.5$, and centered only 8 degrees from the north galactic pole. This field also has a remarkable redshift distribution with two very large over densities centered at z=0.027 and z=0.07, and separated by a large gap in the redshift distribution which intersects the periphery of the large Bootes void region. Note the lower redshift spike includes galaxies of the Coma supercluster (z=0.023) which lies only $\sim$ 1 degree of the NGP. Figure 6.8 shows the redshift distribution of both this field and DARS at the same resolution, (normalised to DARS), and with the respective selection functions

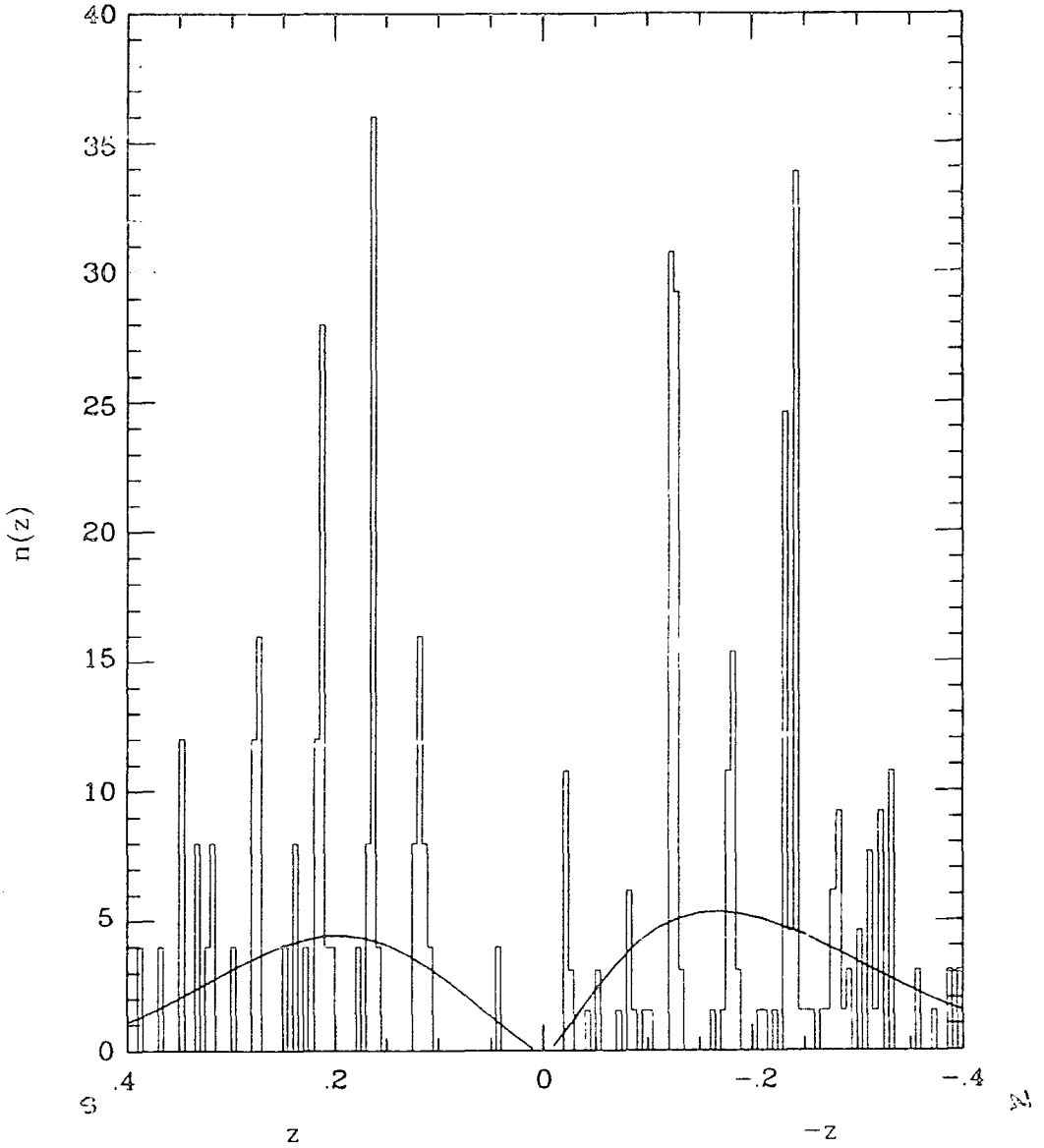


**Figure 6.7 Redshift distribution for the faint survey SGP field (left), and the deep survey of Koo and Kron (right), with selections functions indicated as solid curves and normalised to each data set.**

shown for comparison.

Fitting these surveys together, the resultant redshift distribution suggests a periodicity in the positions of the strongest overdensities, i.e. the spikes identified in the redshift distribution of the SGP field of the faint redshift survey, appear to form part of a much larger series of evenly spaced features of sharp features falling along an axis defined by the North and South Galactic Poles, and spanning at least $1200h^{-1}$Mpc. The combined redshift distribution is

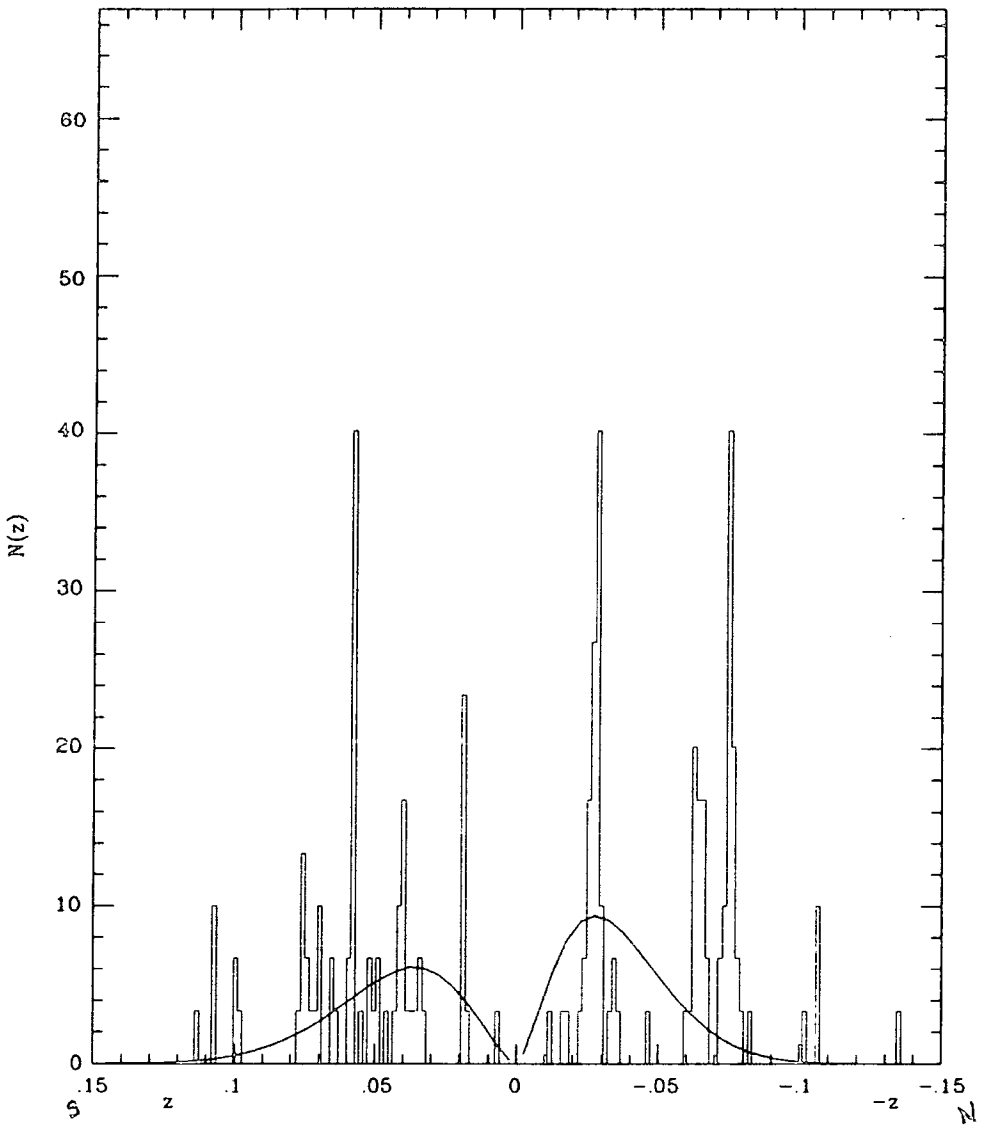


**Figure 6.8 Redshift distribution for the SGP field of the DARS survey (right), and the NP5 field of KOSS (left). Selection functions are shown as solid curves, normalised to each data set.**

shown in Figure 6.9, each redshift survey is adjusted to give approximately the same height at the respective peak of the selection function appropriate to each survey. We also show in this figure the best fitting comoving pair separations for comparison. The positions of strongest overdensities are well matched by choosing $q_o = 0.5$ and a comoving separation of $128h^{-1}$Mpc, demonstrating a possible high degree of regularity of clustering along this line.

At redshifts greater than $z = 0.3$ the selection functions of the faint

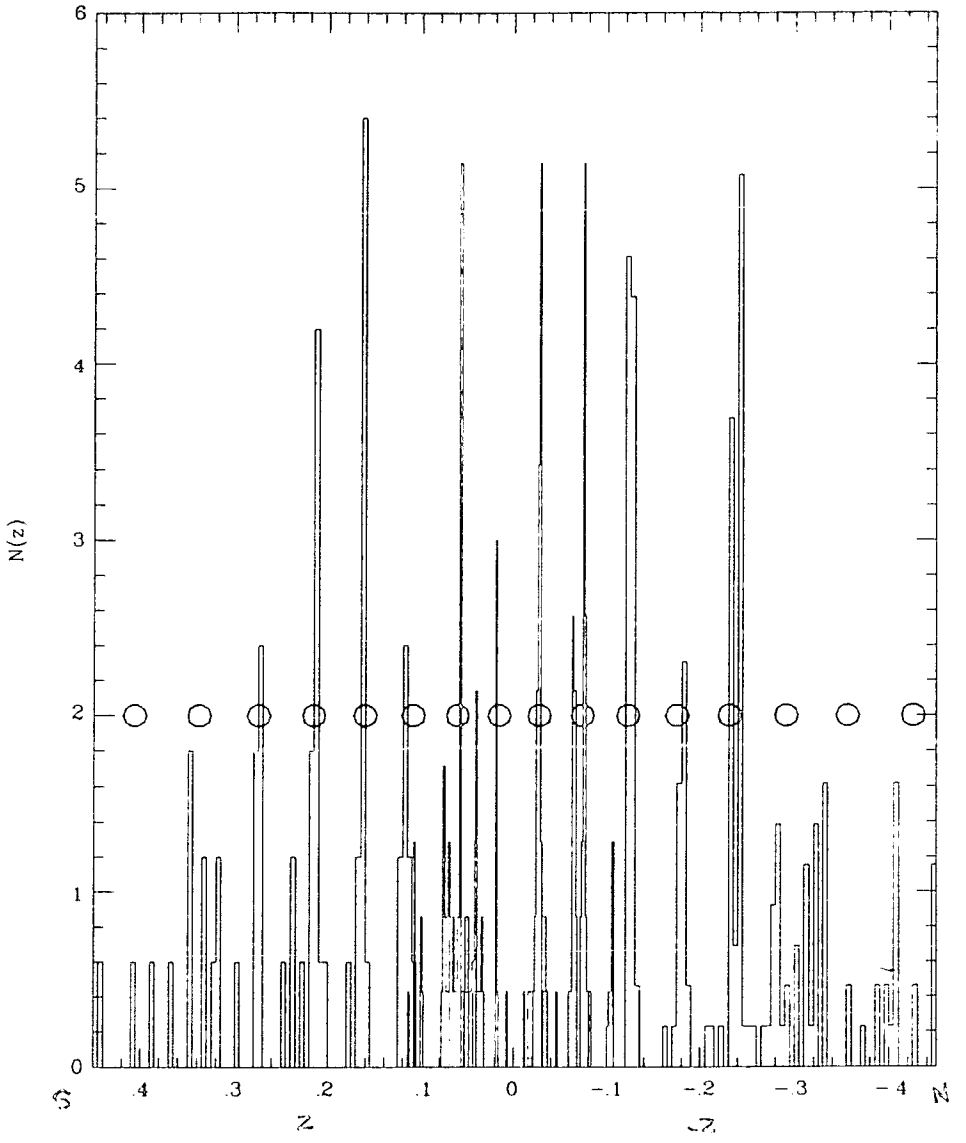


**Figure 6.9 Redshift distribution for the four fields of Figures 6.7 and 6.8, normalised as described above, with circles to indicate a constant comoving separation of $128h^{-1}$Mpc for $q_0 = 0.5$.**

surveys fall off and clustering information becomes uncertain. Interestingly however, there is a rich cluster of galaxies at $z = 0.566$ found by Couch *et al* 1988), is within the SGP field and was identified from a hypersensitised copy of the same AAT plate from which the faint survey SGP field is sampled. This cluster too lies to the expected position of an overdensity continuing the above sequence, however, the great depth means the prediction of its position is dependent on the choice of $q_0$, a point we demonstrate below.

Firstly we calculate the correlation function for the DARS and Kirshner *et al* fields for comparison with the SGP field of the faint survey, this is not possible for Koo and Krons' deep NGP field at present, which is as yet unpublished. Figure 6.10 shows the the correlation functions for these 3 fields, showing large scale correlations from $100h^{-1}$Mpc to $150h^{-1}$Mpc, which, in terms of the simple pair count are highly significant.

We can roughly calculate the maximum probability of finding such a pattern by chance by asking how often each of 11 intervals of width set to be the mean separation between overdensities is occupied by a prominant overdensity. The probability of such an occurrence is given by $n!/n^n$, and for n=11, it is only $1.4 \times 10^{-4}$. This is of course an *overestimate* since the peaks are clearly not randomly distributed within each interval. A more satisfactory approach to assesing the probability of occurence of such a redshift distribution would take into acount galaxy clustering. It would be more sensible, for example, to ask how often would such a pattern be sampled from the various differing N-body simulations constructed to describe the universal distribution of matter.

To examine the degree of regularity in this combined redshift distribution, we first define the mean spike redshifts by running a top hat filter of width $5h^{-1}$Mpc through this data. For the peaks of Koo and Krons' data we have to estimate the positions by eye, since the data are unpublished. Uncertainty in the mean redshift is far smaller than the spacing of these features, and in the case of the spikes at z=0.07 and 0.185 on the NGP, which appear to be 'split', we simply average over the full width of each feature.

A 'cluster-cluster' auto-correlation is now be constructed so that all separations can be examined. This is done in comoving coordinates and shown in Figure 6.11 for various values of $q_o$. This diagram contains all the information on pair separations, which are very clearly non-randomly distributed, showing a pattern reflecting the regularity of the peak separations. Note the smallest pair separation of $\sim$ 125 Mpc is the 'fundamental mode' and is a sharp feature for all values of $q_o$ in the range shown in Figure 6.11, so that the claim for regular spaced overdensities is independent of $q_o$. However larger scale pair separations are more sensitive to the choice of $q_o$ and it can be seen from figure 6.11 that the 'tidiest' or most regular spacing is given by $q_o = 0.5$. This diagram

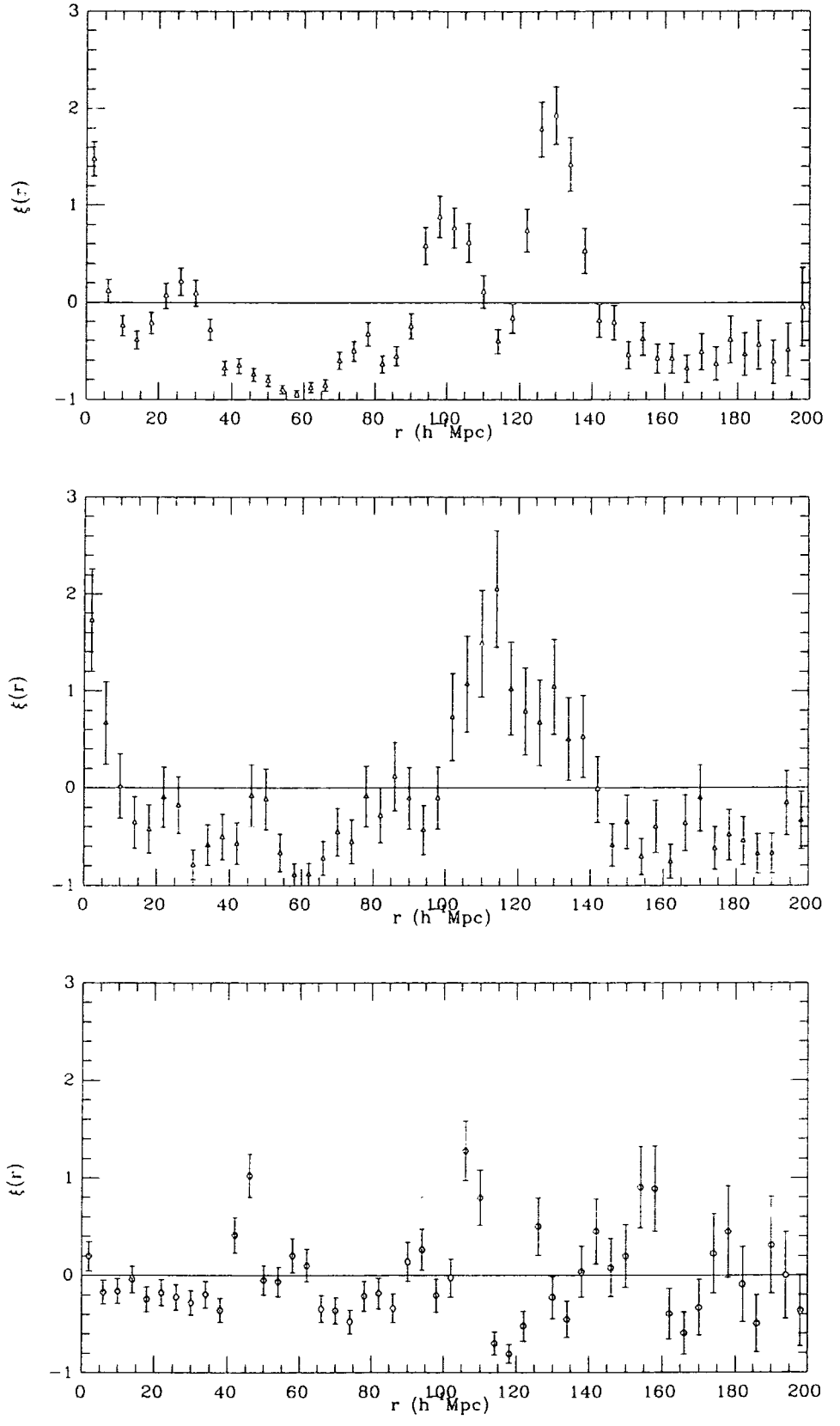


**Figure 6.10 Auto-correlations for NGP (Top) and SGP faint surveys (middle) and the and the DARS field (bottom).**

note, includes the SGP cluster the redshift of which favours $q_o \sim 0.5$, since the cluster lies well away from the 'predicted' position (accepting the reality and significance of this behaviour), than for the other values of $q_o$, this can be seen by comparing the position of the largest scale pair between diagrams.

Clearly at present, it is premature to discuss the implications of using such data for tests of universal geometry, more data of this form must be obtained to firstly establish the significance of these features, but the remarkable pattern of evenly spaced sharp features in a redshift distribution constructed from four completely independent data sets cannot be ignored.

Below we go on to discuss the properties of clustering in the direction of the galactic poles examining the spatial distribution of Abell clusters both close to the poles, and over the whole sky, to examine this behaviour further.

## 6.7 Clusters and Voids on the Galactic Poles

The extent of the 'spike' features as measured from the redshift distributions can be followed over only a few Mpc ($\sim 3h^{-1}$Mpc), due to the narrowness of the fields. However, a number of studies of the distribution of rich clusters on the polar caps have been made with the strong suggestion of very large scale structure in these directions. This data allow us to explore the clustering pattern tranverse to the line of sight for comparison with the narrow cone redshift data discussed above.

The Southern and Northern cap rich cluster correlation functions of Batuski *et al* (1987) and Kopylov *et al* (1986), claim evidence of large scale power in the correlation function. The sample of Kopylov *et al*, of large distance compact and Zwicky rich clusters cover a redshift range $0.05 < z < 0.25$ at $|b| > 60$ about the NGP. They claim, based on a sample of 50 redshifts, an excess correlation between 100 and $150h^{-1}$Mpc. Complementing this work, Batuski *et al* claim a similar result of a 'sizeable bump' in their correlation function at $150h^{-1}$Mpc. This is based on a sample of 225 redshifts of Abell clusters to $z < 0.085$, on both North and South Galactic caps.

It has also been noted by Stevenson (1986) that a large number of rich clusters are found at $z \sim 0.1$ on the SGP, indicating the presence of a supercluster in that direction. To examine the clustering of rich clusters at the poles further, we make use of the carefully compiled catalogue of Abell clusters of Olowin and Corwin (1988), for which 517 have secure redshifts taken from

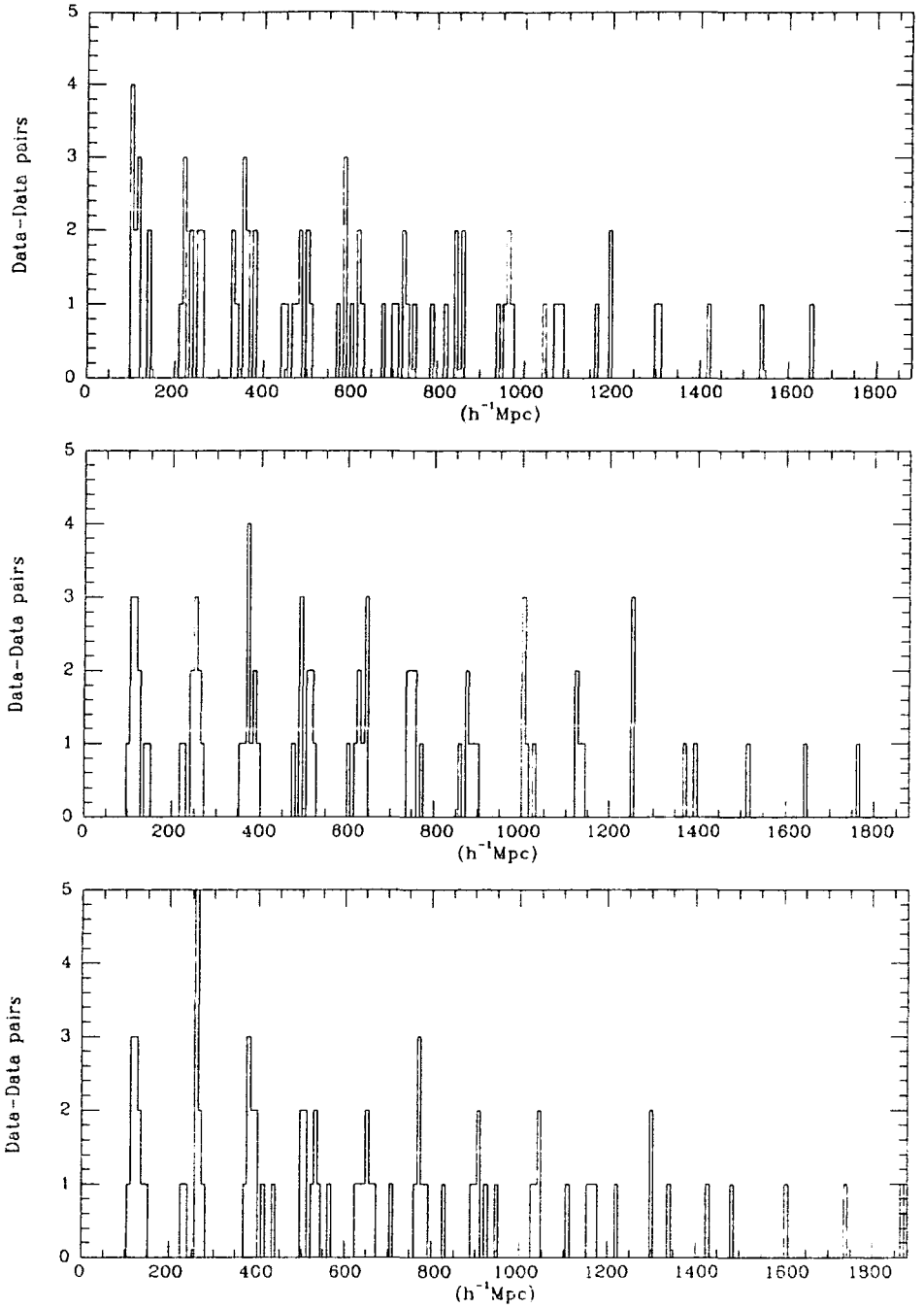


**Figure 6.11 Pair count correlation for strongest overdensities along a line defined by the Galaxy poles, for $q_o$=0.8 (top),$q_o$=0.5 (middle),$q_o$=0.2 (bottom).**

a variety of sources. Examining the association of clusters in the compilation we find a number a rich clusters grouped about the 'spikes' identified in the redshift distributions shown above.

We now examine projections of this cluster catalogue onto the X axis to see to what extent clustering is important along this line. Projecting all clusters within $60h^{-1}$Mpc from an axis with a pole which points to 13hrs 30mins, +27 degrees, (defined by the redshift data discussed above), shows some evidence of a periodicity in the distribution. Curiously however, we find this behaviour is *more* exaggerated when the entire catalogue is projected onto this axis, indicating that structures orthogonal to this line may be present over much larger scales. These distributions are shown in Figure 6.13, clearly a strong periodicity is observed, with overdensities at z=0.03 0.08 on the NGP and z=0.05 on the SGP, with little else between. Note here all measurements are indicated in intervals of redshift for convenience, since distances are proportional to redshift to the depths of this catalogue.

Comparing this with the redshift distribution from the redshift surveys we find interestingly an agreement in positions of cluster overdensities in this projection, with the positions of the 'spikes' identified above from the galaxy distribution along this line of sight. This can be seen by comparison of Figure 6.13 with Figure 6.9. One nearby feature in the galaxy distribution is not matched by the cluster projection; a deficit of clusters is found for $z < 0.02$ in the Southern Galactic Hemisphere. Unfortunately the combination of galactic obscuration the declination limit, result in only a small volume to this low redshift in this part of the sky, and hence a deficiency of observed clusters. The declination limit note effects all depths on the negative X axis, and this can be seen by comparison with the greater number of clusters which are projected onto the positive X axis and demonstrated shortly in Figure 6.14.

Figure 6.13 shows that the contribution to this periodic behaviour is not only from the large groups of clusters noted above lying close to the X axis, but also from association of clusters over the whole survey volume. To investigate this further we examine projections of the catalogue onto 3 orthogonal planes. To do this we must first define the orientation of one of the remaining axes, which can be arbitrary. However it is possible to choose an axis in the YZ plane to align within only 12 degrees of the supergalactic plane defined by de-Vaucouleurs (1972), in other words, we can by suitable choice of axes set up the coordinate system to be within 12 degrees, of super galactic coordinates (note Y axis of the Supergalactic coordinate system is then equivalent to the

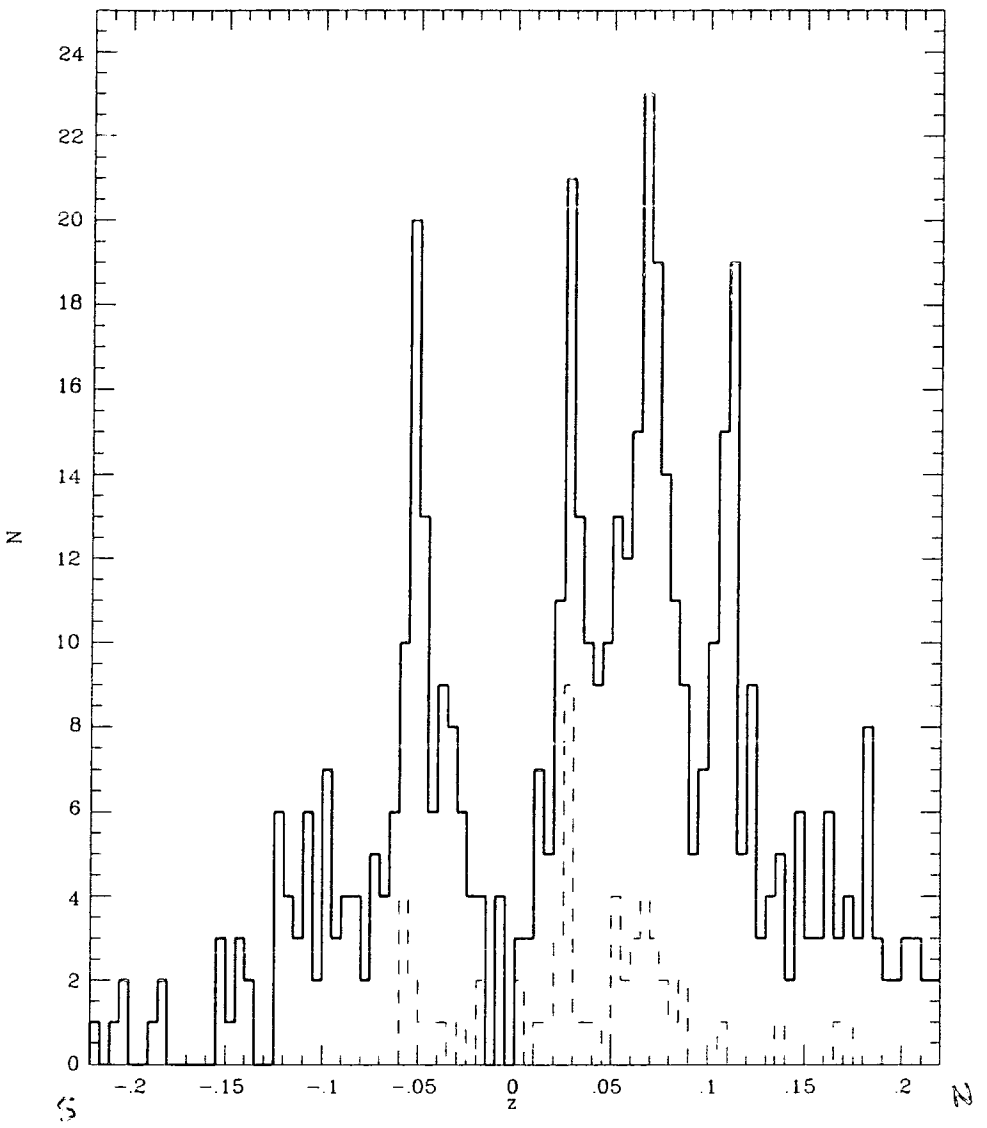


**Figure 6.13 Projection of Abell clusters onto an the X axis (defined in the text), for the full catalogue indicated by solid histogram, and for clusters less than $60h^{-1}$Mpc from this axis, by the light histogram**

X axis here). Note also in these diagrams, the wedge shaped regions in which clusters are not sampled due to galactic obscuration, and declination limit of the Abell catalogue, which is most apparent in Figure 6.14a.

Looking down the Y axis onto the XZ plane (Figure 6.14a) it is apparent that the 1D projection of clusters shows the overdensities which contribution to be extended over the full width of the sample, but with the majority of large overdensities along the X axis at $Z = 0$. Projection onto the XY plane (Figure

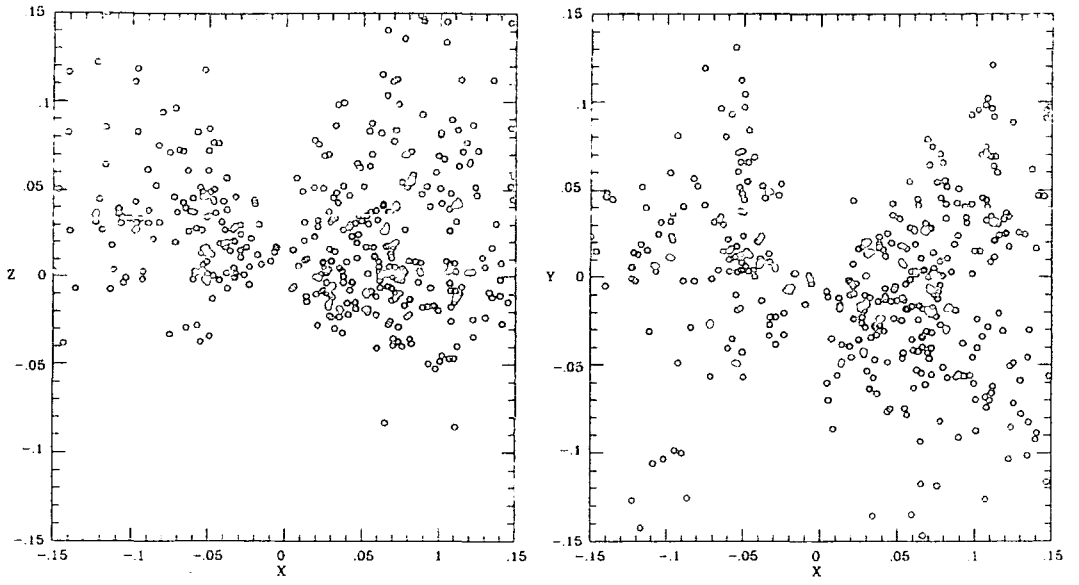


**Figure 6.14 Projection of Abell clusters onto the XZ plane (left), and XY plane (right).**

6.14b) shows what appears to be a rather complex pattern containing some large voids, and does not look as periodic as the XZ projection, indicating that a description of the periodicity along the X axis in terms of planes, would be too simple.

Note that since this system is close to the supergalactic coordinate system and therefore the supergalactic plane is almost orthogonal to the extended features tentatively identified above. And interestingly Tully (1986,1987) has argued that the spatial distribution of Abell clusters in the sample of Struble and Rood (1987), for a very much larger super galactic plane than the local flattened structure found for bright galaxies. In fact we can look for the same with the compilation used here, by forming a 1D projection onto the Z axis of our system. Figure 6.15c does seem to suggest an excess at $Z = 0$ in agreement with Tully, also shown are projections onto the other 2 axes in this system.

It is important to note that the redshift measurements for the Abell clusters

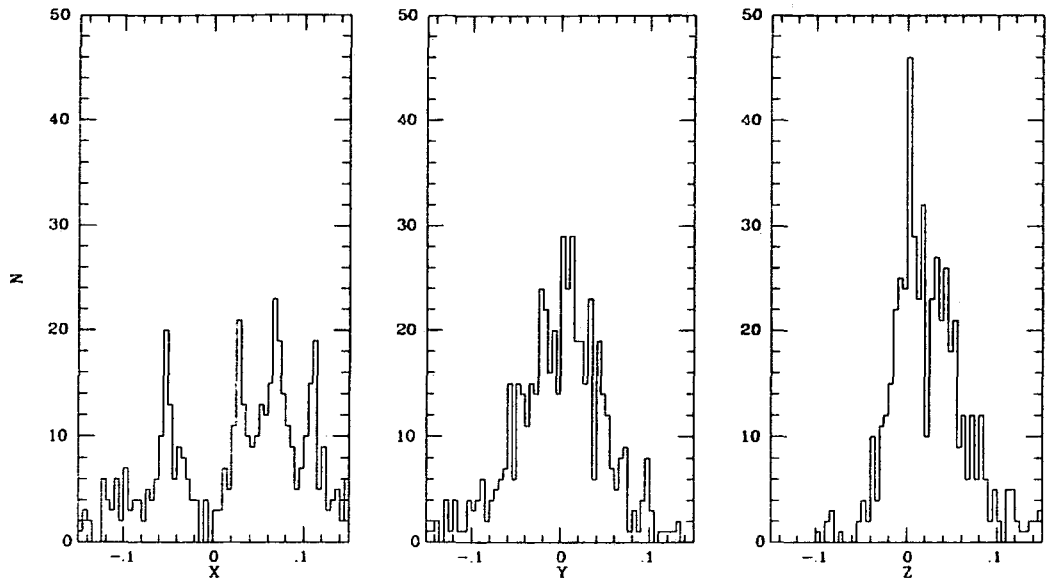


**Figure 6.15 1D Projections of Abell clusters onto the X axis (left), Y axis (center) and Z axis (right) (see text for definition of coordinate system).**

in Olowin and Corwins' compilation are from a number of different authors and so covers the sky heterogeneously. Clearly selection effects in this process are not well controlled and these results must await further cluster redshift measurements. Sutherland (1988) has also noted a more fundamental point, that clusters identified close in projection on the sky may not be unrelated, in that the extended radial densitiy profile of a cluster contributes an excess of galaxies which may enhance the local projected detection of other clusters. Correction for this effect, Sutherland shows, may lead to a significantly reduced cluster correlation function, however, this is not supported from a sample of X-ray selected clusters of Lahav *et al* (1988), which although constitutes only 60 clusters, seems to be more strongly clustered - consistent with the results of Bachall and Soneira (1984b).

We may crudely examine the nature of the structure shown in Figure 6.13, by simply rotating our coordinate system slightly and see the periodic behaviour

in the 1D projection onto the X axis washes out, as would be expected for narrow extended structures. Figure 6.16 shows the 1D projections which are offset from the X axis in RA by $\pm 15$ degrees, and indeed do not show any obvious periodicity, the sharp features of Figure 6.14 are now smoothed in projection along these offset axes.

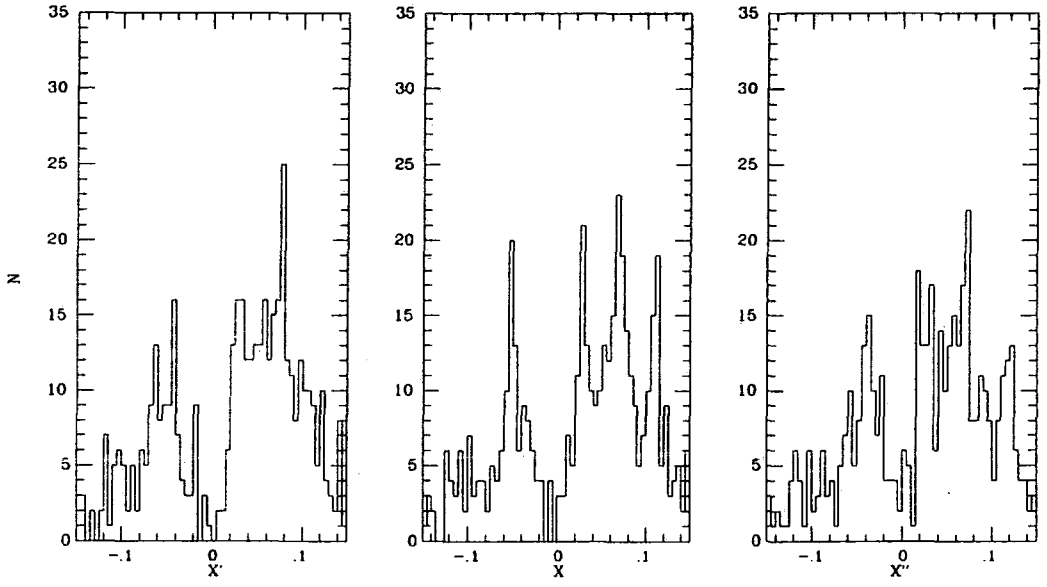


**Figure 6.16 Projection of 517 Abell clusters onto an the X axis (center), and onto two axes pointing 15 degrees away from a pole defining the X axis.**

Greater completeness and depth will be required to examine the distribution of Abell clusters more fully and for now we simply note the strange behaviour of clustering along this axis, which may tentatively indicate a large periodicity and which is coincident with the galaxy distribution along the same axis.

### 6.7.1 Discussion and Conclusions

Unusual clustering patterns in the Abell catalogue have been noted by a number of authors, Tully claims large connected regions of low filling factor from a percolation analysis (Tully 1986). Pietronero (1987) makes an interesting claim

that the observed difference between the amplitude of the correlation functions of rich clusters and galaxies, is as expected if the distribution of galaxies follows a simple fractal pattern over a wide range of scales - a possibility raised by Mandelbrot (1982). The agreement between the position of overdensities of Abell clusters projected onto an axis coincident with those observed by the redshift surveys along this line is interesting, and possibly compelling evidence for at least considering the possibility of a large scale periodicity in the clustering pattern of both galaxies and clusters of galaxies.

These results are tentative at present, and unappealing in terms of standard cosmogonies, requiring perhaps a strong phase correlation on large scales. One interesting possibility for producing such behaviour maybe the very late time phase transition proposed by Hill *et al* (1988), in which the regularly spaced domain walls on scales of order $100h^{-1}$Mpc are produced, and subsequent evolution of the walls will determine the final clustering pattern. This scenario has a particle physics motivation, and since the phase transition is expected to be post-recombination, it has the advantage of producing very large scale structure without significantly perturbing the Microwave background.

## 6.8 Count Variance

Related to the question of large scale structure is the variance in the galaxy number counts. As discussed in Chapter 2.5, field to field variations in the counts are found in the 4m plate $b_j$ counts such that the numbers observed at any magnitude, vary between plates by as much as a factor of $\sim 2$ (Jones *et al* 1989, in preparation), in a systematic way so that fields are either high or low over the full useful magnitude range, with good agreement of the differential count slope between fields.

This variance is far greater than the poisson expectation of only 1%, and seems too large to be fully accounted for by uncertainties is photometric zero-points amounting to $0.^m7$ between extreme fields. We note here that the 197 and SGP fields Peterson *et al* (1979) and Shanks *et al* (1984) represent examples of low and high count fields respectively, and show very different redshift distributions. As discussed above the SGP is distribution is mostly contributed by 4 spike features, but the 197 field shows a much flatter and smoother redshift distribution (see Figure 6.2).

If large scales periodicities are a common feature of the galaxy distribution

then we may expect large field to field variation in the counts, with large numbers of overdensities aligned in only some preferred directions.

Clearly the expected variance depends not only on the spatial distribution of galaxies but on the form of the selection function; a broad flat function will select more groups than a narrow peak. In fact the evolutionary model of Chapter 5 predicts that the redshift distribution will to the limit of 4m plate material, be bell shaped centered on $z = 0.35$, and so strongly influenced by the clustering on the length scale of the SGP data. For example removing the clump in the SGP field at z=0.22 and 0.16 in would reduce the count on the SGP at $b_j = 21$ by a factor of 2 and in line with the 197 field at this magnitude.

## 6.9 Conclusions

From the faint redshift survey we note some evidence for large scale excess in the correlation function, although this result is dominated by two fields for which the clustering shows large gaps and over-densities in the redshift distribution.

At small scales the correlation function does seem to be marginally flatter than that of Hale-Sutton *et al*, and may indicate the effects of evolution. The role of starburst evolution is not clear at present from this data and in addition the majority of small scale pairs are contributed by only two fields, much more data is required before we address the question of dynamical evolution on small scales.

The combined redshift distribution of galaxies selected from four independent redshift surveys close to both the Northern and Southern Galactic poles show an apparent periodicity which extends over at least $1200h^{-1}$Mpc with at least 11 sharp regularly separated overdensities in the redshift distribution. which form a chain along this line.

This observation would seem to be supported by a periodicity observed in projections of Abell Clusters. Peaks in a 1D projection along this same line of sight coincide with 4 of the nearest 'spikes' in the combined galaxy redshift distribution.

These cluster overdensities although mostly concentrated along the Z axis do seem to be extended in 3 dimensions and may trace out a very large scale and complex spatial distribution.

These results are tentative at present but underline the importance of pursuing deep galaxy and cluster redshift surveys. If this behaviour confirmed from a wider sky pattern it would be of great interest for theories of galaxy formation, indicating perhaps the presence of phase correlations over large scales in the primordial density field.

# Chapter 7.

# CONCLUSIONS and DISCUSSION

In previous Chapters we have examined the nature of galaxy evolution and clustering by comparison of the general properties of galaxies, sampled at the current limits of spectroscopy and photometry, with carefully constructed models based on local galaxy distributions.

New spectroscopic redshift survey data is presented from which we determine the redshift distribution of galaxies at magnitudes faint enough to penetrate the galaxy count excess observed in the B passband. This redshift information allows new statistical inferences to be drawn about the history of star formation of the general galaxy population.

## 7.1 Spectral Evolution and Faint Photometry

In chapter 2 we set out our standard no-evolution model which formed the framework for the subsequent analysis of faint galaxy distributions. A comparison of this model with deep CCD galaxy counts and colours, for the $b_J$ and $r_F$ passbands, revealed a number of new results.

We found that traditional methods for modelling the count excess and colour distributions are not able to generate reasonable fits either of these these distributions. In the past other authors have concluded the contrary, but based on brighter photographic photometry and only then by 'tuning' the different star formation histories assumed for the various galaxy types. The CCD differential counts in $b_J$ show a power law slope extending to the current faint limit of $b_J = 25$, with no indication of a turn over at the faintest magnitudes. This behaviour is very difficult to reproduce with monotonically declining star formation rates at earlier times, demonstrating that the old models are increasingly untenable at faint magnitudes.

The CCD colour distribution in $b_J - r_f$ is bimodal. The count excess with respect to the no-evolution model is concentrated at bluer colours, in the colour range $b_J - r_F < 1.6$. In addition a red tail extending over a range $1.6 < b_J - r_F < 3.5$ is observed to $b_J = 24$, which is fully consistent with our no-evolution prediction. This conclusion is in agreement with the observation of unevolved early type optical spectra to $z < 1$, from the very deep spectroscopy of Hamilton 1986 and Gunn 1989.

We also conclude from Chapter 2.9 that a non-evolving, non-standard model will reproduce the number counts, and is allowed by the present uncertainty at the faint end of the galaxy luminosity function. Such models are rather ad-hoc however, and require large populations of low luminosity systems to lie just beneath the present limits on the local faint end luminosity function.

Interpretations of the faint galaxy distributions presented in Chapter 2 span a wide range of possibilities for the counts, and we conclude with confidence only that a clear blue excess is apparent from comparison of deep distributions with our standard no-evolution model and that the red tail of this distribution is fully consistent with our no-evolution model. Finally we stressed the need for redshift information to help discriminate the various interpretations.

### 7.1.1 Faint Spectroscopy and New Descriptions of Evolution

In Chapter 3 we presented the results of a faint galaxy redshift survey, these data represent the faintest complete field galaxy redshift survey to date and sample the counts at magnitudes faint enough to examine the reasons for the count excess. A high degree of completeness of 90% is achieved, for galaxies selected in apparent magnitude slices between $20 < b_J < 21.5$, resulting in a total sample of 189 redshifts covering 5 well separated high galactic latitude fields. The mean redshifts derived from each field are in excellent agreement, we find $\overline{z} = 0.22 \pm 0.015$ in the magnitude range $20.5 < b_J < 21$.

Comparison of the redshift distribution with the models discussed in Chapter 2 favours a new interpretation of the counts, and strengthens our earlier conclusions regarding the difficulties with the standard descriptions for evolution. Firstly we do not find evidence for a high redshift tail to the redshift distribution in this survey, nor is there an excess of intrinsically low luminosity galaxies, required by the radical no-evolution model. In fact the mean redshift is consistent with the standard no-evolution model, but since the counts are in excess of this model by at least 30%, then we conclude that evolution must take place such that only lower luminosity galaxies are significantly influenced.

Luminosity evolution for galaxies at the bright end of the luminosity function must have been very small over the redshift interval $0 < z < 0.5$ and thus the popular luminosity evolution models are restricted to those models producing only a minimal effect, and thus this form of evolution is not the principle reason why the slope of the blue number magnitude counts is steep

at $b_J > 20^m0$.

This result is surprising not only in the context of the traditional luminosity evolution models of Tinsley and Bruzual, because we know that for early type systems their present day red colours imply much higher star formation rates at some time in the past. This suggests that the redshift of galaxy formation is high for any population obeying the single burst c-type models, and that a large proportion of the population might be displaying a fairly constant star formation rate with look-back time, resulting in only minimal evolutionary changes in luminosity and colour. This lack of bright galaxy evolution strongly supports our earlier conclusion from Chapter 2, that the colour distributions to fainter magnitudes show no significant colour evolution.

The major new conclusion from the redshift survey, is that at least one extra evolutionary process needs to be invoked to explain the observed redshift and count distributions at the faint limits of this data. We find that a simple steepening the luminosity function with redshift so that the bright end is not significantly evolved produces an excellent empirical fit to both the number counts and redshift distributions. This may be interpreted as luminosity dependent luminosity evolution.

## 7.2 Spectral Evolution

Extending our analysis to the spectral properties of the galaxies sampled in the faint redshift survey, we find clear evidence for higher star formation compared with local surveys.

The evolution required by the count excess is apparent from a comparison of the emission line strengths of O[II]3727Å of this survey with the shallower DARS survey. The distribution of the equivalent widths of this line for the faint survey, extends to higher values than DARS. We conclude that possible sources of error and systematic effects by no means account for this difference, and that at $z \sim 0.2$, strong emission line objects are present in excess of local galaxies.

The strong lined objects are further investigated via detailed spectral modelling, using stellar synthesis codes and intermediate resolution stellar spectra. We find that at least 30% of objects are undergoing anomalously strong star formation, best explained by short duration ($\leq$0.2Gyrs) enhanced star formation.

This mode of star formation is locally rare, and therefore represents a

strong evolutionary effect at faint magnitudes, and is consistent with evolution found in other deep survey work. In particular the evolution required by the steep faint radio source counts, where starburst activity is argued completely independently, based radio emission properties (see Chapte 3.11 for discussion of this point).

We conclude that the results of Chapter 3 and 4 combined, argue strongly for strong evolution of starburst activity over recent epochs and provide a natural explanation of the blue number count excess.

## 7.3 Starburst Models

We show in Chapter 4 that the effects of even the conversion of small amount of a galaxies mass into stars will, for a short duration burst, have a large effect on the host galaxy, increasing the luminosity of a galaxy significantly, and producing a bluer spectrum. In Chapter 5 we demonstrate, with detailed modelling, that this activity can have an important effect on the faint galaxy counts and colour distributions. By adding recurrent starburst activity into the general field galaxy population we are able to reproduce the observed faint galaxy number counts such that the low luminosity galaxies are most strongly affected.

In detail we find that the simplest model for which burst star formation rates are proportional to gas content cannot produce a steep enough count for $b_J > 23$, without producing unacceptably high mean redshifts. If we insist on accounting for *all* the evolution seen in the counts via the burst model then more promising fits are obtained with a truncated initial mass function so that only high mass stars ($> 3M_{\odot}$) are formed. This removes the constraints on the evolution imposed by accounting for the gas consumption, and allows a larger rate of evolution.

The deep colours distributions provide additional constraints on these models. We find that the blue excess observed in the colour distributions is best matched by a model which includes either bursts slightly longer than the adopted $10^8$ yrs and/or a small amount of reddening (E(B-V)$<$ 0.25), otherwise the predicted colours for the best fit models are too blue.

The primary conclusion of Chapter 5 is then, that we can construct simple models, with evolution dominated by the effects of short bursts of star formation, which do fit the faint galaxy photometric properties, and can simultaneously

reproduce the redshift distribution and spectral properties of the faint redshift survey.

### 7.3.1 Redshifts from Photometry

The above results have important implications for the attempts of some authors to determine galaxy redshifts from photometric data alone. Multicolour data has been used to produce approximate redshifts of faint galaxies (c.f. Koo 1985, Loh and Spillar 1986, Cowie *et al* 1988), this technique relies on a complete knowledge or modelling of galaxy spectral energy distributions, their time-dependence and range. Furthermore, since the evolution is greatest in the blue, those selected at that wavelength are the most important to study for evolutionary purposes and yet the hardest to obtain photometric redshifts for, since their spectral energy distributions are generally flat. The strong effect of bursts on the galaxy population will considerably complicate these attempts, since the combined spectrum of a galaxy and a burst has at least a dependency on galaxy type, burst strength, burst age, duration and redshift, producing a wide range of continuum shapes and colours. Therefore conclusions relating to redshifts which are determined photometrically are, at best, dubious.

### 7.3.2 Starbursts and Dynamical Evolution

The role of galaxy interaction in 'triggering' starburst activity has been pointed out by many authors (Larson and Tinsley 1978, Joseph 1987). However, we have not stressed this strongly in this thesis because it is unclear if interaction is common to all starburst activity or if instead, the majority of bursts are self induced. Careful sample selection criteria are required in order to address this problem: it cannot be concluded that enhanced star formation only accompanies interaction if the galaxies studied are selected because they appear morphologically disturbed in some way.

If interaction is important then, as noted in Chapter 5, the starburst modelling would require modification. For example, this activity is then determined in part by the dynamical evolution of matter and thus may depend sensitively on the choice of cosmological model. We may expect, perhaps, a preferred epoch(s) of starburst activity, linked to the general velocity field, which may have a scale dependency and a complex evolution. At present such dependencies, if any, can only be examined empirically.

## 7.4 Large Scale Structure

We claim tentative evidence of large scale regular periodicity in the galaxy and cluster spatial distribution. This is evidenced from the 2-point spatial correlation of galaxies in the faint survey and results from the regularity of redshift distribution in the SGP field. This behaviour is repeated in 3 other independent redshift surveys. These surveys lie close to the galactic poles and combined, display an apparent periodicity extending over $\sim 1200h^{-1}$Mpc. We also conclude a similar pattern in the spatial distribution of Abell clusters.

These results, if confirmed from a wider sky pattern, are not easily understood in terms of the conventional picture of clustering grown from gravitational instability from simple scale free initial conditions within the framework of standard linear theory, assumed in most descriptions. However these assumptions are only justified in the absence of a firm physical model for the seeding of density perturbations, and other exciting and very different explanations for the growth of structure have been suggested by some authors, inspired by the newly realised self-organising and complex evolutionary behaviour common to many physical systems (see Davies 1988, Prigogine 1988).

An interesting and perhaps related point is the observation that redshift survey work throws up large scale voids in the galaxy distribution of order the sample depth - no matter the size of the survey, from galaxy local galaxy redshift surveys to the larger volume rich cluster studies. This behaviour we find here also (see the 529 field of Figure 6.1). Indeed the high degree of inhomogeneity in the very large redshift survey of Huchra and Geller and collaborators, makes it very difficult to derive an accurate corelation function for their sample, de Lapparent *et al* (1986), they quote a correlation length with a $1\sigma$ error of 70%.

These points are emphasised by proponents of the fractal description of galaxy clustering (see Pietroneiro 1988, Scheaffer 1986, Mandelbrot 1987) in which a scale free inhomogeneous distribution is argued to extend over a range of scales much larger than the usually accepted corelation length. With such a mass distribution, note, the common assumption that with larger samples of galaxies better estimates the correlation function or mean luminosity density are allowed, becomes a nonsense over the range of scales to which any fractal pattern may apply.

## 7.5 Future Work

### 7.5.1 Starburst Models

An obvious extension of the Models of starburst evolution developed in Chapter 5, is to apply them to the faint radio source counts discussed in Chapter 4.11. Constraints on the form of the star formation rate at the high mass end of the initial mass function may be obtained by comparison of these faint source counts with the models of Chapter 5. Using existing redshift and optical colours for these faint sources we may separate the radio starburst population from the populations of local late type spirals and strongly evolving double lobed bright elliptical galaxy population. One would hope to obtain a self consistent picture for the evolution required by both the radio and optical source counts.

Modelling the Far Infra-red emission would then follow, since here knowledge of the rate of massive star formation determines the intensity and temperature of the Lyman continuum radiation field. The IRAS point source survey and the follow-up redshift surveys will provide the essential data for this work.

In order to examine the connection between galaxy interaction and burst activity samples of galaxies with spectral evidence of enhanced star formation are required. 2 dimensional velocity information and careful dynamical modelling would then reveal if these systems had suffered recent gravitational disturbance.

### 7.5.2 Bright Galaxy Evolution

The clear result to emerge from this thesis is the need to abandon earlier expectations of the form of galaxy evolution, with important implications for galaxy formation. The question at what redshift did the majority of star formation take place in bright early type systems in now restricted to two increasingly constrained possibilities. Firstly for $b_j > 24$ we may expect a new mode of evolution to become important. The count excess at these magnitudes is not easily reproduced with the burst model of chapter 5 unless we suppress low mass star formation. We may reason that late epoch ($z < 5$) density evolution may feasibly assemble the bright end of the luminosity function, and the early high star formation (required by the present day colours) lifts the luminosity of these otherwise lower luminosity systems so that they are included in the counts at faint magnitudes. Such strong star forming sub-units will naturally

be blue, as required by the faint colour distributions. Subsequent dynamical evolution and the cessation of strong star formation, might be supposed to build up the red tail to the faint colour distributions - for observation at much lower redshifts. Such a picture for galaxy formation is expected in the popular Cold-Dark-Matter scenario, in which low redshifts galaxy formation and extensive merging is expected (Frenk *et al* 1988).

If we prefer a simpler single collapse for galaxy formation the early epoch of strong star formation is restricted to $z > 5$, since the high luminosities generated would be apparent as bright as $b_J = 20$ (without significant reddening - see chapter 2.8). In which case we must expect to find indications of a hump-like count excess in the near-infrared, unless again, dynamical evolution is important. Deep area photometry in the near-infrared and modelling along the lines of Chapter 2 are required to address this possibility.

However, no indication of a very high redshift excess has been uncovered from extensions from the $b_J$ selected redshift survey work of Colless *et al* 1989, who have obtained a redshift distribution to $b_J = 22.5$. The results are consistent with the expectations based on the starburst model of Chapter 5: the mean redshift is in agreement with the no-evolution and yet the count excess is a factor 2.5 higher than the survey presented here, and again a large fraction of strong lined objects is sampled.

Further deep field redshift surveys must be pursued to even fainter limits, as the only reliable discriminator of the above possibilities for galaxy formation. Colour selecting the bluest objects at $b_j > 23$ for spectroscopy will be most useful approach, since here the evolutionary excess is greatest. Given our experience of the flat spectrum sources in the faint redshift survey, we may reasonably expect strong line emission from such sources, considerably reducing the task of obtaining redshift information at such faint magnitudes with the presently available techniques. Even a handful of reliable redshifts for faint blue objects would be enough to discriminate the above possibilities and may be regarded as as one of the most direct tests of the CDM picture of galaxy formation.

### 7.5.3 Large Scale Structure

The claimed large scale regularities in the deep galaxy and cluster redshift surveys, of Chapter 6, must be followed up with care before we can be confident

of claiming such unexpected behaviour. Frustratingly little 3D data on scales above 50h-1Mpc exists other than by implication from projected catalogues, but with tentative indications of interesting large scale features. The recent availability of multi-object fibre spectroscopy in both the northern and southern hemispheres could be exploited here.

Redshifts for the remaining Large distance class clusters is an obvious goal, in particular the spatial distribution of southern rich clusters of Olowin and Corwin sample would provide the most efficient way of extending our information on the clustering of rich clusters for which at present, there is virtually no reliable redshift information, by providing full sky coverage.

# Appendix A.

## Redshift Survey Catalogue.

See Chapter 3.8 for description of this catalogue.

**Table 2:** *Catalogue*

| # | R.A. | DEC | $m_{b_j}$ | $z_{em}$ | $z_{abs}$ | r | $W_\lambda(\AA)$ |
|---|---|---|---|---|---|---|---|
| | SGP | Field | | | | | |
| 1 | 005427.32 | -275528.9 | 21.48 | .36911 | | | 31 |
| 2 | 005438.83 | -275342.4 | 21.08 | .21523 | | | 19 |
| 3 | 005435.77 | -275543.7 | 21.41 | .38968 | | | 16 |
| 4 | 005349.41 | -275140.0 | 20.97 | .11200 | | | 58 |
| 5 | 005428.35 | -275106.8 | 20.83 | .24881 | | | 25 |
| 6 | 005438.06 | -275608.4 | 20.86 | .31960 | | | 30 |
| 7 | 005516.19 | -274944.9 | 21.04 | | .27529 | 4.79 | |
| 8 | 005520.72 | -275238.6 | 21.47 | | .27508 | 2.74 | 3 |
| 9 | 005501.45 | -275202.1 | 21.16 | | | | |
| 10 | 005508.94 | -275231.4 | 20.66 | | .16117 | 3.27 | 2 |
| 11 | 005517.51 | -274935.8 | 21.09 | .15772 | | | 84 |
| 12 | 005524.95 | -275441.1 | 21.42 | .11678 | | | 47 |
| 13 | 005518.33 | -275622.3 | 20.59 | .21397 | | | 48 |
| 14 | 005417.94 | -275244.5 | 21.01 | | | | |
| 15 | 005423.28 | -275613.8 | 21.40 | .22541 | | | 28 |
| 16 | 005410.15 | -275920.8 | 21.12 | .20303 | | | 41 |
| 17 | 005408.64 | -275549.6 | 21.25 | .31907 | | | 27 |
| 18 | 005418.73 | -275742.4 | 21.02 | .40542 | | | 11 |
| 19 | 005419.05 | -275149.4 | 20.72 | .16581 | | | 22 |
| 20 | 005412.29 | -275615.4 | 21.26 | .34892 | | | 14 |
| 21 | 005406.73 | -274939.6 | 20.85 | .21324 | | | 17 |
| 22 | 005353.07 | -275912.0 | 20.65 | .16793 | | | 24 |
| 23 | 005353.53 | -275933.1 | 21.03 | .10517 | | | 41 |
| 24 | 005347.74 | -275804.8 | 21.48 | | | | |
| 25 | 005357.36 | -275453.6 | 20.61 | .11501 | | | 23 |
| 26 | 005357.12 | -275351.9 | 20.87 | .11567 | | | 73 |
| 27 | 005457.86 | -275902.5 | 21.39 | .27550 | | | 15 |
| 28 | 005453.71 | -275854.1 | 20.81 | | .27453 | 3.12 | 11 |
| 29 | 005440.41 | -275616.0 | 21.31 | | | | |
| 30 | 005444.88 | -275418.2 | 21.13 | .21554 | | | 33 |
| 31 | 005440.49 | -275805.8 | 21.18 | .21363 | | | 19 |
| 32 | 005526.93 | -275753.3 | 21.44 | .12467 | | | 71 |
| 33 | 005444.75 | -275656.0 | 20.52 | .29805 | | | 16 |
| 34 | 005426.17 | -275233.8 | 20.78 | .16043 | | | 16 |
| 35 | 005456.37 | -275139.6 | 21.19 | .16288 | | | 35 |
| 36 | 005506.49 | -275313.6 | 20.91 | .16073 | | | 32 |
| 37 | 005406.27 | -275652.7 | 21.47 | .16194 | | | 15 |
| 38 | 005412.76 | -275646.5 | 20.94 | | | | |
| 39 | 005348.76 | -275933.4 | 20.54 | | | | |
| 40 | 005357.52 | -274959.1 | 21.35 | .44423 | | | 76 |
| 41 | 005443.36 | -275636.6 | 20.50 | | .16453 | 4.27 | 3 |
| 42 | 005355.88 | -275319.2 | 21.28 | .21181 | | | 30 |
| 43 | 005353.16 | -275526.9 | 21.49 | .34616 | | | 5 |
| 44 | 005346.94 | -275039.1 | 21.45 | | | | |

| # | R.A. | DEC | $m_{b_j}$ | $z_{em}$ | $z_{abs}$ | r | $W_\lambda(\AA)$ |
|---|---|---|---|---|---|---|---|
| 45 | 005518.155 | -275237.99 | 20.50 | | .210 | | |
| 46 | 005417.560 | -275307.35 | 20.57 | .21563 | .21552 | 3.12 | 6 |
| 47 | 005440.920 | -275836.89 | 20.60 | .16204 | | | 55 |
| 48 | 005519.276 | -275628.24 | 20.66 | | | | |
| 49 | 005450.541 | -275912.10 | 20.70 | .27565 | .27574 | 3.06 | 24 |
| 50 | 005356.059 | -275558.63 | 20.80 | | .17933 | 4.08 | |
| 51 | 005349.354 | -275745.92 | 20.82 | | .21186 | 4.54 | 2 |
| 52 | 005505.948 | -274929.14 | 20.85 | | .21245 | 5.08 | |
| 53 | 005454.412 | -275459.61 | 20.90 | .11712 | | | 47 |
| 54 | 005509.216 | -275022.41 | 20.94 | .163 | | | 15 |
| 55 | 005514.116 | -275540.69 | 20.98 | .04089 | | | 100 |
| 56 | 005358.479 | -275300.42 | 21.02 | | .27477 | 3.38 | 4 |
| 57 | 005451.546 | -275625.89 | 21.04 | .11363 | | | 98 |
| 58 | 005418.723 | -275006.78 | 21.08 | .31942 | .32028 | 3.44 | 9 |
| 59 | 005444.169 | -275116.87 | 21.11 | .11978 | .12159 | 2.49 | 13 |
| 60 | 005452.453 | -274925.86 | 21.13 | .33393 | | | 18 |
| 61 | 005348.905 | -275559.35 | 21.17 | .23585 | | | 49 |
| 62 | 005521.073 | -275447.02 | 21.22 | | | | |
| 63 | 005349.809 | -275616.70 | 21.26 | | .27801 | 2.14 | |
| 64 | 005455.129 | -275524.70 | 21.29 | | | | |
| 65 | 005500.627 | -275033.81 | 21.33 | .23588 | | | 43 |
| 66 | 005415.314 | -275006.02 | 21.39 | .33294 | | | 30 |
| 67 | 005413.846 | -275537.61 | 21.40 | .34677 | .34717 | 2.91 | 23 |
| 67 | 005448.863 | -274938.72 | 21.42 | | | | |
| 69 | 005345.582 | -275930.10 | 21.45 | | | | |
| 70 | 005419.610 | -275331.01 | 21.47 | | .21160 | | 6 |
| 71 | 005519.228 | -275735.87 | 21.48 | .16276 | | | 25 |
| | 197 | Field | | | | | |
| 1 | 020013.48 | -500532.6 | 21.03 | .17298 | | | 33 |
| 2 | 015942.60 | -500227.6 | 21.48 | | | | |
| 3 | 020000.16 | -500519.6 | 20.81 | .35176 | | | 20 |
| 4 | 015957.29 | -500212.0 | 21.08 | .14387 | | | 19 |
| 5 | 020001.53 | -500545.6 | 21.33 | | | | |
| 6 | 015947.76 | -500210.3 | 21.45 | .101 | | | 15 |
| 7 | 015935.40 | -500509.2 | 21.04 | .08906 | | | 39 |
| 8 | 015929.31 | -500536.2 | 20.73 | .35088 | | | 31 |
| 9 | 020025.26 | -500255.5 | 20.98 | | .30691 | 2.25 | |
| 10 | 020037.34 | -500428.2 | 20.74 | .10141 | | | 28 |
| 11 | 020033.78 | -500907.1 | 21.34 | .21707 | | | 24 |
| 12 | 020050.33 | -500503.7 | 21.15 | .20820 | | | 46 |
| 13 | 020029.85 | -500259.7 | 20.90 | .30654 | | | 10 |
| 14 | 020038.21 | -500249.9 | 20.59 | .47360 | | | 10 |
| 15 | 020041.48 | -500812.5 | 21.23 | | .217 | | |
| 16 | 020027.16 | -500614.2 | 20.82 | .38555 | | | 15 |
| 17 | 020034.99 | -500152.9 | 20.93 | .37552 | | | 15 |

| # | R.A. | DEC | $m_{b_j}$ | $z_{em}$ | $z_{abs}$ | r | $W_\lambda(\AA)$ |
|---|---|---|---|---|---|---|---|
| 18 | 020012.62 | -495934.6 | 20.78 | .21184 | | | 14 |
| 19 | 015953.04 | -500847.1 | 21.37 | .20740 | | | 54 |
| 20 | 020056.62 | -500005.0 | 21.25 | .10018 | | | 70 |
| 21 | 020005.16 | -500632.7 | 20.95 | .10128 | | | 33 |
| 22 | 020105.47 | -495919.6 | 21.41 | .35092 | | | 49 |
| 23 | 020020.14 | -495927.8 | 21.28 | .30886 | | | 8 |
| 24 | 020030.79 | -495853.4 | 21.13 | | | | |
| 25 | 020102.24 | -495453.4 | 20.61 | .30693 | | | 13 |
| 26 | 015912.80 | -500402.7 | 21.43 | | | | |
| 27 | 015909.68 | -495907.3 | 20.65 | .18464 | | | 36 |
| 28 | 015908.59 | -500251.8 | 21.19 | | | | |
| 29 | 015918.54 | -500527.3 | 21.48 | .19607 | | | 26 |
| 30 | 015919.53 | -495905.8 | 21.32 | .38389 | | | 30 |
| 31 | 015923.49 | -495903.3 | 20.90 | .18375 | | | 37 |
| 32 | 020045.41 | -495406.8 | 20.76 | .26427 | | | 17 |
| 33 | 020029.66 | -495105.5 | 21.22 | .19391 | | | 13 |
| 34 | 015950.13 | -495207.7 | 21.34 | | .384 | | |
| 35 | 020004.07 | -495450.8 | 20.62 | .26524 | | | 28 |
| 36 | 020008.18 | -495152.1 | 21.36 | | | | |
| 37 | 015941.36 | -495334.8 | 21.21 | | | | |
| 38 | 015912.50 | -495406.9 | 20.68 | | .22507 | 2.20 | |
| 39 | 020014.56 | -495407.5 | 21.39 | | | | |
| | MT | Field | | | | | |
| 1 | 220229.50 | -185501.92 | 20.50 | .34648 | .34643 | 2.57 | 11 |
| 2 | 220237.69 | -185136.06 | 20.52 | .18995 | .18976 | 3.29 | 15 |
| 3 | 220336.63 | -184127.90 | 20.54 | .21214 | | | 32 |
| 4 | 220336.25 | -184642.29 | 20.56 | .16036 | | | 32 |
| 5 | 220237.10 | -190504.55 | 20.58 | | .149 | | |
| 6 | 220320.84 | -184707.09 | 20.65 | | .24143 | 3.74 | 8 |
| 7 | 220328.41 | -190650.77 | 20.66 | | .13503 | 5.89 | |
| 8 | 220329.60 | -190603.66 | 20.67 | | .13455 | 3.88 | |
| 9 | 220356.29 | -190350.90 | 20.68 | | .30908 | 3.61 | |
| 10 | 220242.69 | -190014.35 | 20.73 | | | | |
| 11 | 220251.06 | -185350.54 | 20.75 | | .23733 | 5.41 | 3 |
| 12 | 220309.27 | -190630.20 | 20.77 | .32796 | .32807 | 2.85 | 28 |
| 13 | 220233.18 | -185715.37 | 20.81 | .23762 | .23816 | 3.40 | 15 |
| 14 | 220232.63 | -184651.72 | 20.84 | | .26348 | 3.06 | 22 |
| 15 | 220242.60 | -185744.35 | 20.86 | .20993 | .21092 | 2.98 | 19 |
| 16 | 220243.85 | -185314.36 | 20.87 | | | | |
| 17 | 220207.86 | -184911.64 | 20.89 | .23587 | | | 55 |
| 18 | 220342.20 | -184845.29 | 20.92 | .23836 | | | 35 |
| 19 | 220208.70 | -185452.20 | 20.95 | .22947 | | | 14 |
| 20 | 220302.87 | -190651.27 | 20.95 | .15366 | | | 14 |
| 21 | 220204.78 | -184301.39 | 20.96 | | | | |
| 22 | 220315.94 | -184700.08 | 21.01 | .27236 | | | 23 |

| # | R.A. | DEC | $m_{b_j}$ | $z_{em}$ | $z_{abs}$ | r | $W_\lambda(\AA)$ |
|---|---|---|---|---|---|---|---|
| 23 | 220236.06 | -184107.06 | 21.04 | .18611 | | | 24 |
| 24 | 220247.82 | -190250.07 | 21.05 | .33339 | .32807 | 2.85 | 12 |
| 25 | 220231.04 | -185340.74 | 21.07 | | | | |
| 26 | 220400.99 | -184554.72 | 21.09 | | | | |
| 27 | 220332.23 | -190325.63 | 21.12 | .151 | | | 10 |
| 28 | 220249.97 | -184552.76 | 21.14 | .36234 | .36183 | 2.83 | 18 |
| 29 | 220215.92 | -184733.05 | 21.16 | .284 | | | 22 |
| 30 | 220223.59 | -184848.81 | 21.21 | .186 | | | 25 |
| 31 | 220235.22 | -190712.88 | 21.22 | | | | |
| 32 | 220324.56 | -185406.40 | 21.22 | .17449 | | | 40 |
| 33 | 220312.61 | -185831.80 | 21.23 | | | | |
| 34 | 220344.61 | -184427.73 | 21.26 | | | | |
| 35 | 220231.39 | -190523.19 | 21.28 | .29912 | .29974 | 2.53 | 26 |
| 36 | 220335.91 | -185504.55 | 21.28 | .42352 | | | 50 |
| 37 | 220341.03 | -184244.53 | 21.30 | .17508 | | | 15 |
| 38 | 220253.35 | -185412.57 | 21.34 | .09678 | | | 52 |
| 39 | 220312.68 | -185159.60 | 21.36 | | | | |
| 40 | 220208.39 | -185224.81 | 21.38 | | | | |
| 41 | 220313.19 | -185332.52 | 21.41 | | | | |
| 42 | 220223.63 | -184621.97 | 21.44 | | | | |
| 43 | 220400.52 | -185307.76 | 21.47 | | | | |
| 44 | 220230.15 | -185845.47 | 21.49 | .14589 | | | 46 |
| | 419 | Field | | | | | |
| 1 | 035544.54 | -311132.6 | 20.42 | .16605 | | | 17 |
| 2 | 035538.54 | -310907.5 | 20.67 | | .17402 | 3.24 | 18 |
| 3 | 035527.93 | -311026.9 | 20.88 | .10763 | | | 10 |
| 4 | 035534.46 | -311246.3 | 20.26 | .22450 | | | 25 |
| 5 | 035515.32 | -311147.7 | 20.01 | .29929 | | | 10 |
| 6 | 035546.82 | -311233.1 | 20.06 | .13977 | | | 49 |
| 7 | 035515.35 | -310300.9 | 20.28 | .36000 | | | 10 |
| 8 | 035544.35 | -310410.1 | 20.70 | .17391 | | | 20 |
| 9 | 035515.70 | -310207.8 | 20.89 | .21999 | | | 23 |
| 10 | 035519.87 | -310424.6 | 20.99 | .14169 | | | 33 |
| 11 | 035548.03 | -305736.6 | 20.91 | .24242 | | | 11 |
| 12 | 035507.95 | -310300.3 | 20.94 | .16663 | | | 37 |
| 13 | 035531.05 | -310340.5 | 20.93 | | | | |
| 14 | 035547.09 | -310414.2 | 20.66 | | .17347 | 3.52 | |
| 15 | 035516.60 | -310116.5 | 20.86 | .32578 | | | 10 |
| 16 | 035511.20 | -310112.7 | 20.77 | | .20741 | 3.01 | 11 |
| 17 | 035413.74 | -305630.8 | 20.18 | | | | |
| 18 | 035405.66 | -305442.5 | 20.13 | .19860 | .19824 | 4.88 | 7 |
| 19 | 035452.54 | -305514.5 | 20.11 | .09337 | | | 26 |
| 20 | 035425.73 | -311205.6 | 20.38 | .17636 | .17746 | 3.41 | 4 |
| 21 | 035405.57 | -305255.1 | 20.81 | .14138 | | | 51 |
| 22 | 035416.73 | -305523.1 | 20.23 | | .23329 | 5.09 | |

| # | R.A. | DEC | $m_{b_j}$ | $z_{em}$ | $z_{abs}$ | r | $W_\lambda(\AA)$ |
|---|---|---|---|---|---|---|---|
| 23 | 035425.76 | -310637.8 | 20.36 | .06110 | | | 26 |
| 24 | 035444.68 | -305328.0 | 20.03 | .25415 | .25420 | 4.68 | 3 |
| 25 | 035450.61 | -305344.1 | 20.99 | | | | |
| 26 | 035420.00 | -305518.3 | 20.99 | .25323 | | | 29 |
| 27 | 035450.61 | -305344.1 | 20.99 | .20355 | | | 65 |
| 28 | 035412.31 | -311307.1 | 20.16 | .12501 | .12443 | 3.14 | 10 |
| 29 | 035447.21 | -310935.6 | 20.73 | | | | |
| 30 | 035434.30 | -310848.3 | 20.14 | .23180 | | | 34 |
| 31 | 035413.35 | -311243.5 | 20.57 | .19362 | .19344 | 4.24 | 25 |
| 32 | 035454.78 | -310518.0 | 20.52 | | .29950 | 5.0 | |
| 33 | 035428.43 | -311109.7 | 20.88 | .20197 | | | 33 |
| 34 | 035453.45 | -311201.5 | 20.99 | | | | |
| 35 | 035506.18 | -305813.2 | 20.62 | .26490 | | | 52 |
| 36 | 035448.88 | -305741.5 | 20.53 | .23286 | | | 8 |
| 37 | 035453.43 | -310225.9 | 20.49 | | | | |
| 38 | 035501.16 | -310025.2 | 20.46 | | .20709 | 3.18 | 1 |
| | 529 | Field | | | | | |
| 1 | 205650.66 | -252453.9 | 20.88 | .19880 | | | 59 |
| 2 | 205639.14 | -252335.5 | 20.81 | | .19861 | 2.46 | |
| 3 | 205610.44 | -252115.1 | 20.63 | .10855 | | | 40 |
| 4 | 205626.45 | -252236.0 | 20.69 | | .30111 | 3.79 | 2 |
| 5 | 205609.03 | -252029.4 | 20.00 | .18739 | | | 25 |
| 6 | 205649.80 | -252342.3 | 20.89 | | .29905 | 2.72 | |
| 7 | 205635.31 | -253101.7 | 20.83 | .19797 | | | 24 |
| 8 | 205634.67 | -253121.6 | 20.94 | .19780 | | | 22 |
| 9 | 205556.95 | -252716.4 | 20.73 | .17182 | | | 11 |
| 10 | 205543.09 | -252713.4 | 20.31 | | .17914 | 3.04 | 9 |
| 11 | 205535.16 | -252827.8 | 20.04 | | .16477 | 5.73 | 2 |
| 12 | 205556.14 | -253113.8 | 20.04 | .13581 | | | 42 |
| 13 | 205514.91 | -252344.3 | 20.94 | .43574 | | | 16 |
| 14 | 205517.22 | -253107.6 | 20.10 | | .17035 | 3.54 | |
| 15 | 205615.02 | -252638.3 | 20.94 | | | | |
| 16 | 205623.78 | -252605.1 | 20.27 | | | | |
| 17 | 205552.48 | -252310.6 | 20.69 | | .18563 | 1.82 | 2 |
| 18 | 205553.45 | -252530.5 | 20.67 | .30043 | | | 23 |
| 19 | 205630.83 | -252728.1 | 20.63 | .29014 | .29100 | 6.0 | 5 |
| 20 | 205604.45 | -252452.1 | 20.46 | | | | |
| 21 | 205626.06 | -252739.2 | 20.42 | .18623 | | | 8 |
| 22 | 205633.42 | -252848.7 | 20.44 | .204 | | | 9 |
| 23 | 205610.80 | -252151.9 | 20.06 | .32002 | | | 13 |
| 24 | 205545.94 | -252231.2 | 20.54 | | .317 | | |
| 25 | 205544.69 | -252208.4 | 20.56 | .20396 | | | 51 |
| 26 | 205555.59 | -252135.6 | 20.98 | | | | |
| 27 | 205643.05 | -252737.4 | 20.92 | | | | |

| # | R.A. | DEC | $m_{b_j}$ | $z_{em}$ | $z_{abs}$ | r | $W_\lambda(\AA)$ |
|---|---|---|---|---|---|---|---|
| 28 | 205551.52 | -252019.0 | 20.97 | | | | |
| 29 | 205555.06 | -252026.1 | 20.67 | .16855 | | | 35 |
| 30 | 205504.63 | -251911.5 | 20.66 | | | | |
| 31 | 205517.39 | -251727.1 | 20.37 | | .18397 | 2.99 | 2 |
| 32 | 205520.16 | -252001.1 | 20.10 | .18683 | | | 20 |
| 33 | 205521.70 | -251811.9 | 20.27 | .18631 | | | 5 |
| 34 | 205648.84 | -251839.5 | 20.24 | | | | |
| 35 | 205643.52 | -251657.1 | 20.60 | .19841 | | | 11 |
| 36 | 205611.70 | -251832.6 | 20.04 | .06699 | | | 32 |
| 37 | 205613.66 | -251324.8 | 20.48 | | .13350 | | 2 |
| 38 | 205624.91 | -251643.4 | 20.60 | .31855 | | | 19 |
| 39 | 205602.59 | -251858.8 | 20.81 | | | | |
| 40 | 205625.19 | -251411.7 | 20.48 | .31730 | | | 29 |
| 41 | 205610.44 | -251258.1 | 20.94 | .17153 | | | 14 |
| 42 | 205517.56 | -253030.0 | 20.23 | | .17041 | 3.09 | |
| 43 | 205520.84 | -253104.5 | 20.60 | | .20093 | 3.50 | 11 |
| 44 | 205637.72 | -252415.4 | 20.40 | .05591 | | | 33 |

# Appendix B.

## Spectral Catalogue

See Chapter 3.8 for details.

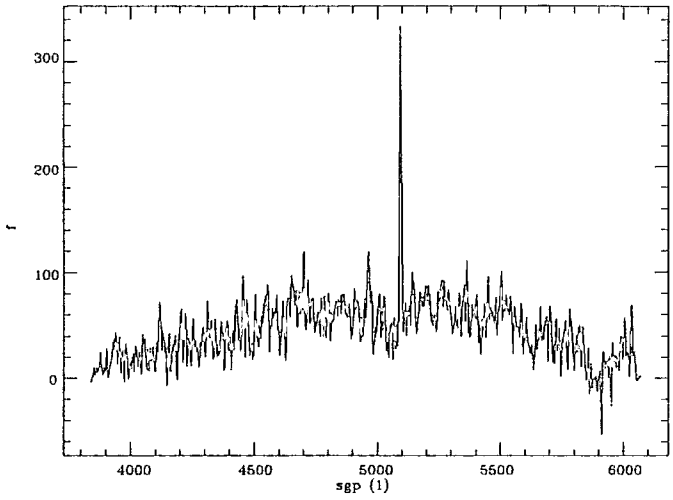
f
sgp (1)

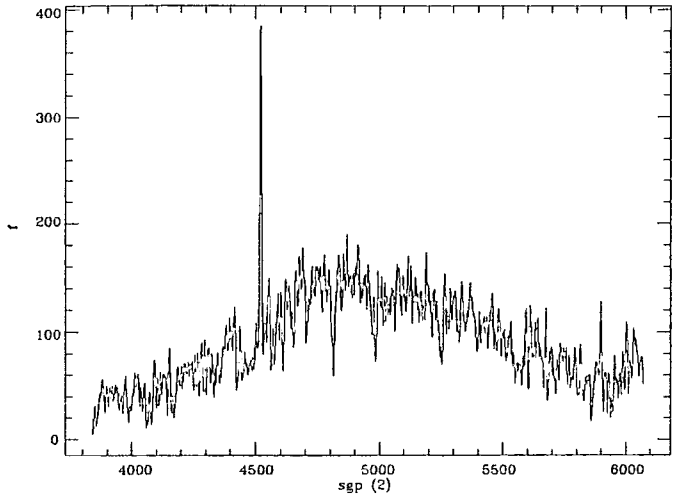
f
sgp (2)

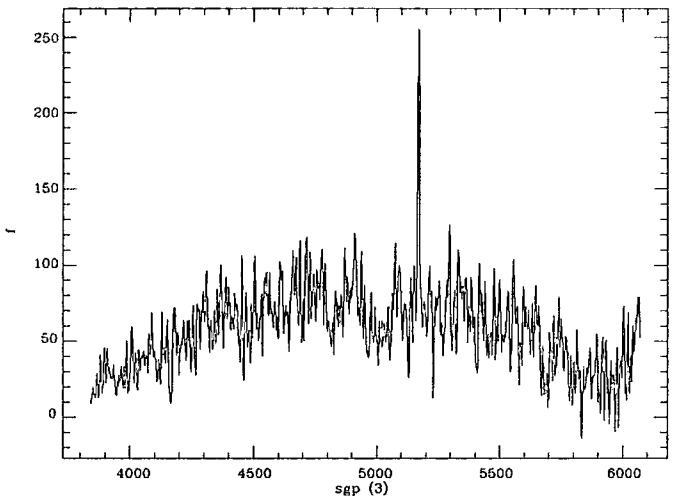
f
sgp (3)

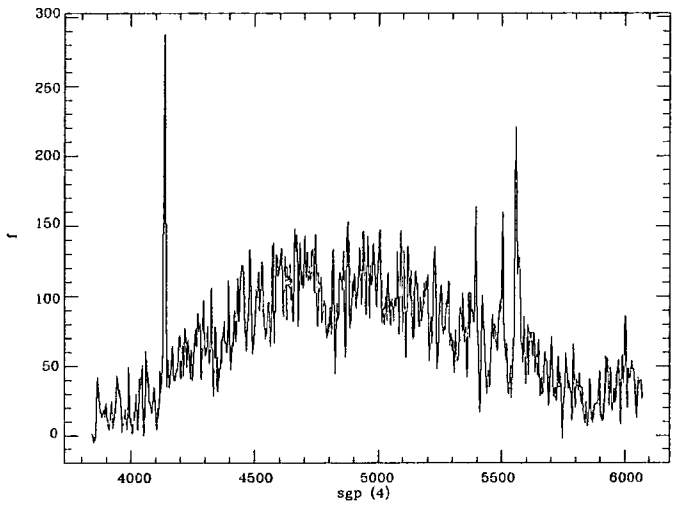
f
sgp (4)

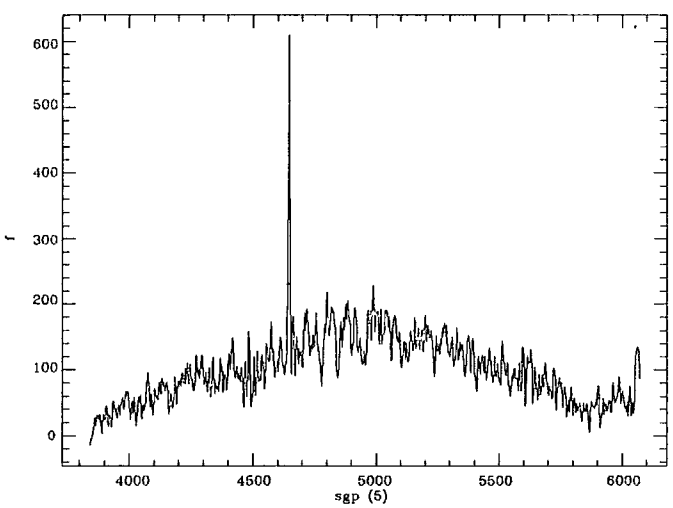
f
sgp (5)

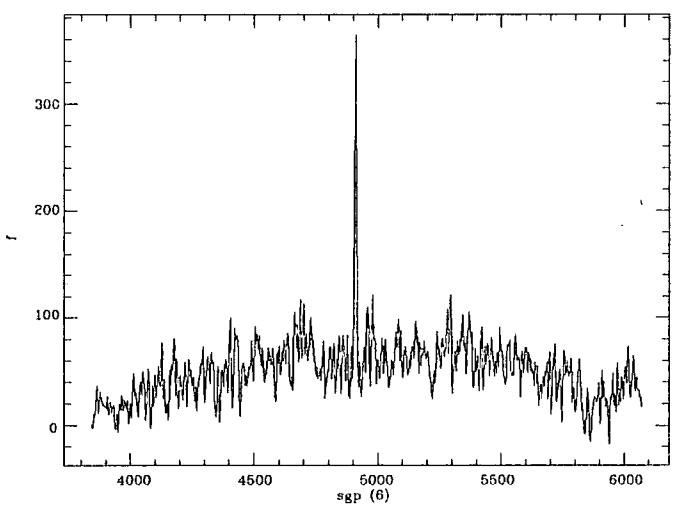
f
sgp (6)

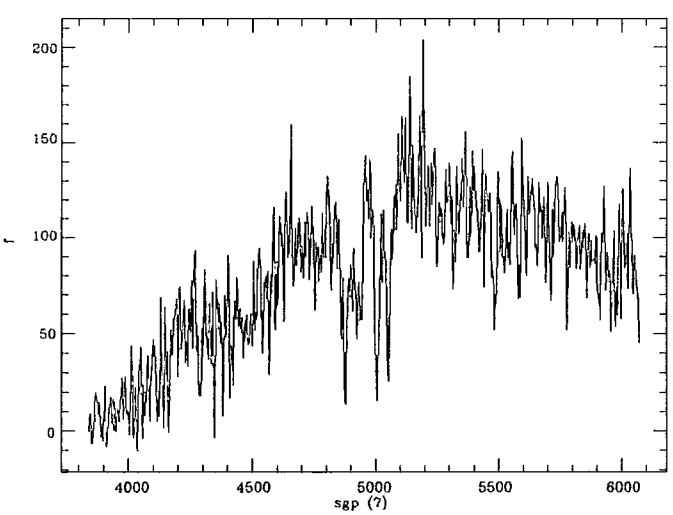
f
sgp (7)

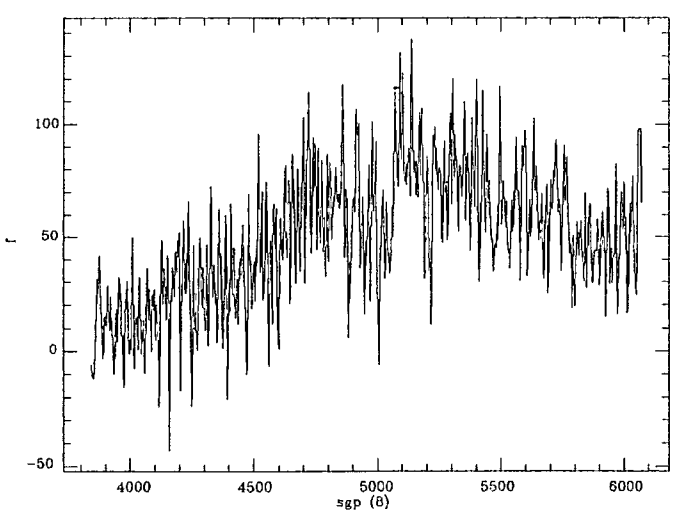
f
sgp (8)

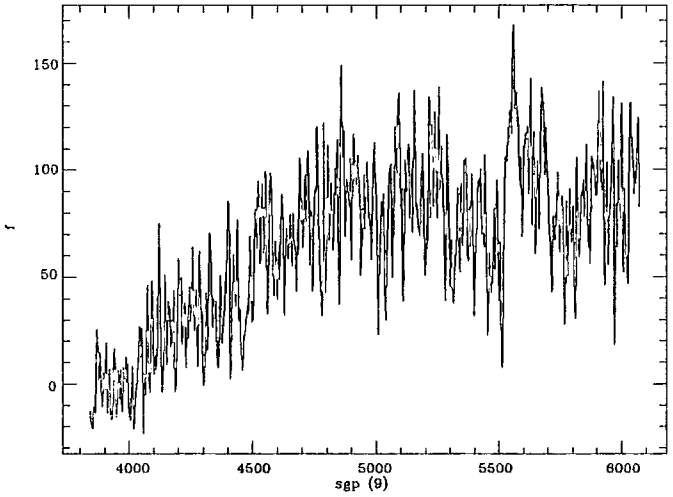
f
sgp (9)

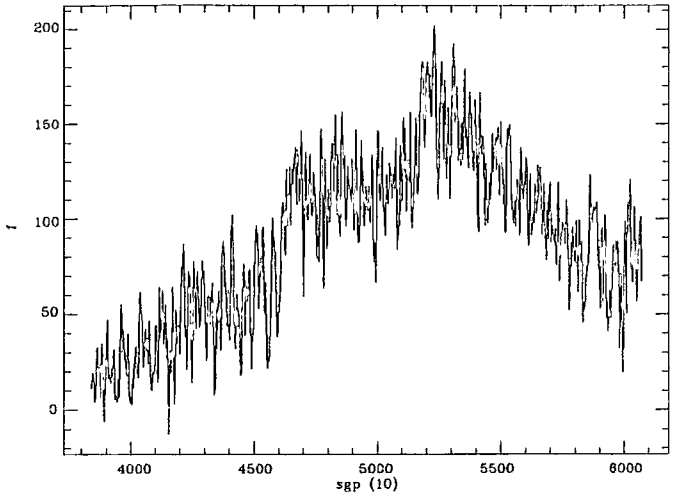
f
sgp (10)

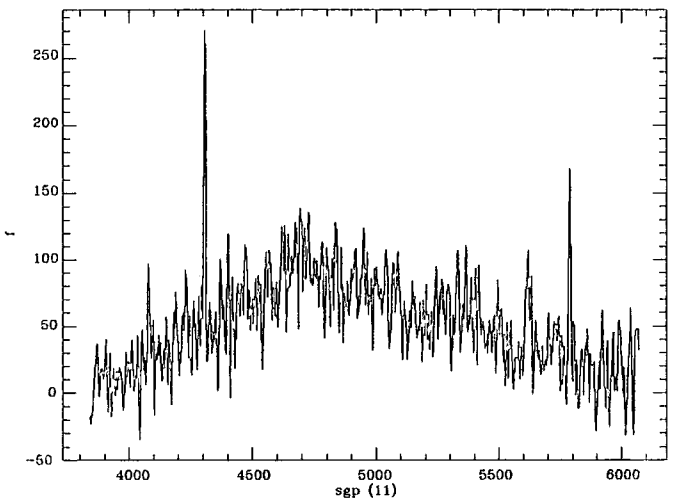
f
sgp (11)

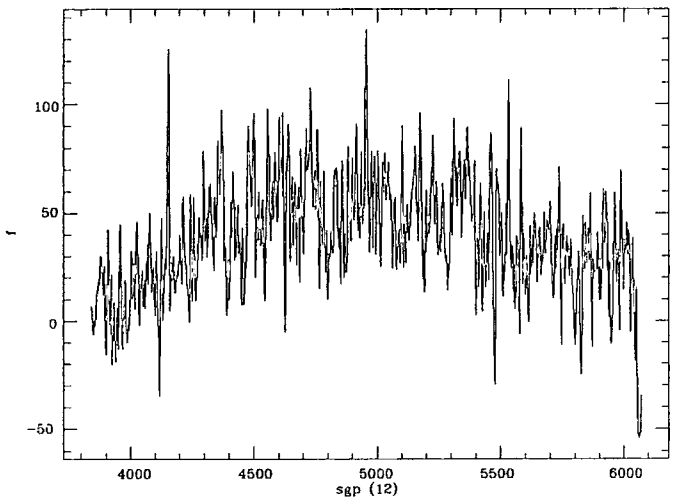
f
sgp (12)

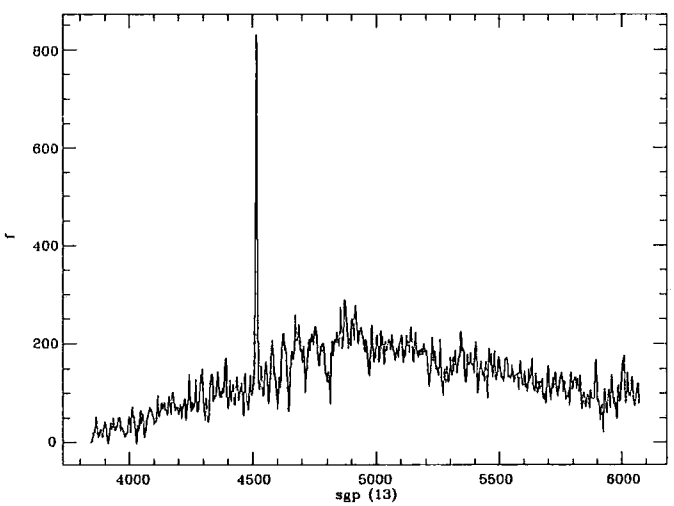
f
sgp (13)

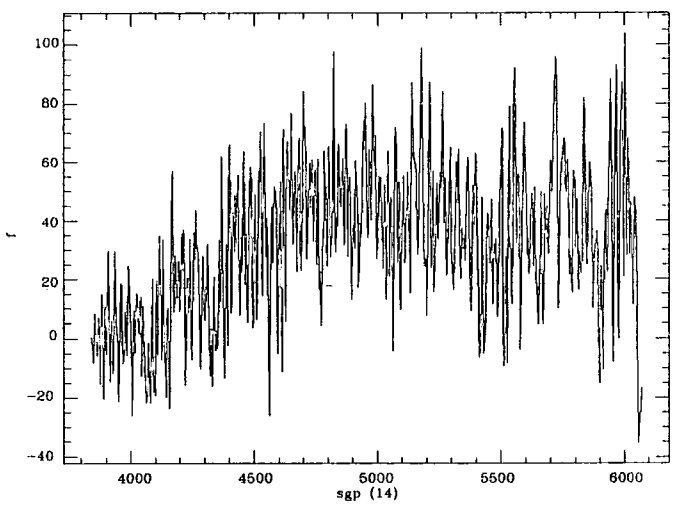
f
sgp (14)

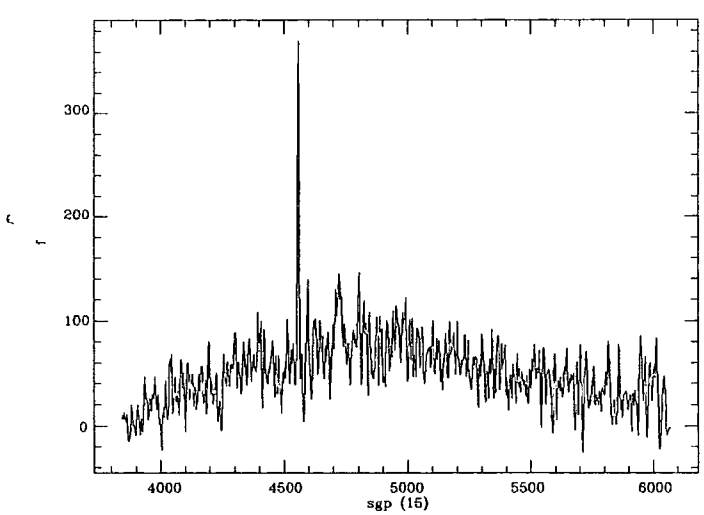
f
sgp (15)

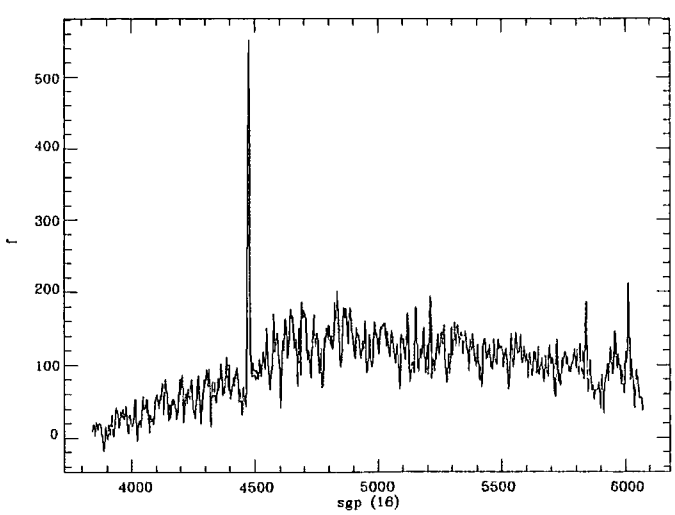
f
sgp (16)

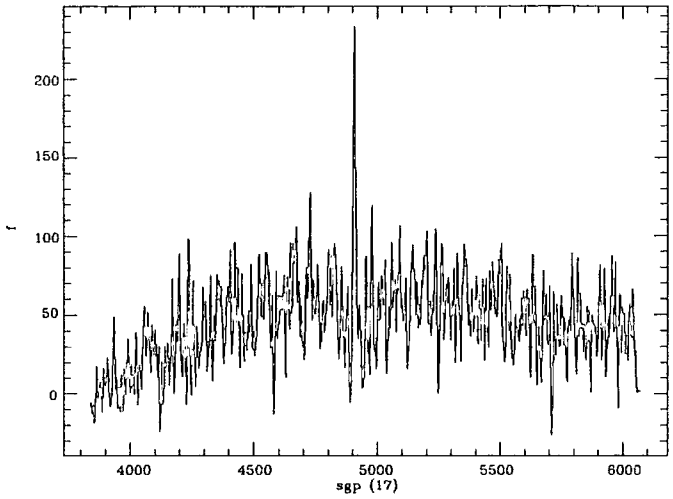
f
sgp (17)

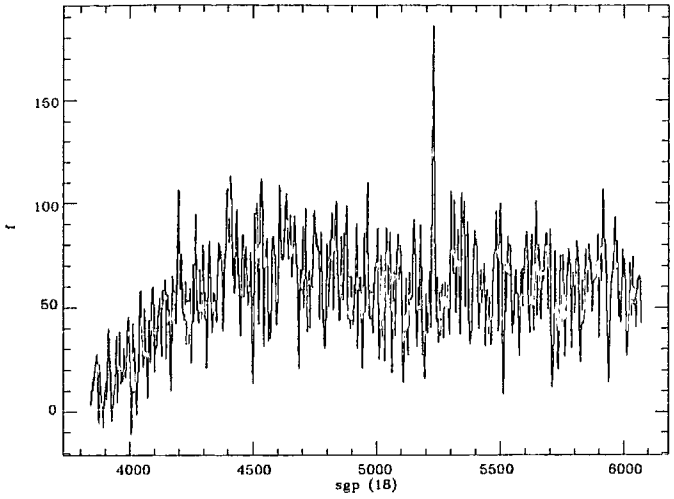
f
sgp (18)

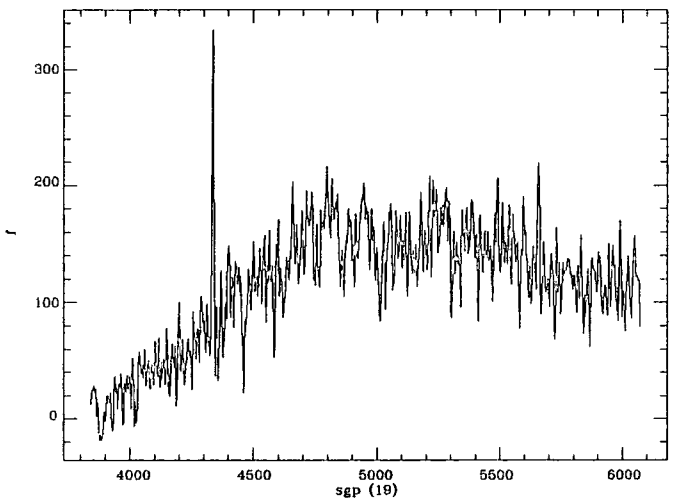
f
sgp (19)

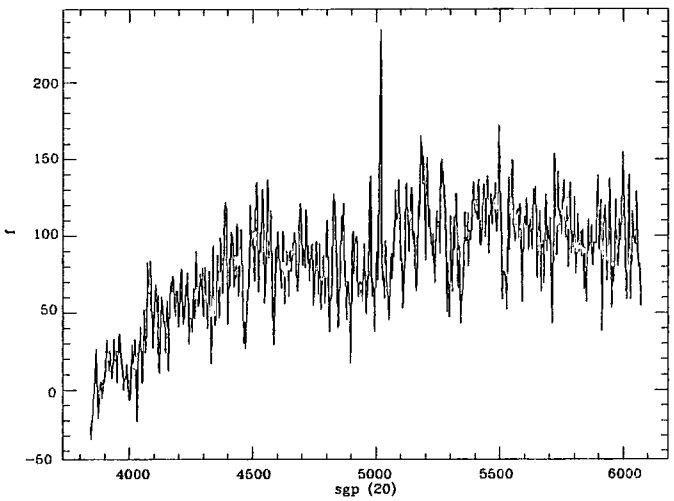
f
sgp (20)

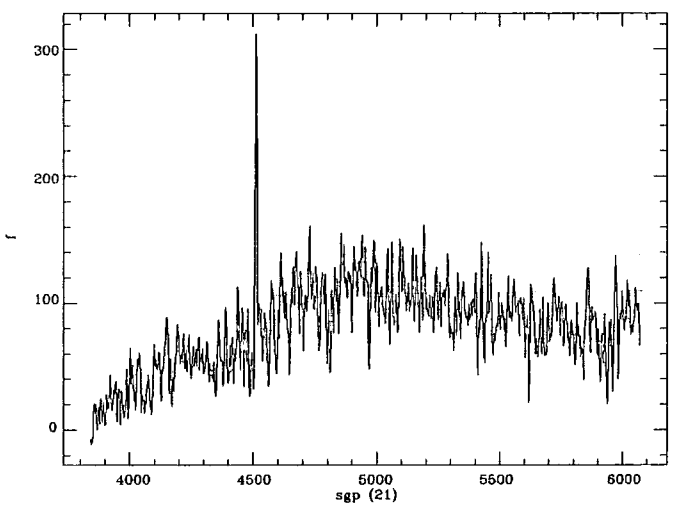
f
sgp (21)

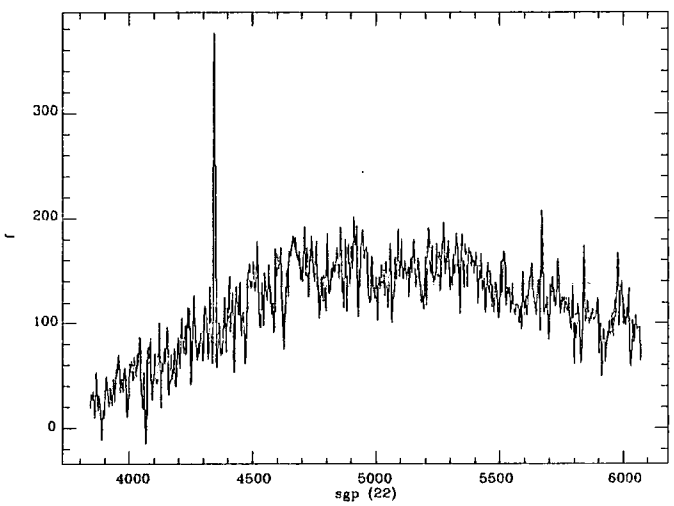
f
sgp (22)

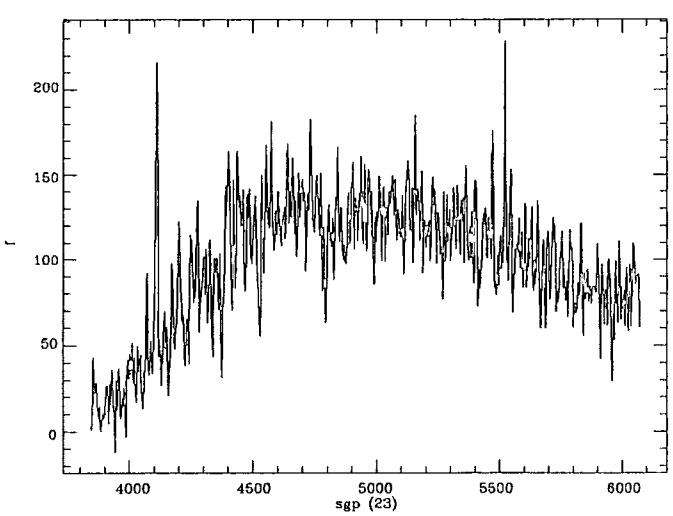
f
sgp (23)

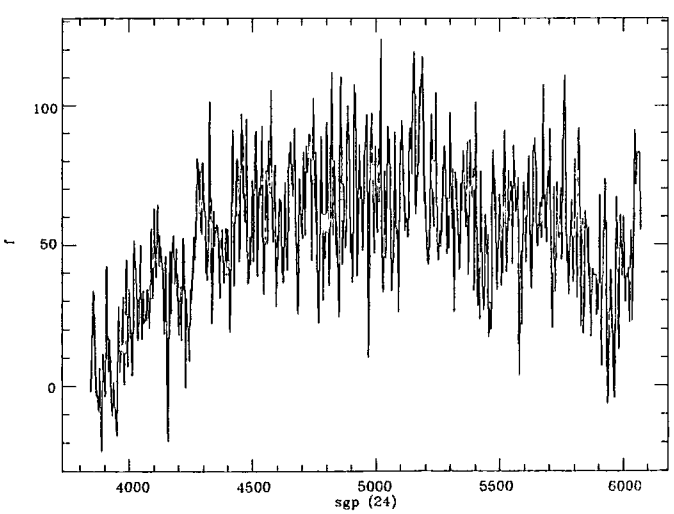
f
sgp (24)

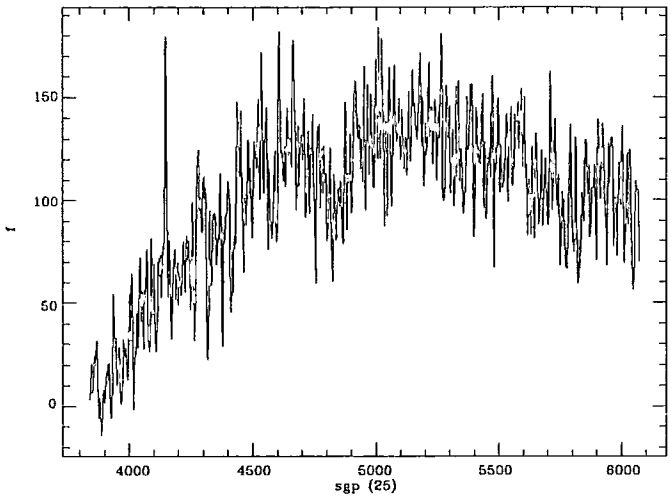
f
sgp (25)

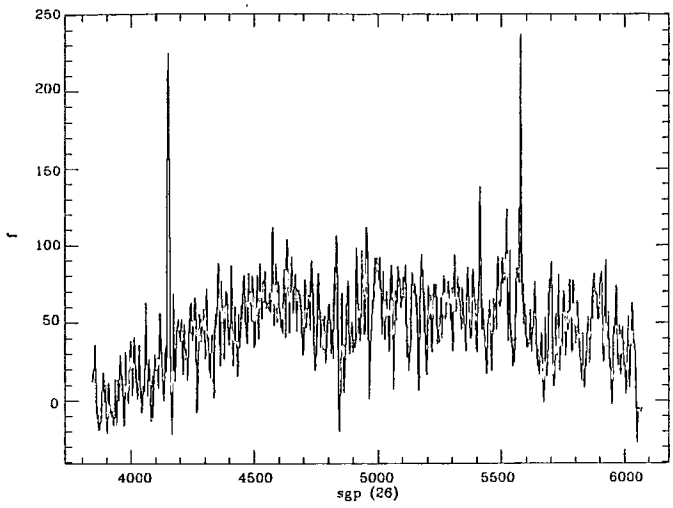
f
sgp (26)

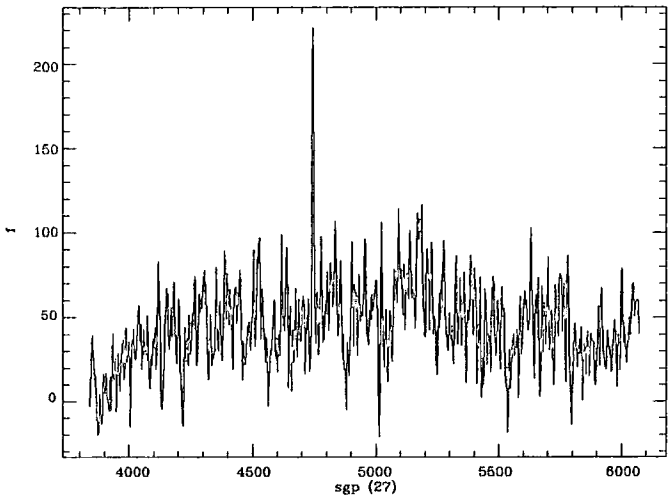
f
sgp (27)

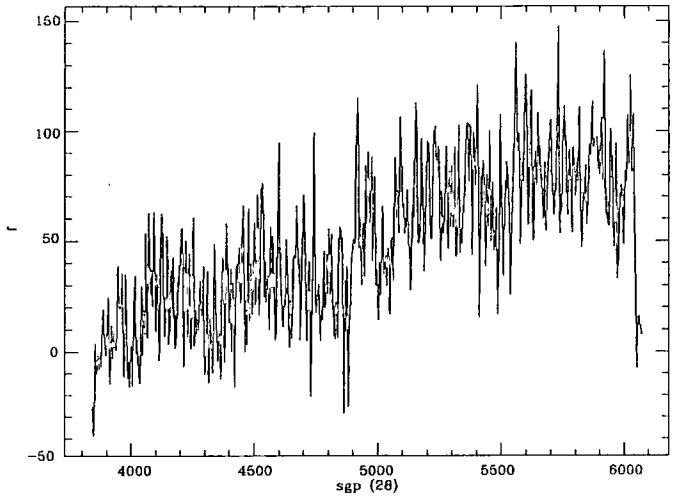
f
sgp (28)

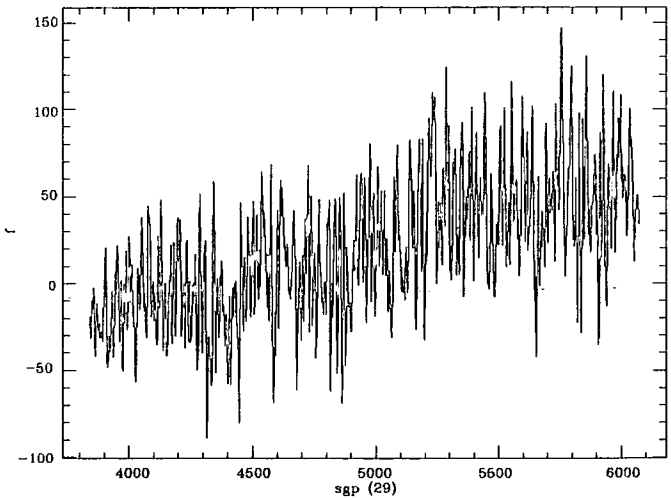
f
sgp (29)

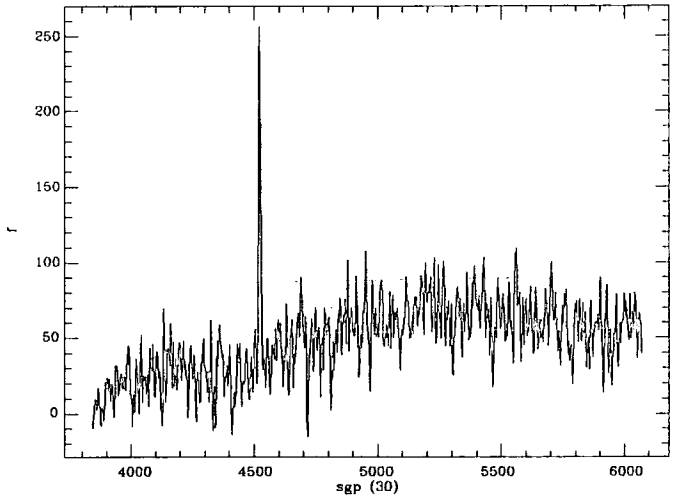
f
sgp (30)

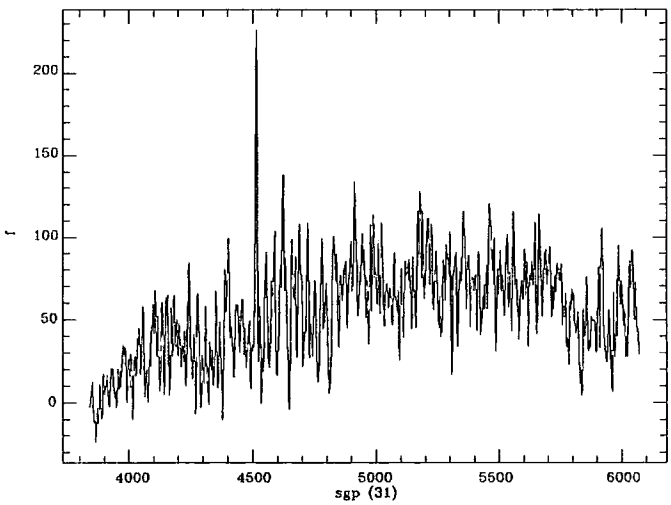
f
sgp (31)

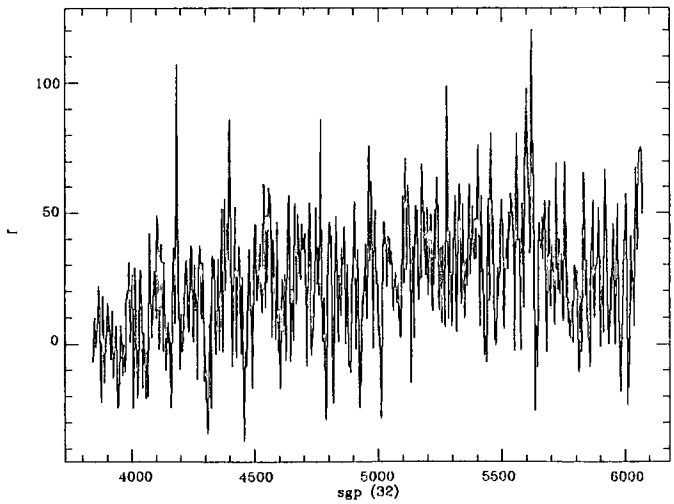
f
sgp (32)

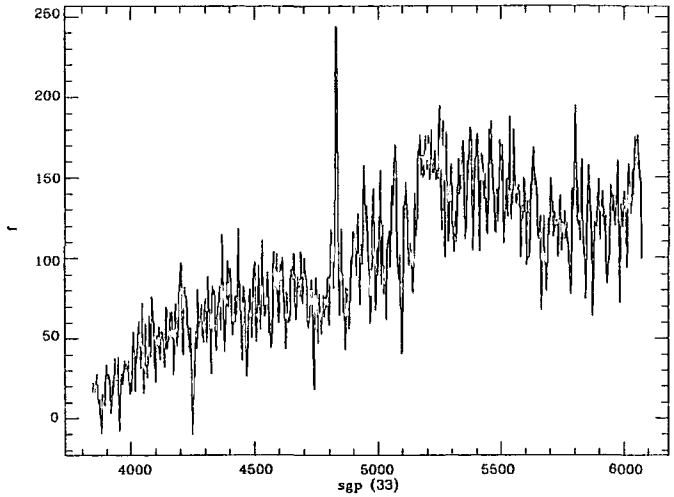
f
sgp (33)

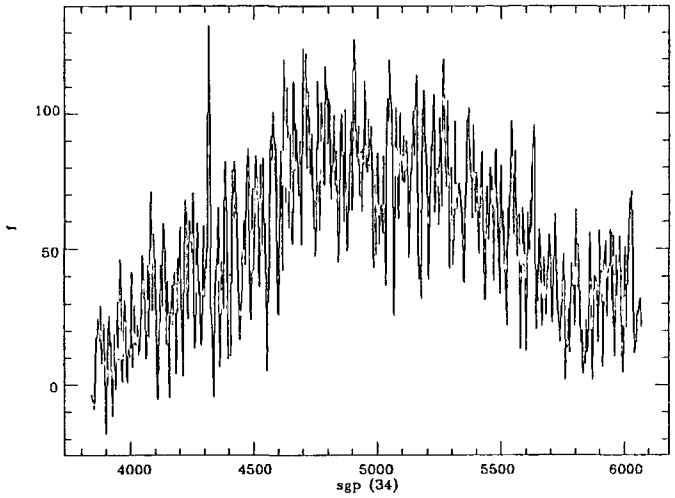
f
sgp (34)

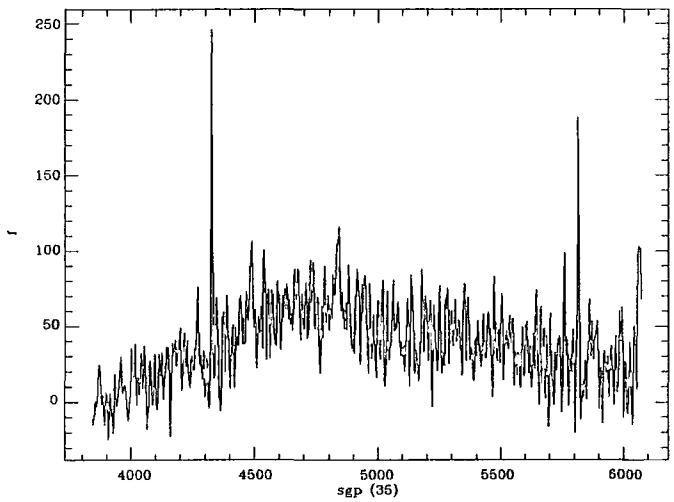
f
sgp (35)

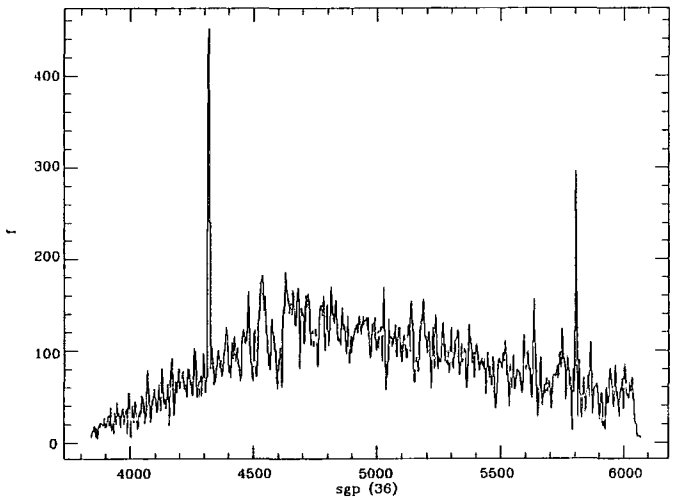
f
sgp (36)

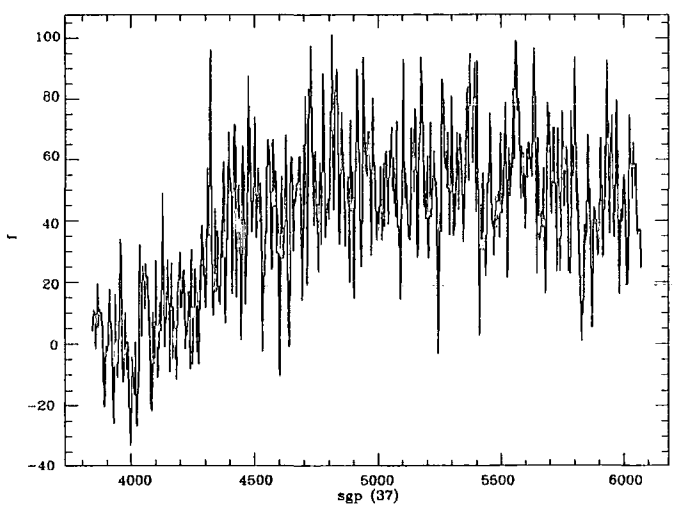
f
sgp (37)

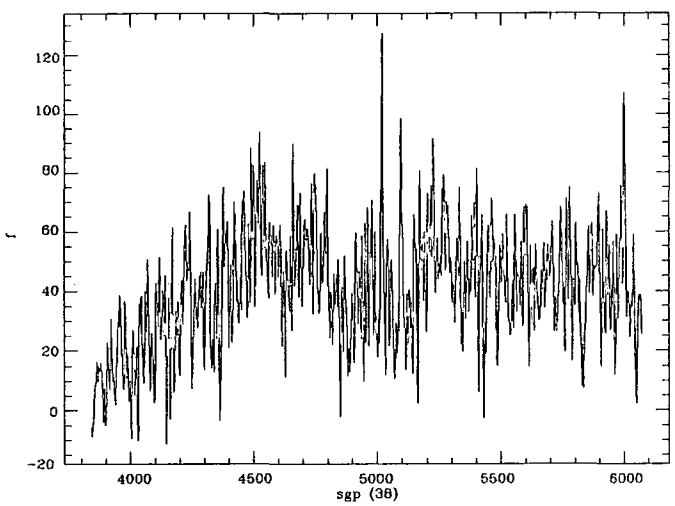
f
sgp (38)

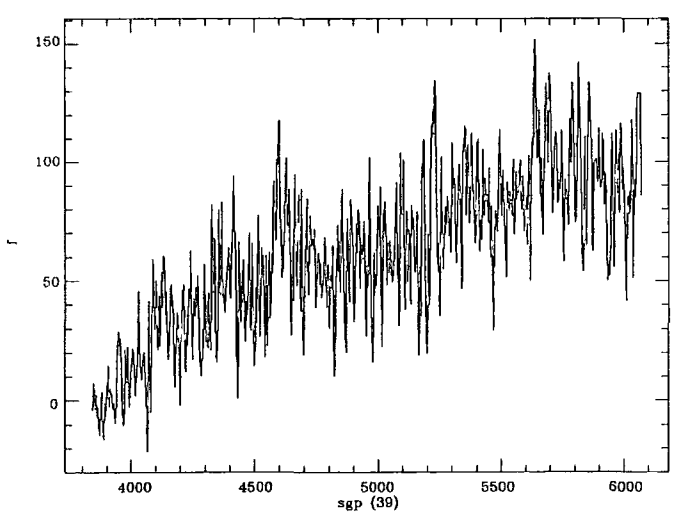
f
sgp (39)

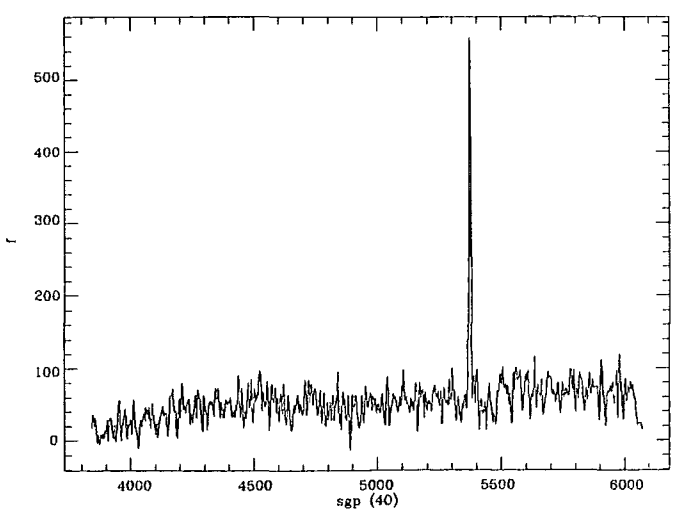
f
sgp (40)

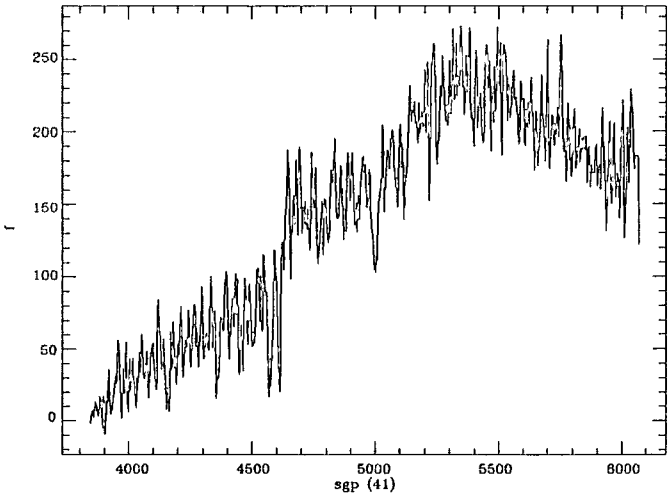
r
sgp (41)

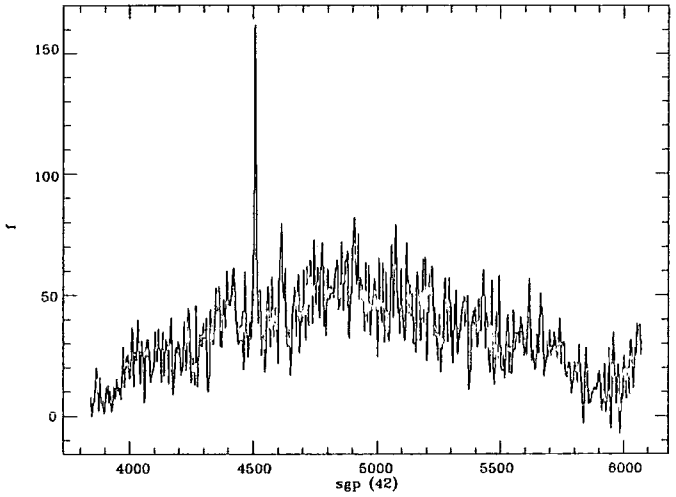
r
sgp (42)

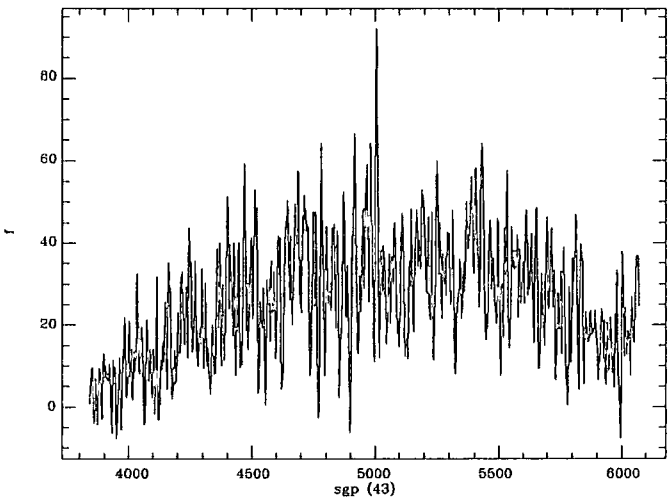
r
sgp (43)

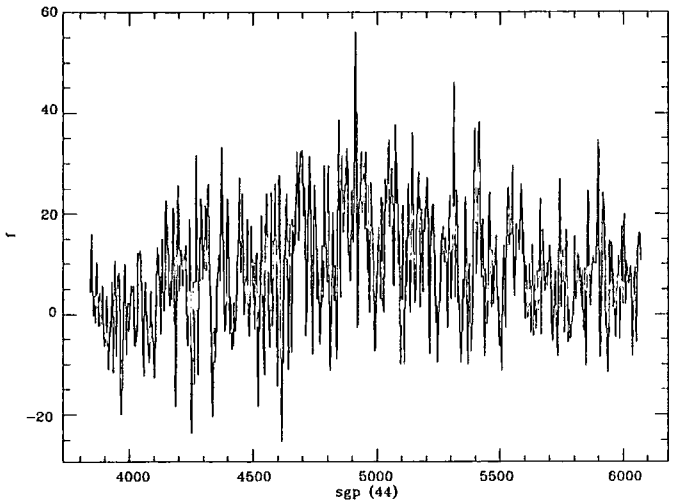
r
sgp (44)

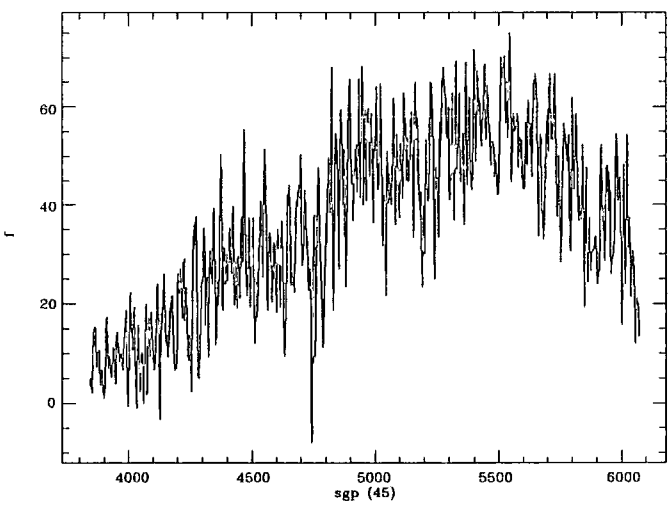
r
sgp (45)

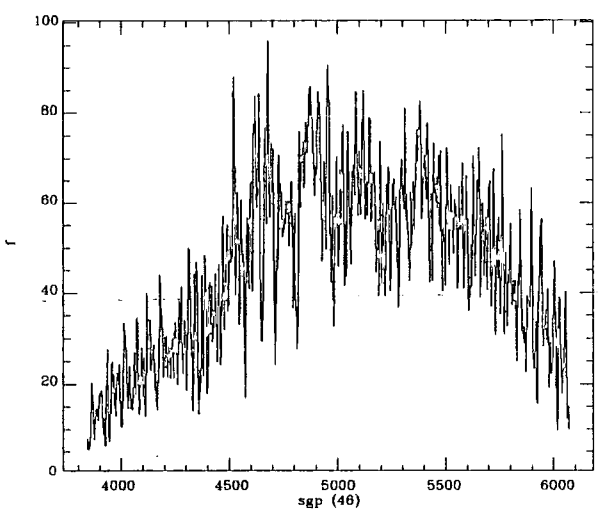
r
sgp (46)

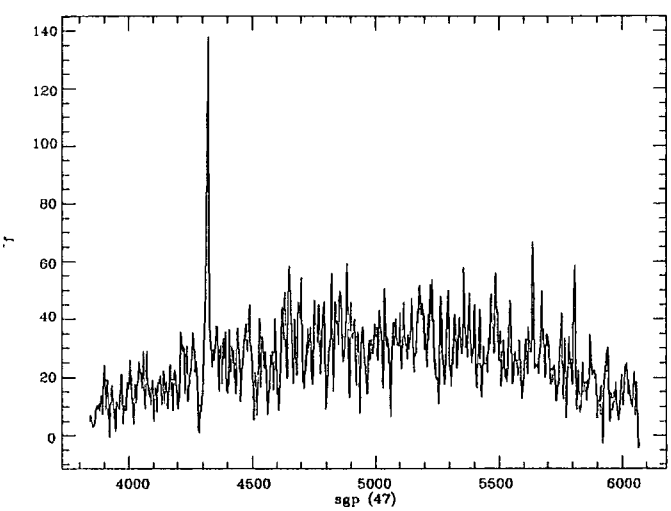
r
sgp (47)

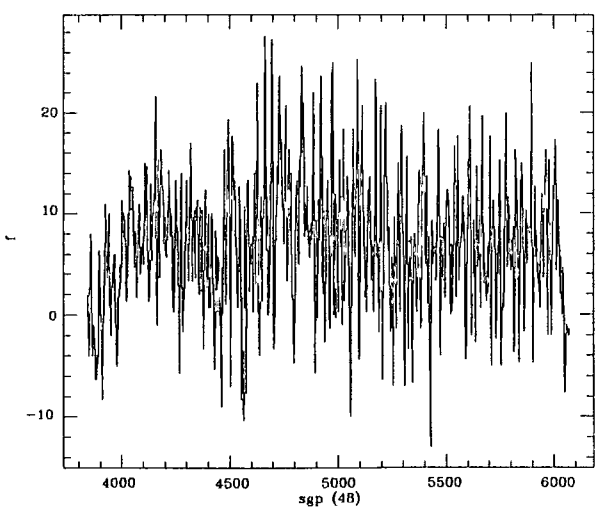
r
sgp (48)

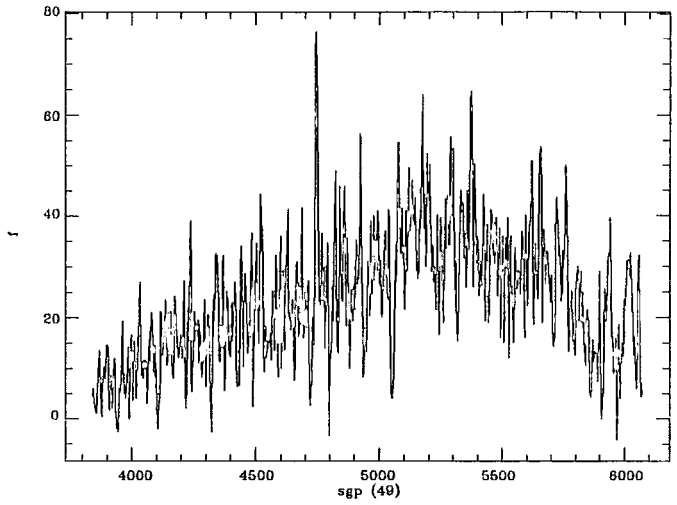
f
sgp (49)

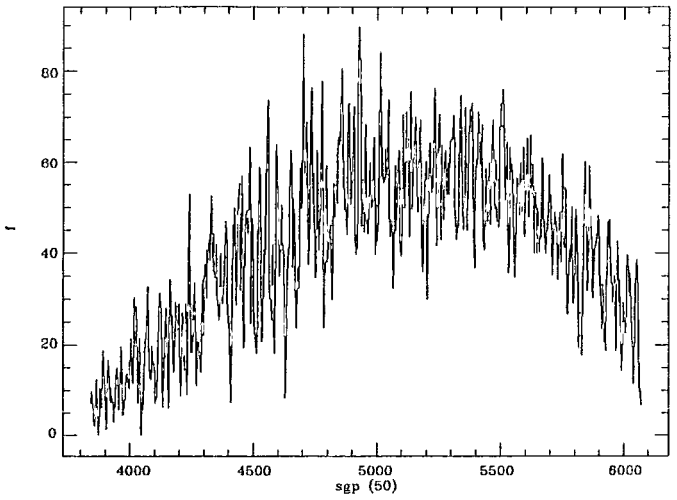
f
sgp (50)

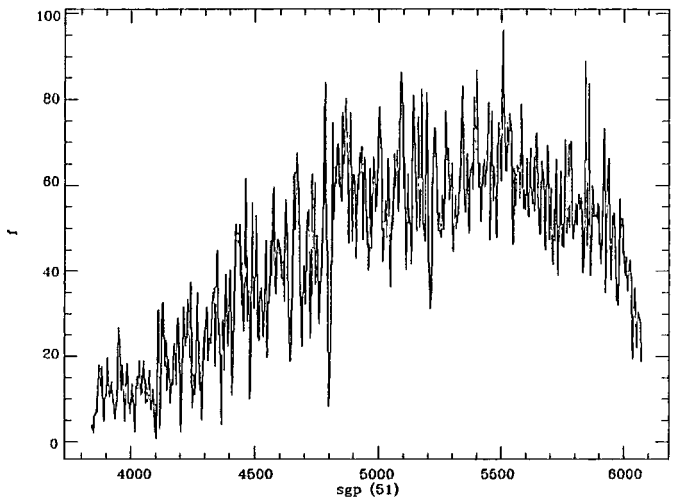
f
sgp (51)

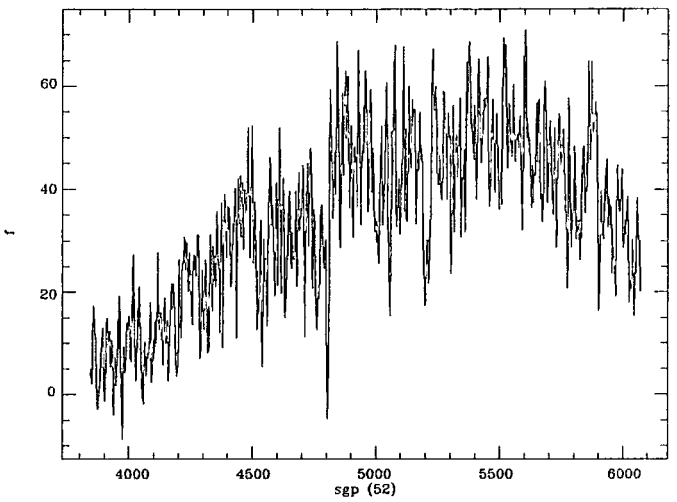
f
sgp (52)

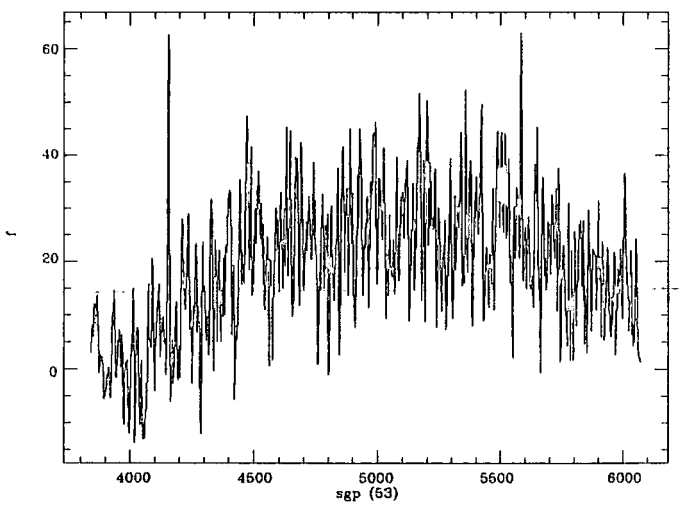
f
sgp (53)

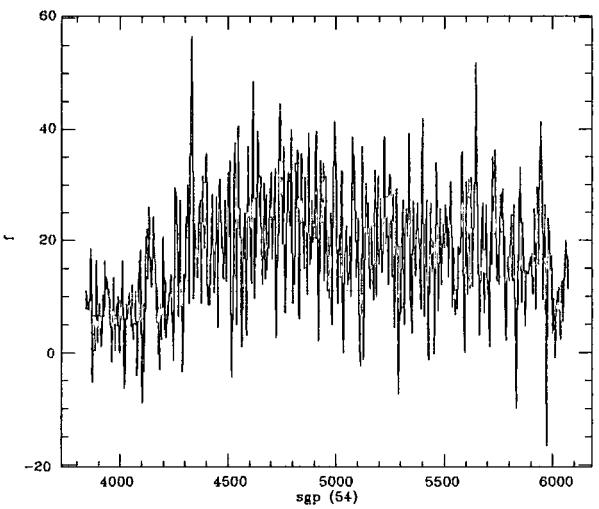
f
sgp (54)

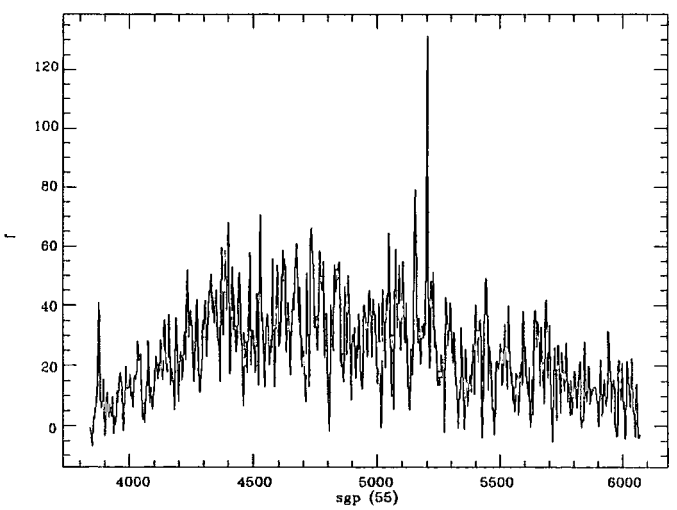
f
sgp (55)

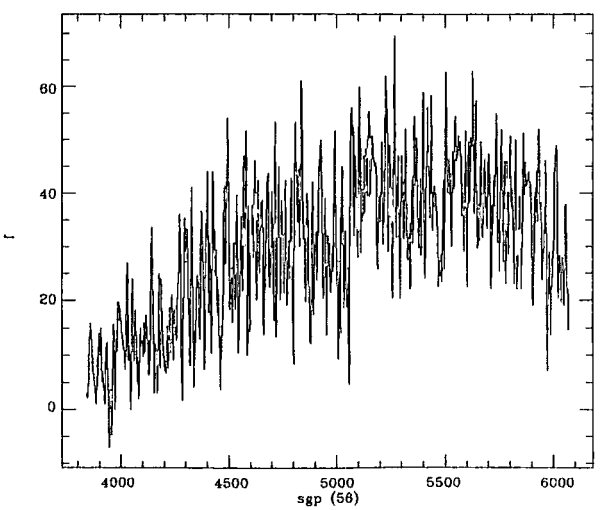
f
sgp (56)

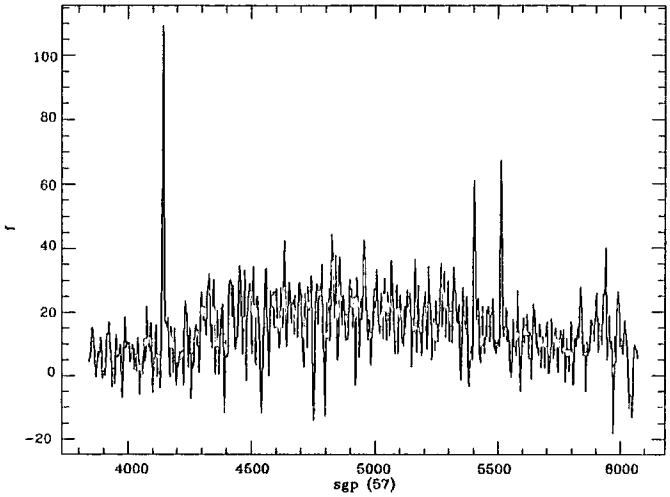
f
sgp (57)

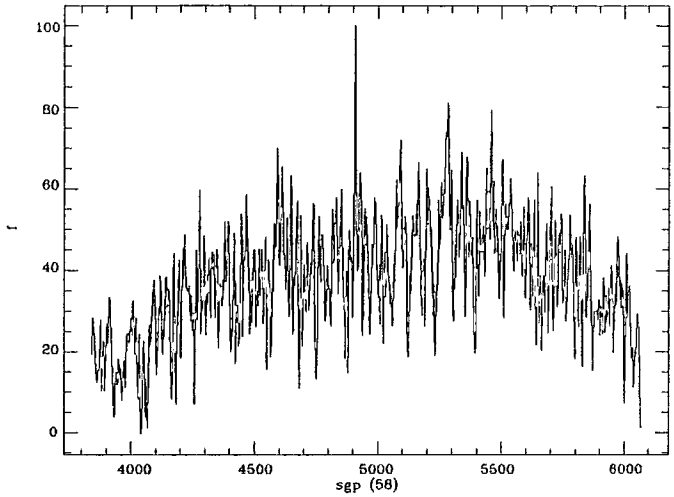
f
sgp (58)

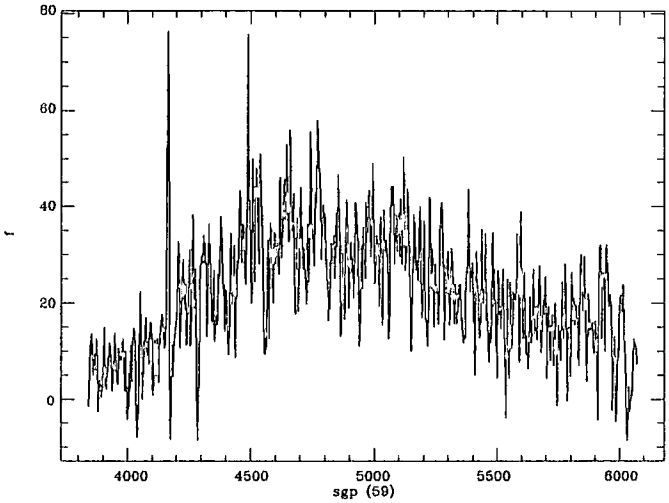
f
sgp (59)

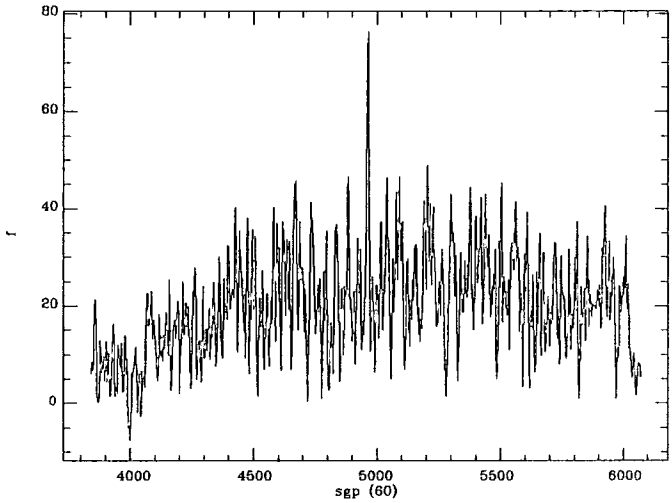
f
sgp (60)

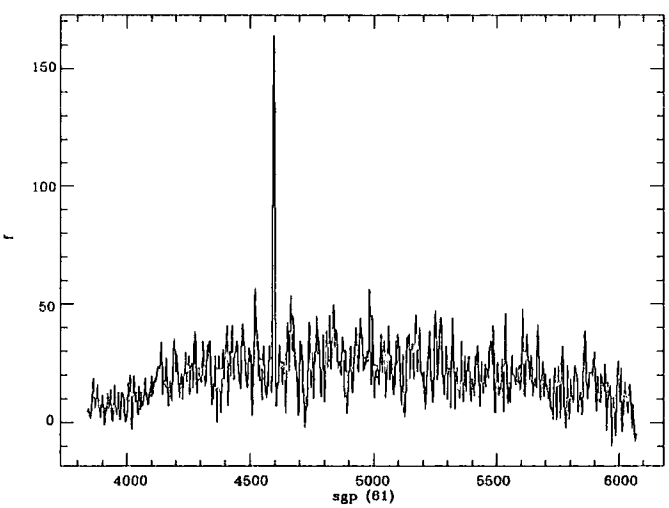
f
sgp (61)

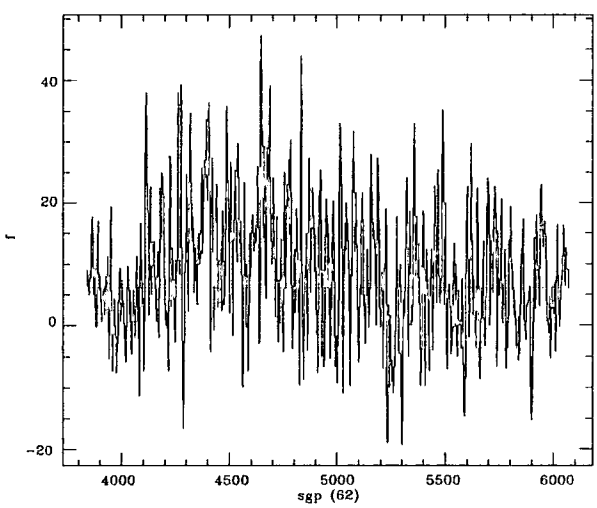
f
sgp (62)

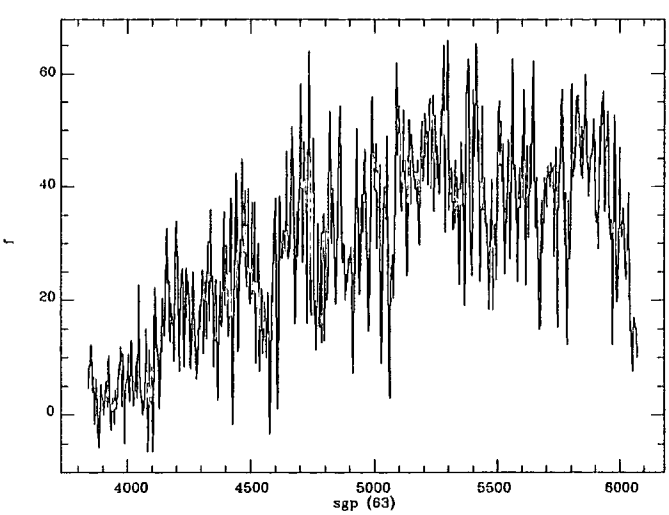
f
sgp (63)

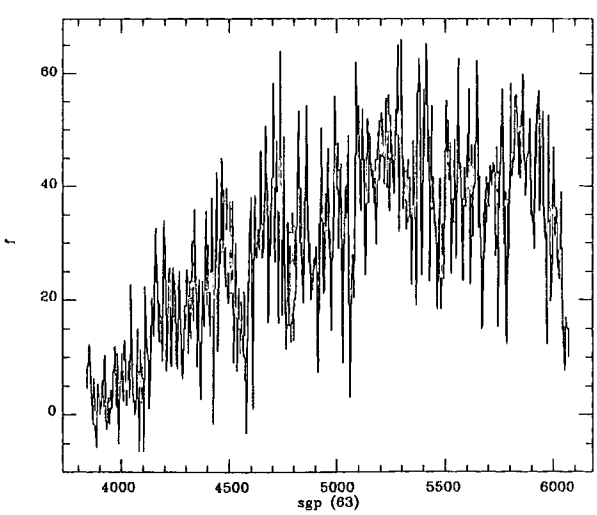
f
sgp (63)

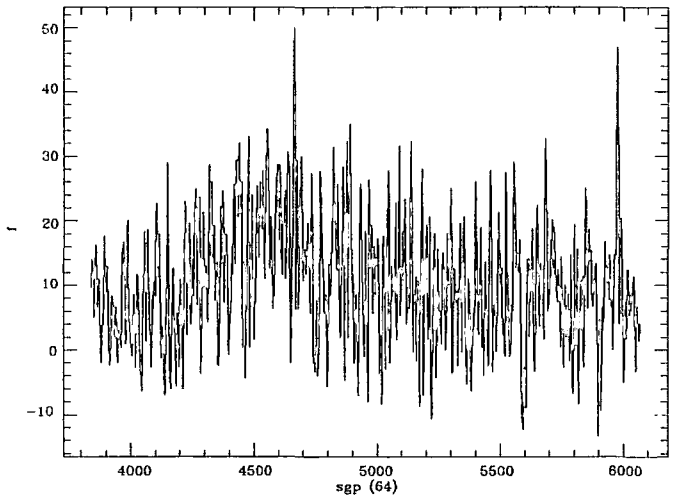
f
sgp (64)

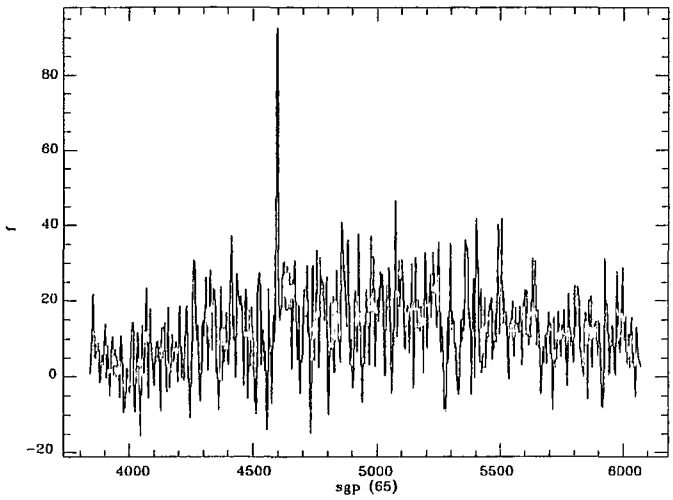
f
sgp (65)

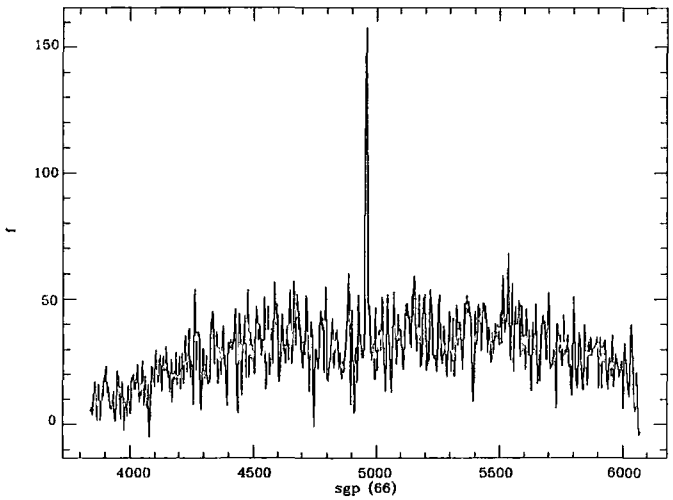
f
sgp (66)

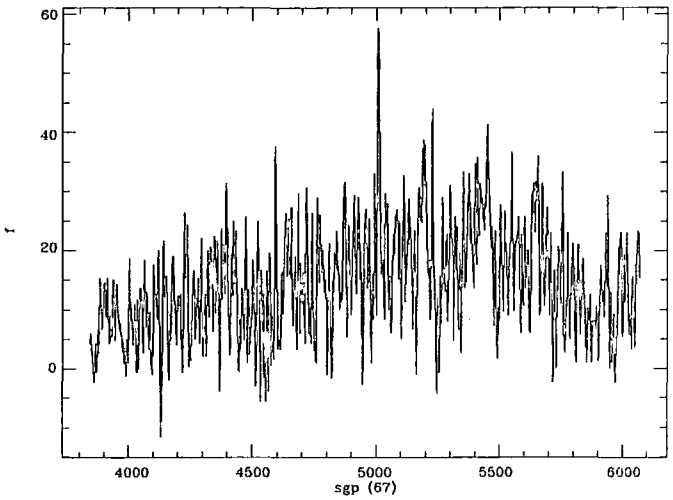
f
sgp (67)

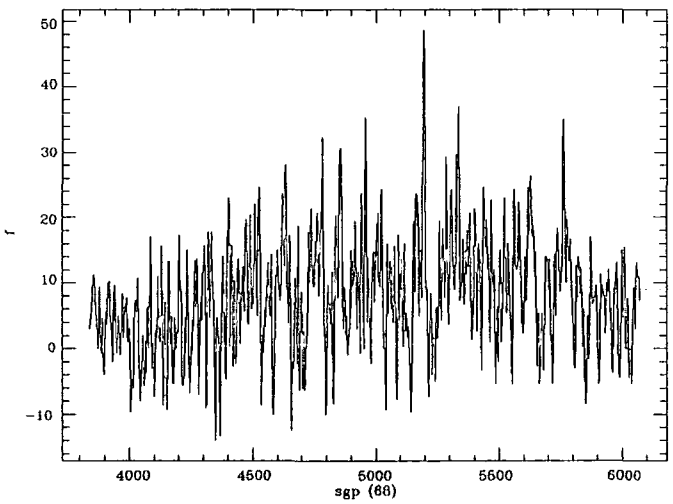
f
sgp (68)

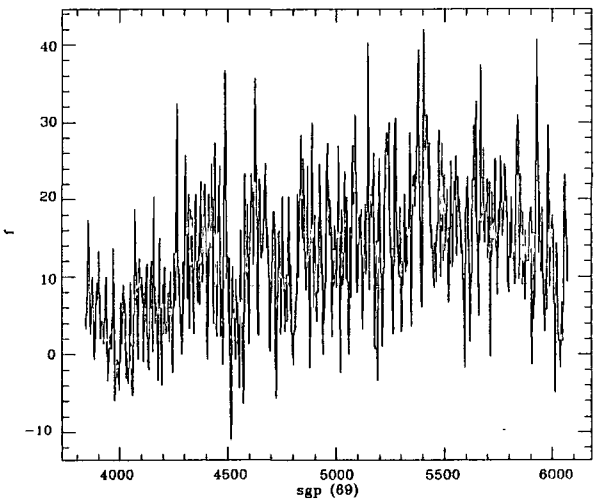
f
sgp (69)

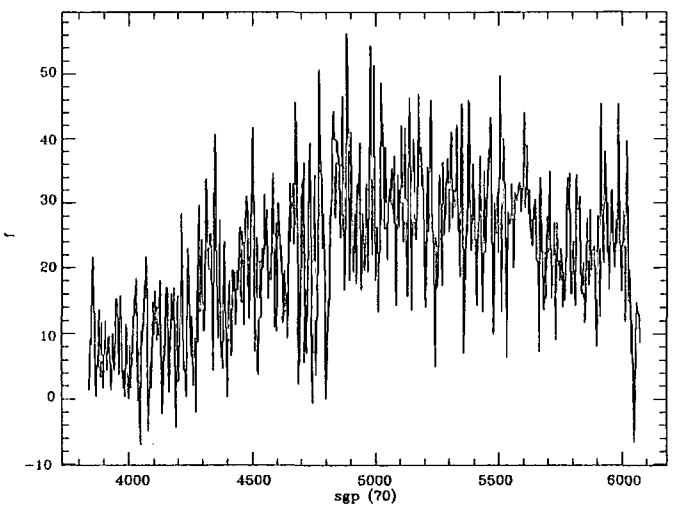
f
sgp (70)

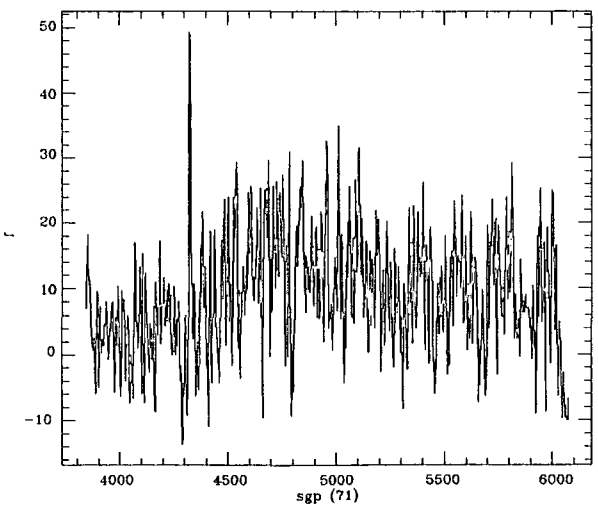
f
sgp (71)

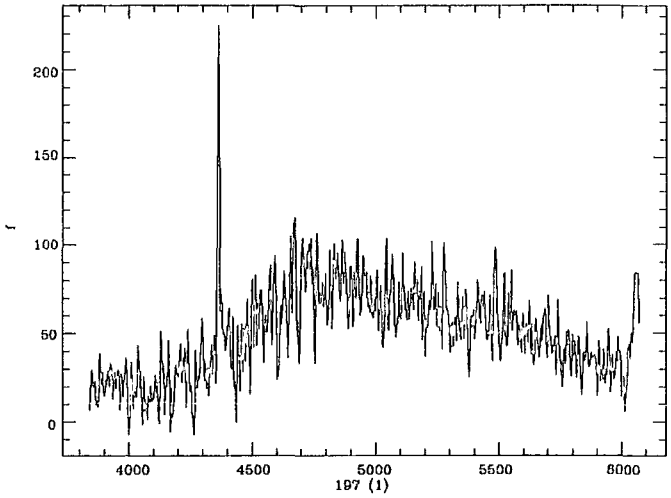
f
4000
4500
5000
5500
6000
197 (1)

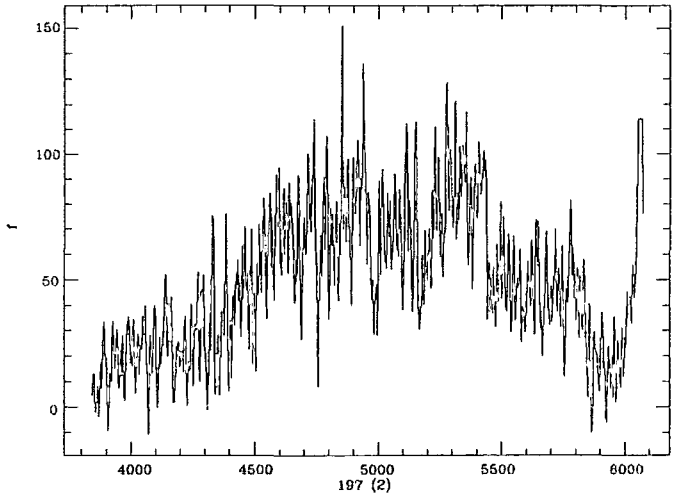
f
4000
4500
5000
5500
6000
197 (2)

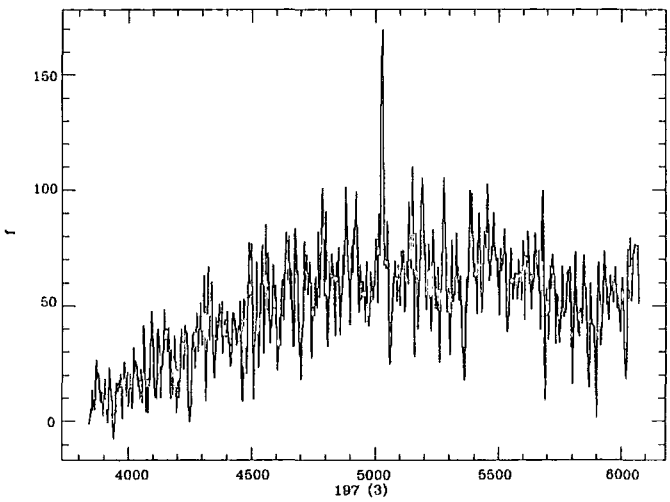
f
4000
4500
5000
5500
6000
197 (3)

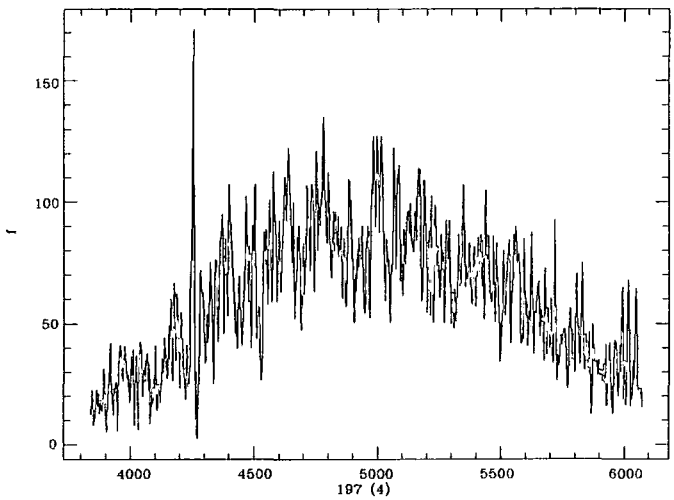
f
4000
4500
5000
5500
6000
197 (4)

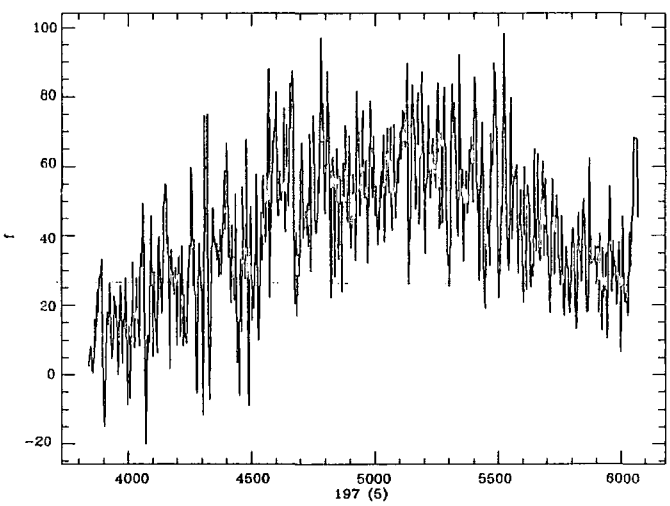
f
4000
4500
5000
5500
6000
197 (5)

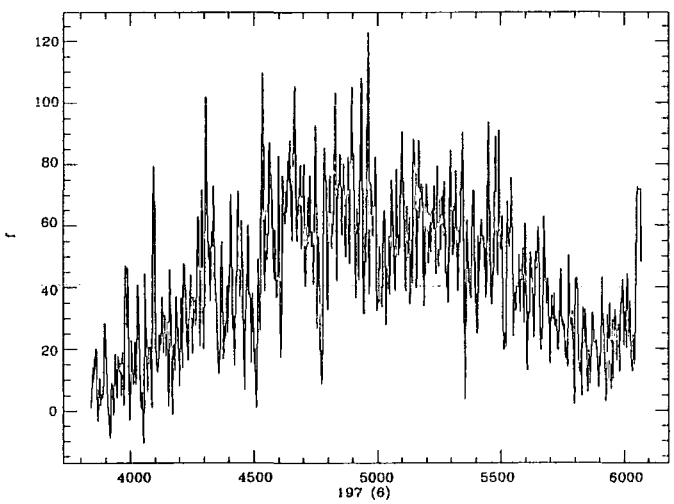
f
4000
4500
5000
5500
6000
197 (6)

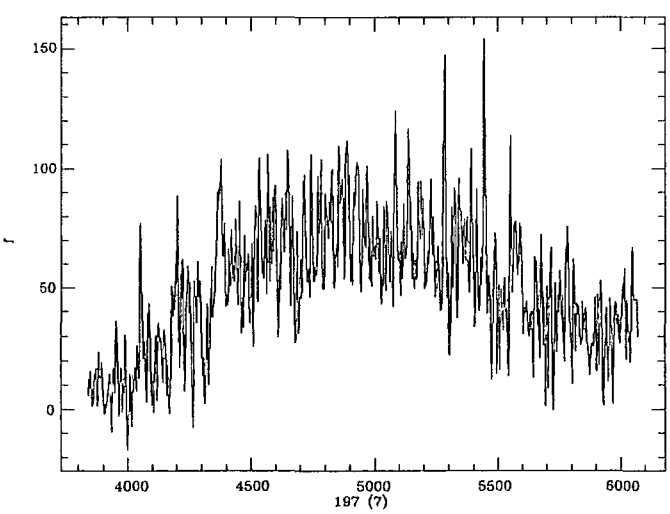
f
4000
4500
5000
5500
6000
197 (7)

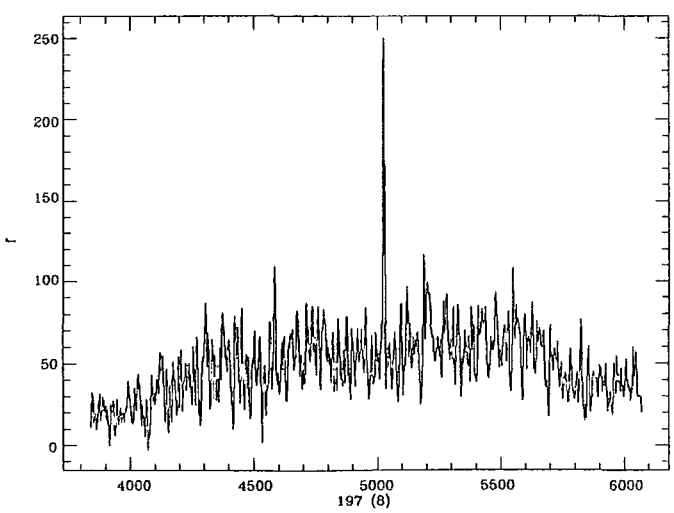
f
4000
4500
5000
5500
6000
197 (8)

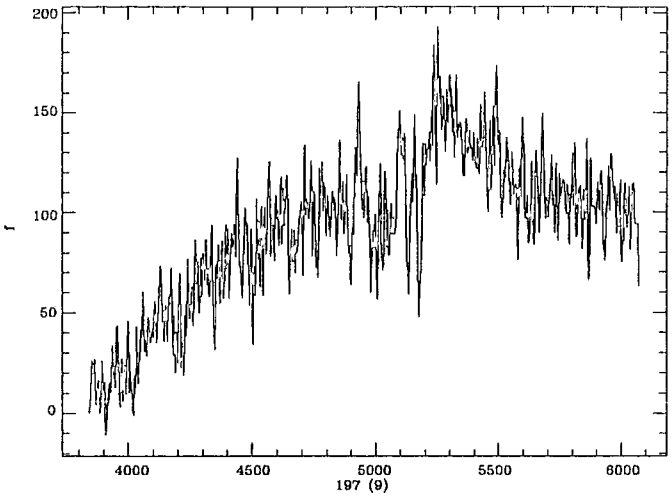
f
4000
4500
5000
5500
6000
197 (9)

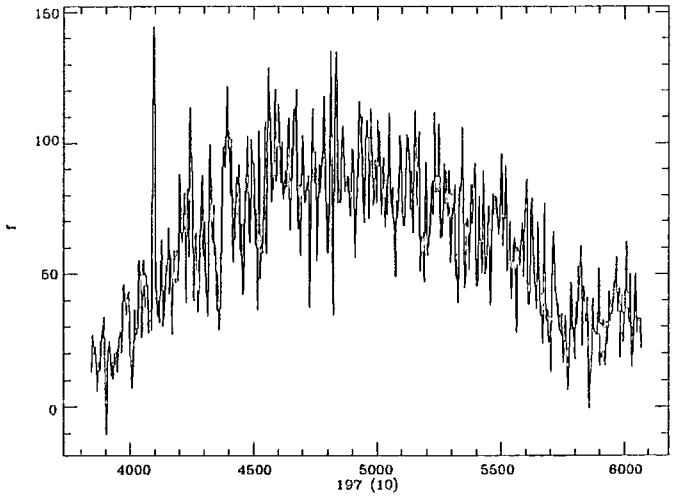
f
4000
4500
5000
5500
6000
197 (10)

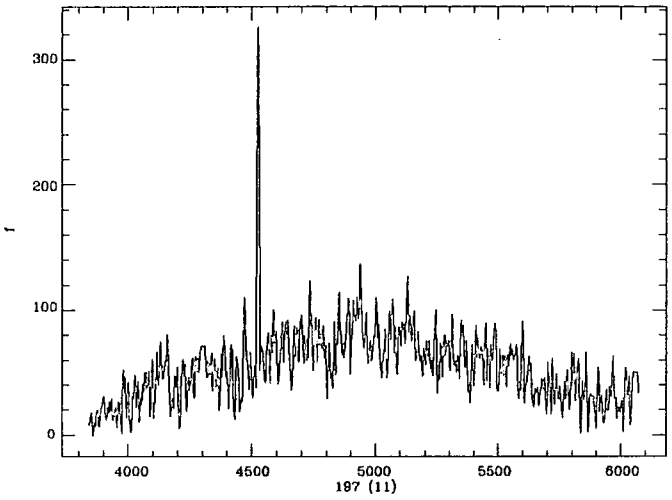
f
4000
4500
5000
5500
6000
197 (11)

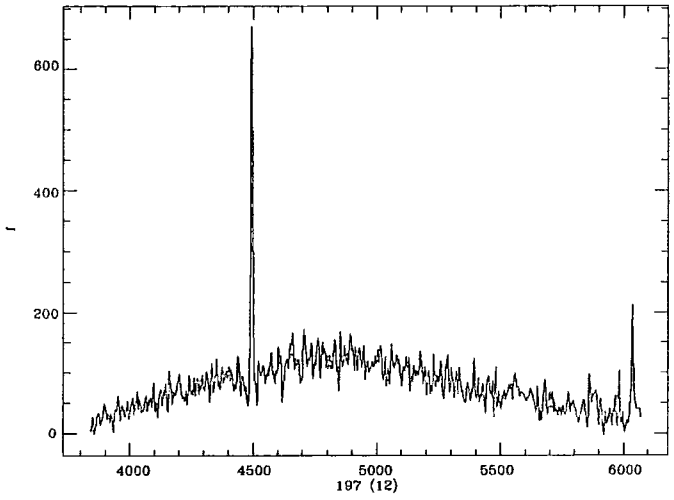
f
4000
4500
5000
5500
6000
197 (12)

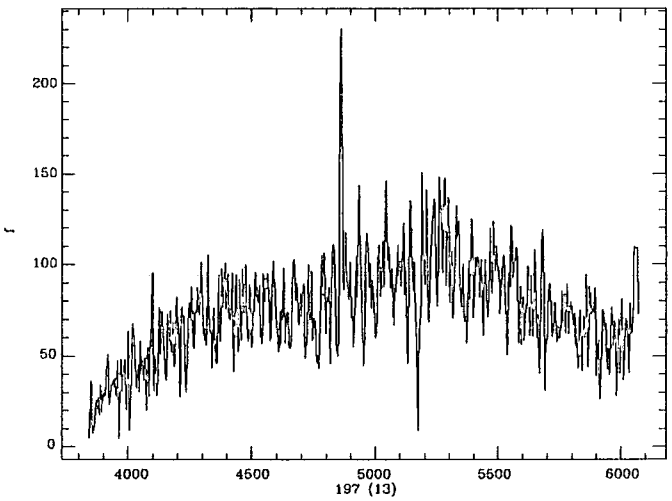
f
4000
4500
5000
5500
6000
197 (13)

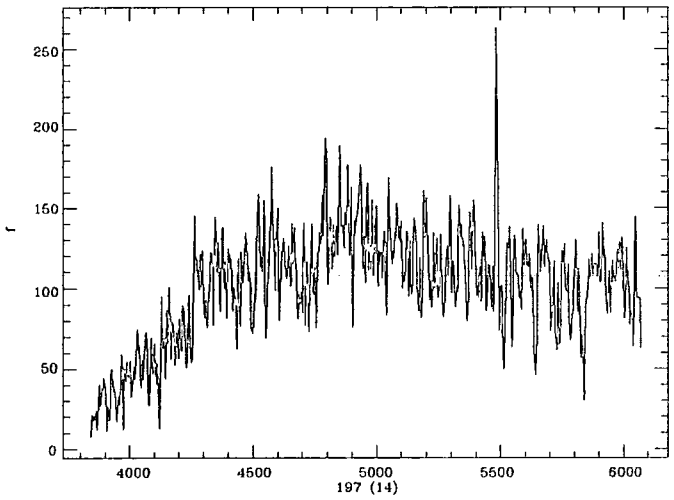
f
4000
4500
5000
5500
6000
197 (14)

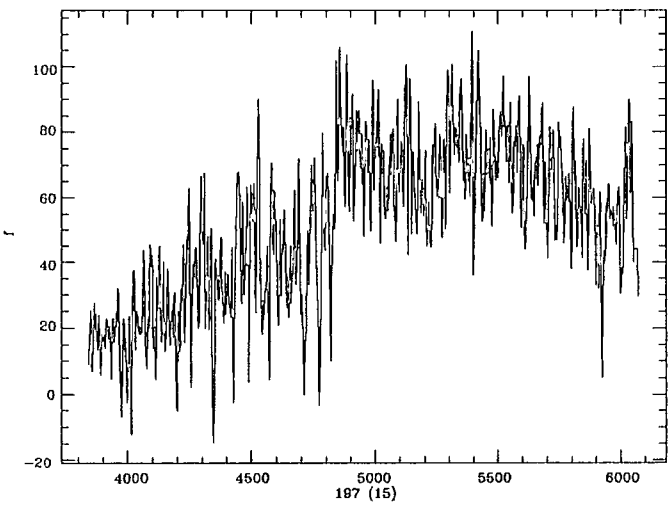
f
4000
4500
5000
5500
6000
197 (15)

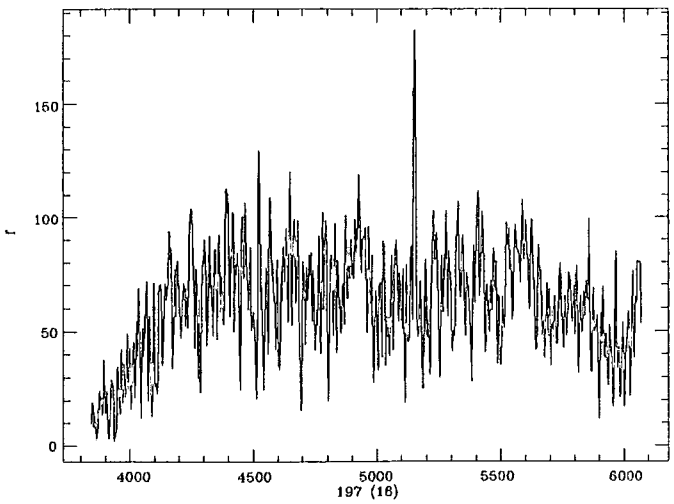
f
4000
4500
5000
5500
6000
197 (16)

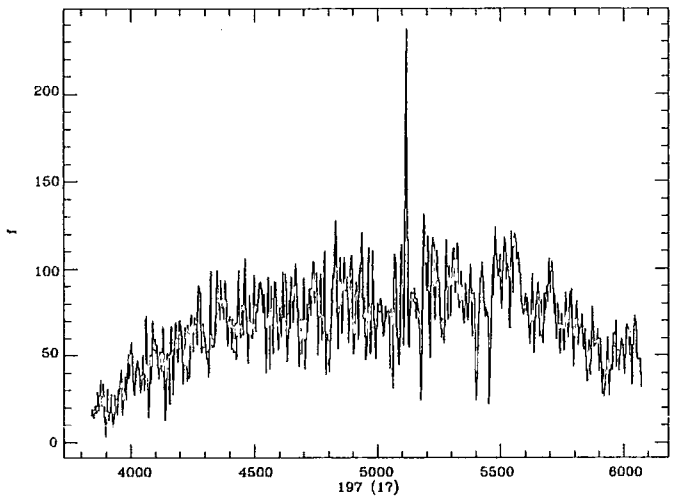
f
0
50
100
150
200
4000
4500
5000
5500
6000
197 (17)

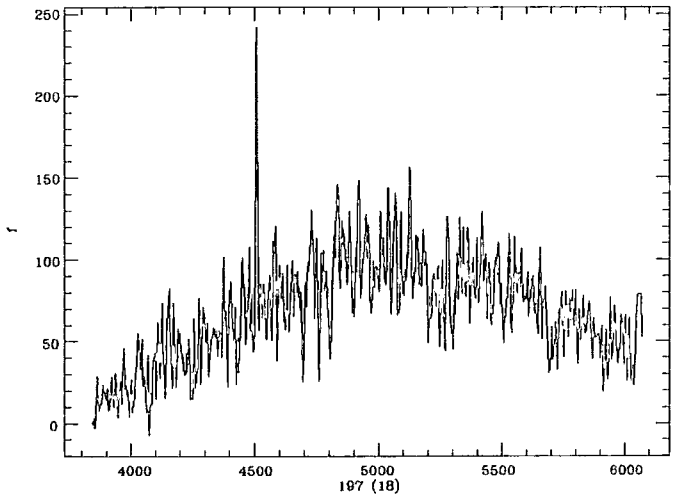
f
0
50
100
150
200
250
4000
4500
5000
5500
6000
197 (18)

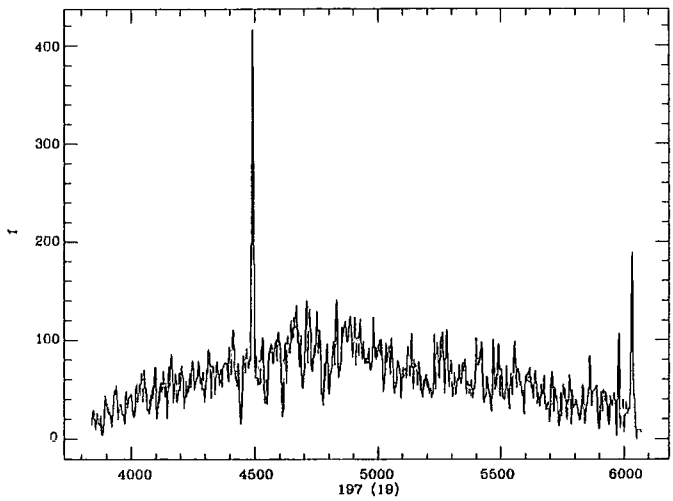
f
0
100
200
300
400
4000
4500
5000
5500
6000
197 (19)

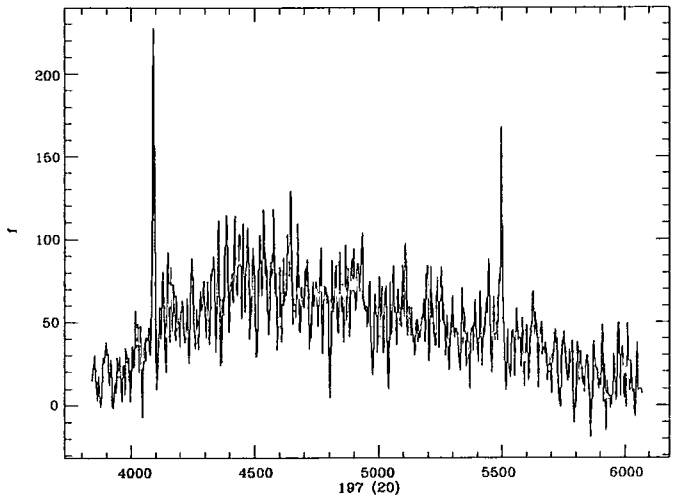
f
0
50
100
150
200
4000
4500
5000
5500
6000
197 (20)

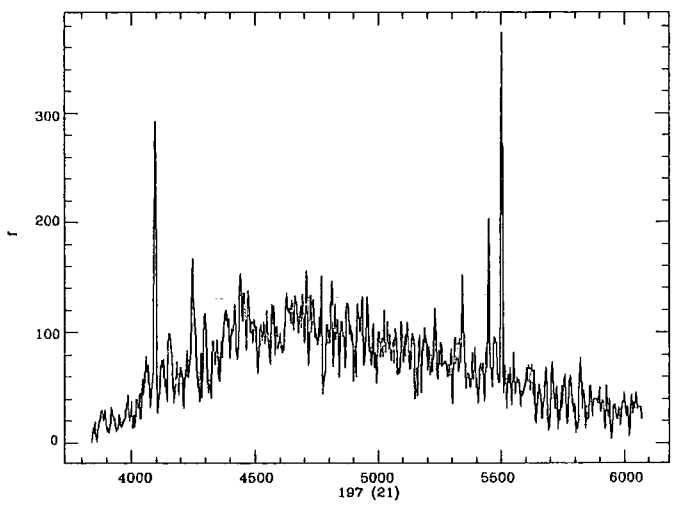
f
0
100
200
300
4000
4500
5000
5500
6000
197 (21)

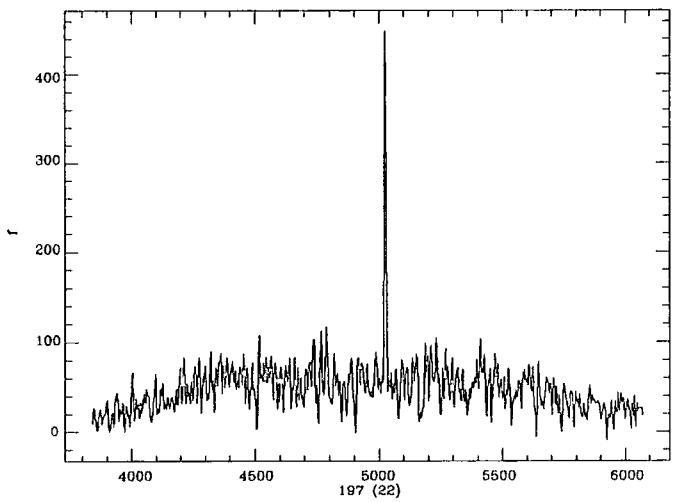
f
0
100
200
300
400
4000
4500
5000
5500
6000
197 (22)

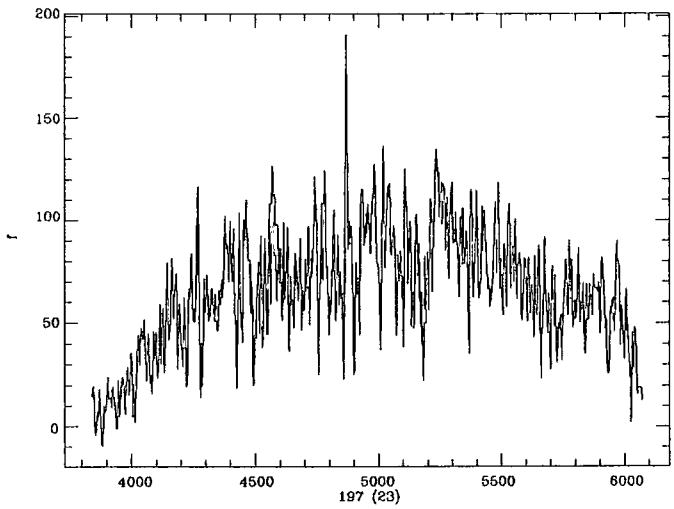
f
0
50
100
150
200
4000
4500
5000
5500
6000
197 (23)

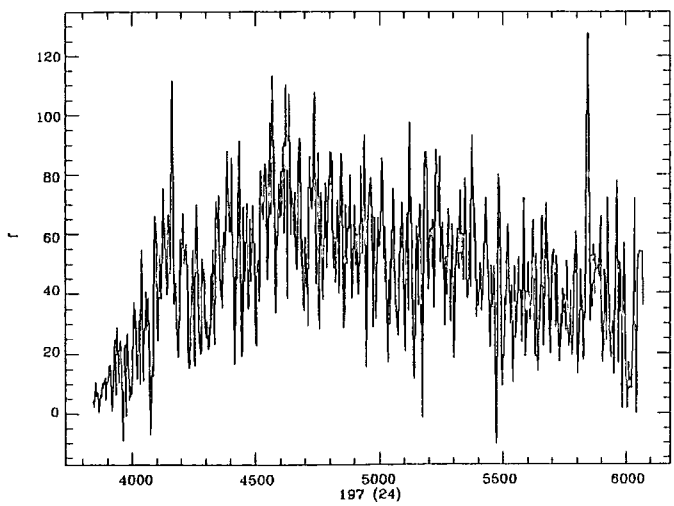
f
0
20
40
60
80
100
120
4000
4500
5000
5500
6000
197 (24)

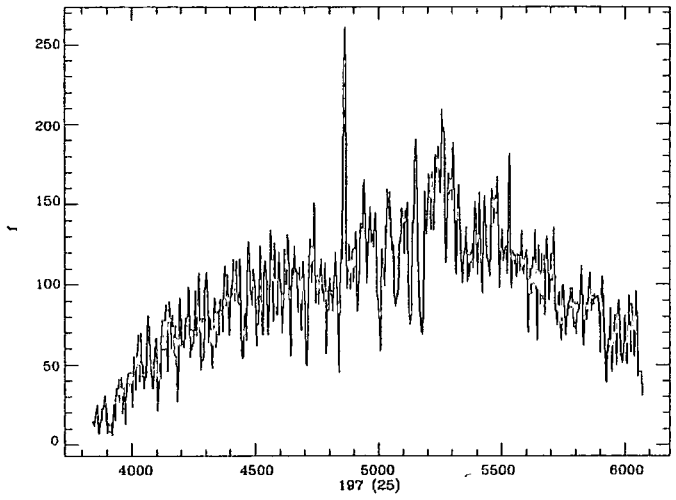
f
4000
4500
5000
5500
6000
197 (25)

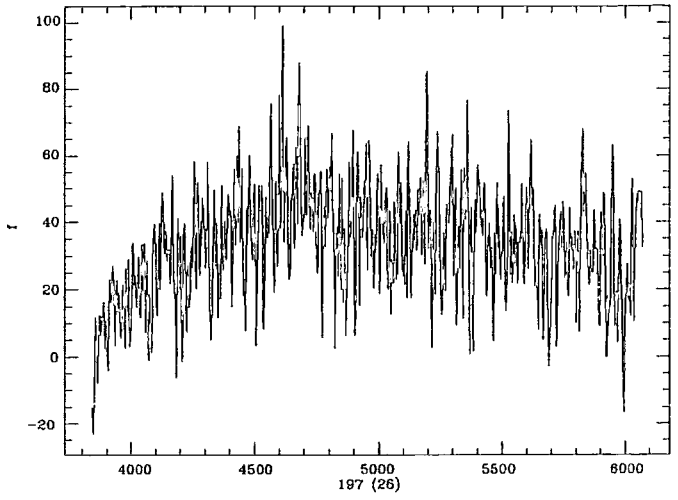
f
4000
4500
5000
5500
6000
197 (26)

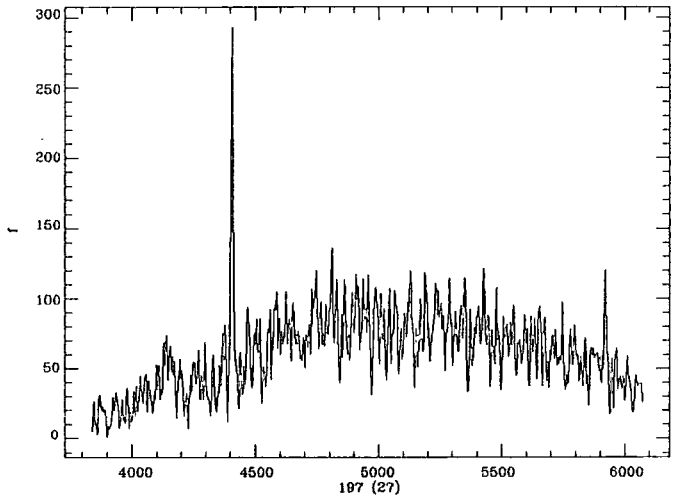
f
4000
4500
5000
5500
6000
197 (27)

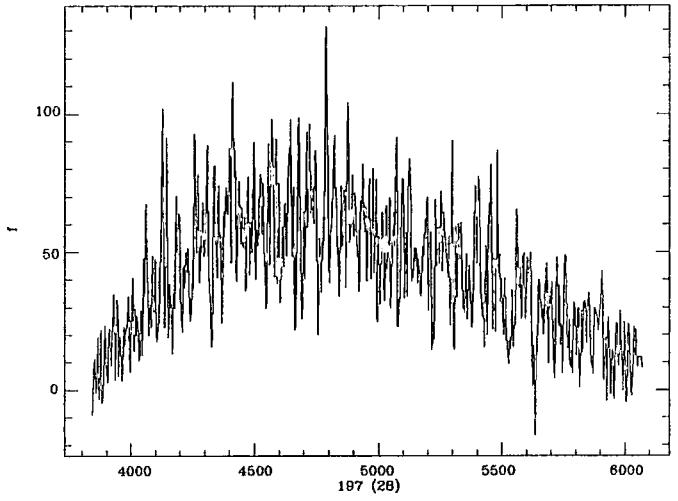
f
4000
4500
5000
5500
6000
197 (28)

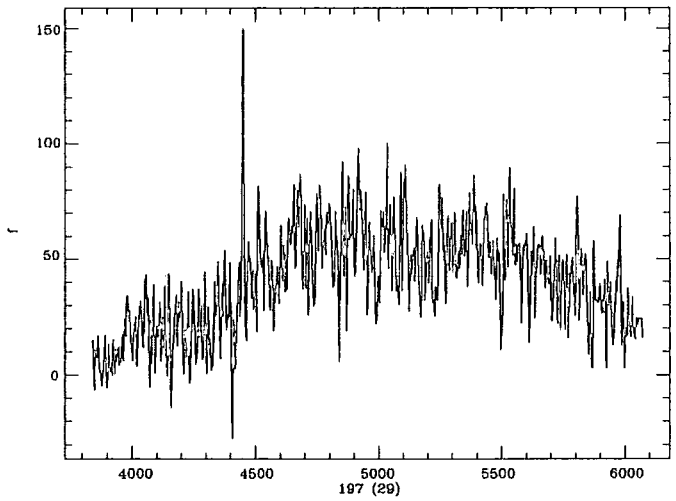
f
4000
4500
5000
5500
6000
197 (29)

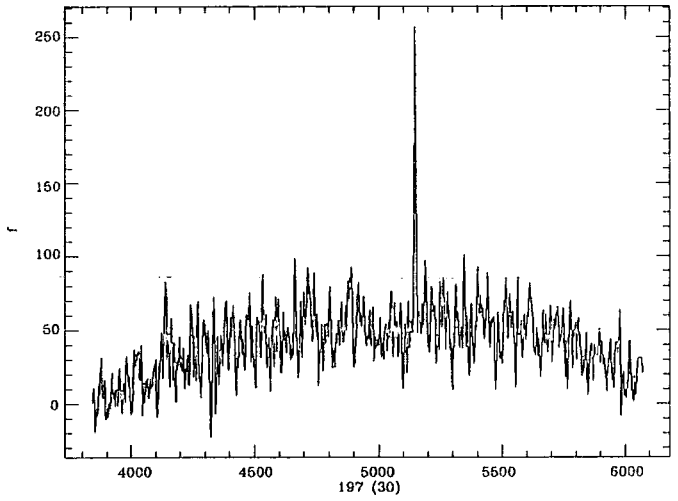
f
4000
4500
5000
5500
6000
197 (30)

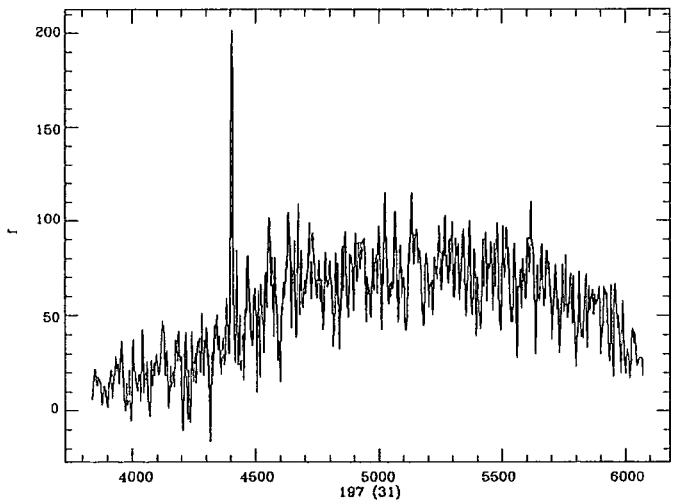
f
4000
4500
5000
5500
6000
197 (31)

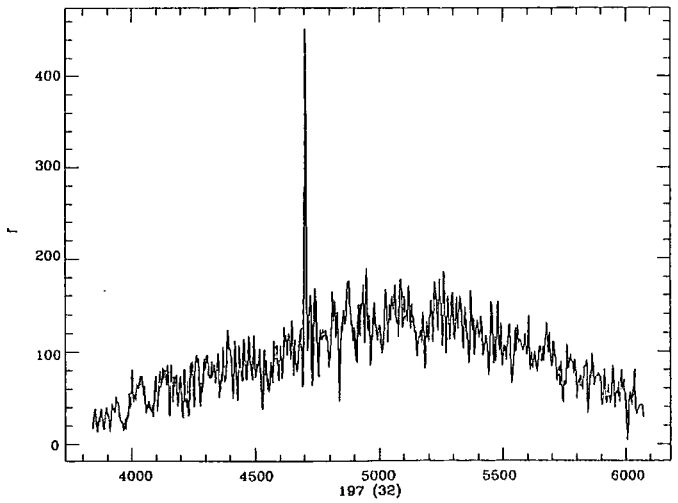
f
4000
4500
5000
5500
6000
197 (32)

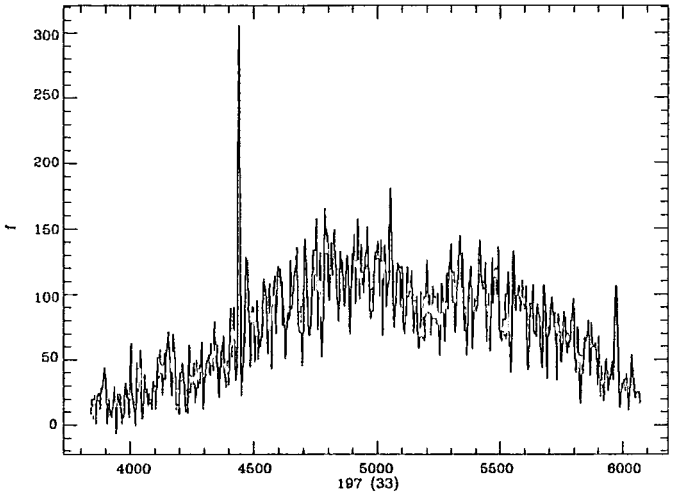
f
4000
4500
5000
5500
6000
197 (33)

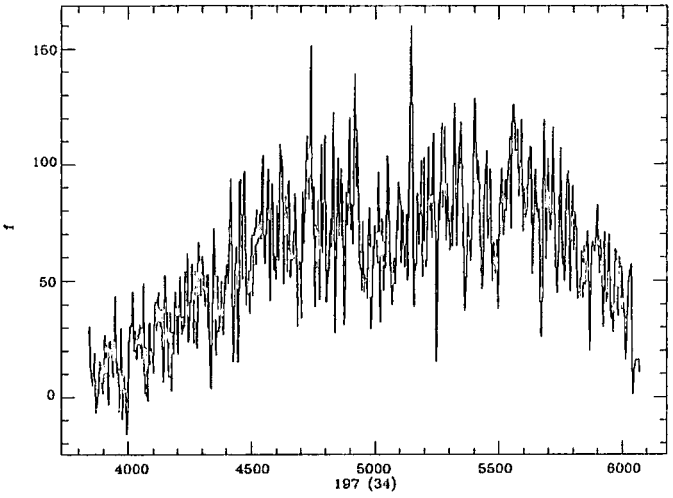
f
4000
4500
5000
5500
6000
197 (34)

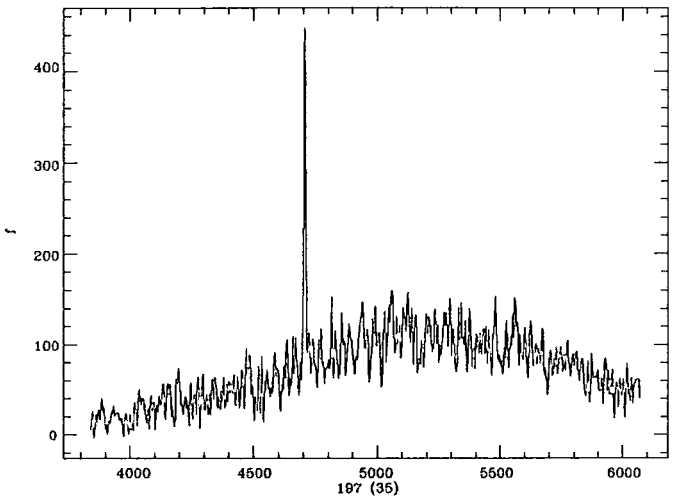
f
4000
4500
5000
5500
6000
197 (35)

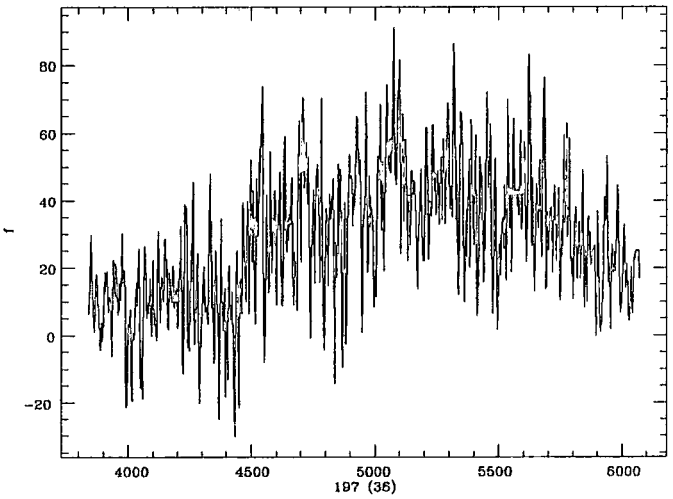
f
4000
4500
5000
5500
6000
197 (36)

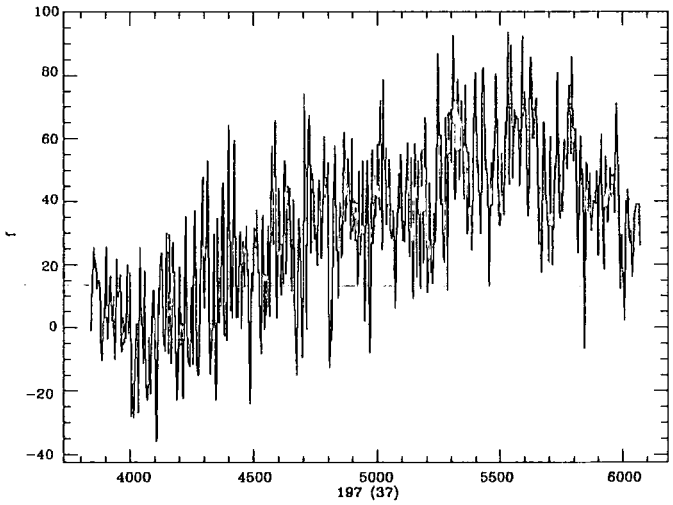
f
4000
4500
5000
5500
6000
197 (37)

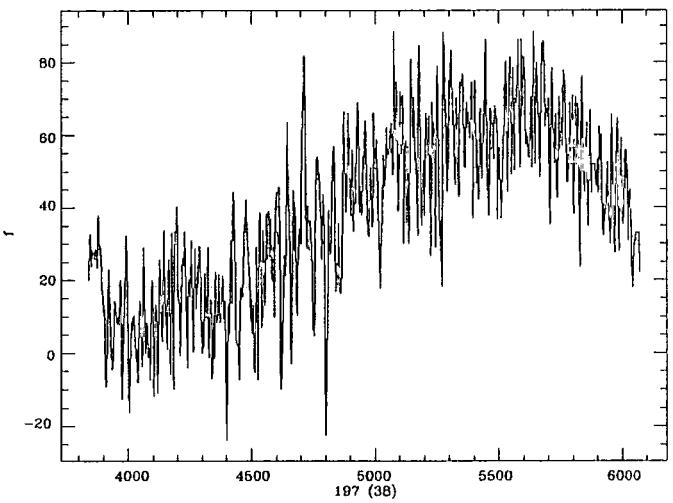
f
4000
4500
5000
5500
6000
197 (38)

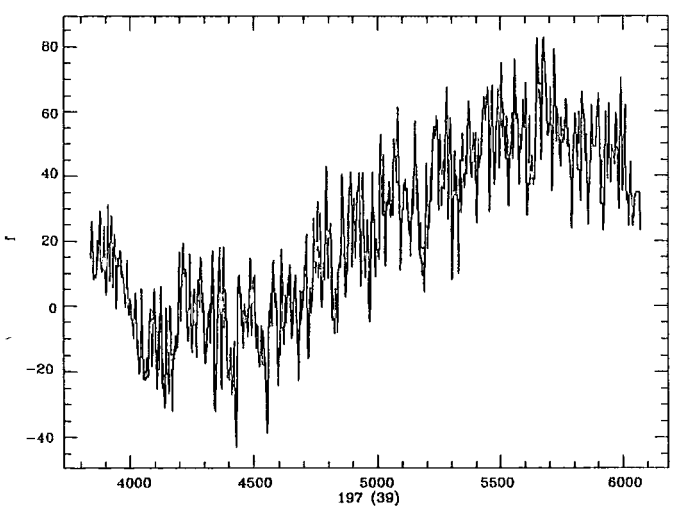
f
4000
4500
5000
5500
6000
197 (39)

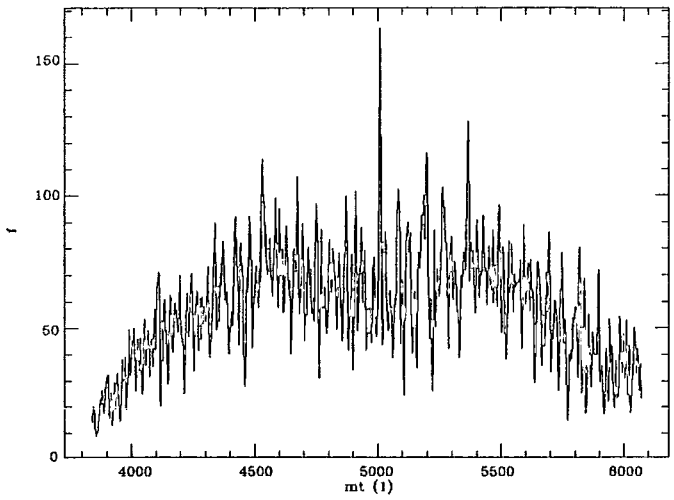
f
mt (1)

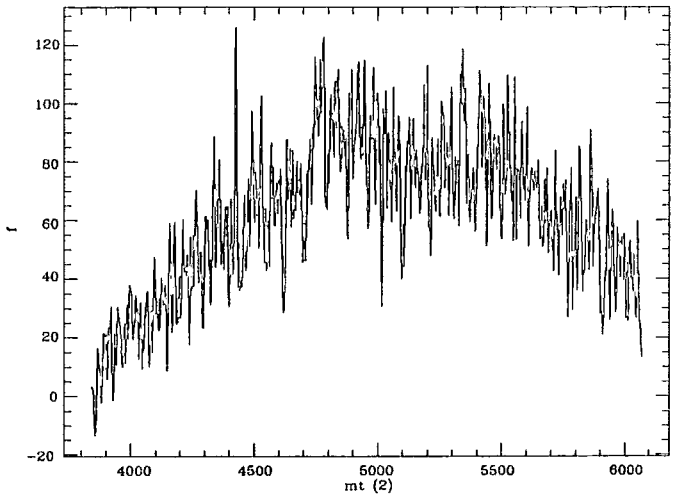
f
mt (2)

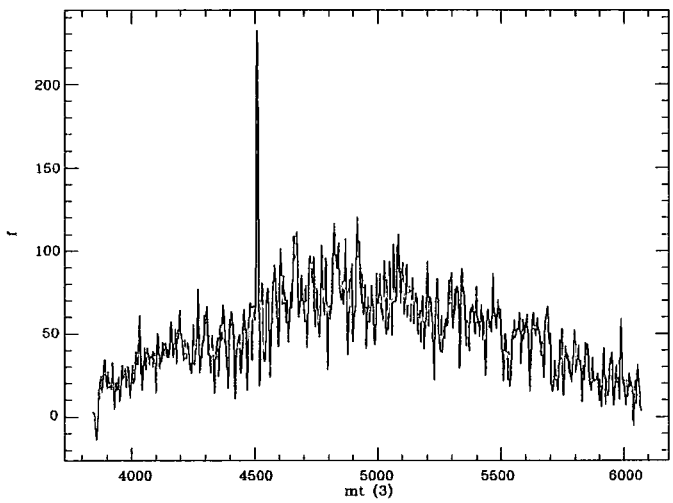
f
mt (3)

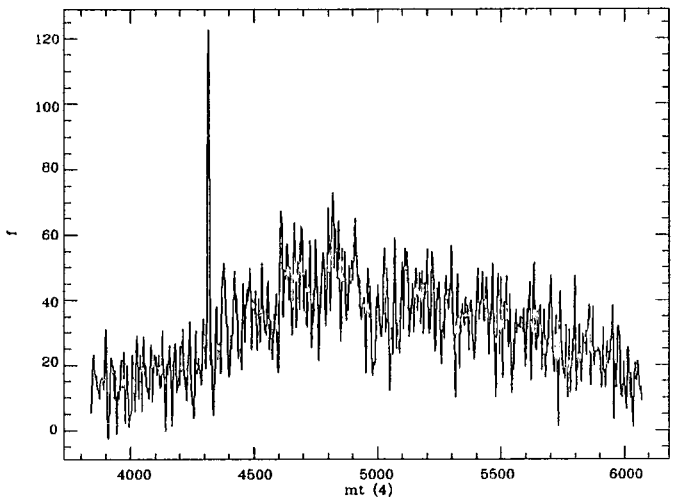
f
mt (4)

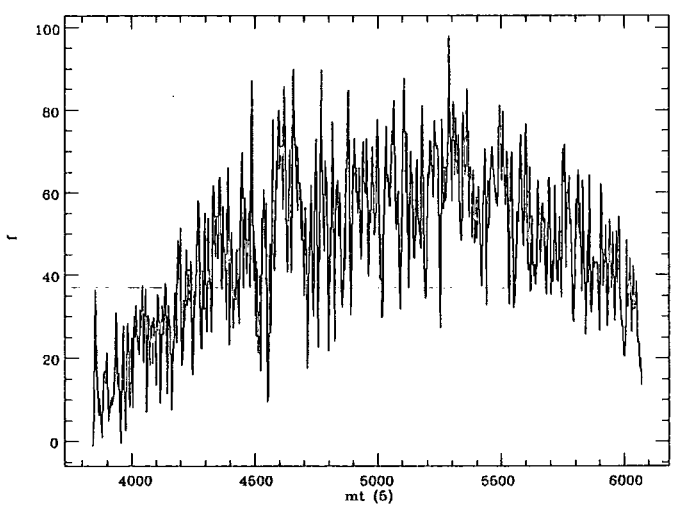
f
mt (5)

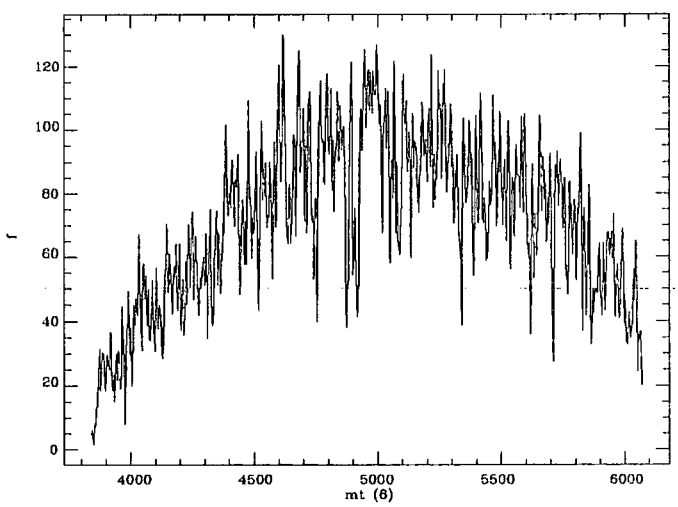
f
mt (6)

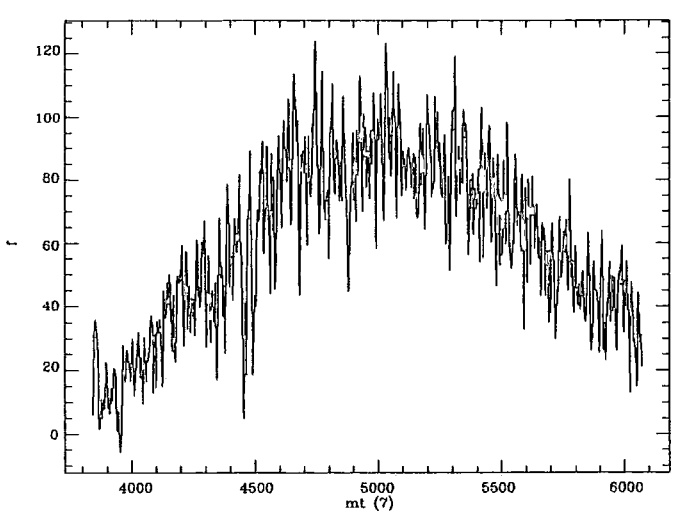
f
mt (7)

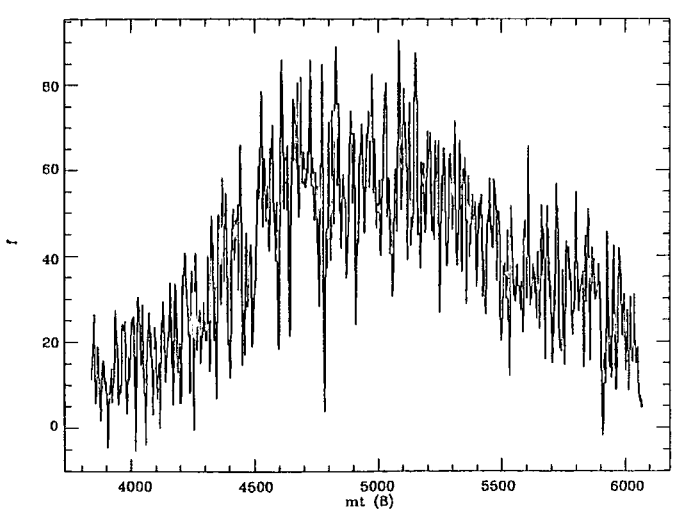
f
mt (8)

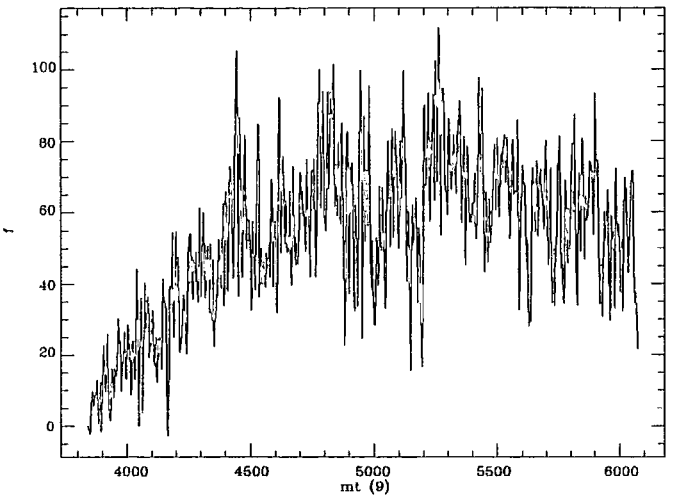
f
mt (9)

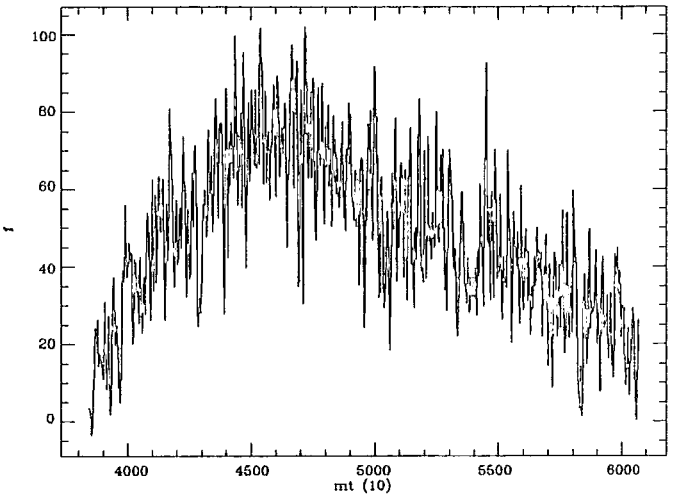
f
mt (10)

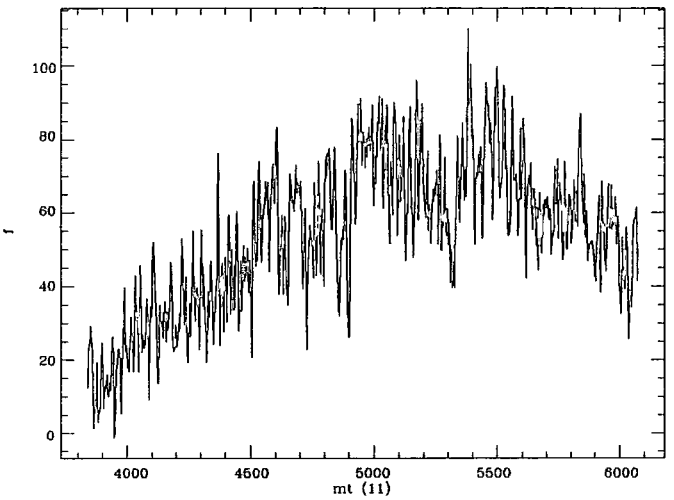
f
mt (11)

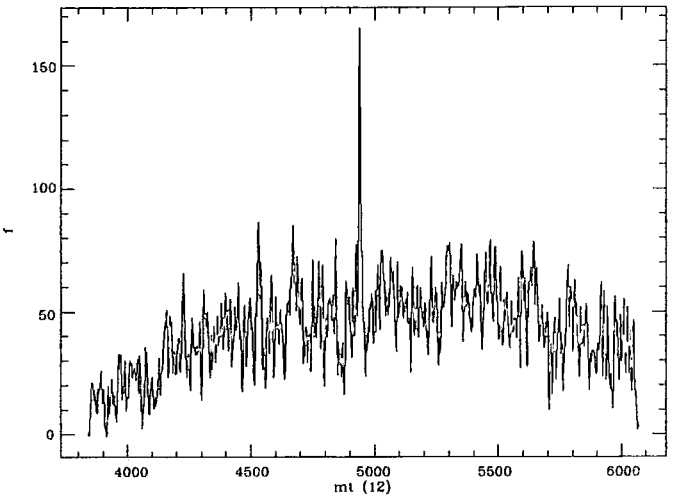
f
mt (12)

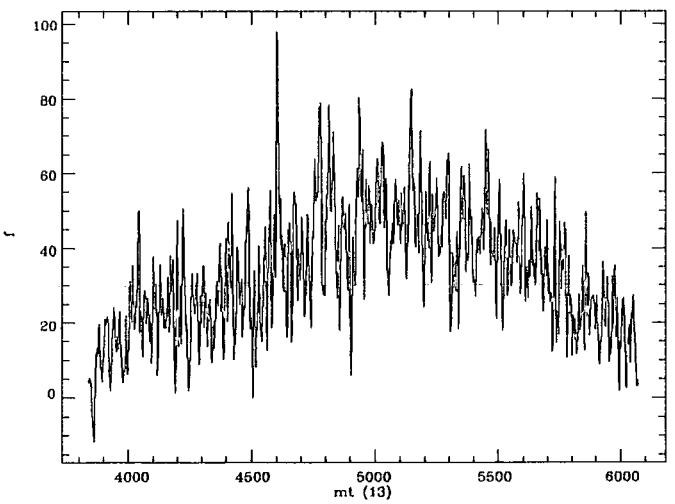
f
mt (13)

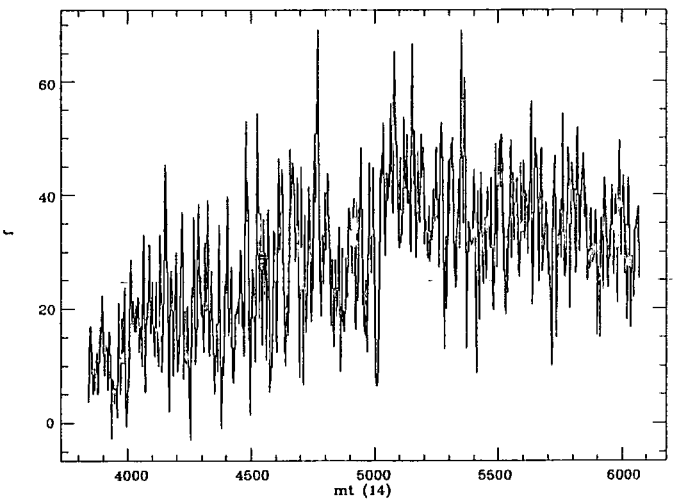
f
mt (14)

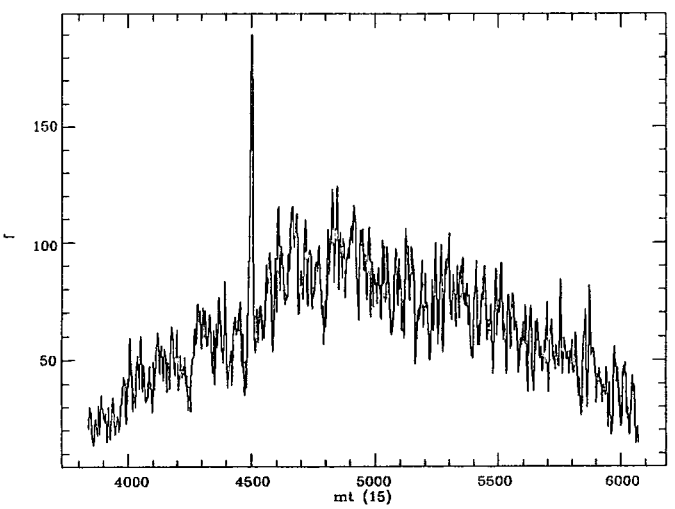
f
mt (15)

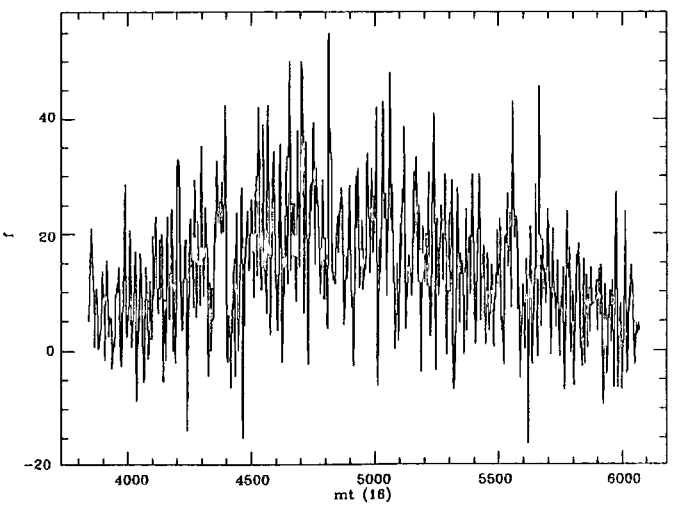
f
mt (16)

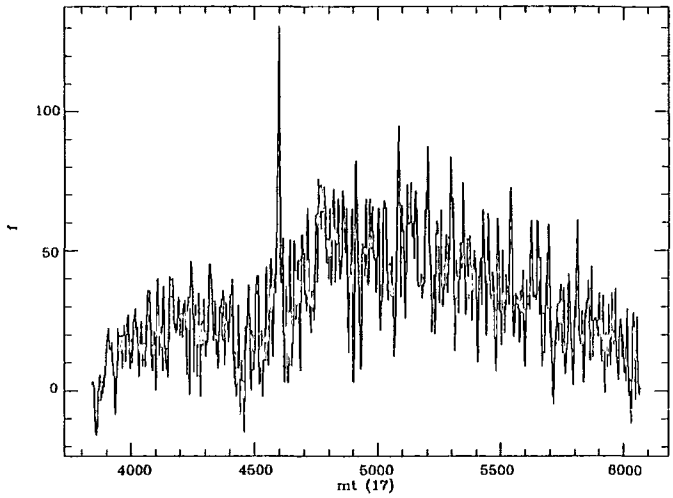
f
100
50
0
4000
4500
5000
5500
6000
mt (17)

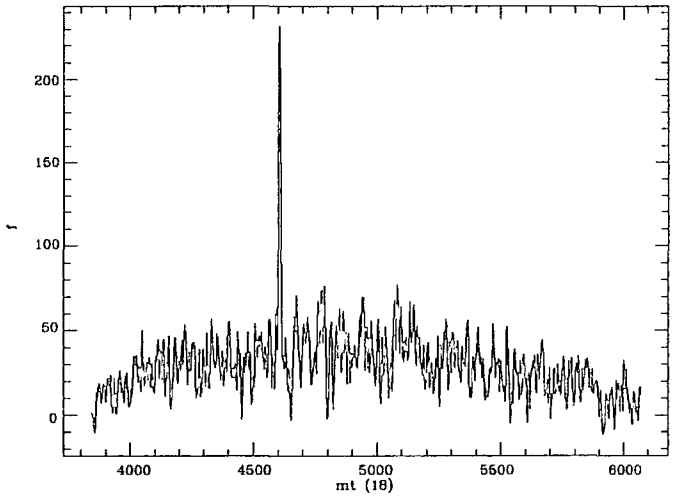
f
200
150
100
50
0
4000
4500
5000
5500
6000
mt (18)

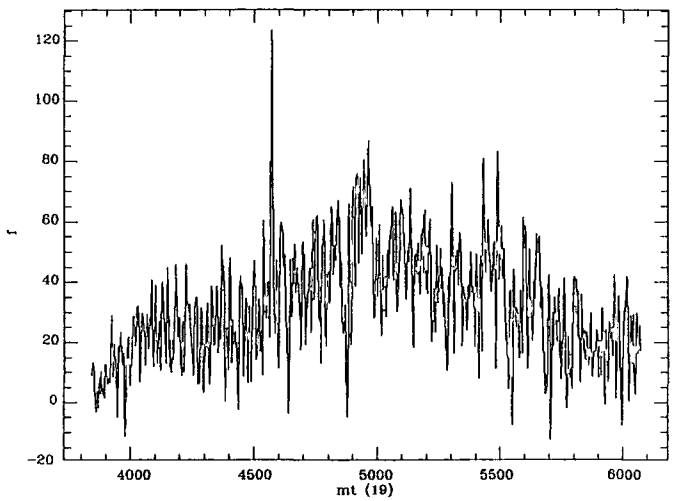
f
120
100
80
60
40
20
0
-20
4000
4500
5000
5500
6000
mt (19)

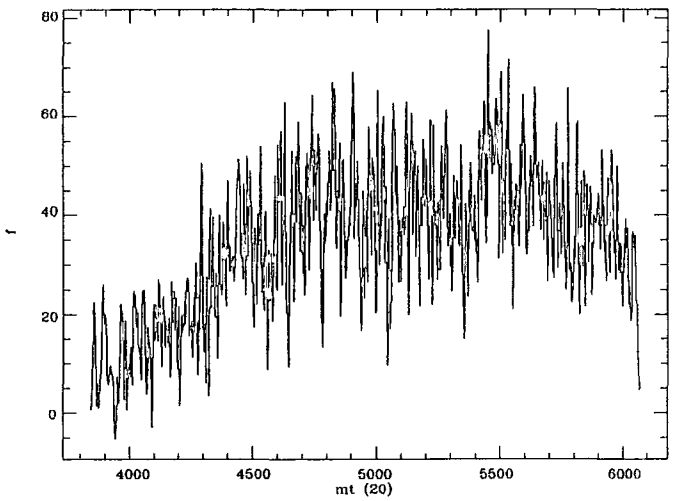
f
80
60
40
20
0
4000
4500
5000
5500
6000
mt (20)

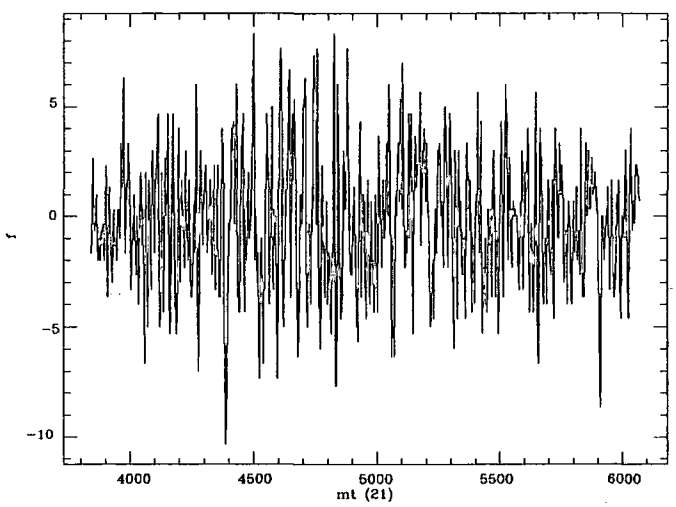
f
5
0
-5
-10
4000
4500
5000
5500
6000
mt (21)

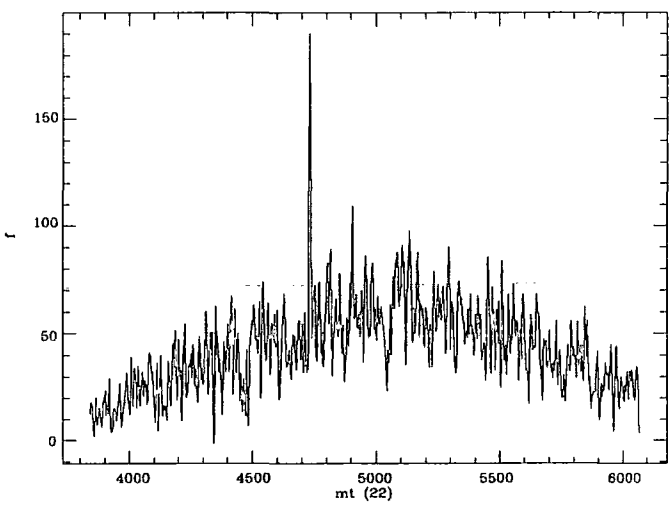
f
150
100
50
0
4000
4500
5000
5500
6000
mt (22)

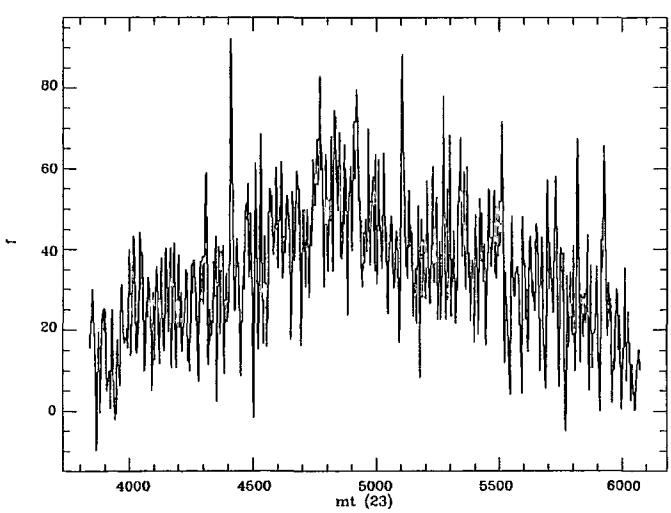
f
80
60
40
20
0
4000
4500
5000
5500
6000
mt (23)

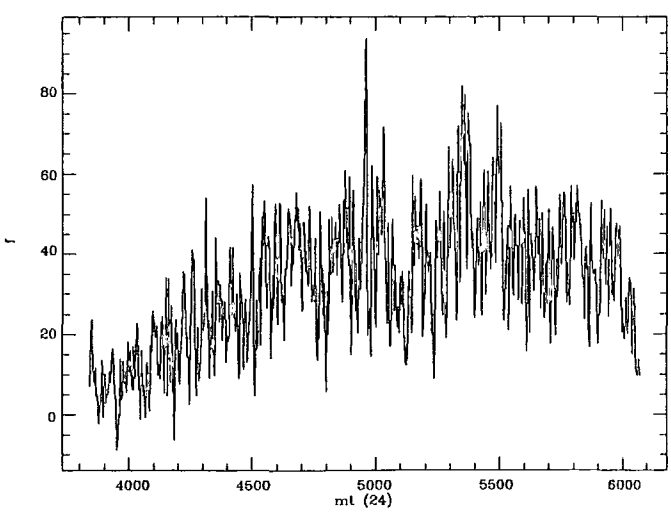
f
80
60
40
20
0
4000
4500
5000
5500
6000
mt (24)

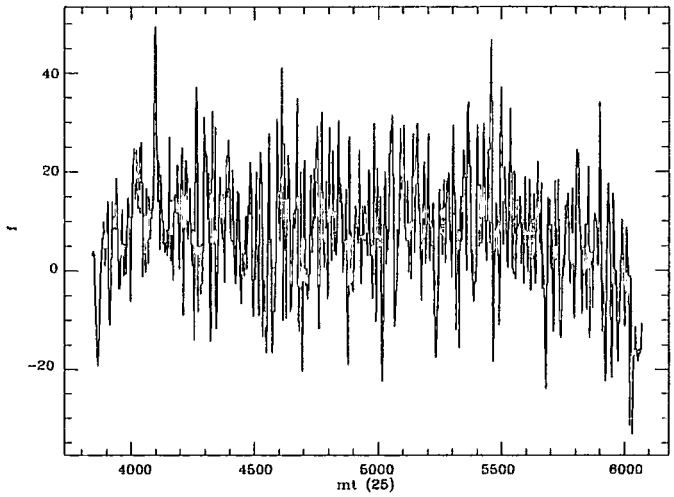
f
40
20
0
-20
4000
4500
5000
5500
6000
mt (25)

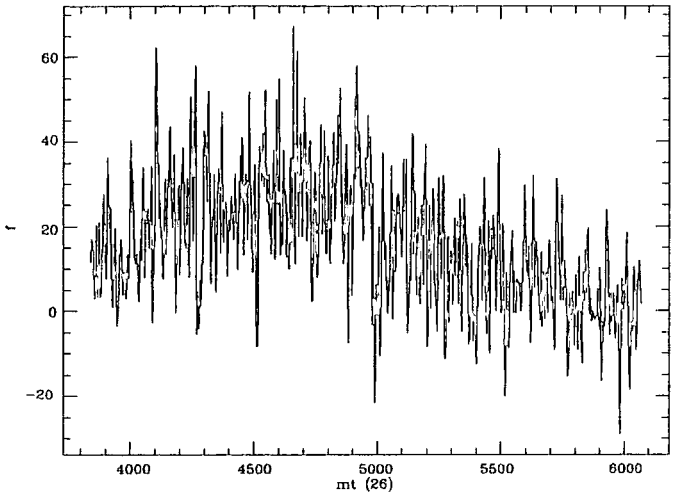
f
60
40
20
0
-20
4000
4500
5000
5500
6000
mt (26)

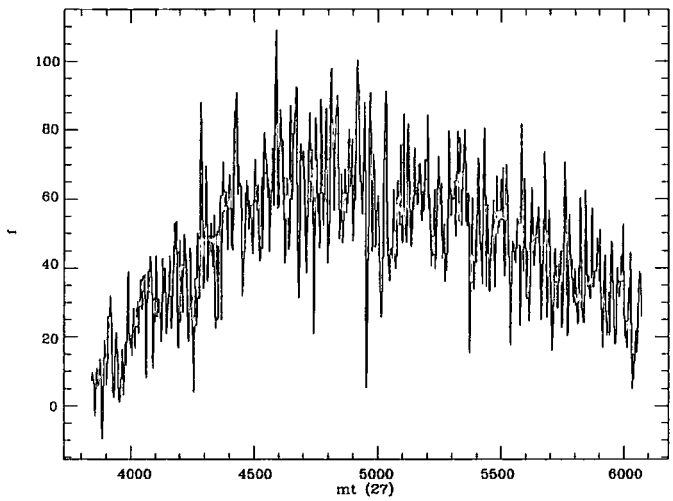
f
100
80
60
40
20
0
4000
4500
5000
5500
6000
mt (27)

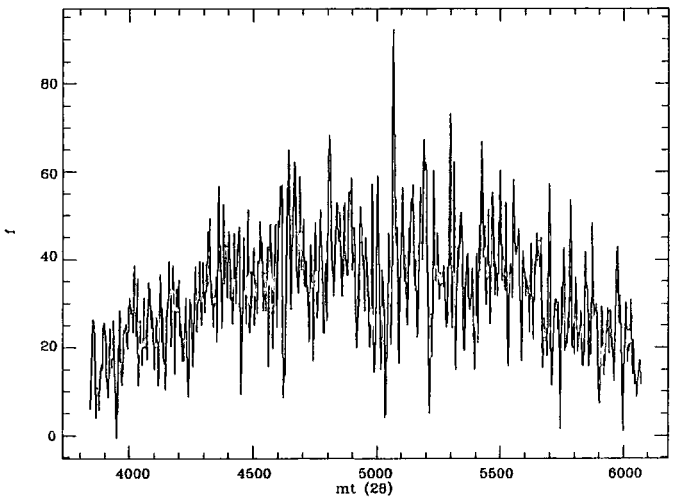
f
80
60
40
20
0
4000
4500
5000
5500
6000
mt (28)

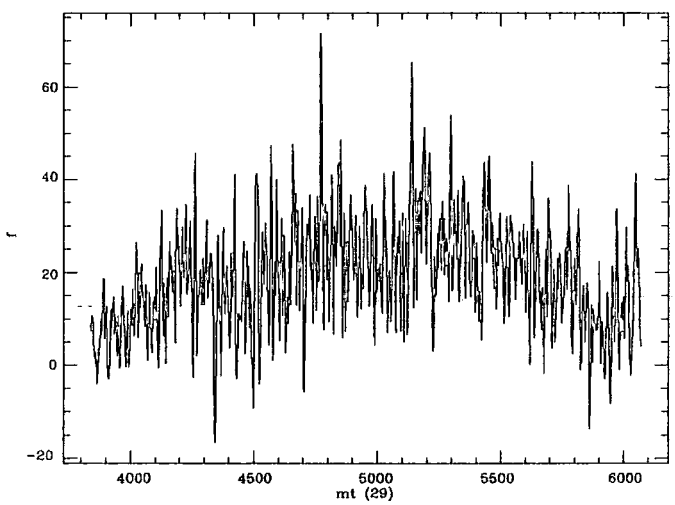
f
60
40
20
0
-20
4000
4500
5000
5500
6000
mt (29)

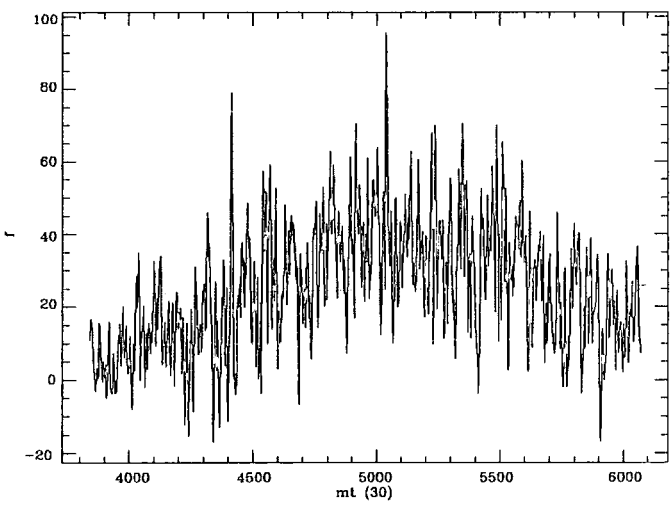
f
100
80
60
40
20
0
-20
4000
4500
5000
5500
6000
mt (30)

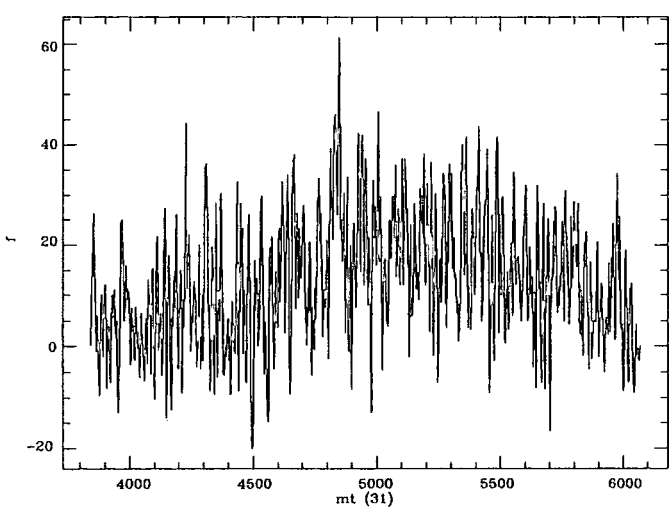
f
60
40
20
0
-20
4000
4500
5000
5500
6000
mt (31)

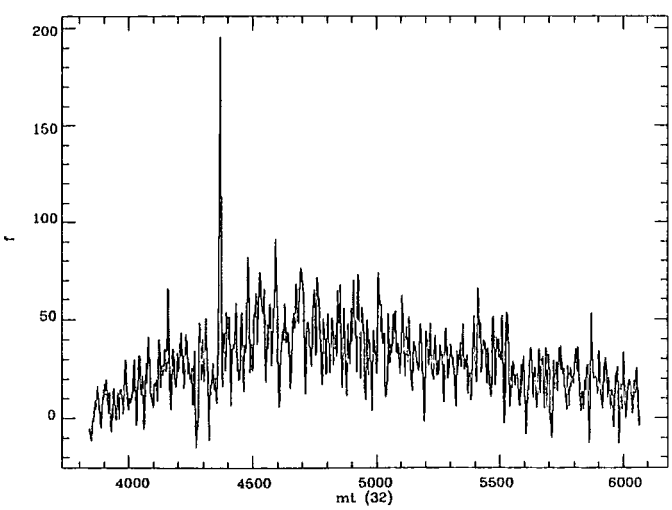
f
200
150
100
50
0
4000
4500
5000
5500
6000
mt (32)

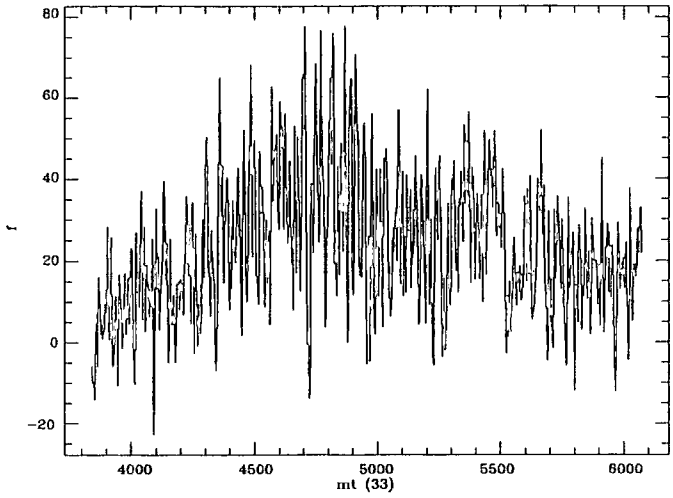
f
mt (33)

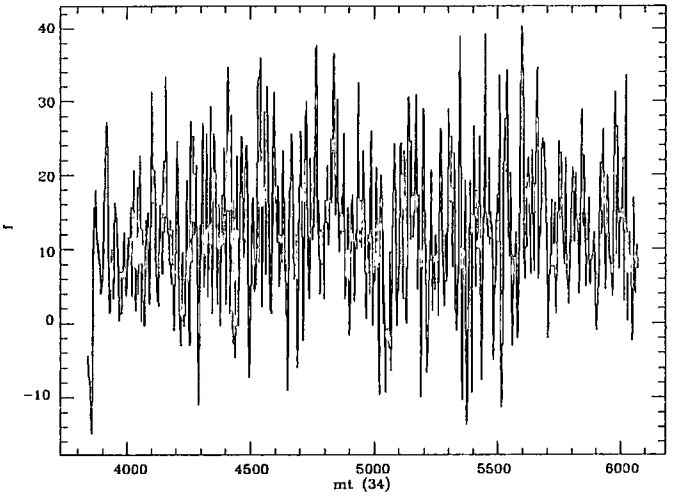
f
mt (34)

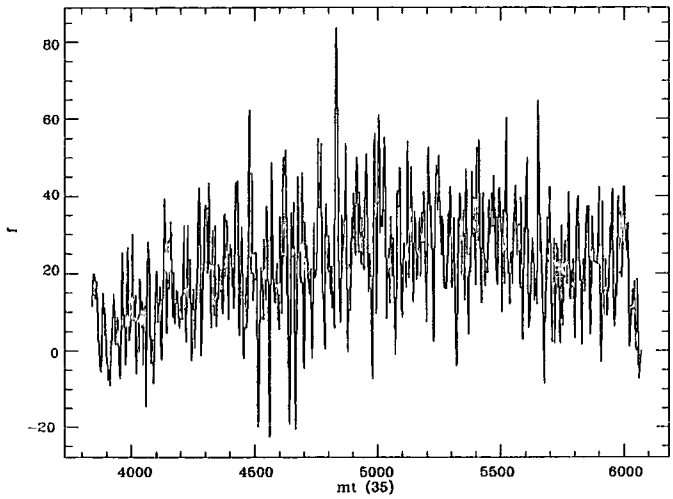
f
mt (35)

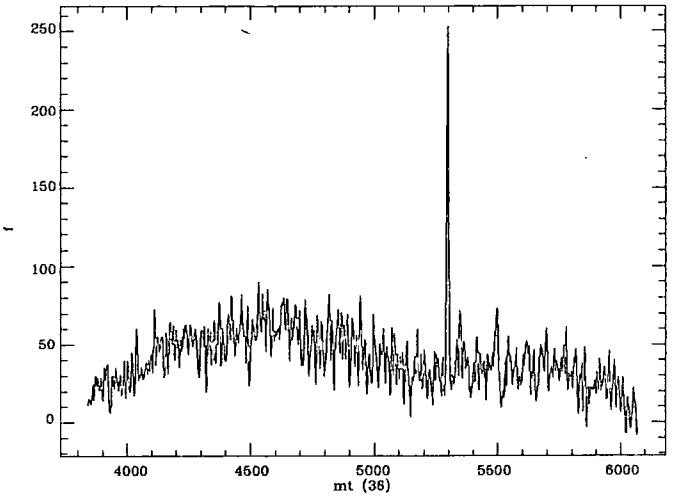
f
mt (36)

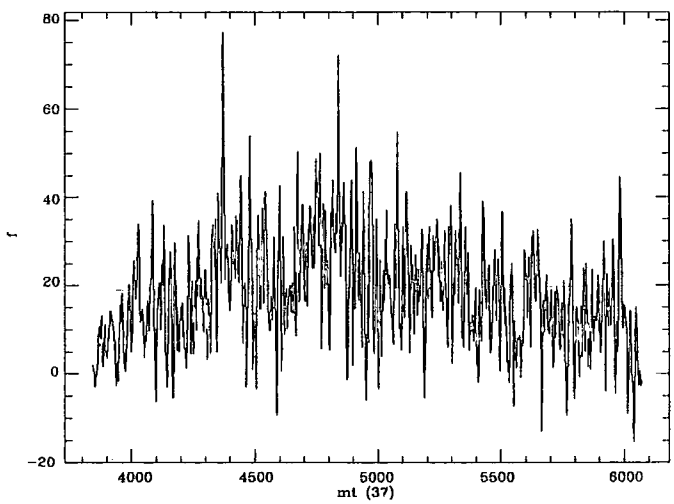
f
mt (37)

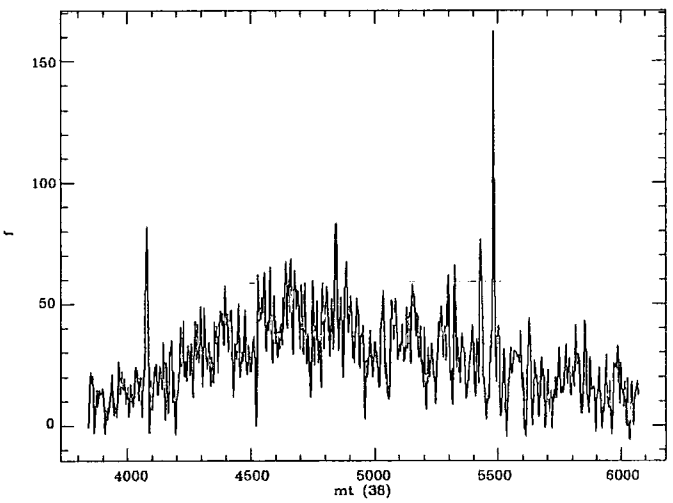
f
mt (38)

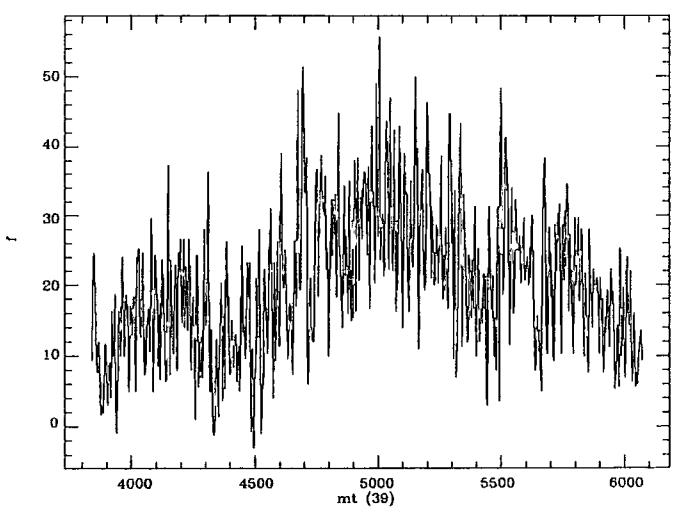
f
mt (39)

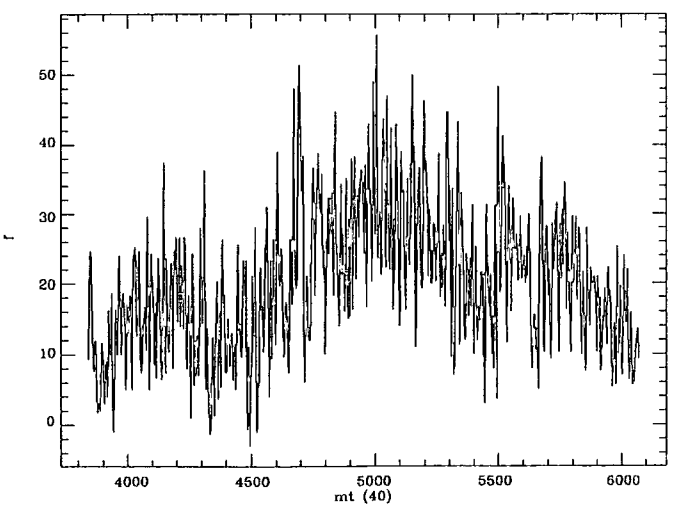
f
mt (40)

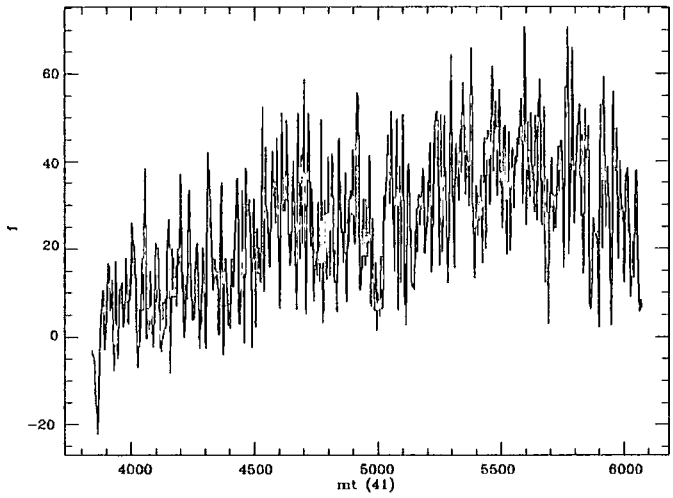
f
60
40
20
0
-20
4000
4500
5000
5500
6000
mt (41)

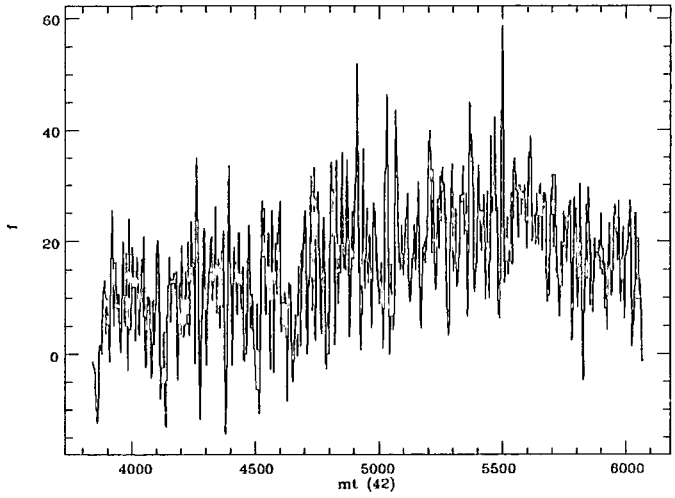
f
60
40
20
0
4000
4500
5000
5500
6000
mt (42)

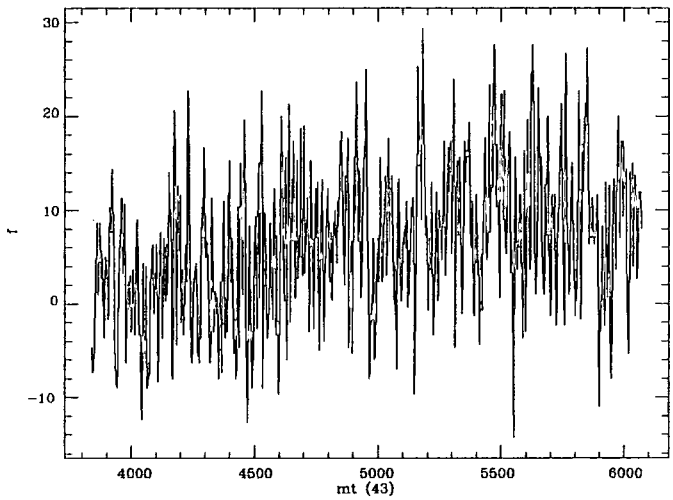
f
30
20
10
0
-10
4000
4500
5000
5500
6000
mt (43)

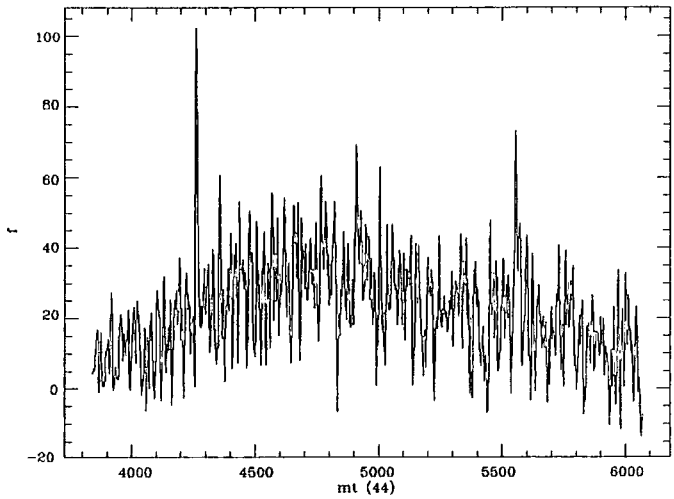
f
100
80
60
40
20
0
-20
4000
4500
5000
5500
6000
mt (44)

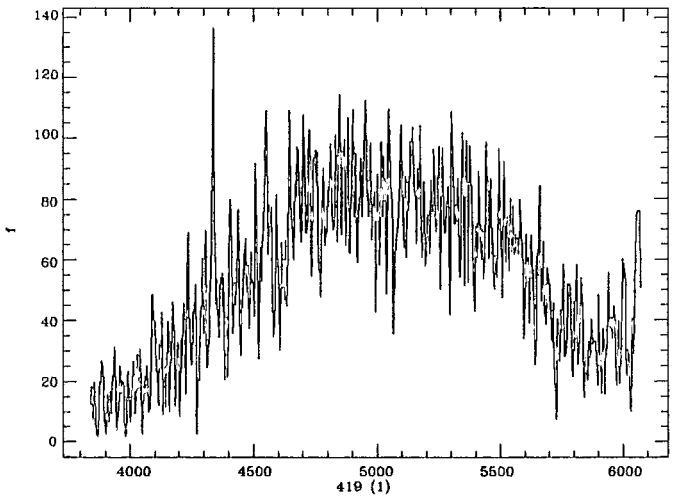
f
4000
4500
5000
5500
6000
419 (1)

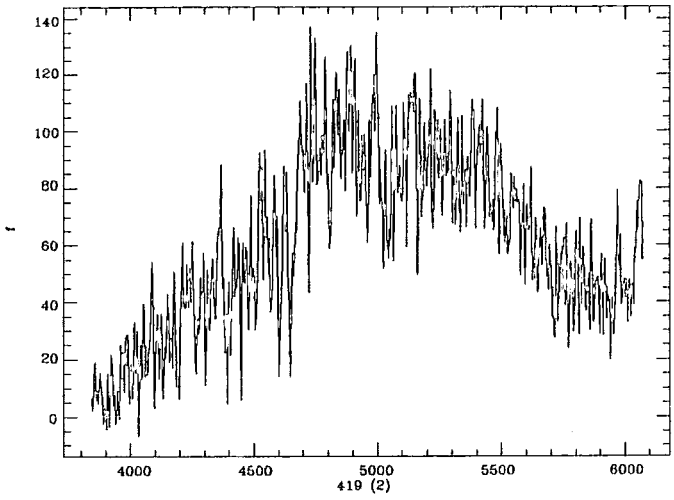
f
4000
4500
5000
5500
6000
419 (2)

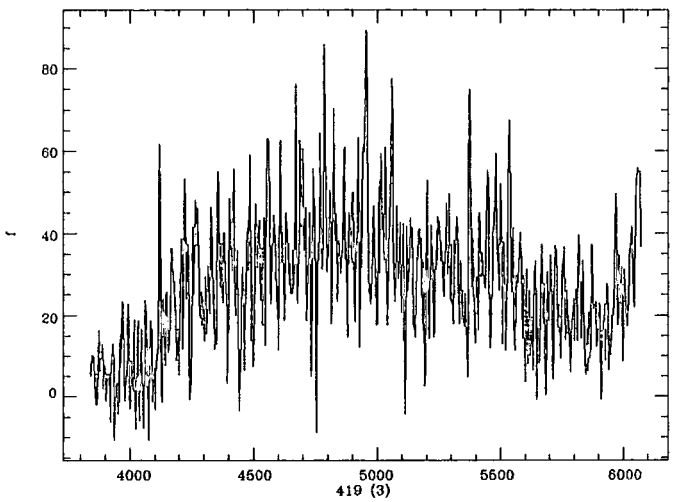
f
4000
4500
5000
5500
6000
419 (3)

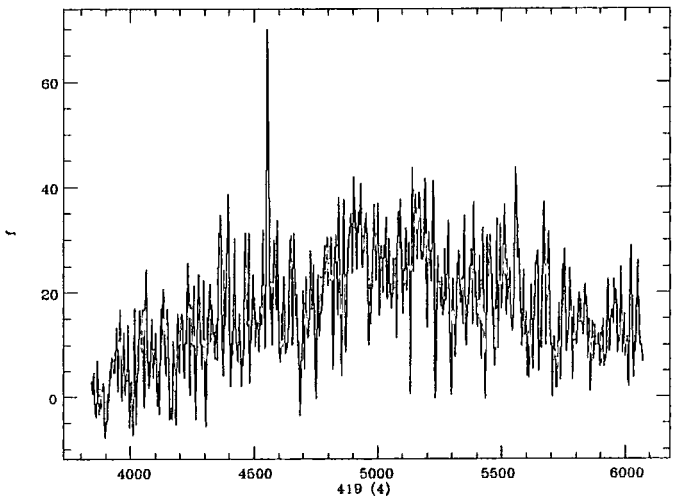
f
4000
4500
5000
5500
6000
419 (4)

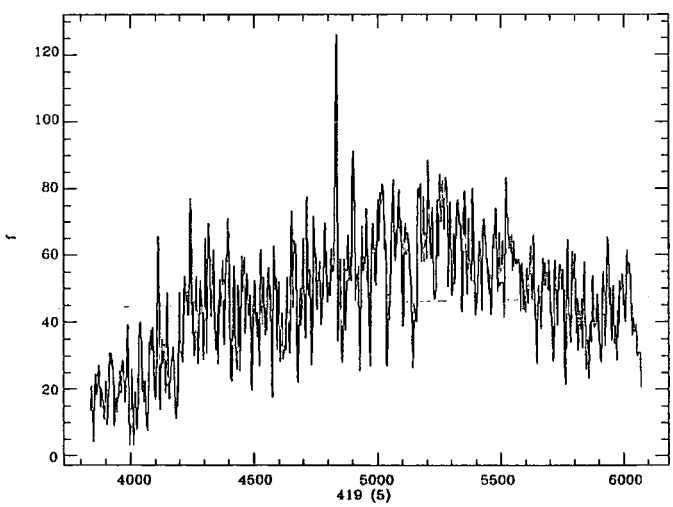
f
4000
4500
5000
5500
6000
419 (5)

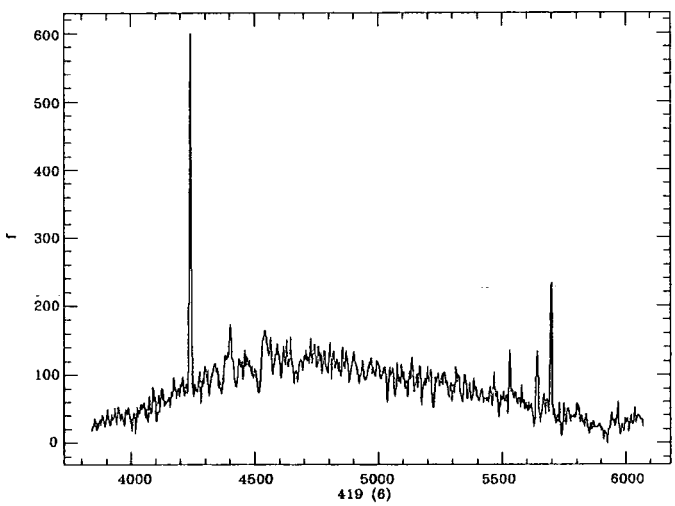
f
4000
4500
5000
5500
6000
419 (6)

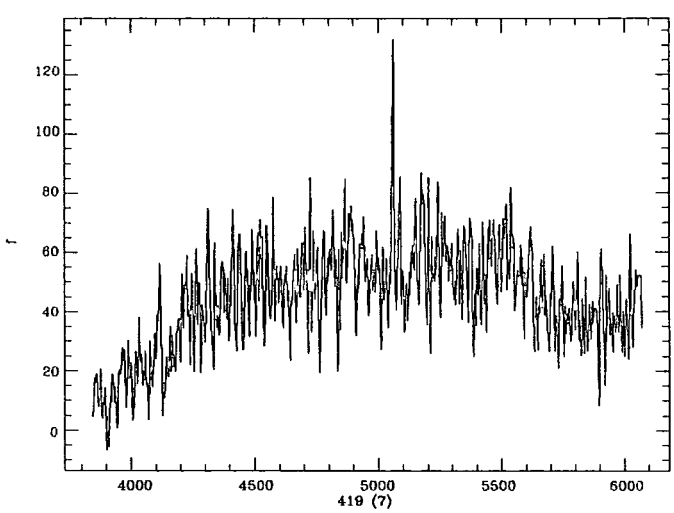
f
4000
4500
5000
5500
6000
419 (7)

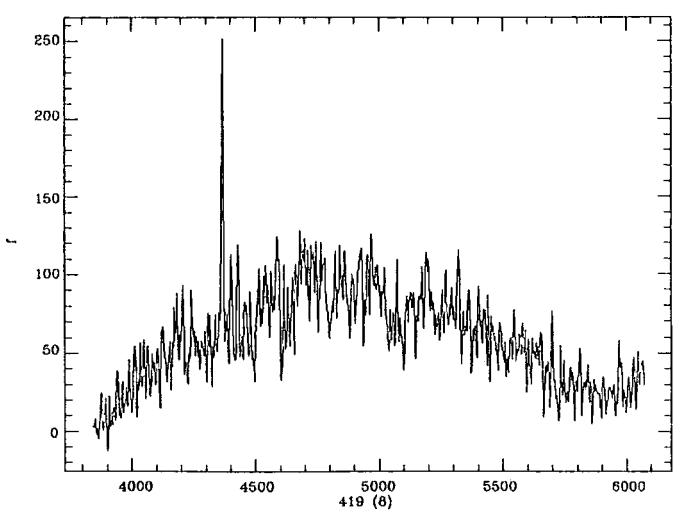
f
4000
4500
5000
5500
6000
419 (8)

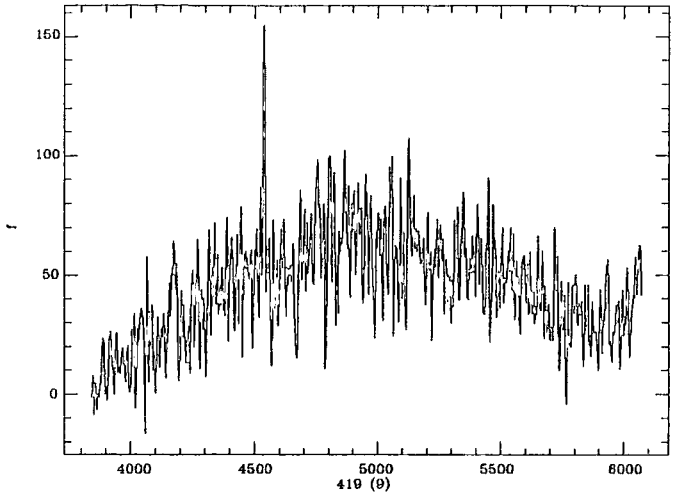
f
150
100
50
0
4000
4500
5000
5500
6000
419 (9)

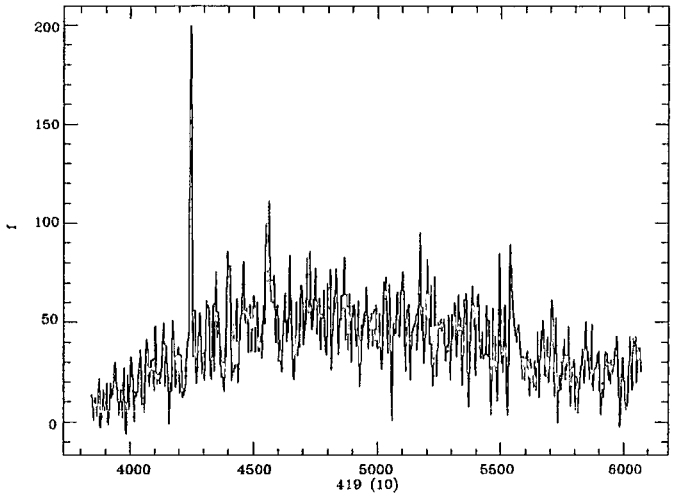
f
200
150
100
50
0
4000
4500
5000
5500
6000
419 (10)

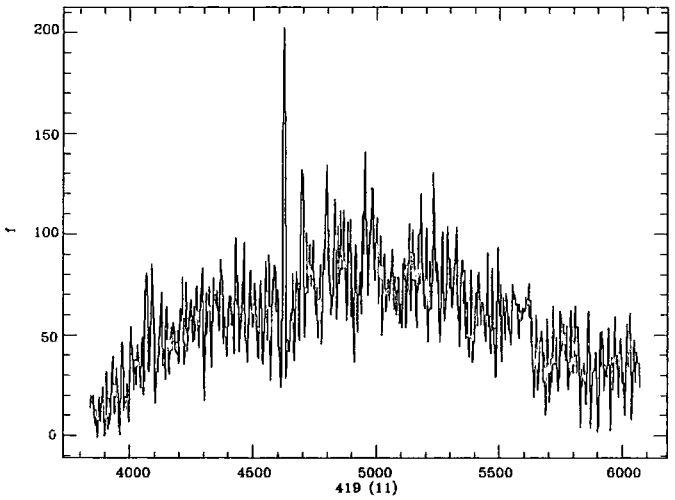
f
200
150
100
50
0
4000
4500
5000
5500
6000
419 (11)

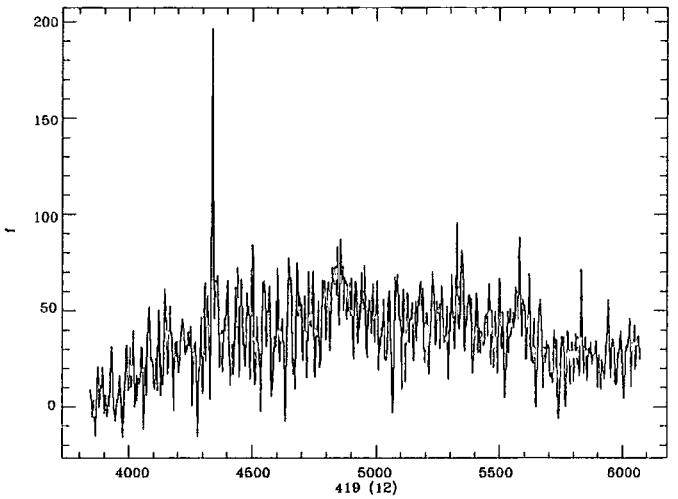
f
200
150
100
50
0
4000
4500
5000
5500
6000
419 (12)

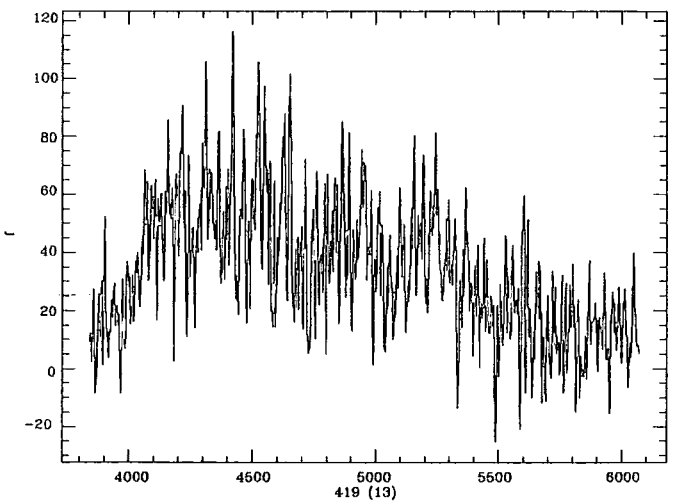
f
120
100
80
60
40
20
0
-20
4000
4500
5000
5500
6000
419 (13)

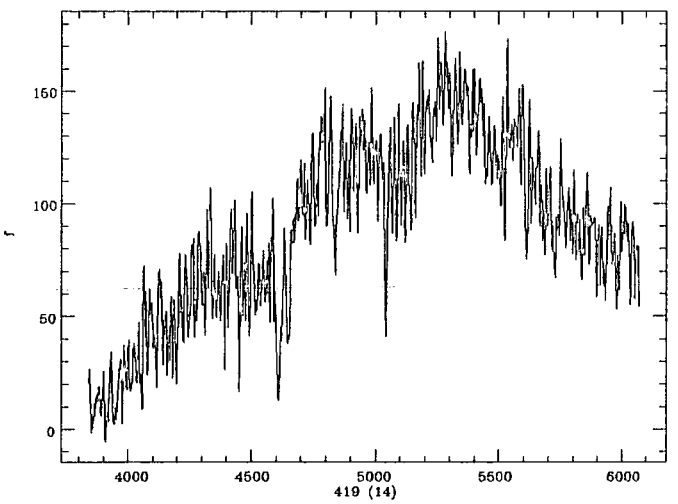
f
150
100
50
0
4000
4500
5000
5500
6000
419 (14)

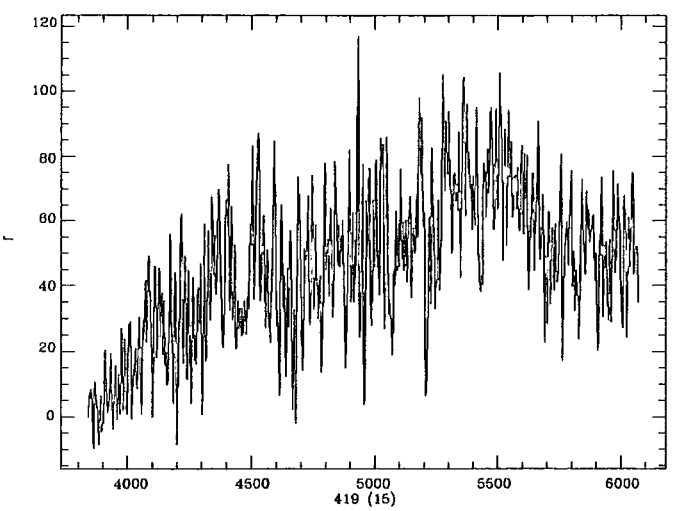
f
120
100
80
60
40
20
0
4000
4500
5000
5500
6000
419 (15)

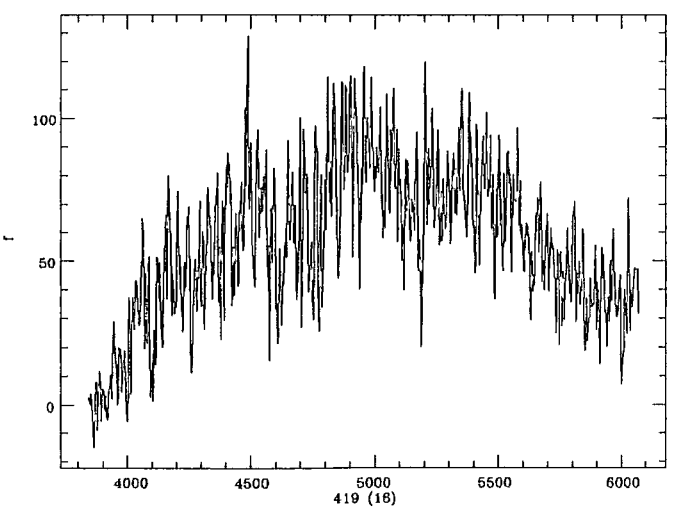
f
100
50
0
4000
4500
5000
5500
6000
419 (16)

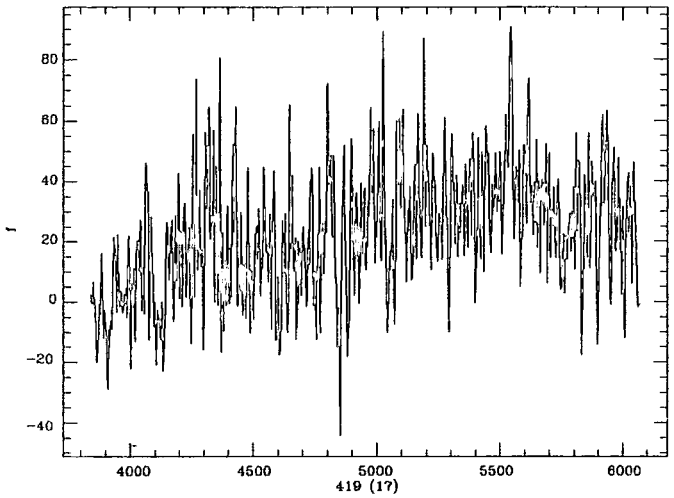
f
4000
4500
5000
5500
6000
419 (17)

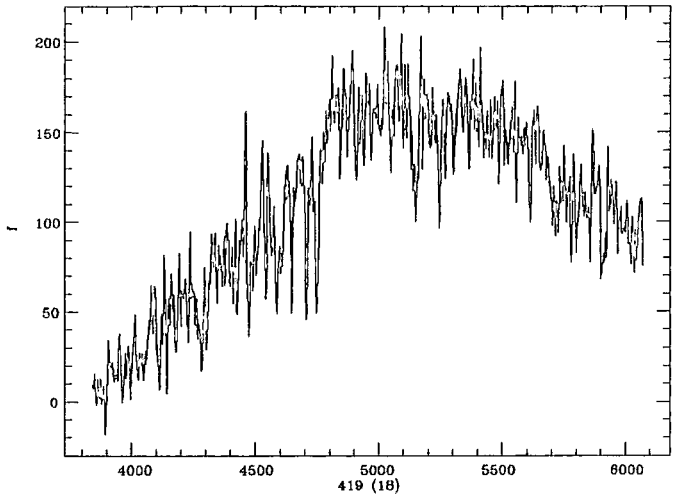
f
4000
4500
5000
5500
6000
419 (18)

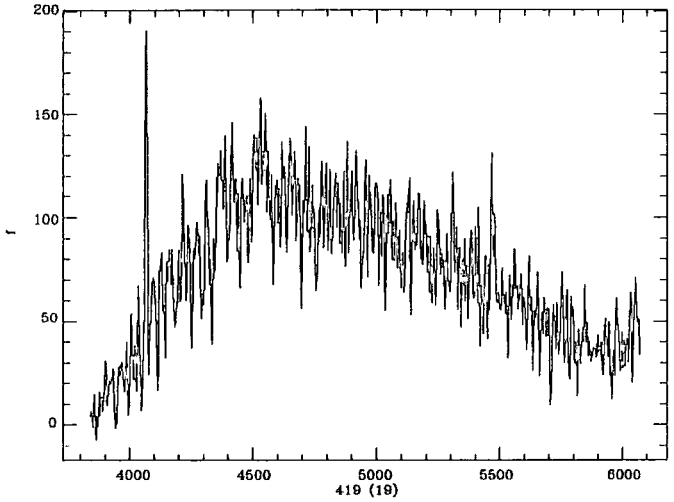
f
4000
4500
5000
5500
6000
419 (19)

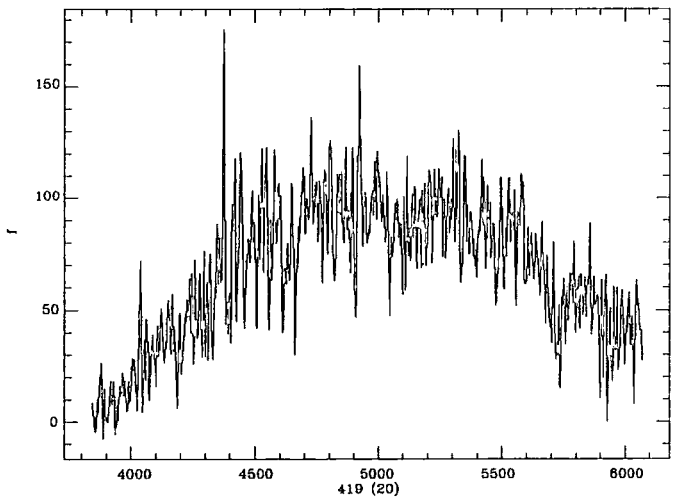
f
4000
4500
5000
5500
6000
419 (20)

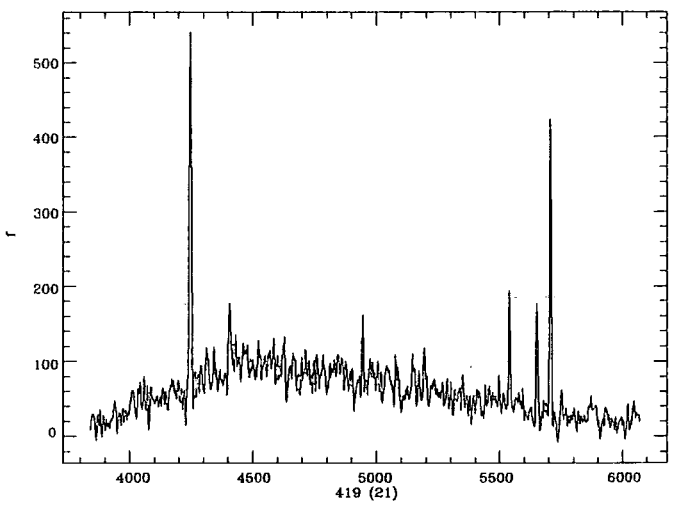
f
4000
4500
5000
5500
6000
419 (21)

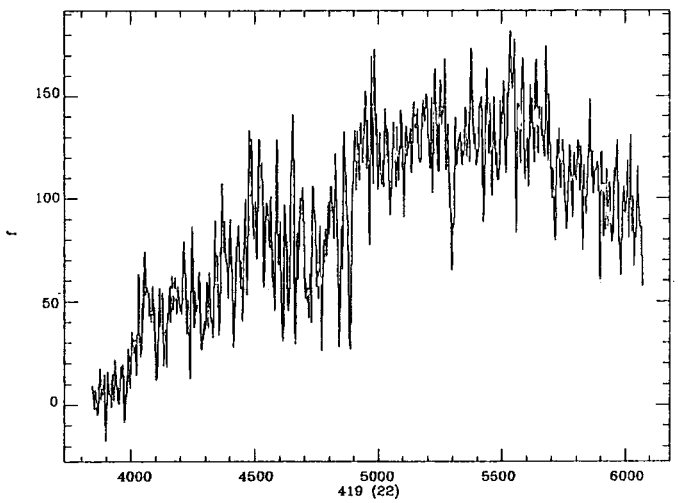
f
4000
4500
5000
5500
6000
419 (22)

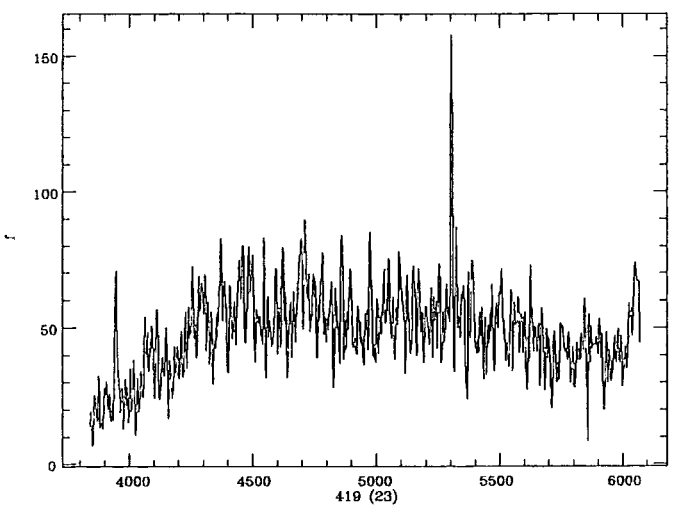
f
4000
4500
5000
5500
6000
419 (23)

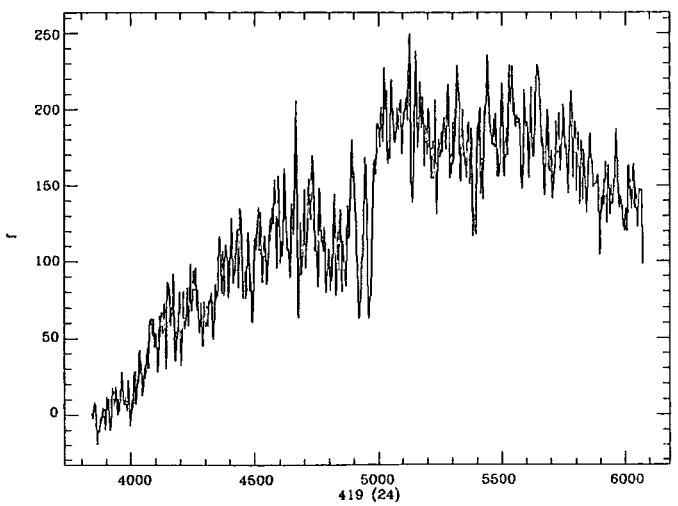
f
4000
4500
5000
5500
6000
419 (24)

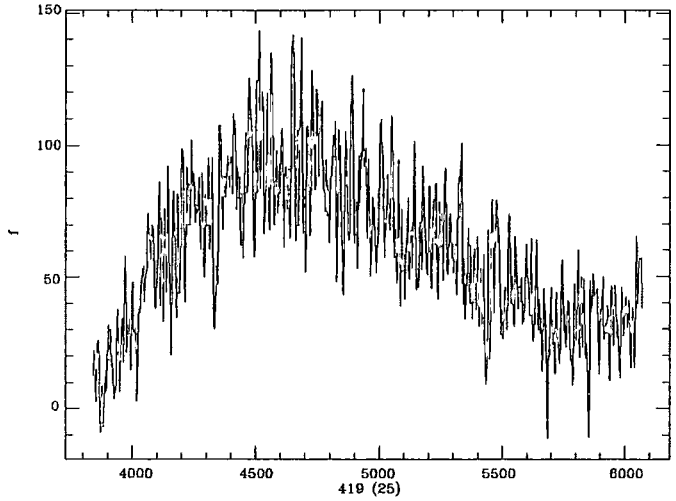
f
4000
4500
5000
5500
6000
419 (25)

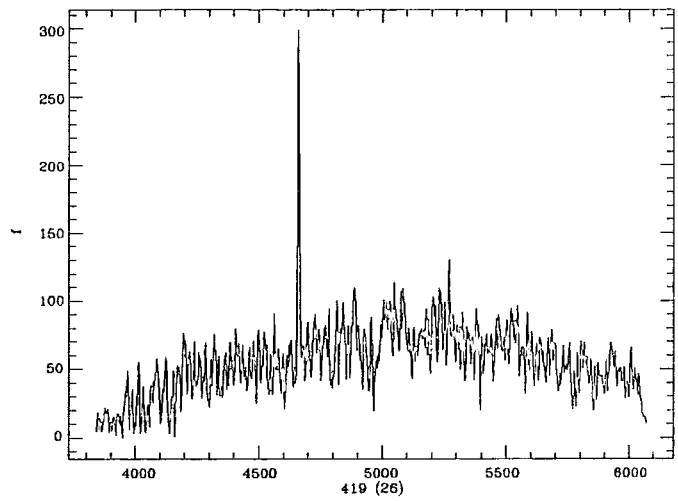
f
4000
4500
5000
5500
6000
419 (26)

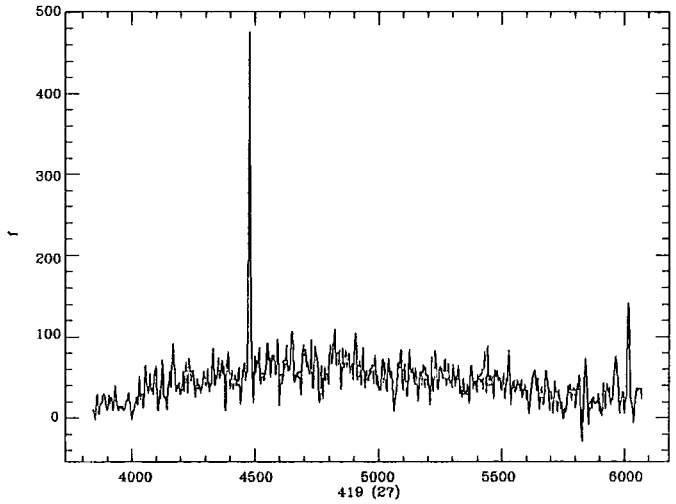
f
4000
4500
5000
5500
6000
419 (27)

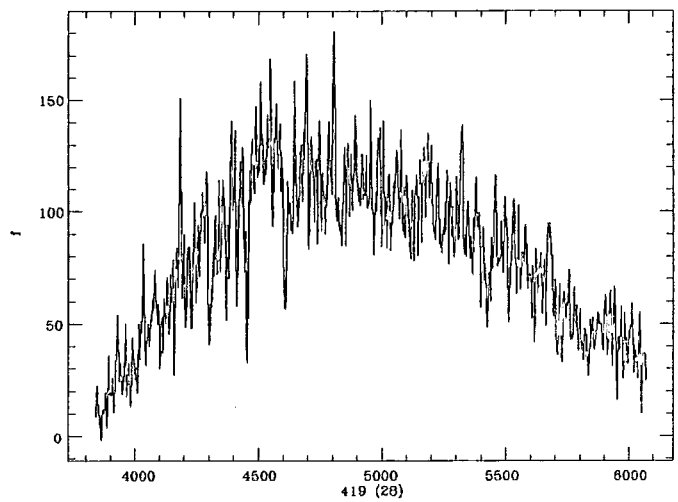
f
4000
4500
5000
5500
6000
419 (28)

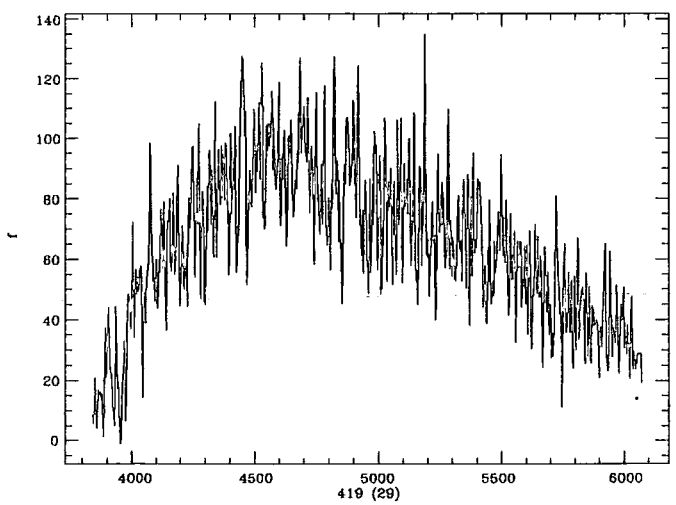
f
4000
4500
5000
5500
6000
419 (29)

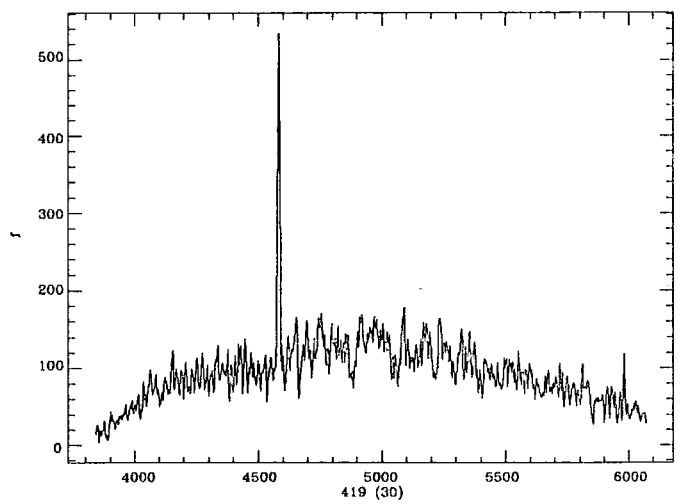
f
4000
4500
5000
5500
6000
419 (30)

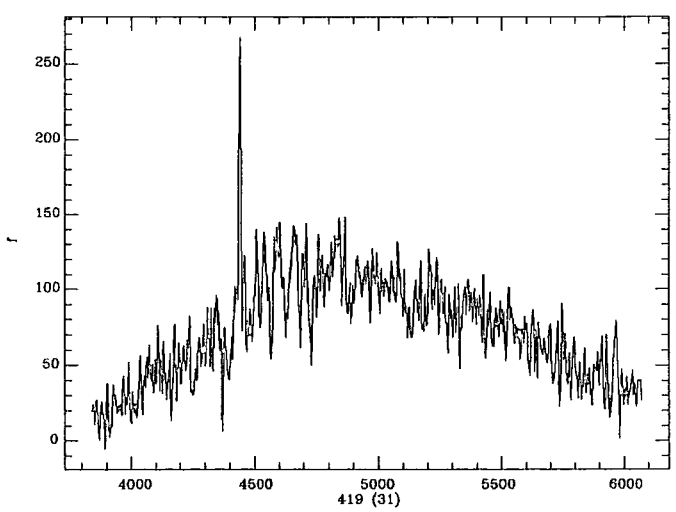
f
4000
4500
5000
5500
6000
419 (31)

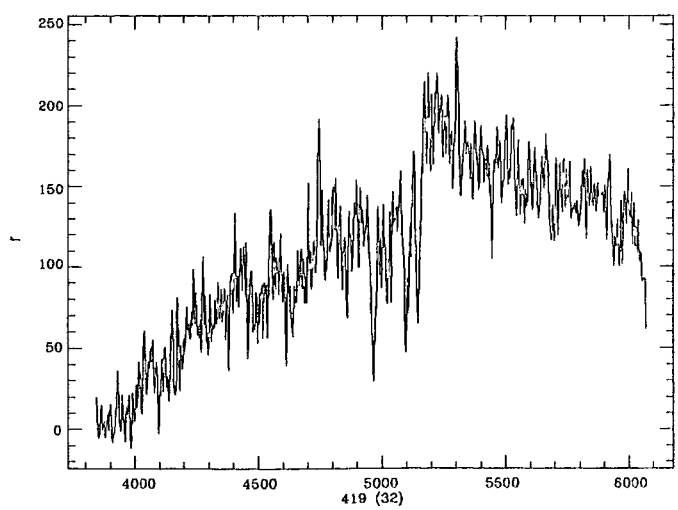
f
4000
4500
5000
5500
6000
419 (32)

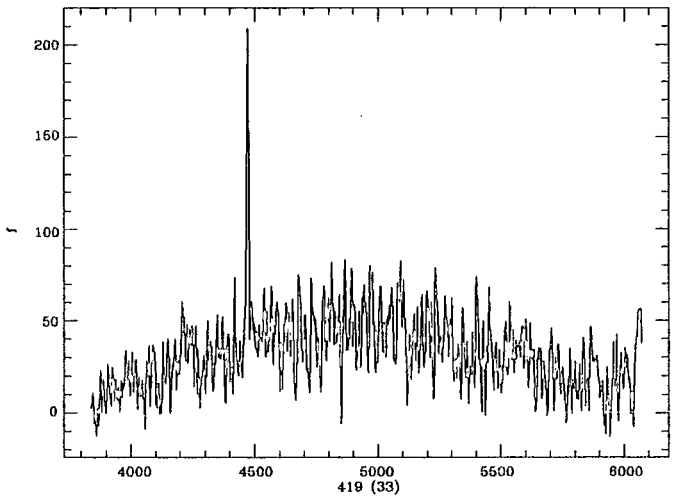
f
200
150
100
50
0
4000
4500
5000
5500
6000
419 (33)

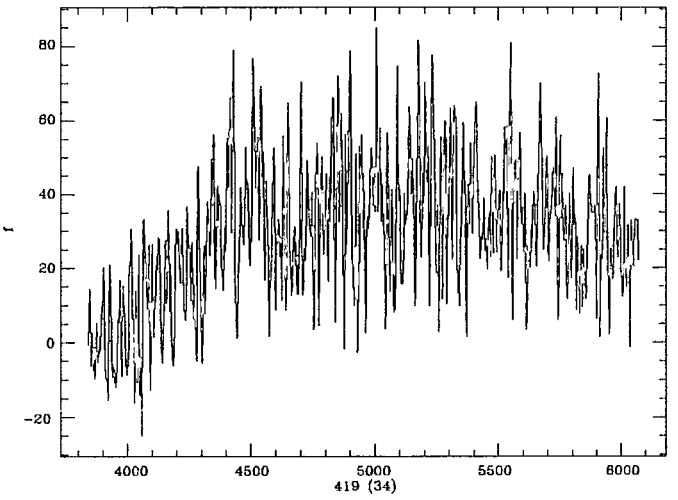
f
80
60
40
20
0
-20
4000
4500
5000
5500
6000
419 (34)

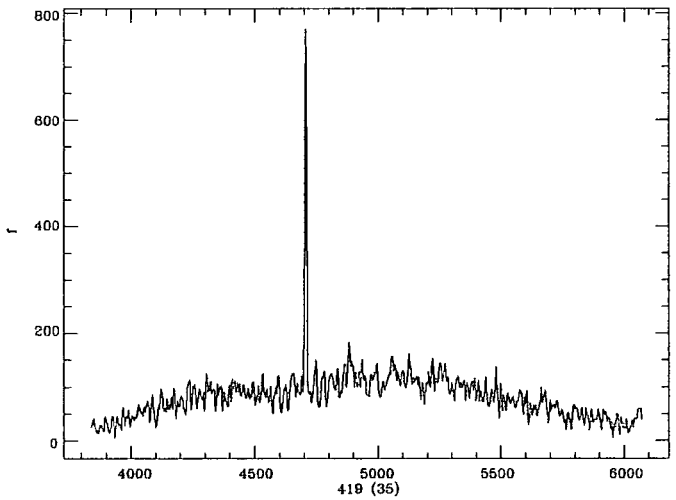
f
800
600
400
200
0
4000
4500
5000
5500
6000
419 (35)

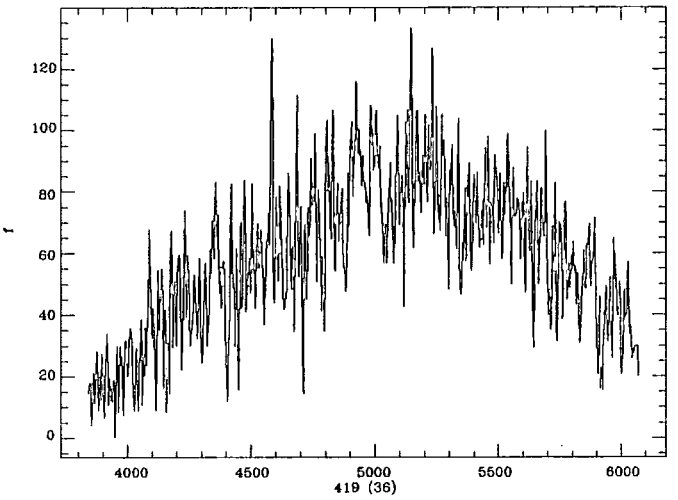
f
120
100
80
60
40
20
0
4000
4500
5000
5500
6000
419 (36)

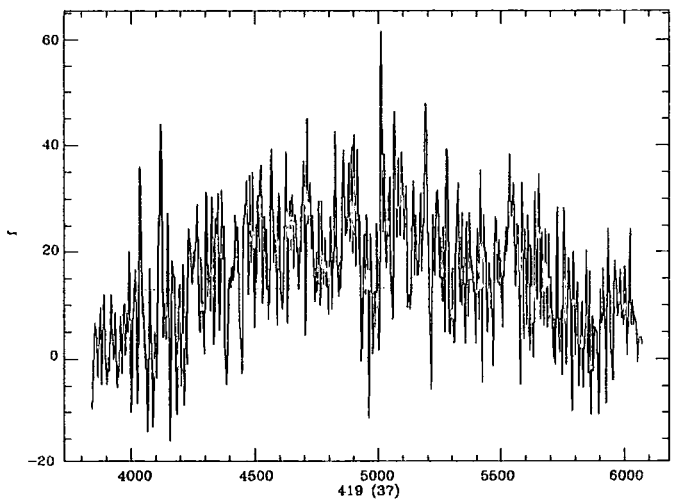
f
60
40
20
0
-20
4000
4500
5000
5500
6000
419 (37)

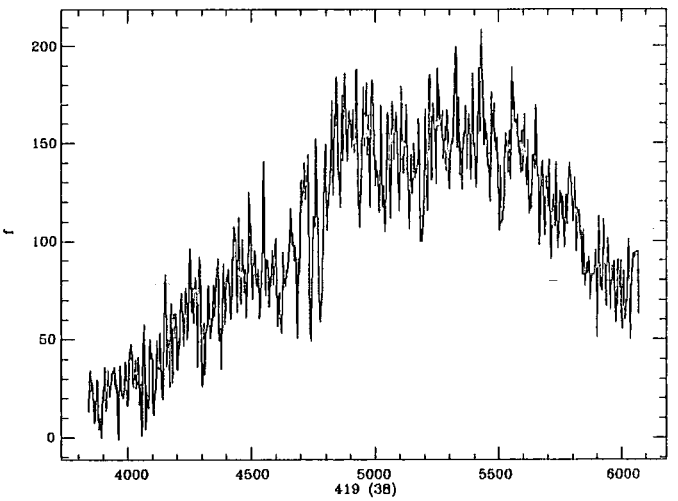
f
200
150
100
50
0
4000
4500
5000
5500
6000
419 (38)

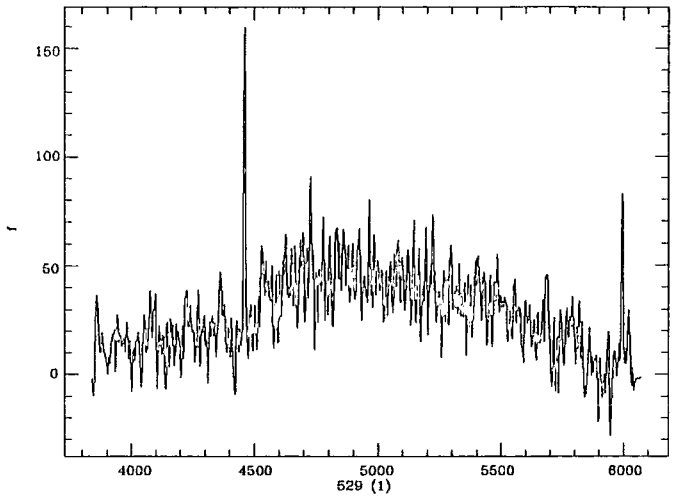
f
4000
4500
5000
5500
6000
529 (1)

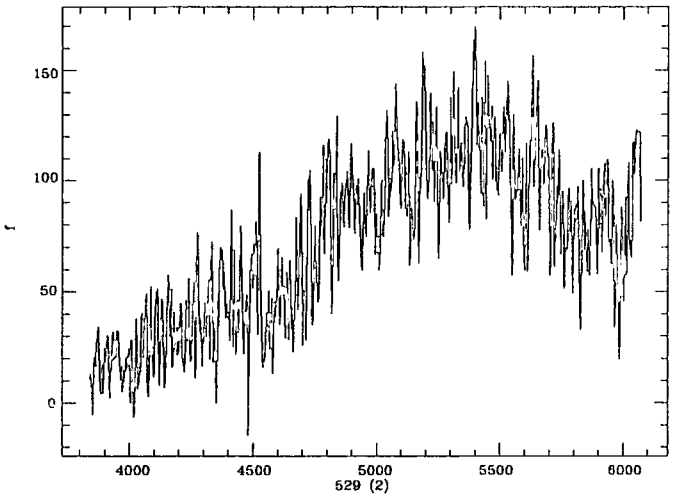
f
4000
4500
5000
5500
6000
529 (2)

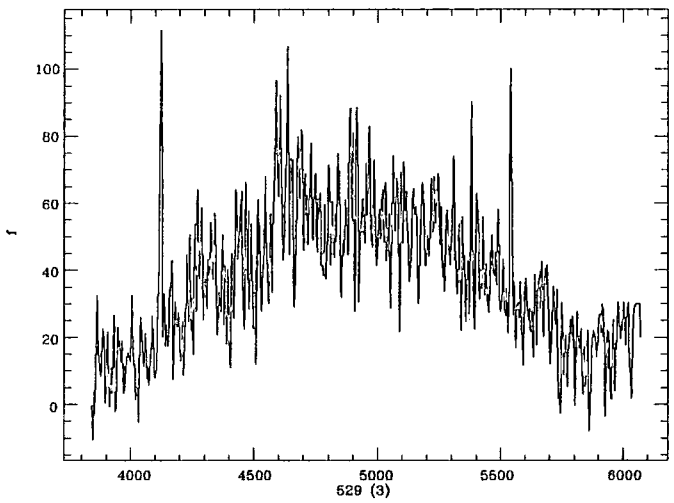
f
4000
4500
5000
5500
6000
529 (3)

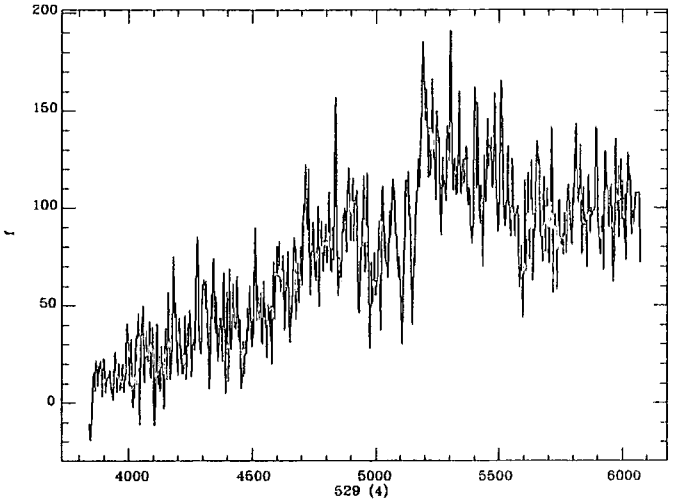
f
4000
4500
5000
5500
6000
529 (4)

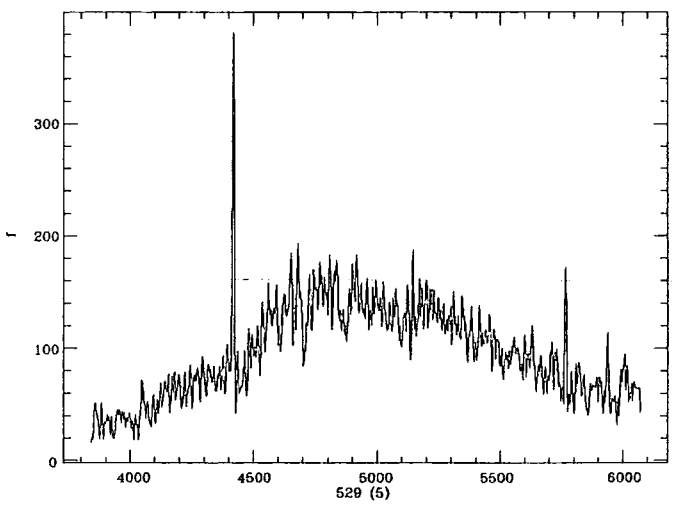
f
4000
4500
5000
5500
6000
529 (5)

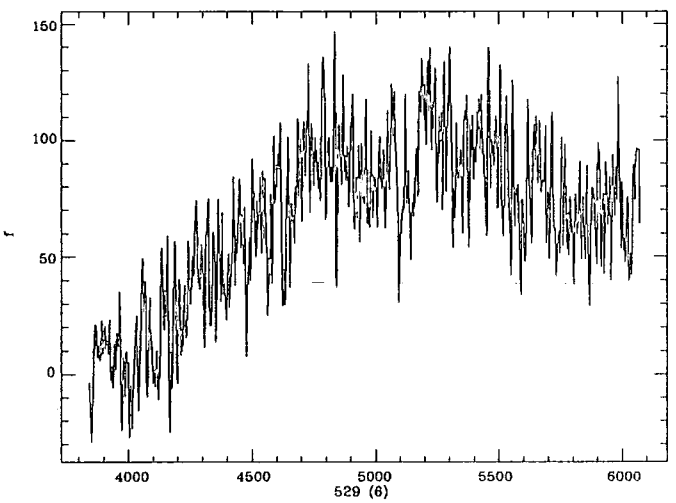
f
4000
4500
5000
5500
6000
529 (6)

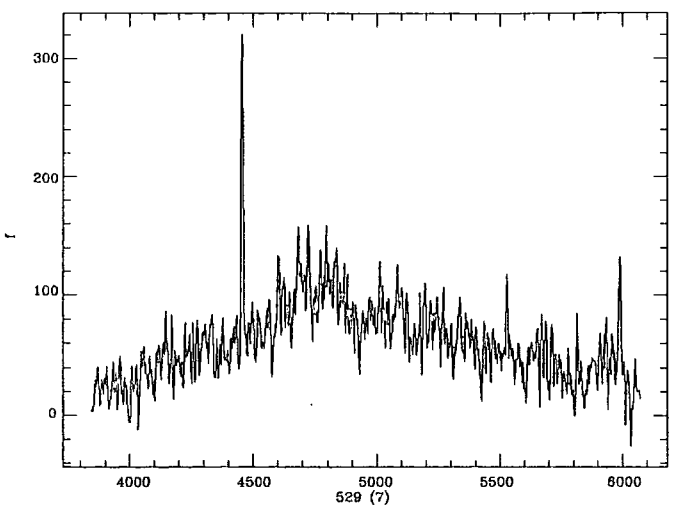
f
4000
4500
5000
5500
6000
529 (7)

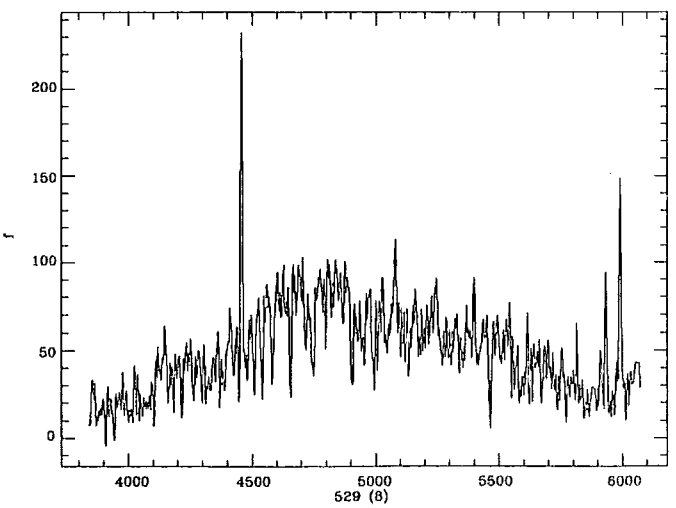
f
4000
4500
5000
5500
6000
529 (8)

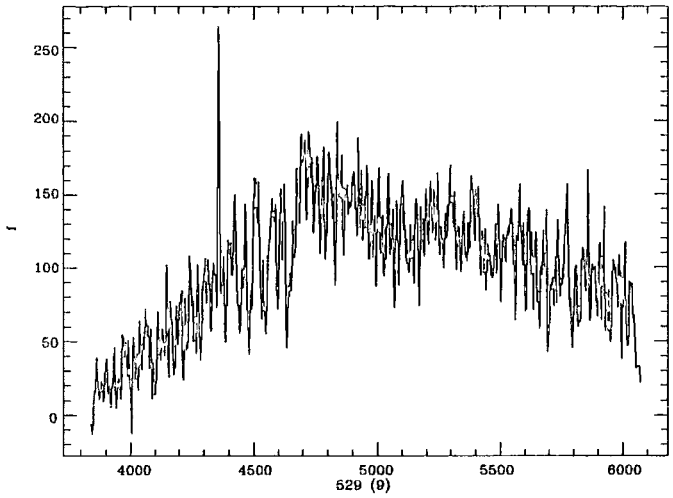
f
4000
4500
5000
5500
6000
529 (9)

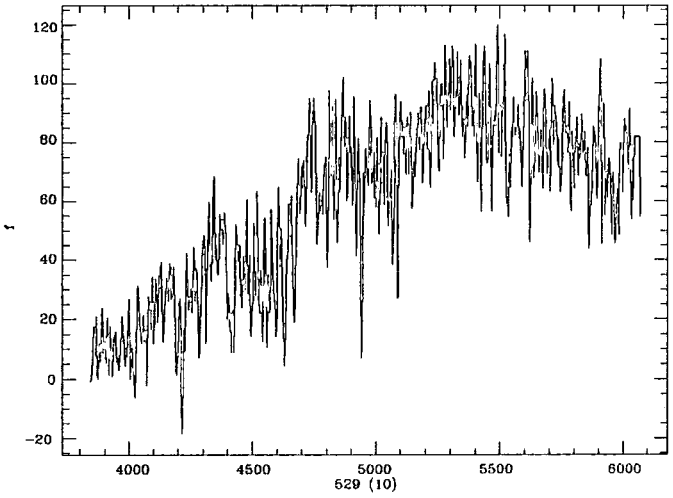
f
4000
4500
5000
5500
6000
529 (10)

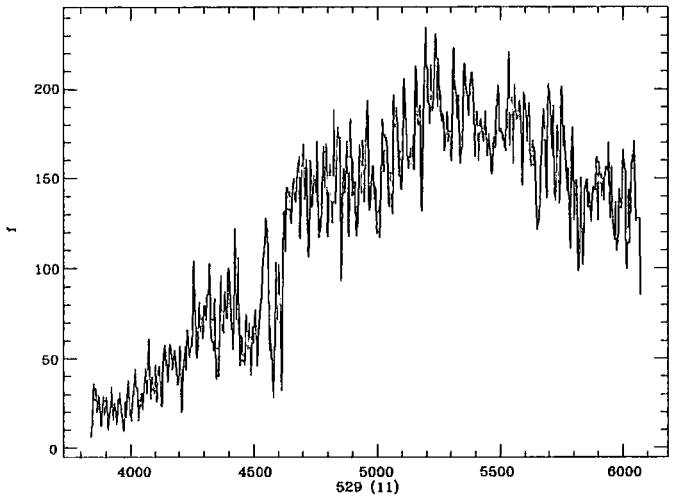
f
4000
4500
5000
5500
6000
529 (11)

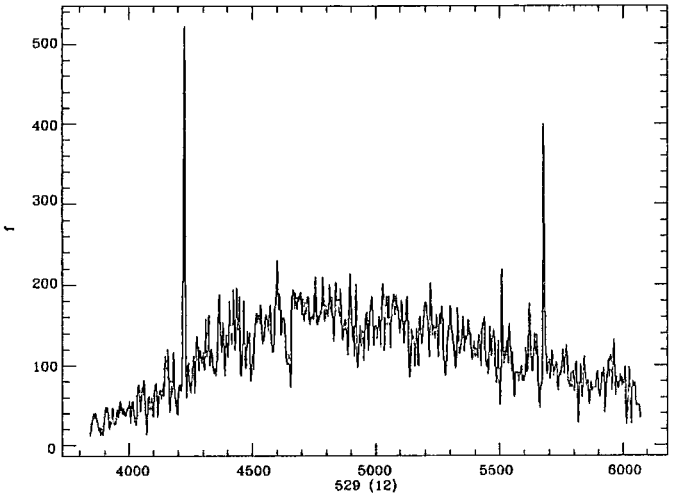
f
4000
4500
5000
5500
6000
529 (12)

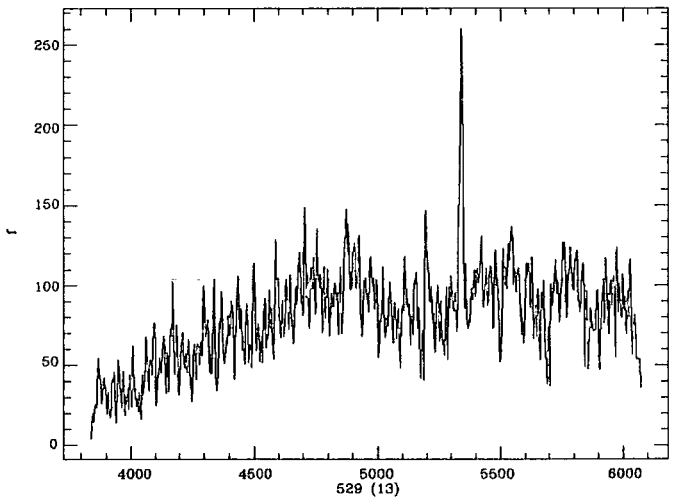
f
4000
4500
5000
5500
6000
529 (13)

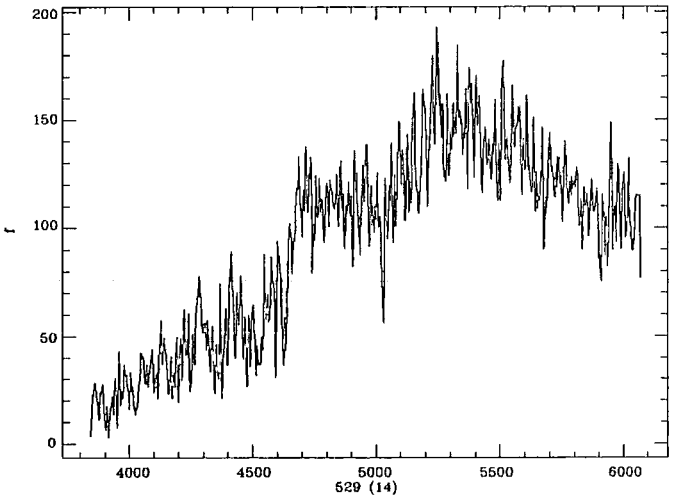
f
4000
4500
5000
5500
6000
529 (14)

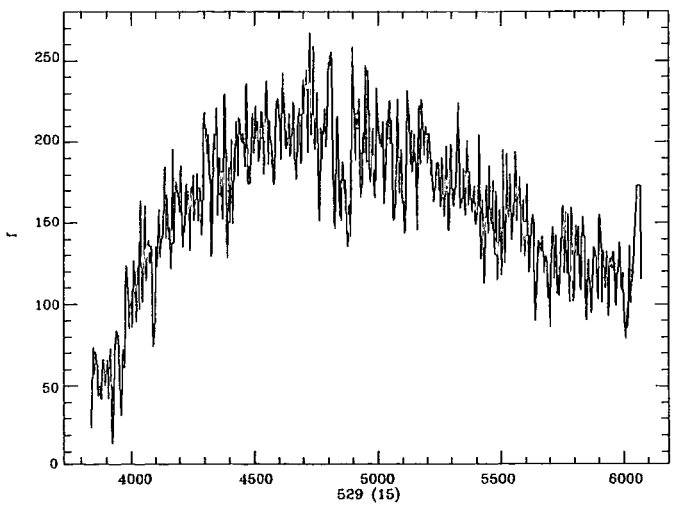
f
4000
4500
5000
5500
6000
529 (15)

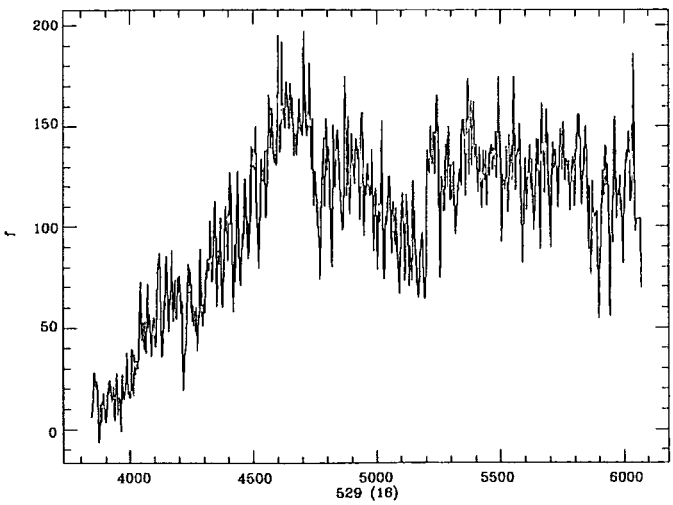
f
4000
4500
5000
5500
6000
529 (16)

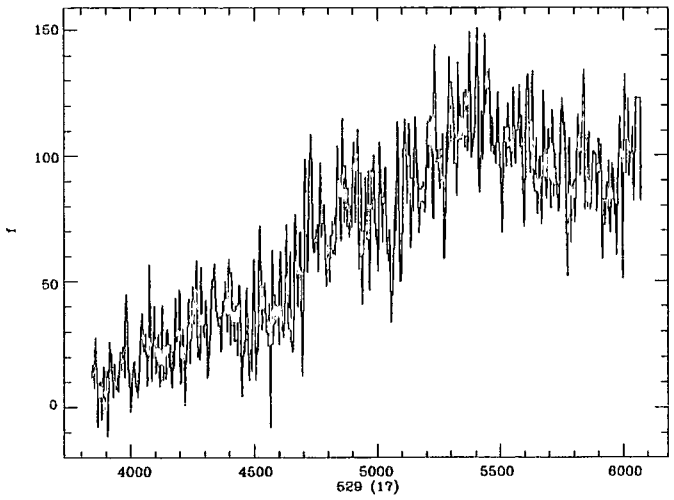
f
0
50
100
150
4000
4500
5000
5500
6000
529 (17)

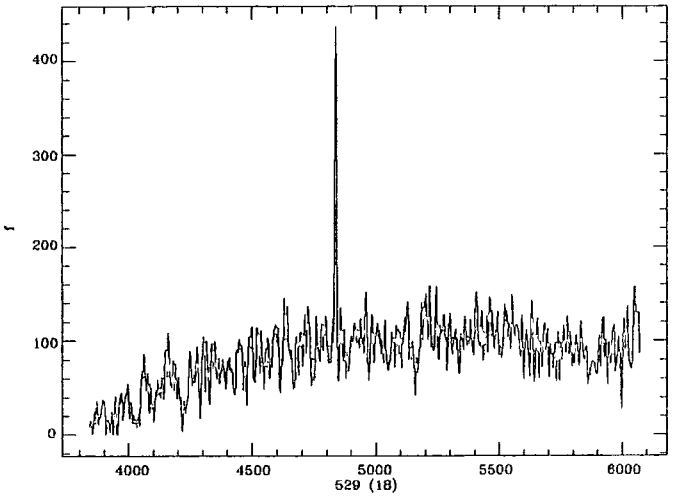
f
0
100
200
300
400
4000
4500
5000
5500
6000
529 (18)

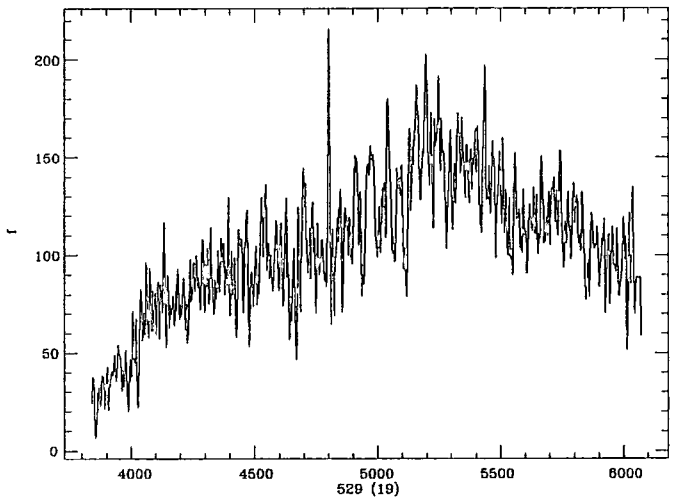
f
0
50
100
150
200
4000
4500
5000
5500
6000
529 (19)

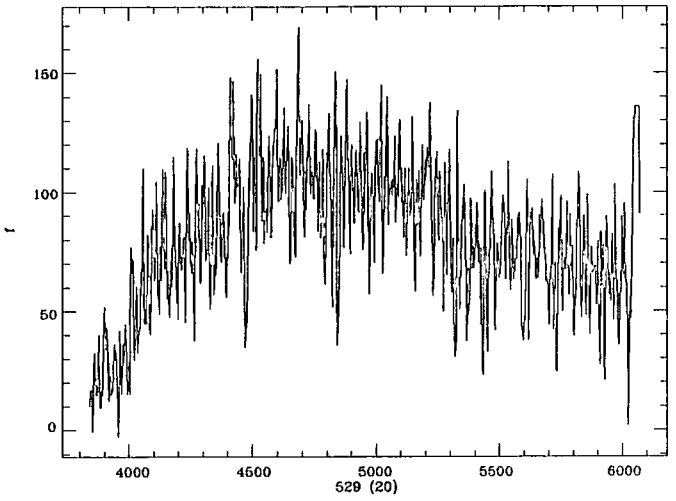
f
0
50
100
150
4000
4500
5000
5500
6000
529 (20)

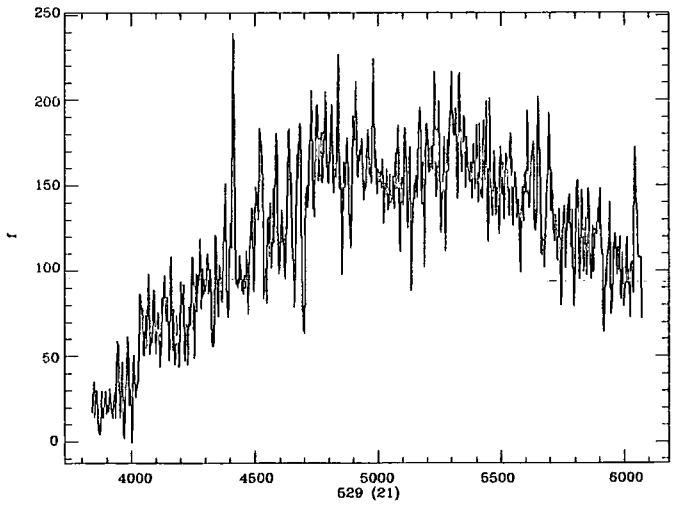
f
0
50
100
150
200
250
4000
4500
5000
5500
6000
529 (21)

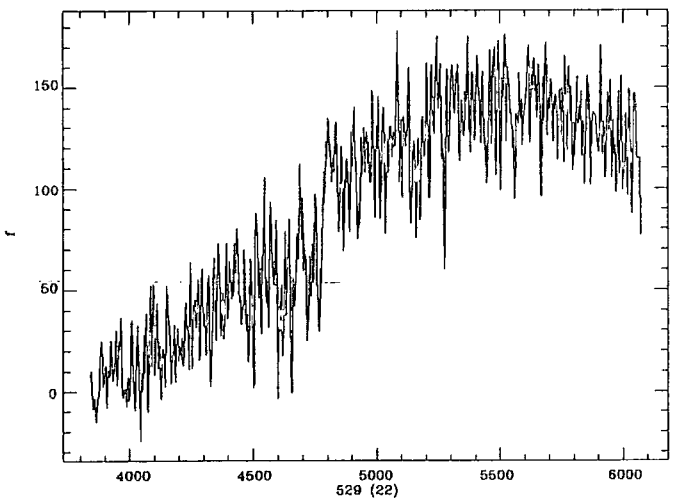
f
0
50
100
150
4000
4500
5000
5500
6000
529 (22)

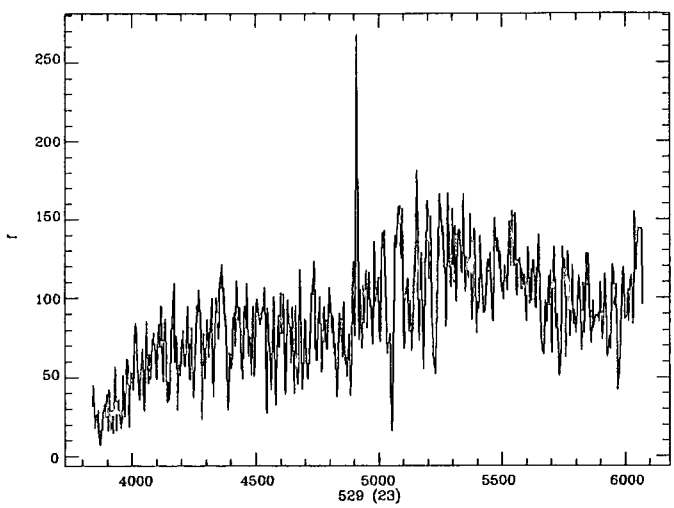
f
0
50
100
150
200
250
4000
4500
5000
5500
6000
529 (23)

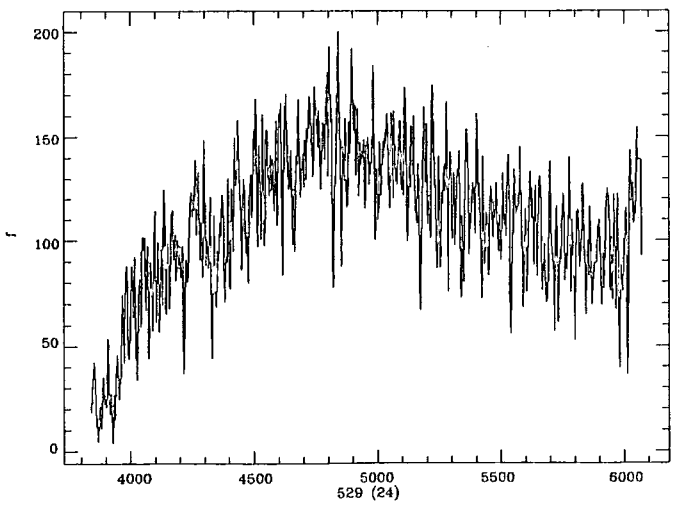
f
0
50
100
150
200
4000
4500
5000
5500
6000
529 (24)

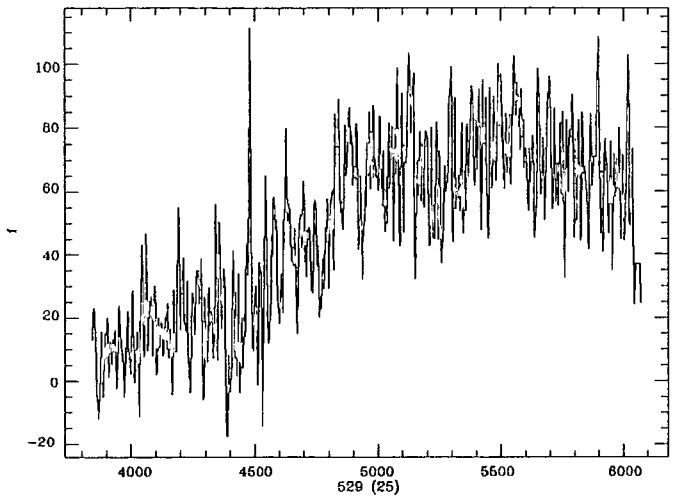
f
4000
4500
5000
5500
6000
529 (25)

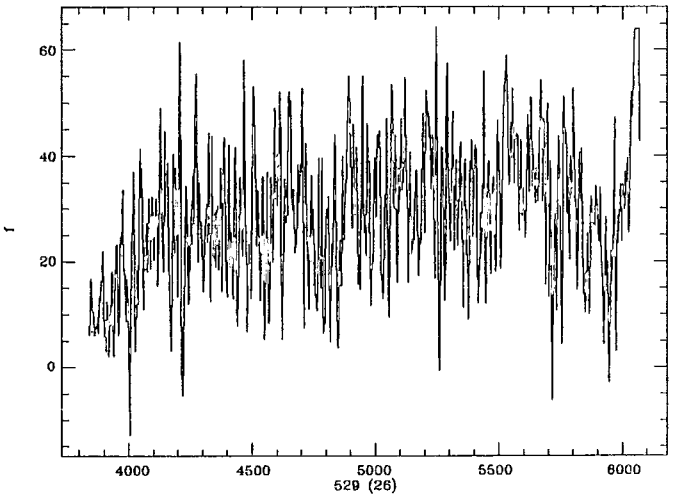
f
4000
4500
5000
5500
6000
529 (26)

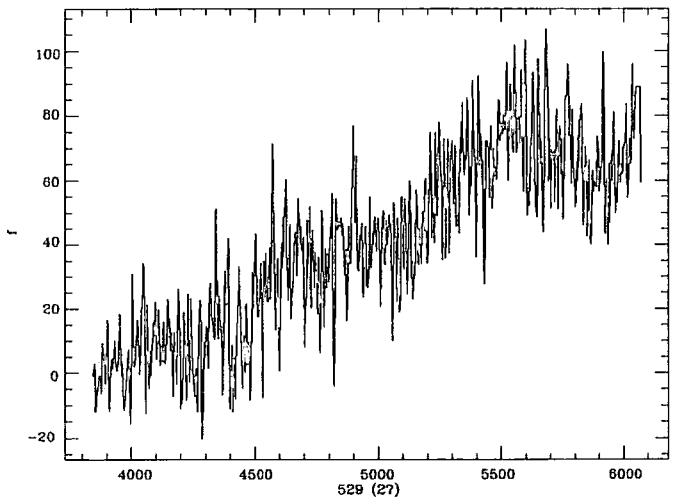
f
4000
4500
5000
5500
6000
529 (27)

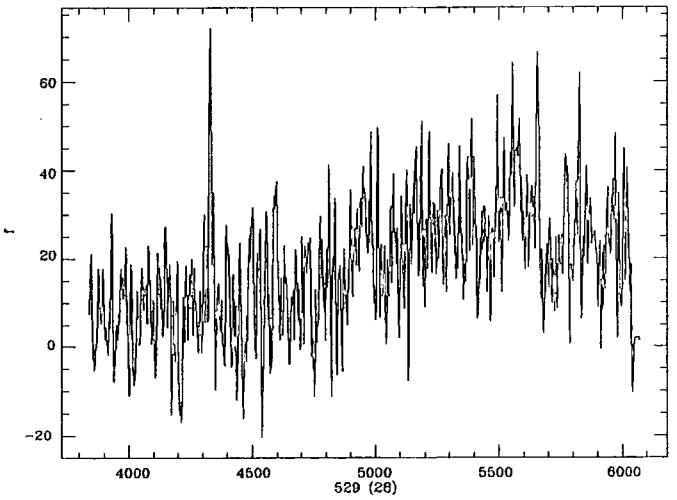
f
4000
4500
5000
5500
6000
529 (28)

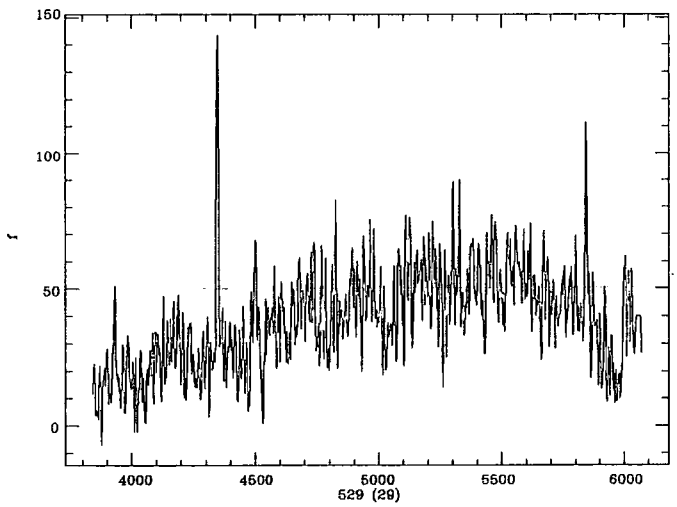
f
4000
4500
5000
5500
6000
529 (29)

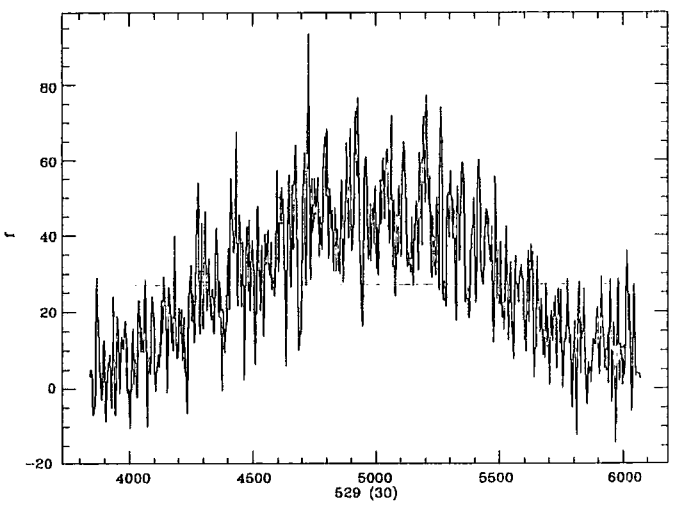
f
4000
4500
5000
5500
6000
529 (30)

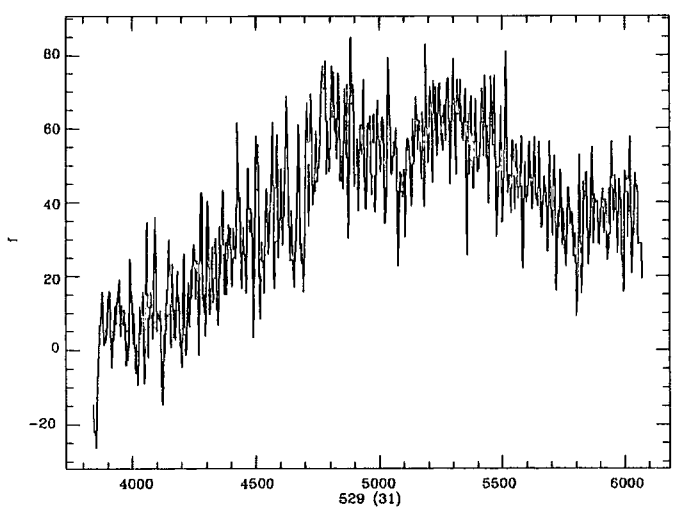
f
4000
4500
5000
5500
6000
529 (31)

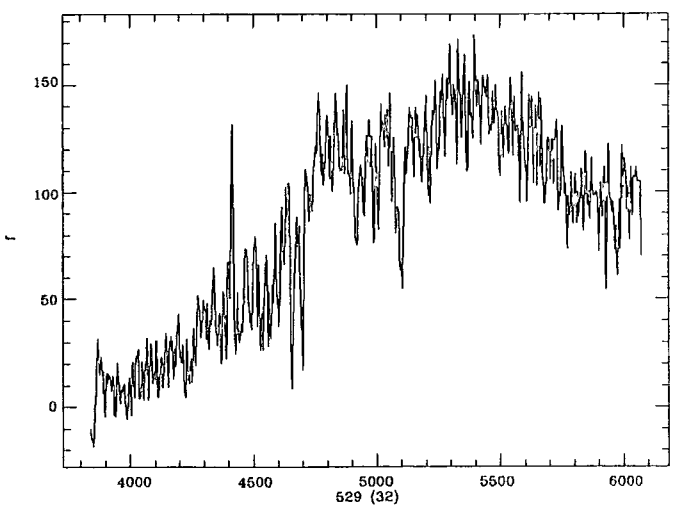
f
4000
4500
5000
5500
6000
529 (32)

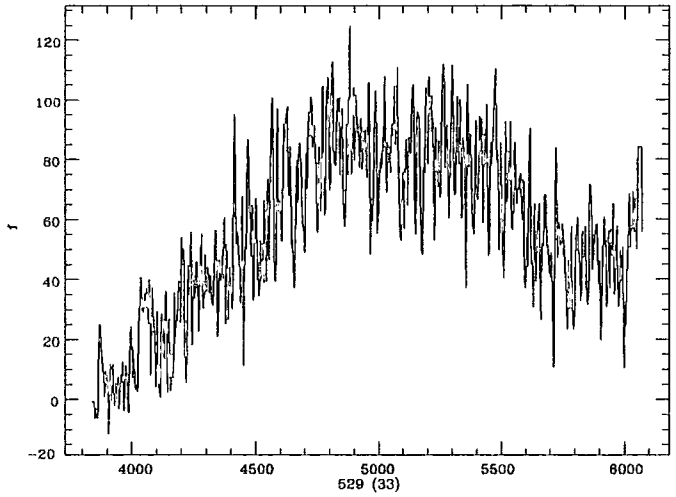
f
4000
4500
5000
5500
6000
529 (33)

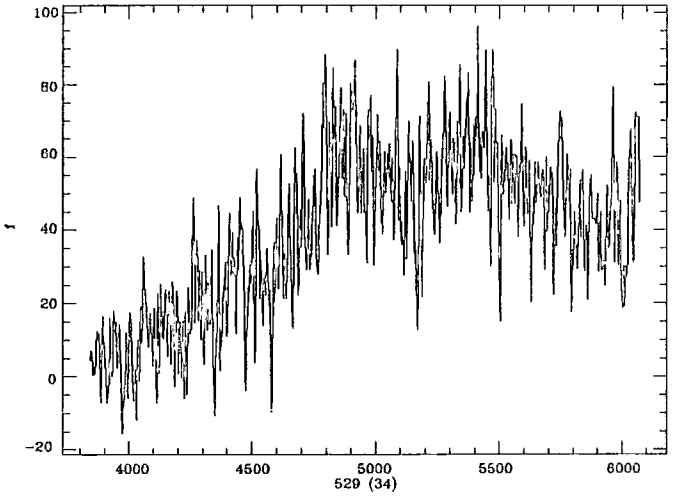
f
4000
4500
5000
5500
6000
529 (34)

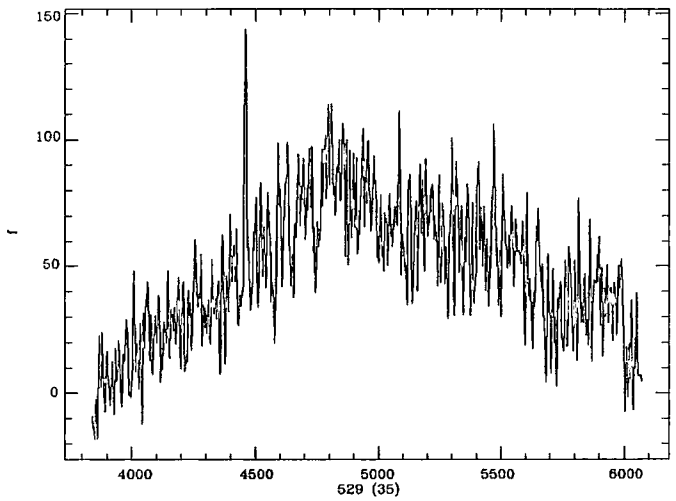
f
4000
4500
5000
5500
6000
529 (35)

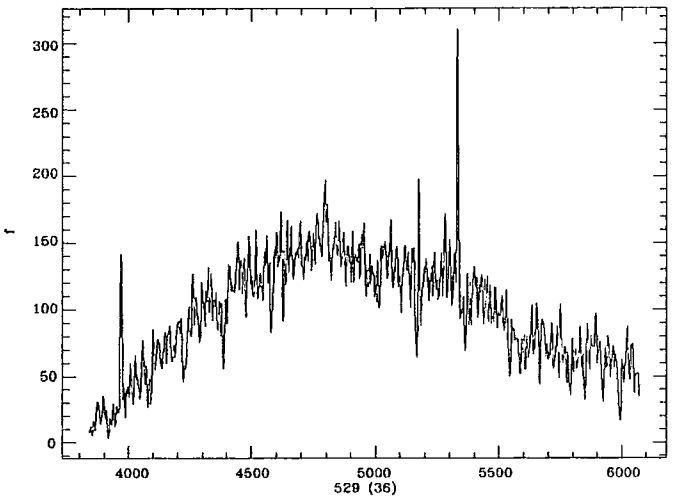
f
4000
4500
5000
5500
6000
529 (36)

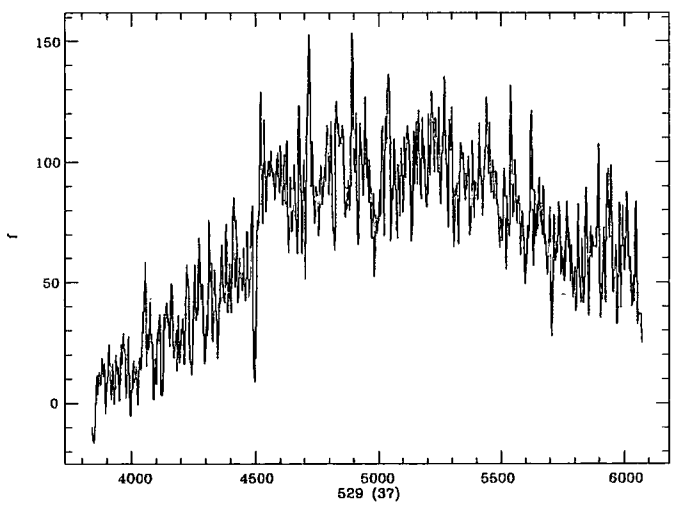
f
4000
4500
5000
5500
6000
529 (37)

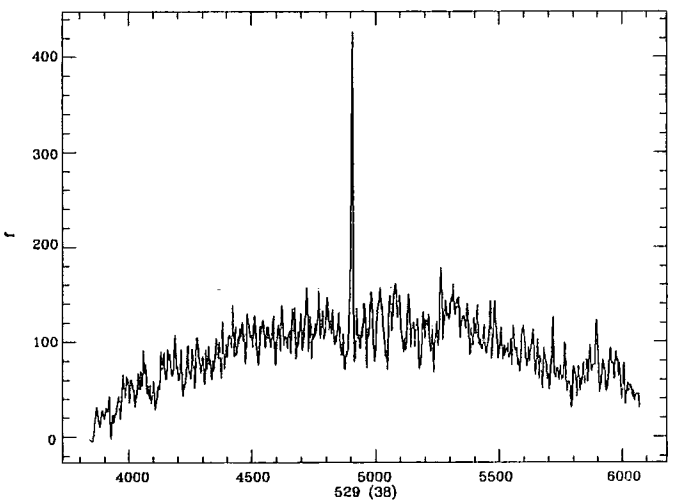
f
4000
4500
5000
5500
6000
529 (38)

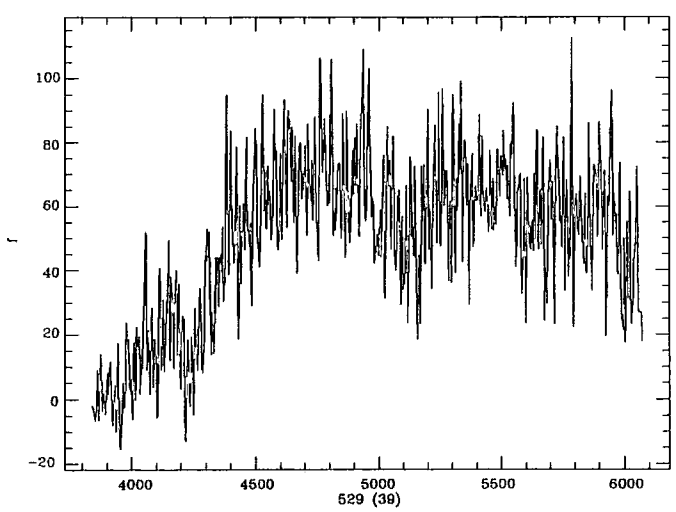
f
4000
4500
5000
5500
6000
529 (39)

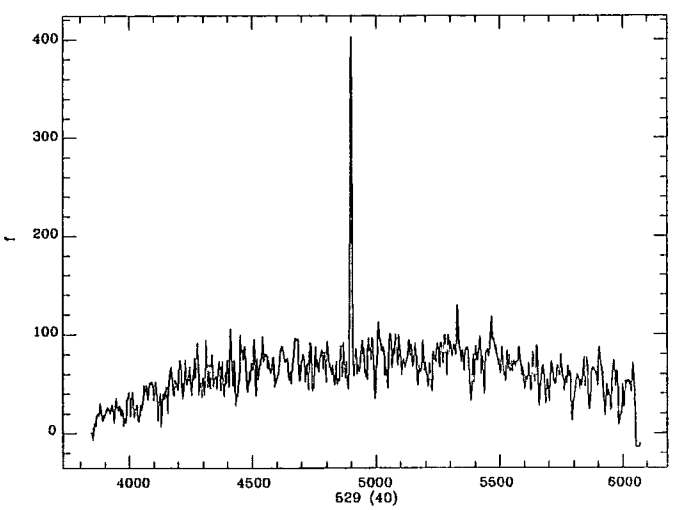
f
4000
4500
5000
5500
6000
529 (40)

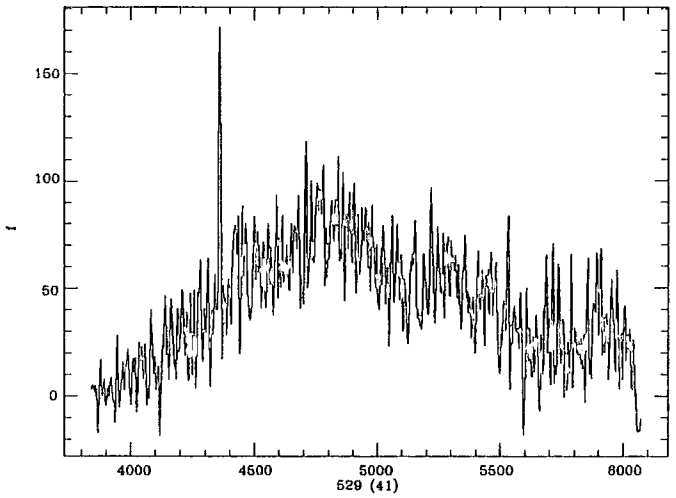
f
150
100
50
0
4000
4500
5000
5500
6000
529 (41)

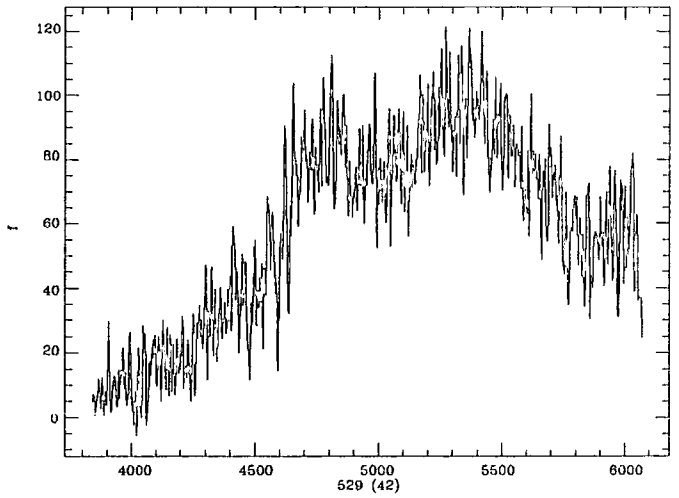
f
120
100
80
60
40
20
0
4000
4500
5000
5500
6000
529 (42)

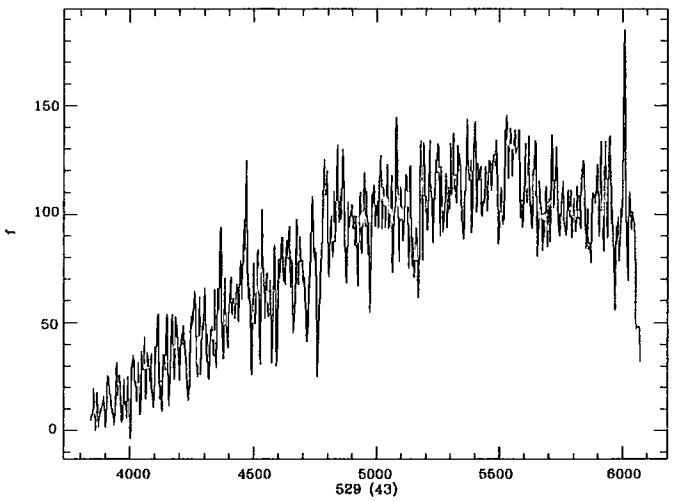
f
150
100
50
0
4000
4500
5000
5500
6000
529 (43)

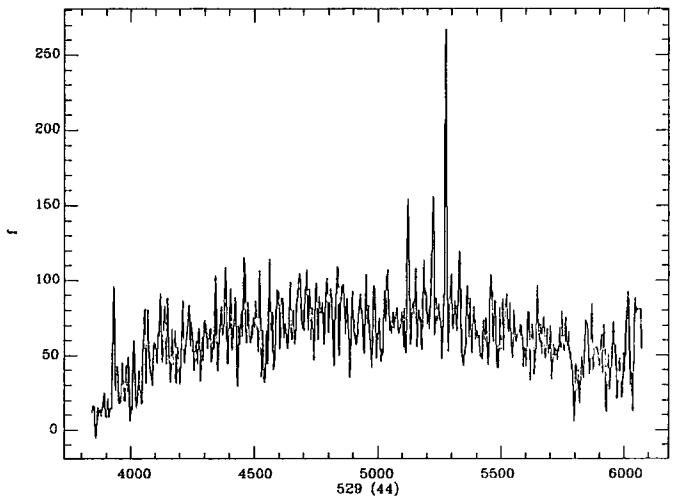
f
250
200
150
100
50
0
4000
4500
5000
5500
6000
529 (44)

## Acknowledgements.

I am Particularly grateful to my thesis supervisor Professor Richard Ellis for clear ideas, guidance and abundant enthusiasm during this work.

Many others contributed invaluably along the way, especially Tom Shanks whose imagination, warm humour and abuse were all appreciated (in that order).

In all of this work Paolo Salucci has taken a keen interest and provided many helpful and invaluable insights. Nigel Metcalfe has been a great help throughout, straightening out crooked ideas and bad fortran. Dick Fong is heartily thanked for his help with mathematical problems, great patience, a stolen calculator and an old pipe.

I have also had invaluable discussion on matters relating directly to this work most notably with Ray Sharples, Warwick Couch, Carlos Frenk and Gus Oemler and Gustavo Bruzual. Their help and experience are much appreciated.

Warrick Couch is also thanked for his expert assistance with the FOCAP observations and I also thank again Gus Oemler, for 9 enjoyable nights at KPNO, learning the art of CCD imaging.

Software for data reduction and modelling has been kindly provided by Gustavo Bruzual, Ray Sharples, Warrick Couch, and John Lucey, for which I am indebted.

I am hugely grateful to Alan Lotts for support on all aspects of computing - soft, hard and unbelievable.

I am also indebted to Richard Myers for his expert technical help and software. In addition he is thanked for *hours* of enjoyable and stimulating debate on many political, philosophical and historical matters.

I would also like to thank the following friends and collegues and friends at the Durham Physics Department for many interesting and helpful discussions over the years: John Lucey, Jeremy Allington-Smith, Iain MacLaren, Fred Stevenson, Brian Boyle, Bahram Mobasher, Laurence Jones, Duncan Hale-Sutton, Nial Tanvir, Ben Moore, Richard Bower, Ioannis Georgantopolous and Kevin Yau ...and on my travels (and their), Dave Koo, George Efstathiou, Simon White, Steve Phillipps, Yanick Mellier, Keith Ashmann and Will Saunders.

I also take this opportunity to thank my high school physics teacher, John Eyre, who spawned my passion for cosmology, with off-syllabus descriptions of the Big Bang and Black Holes.

I would like to thank Mike Breare for his generosity over the years. I would also like to thank the SERC for a research studentship and for provision of the excellent STARLINK facility on which all computing was carried out.

Finally, for their friendship and much more, I thank my house mates Lizzy, Ben, Suzanne and Jonathan, so too all my friends who drank and drink at the 'Vic'.

# REFERENCES


Augarde R., Lequeux J., 1985 *Astron. Astrphys* 147,273

Bachall N.A., Soneira R.M., 1984 *Astrophys. J.* 277,27

Baldwin, J A, Phillips, M M and Terlevich, R 1981 *Publ. Astr. Soc. Pacific*, 93, 5.

Baron E., White S.D.M., 1987 *Astrophys. J.* 322,585

Bardeen J.M., Bond J.R., Efstathiou G., 1987 *Astrophys. J.* 321,28

Batuski D.J., Burns J.O., 1985 *Astrophys. J.* 299,5

Batuski D.J., Burns J.O., Mellott A., 1987 in *Large scale Structures in the universe* eds Ardouze, J and Szalay, A.S. (Reidel). p543

Bean, A J, 1983 *Ph D Thesis* University of Durham.

Bean A.J., Efstathiou G., Ellis R.S., Peterson B.A., Shanks T., 1983 *Mon. Not. R. astr. Soc.* 205, 605.

Biermann P., Eckart A., Witzel A., 1985 *Astron. J.* 92, 94

Bhavsar S.P, Ling E.M., 1988 preprint

Bolzano V., 1983 *Astrophys. J.*, 268, 602.

Bonner W.B., 1957 *Mon. Not. R. astr. Soc.* 117, 111.

Bothun, G D, 1984 *Astrophys J.*, 277,532

Boyle B.J., 1986 Ph.D. *University of Durham*

Broadhurst T.J., Ellis R.S., Shanks T., 1988 *Mon. Not. R. astr. Soc.* 235, 827.

Broadhurst T.J., Salucci P., 1989 *The epoch of galaxy Formation*p379 Eds: Frenk C.S, Ellis R.S, Shanks T., Heavens A.F, Peacock J.A.

Bruzual, G, 1983 *Astrophys. J.*, 273, 105.

Bruzual, G, and Kron R.G. 1980 *Astrophys. J.*, 219, 18.

Bruzual G., 1986 in *Spectral Evolution of Galaxies*, eds Chiosi, C and Renzini, A. (Reidel), p419.

Brown G.S., And Tinsley B.M., 1974 *Astrophys. J.*, 194, 555

Butcher, H., Oemler, A., 1978a *Astrophys. J.* 219, 18.

Butcher, H., Oemler, A., 1978b *Astrophys. J.* 226, 559.

Chincarini G., Vettolani G., 1987*Observational Cosmology, IAU Symposium 124*, eds. Hewitt et al, D. Reidel Publ. Co., p275

Chincarini G., Goivanelli R., Haynes M.P., 1983 *Astron. Astrophys J.* 121,5

Colless M., Ellis R.S., Taylor K., 1989 *The epoch of galaxy Formation*p379 Eds: Frenk C.S, Ellis R.S, Shanks T., Heavens A.F, Peacock J.A.

Comte, G., 1985 in *Spectral Evolution of Galaxies*, eds Chiosi, C and Renzini, A. (Reidel), p419.

Condon J.J. and Mitchell K.J., 1984 *Astron. J.* 89 610

Condon J.J. 1984 *Astrophys. J.* 287 461

Condon J.J, 1987 in *Starburst and Galaxy Evolution*, eds Thuan T.X., Montmerle T., Tran Thahn Van J. (Editions Frontieres), p425

Couch,W J, Sharples,R M 1987 *Mon. Not. R. astr. Soc.* 229, 423.

Couch W.J., Ellis R.S., Malin D., Maclaren I.M. 1988 *Preprint*

Cowie L.L., Lilly S.J., Gardner J., McLean I., 1988 *Astrophys. J.Lett* 332,L29

DaCosta L.N., Pellegrini P.S., Sargent W.L.W., Tohnry J., Davis M., Meibin A., Latham D.W., Menzies J.W., Coolson I.A., 1988 *Astrophys. J.* 327 544

Davies P., 1987 *the Cosmic Blueprint* (London:Heinemann)

de Lapperant V., Geller M.J., Huchra J.P., 1986 *Astrophys. J.Lett* 202,L1

de Lapperant V., Geller M.J., Huchra J.P., 1986 *Large scale Structures in the universe*p519 eds Ardouze, J and Szalay, A.S. (Reidel).

de Vaucouleurs G., 1975 *Astrophys. J.* 202 610

Davies J.I., Phillipps, S., Disney M.J., 1988 *Mon. Not. R. astr . Soc. Lett.* 231,69.

Davis M., Efstathiou G., Frenk C.S., White S.D.M., 1985 *Astrophys. J.* 292,371

Disney M.J., 1976 Nature 263,573

Disney M.J., Phillipps, S., 1983 *Mon. Not. R. astr . Soc.* 205, 1253.

Donnelly R.H., Partridge R.B., Windhorst R., 1987 *Astrophys. J.* 321.94.

Dressler, A and Gunn, J E 1983 *Astrophys. J.* **263**, 533.

Dressler, A and Gunn, J E Schneider D.P., 1985 *Astrophys. J.* **294**, 70.

Efstathiou, G.P., Ellis, R.S., Peterson,B.A. 1988 *Mon. Not. R. astr. So c.* **232**, 431.

Efstathiou, G.P., Bond, J.R., 1987 *Mon. Not. R. astr. So c.* **227**, 38p.

Einasto J., Klypin A.A., Saar E., Shandarin S.F., 1984 *Mon. Not. R. astr. So c.* **206**, 529.

Ellis J.R., *Phil. Trans. R. Soc. Lond.* 1986 A **320** 475

Ellis, R.S., Fong, R., Phillipps, S., 1978 *Mon. Not. R. astr . Soc.* **178**, 163.

Ellis, R.S. 1982 *The Origin and Evolution of Galaxies, Ed.Jones B.J. Jones J.E., Reidel, Dordrecht Holland*

Ellis, R.S., Gray, P.M., Carter, D., Godwin, J., 1984 *Mon. Not. R. astr . Soc.* 206, 285

Ellis, R S, Couch, W J, MacLaren, I and Koo, D 1985 *Mon. Not. R. astr. Soc.* 217, 239.

Ellis, R S and Parry, I R 1987, *Instrumentation in Astronomy*, Santa Cruz Summer Workshop, in press.

Ellis, R S 1987a, *Observational Cosmology, IAU Symposium 124*, eds. Hewitt et al, D. Reidel Publ. Co., p367.

Ellis, R S 1987b, *High Redshift and Primeval Galaxies*, Third IAP Astrophysics Conference, eds. Bergeron et al, in press.

Fromalont E.B., Kellermann K.I., Wall J.V., Weistrop R.A., 1984 *Science* 225 23

Gallager J.S. Hunter D.A., Tutakov R., 1984 *Astrophys. J.*, 284,544

Gray, P.M. 1986 Proc. SPIE 627, 96.

Groth E.J., Peebles P.J.E., 1977 *Astrophys. J.* 217,385

Gunn J., 1989 *The epoch of galaxy Formation*p167 Eds: Frenk C.S, Ellis R.S, Shanks T., Heavens A.F, Peacock J.A.

Guth A., 1981 *Phys. Rev.*D23,347

Hale-Sutton D.H., Shanks T., Fong D., Metcalfe N., *Mon. Not. R. astr . Soc.* in press

Hamilton D., 1986 in *Spectral Evolution of Galaxies*, eds Chiosi, C and Renzini, A. (Reidel), p419.

Hauser M.G., Peebles P.J.E., *Astrophys. J.*, 185,757

Hill T.C. Scramm D.N., Fry J.N., 1988 *Preprint*

Houck J.R.,Hacking P., 1987 *Astrophys. J.*, 63,311

Hucra J.P., 1977a *Astrophys. J.*, 217,928

Hucra J.P., 1977b *Astrophys. J.*, 235,17

Joseph R.D., 1987 in *Starburst and Galaxy Evolution*, eds Thuan T.X., Montmerle T., Tran Thahn Van J. (Editions Frontieres), p425

Frenk C.S, White S.D.M., Davis M., Efstathiou G., 1988 *Astrophys. J.* 327, 507.

Gregory S.A., Thompson L.A., 1978 *Astrophys. J.* 222, 784.

Jacoby, G.H., Hunter, D.A., Christian, C.A. *Astrophys. J.*, 237,692

Kennicutt R.C., 1983 *Astrophys. J.*, 272,54

King, C R and Ellis, R S 1985 *Astrophys. J.*,288, 456.

Kirshner R.P., Oemler A., Schecter P., Schectman S.A., 1981 *Astrophys. J. Lett* 248,L57

Kirshner R.P., Oemler A., Schecter P., 1983 *Astron. J.* 83 1549

Koo, D C 1981 Ph.D *Thesis University of California, Berkeley*

Koo, D.C. 1985 *Astron.J.* 90,418

Koo, D C 1986a in *Spectral Evolution of Galaxies*, eds Chiosi, C and Renzini, A. (Reidel), p419.

Koo, D C 1986b *Astrophys. J.* 311, 651.

Koo, D C 1987 in *Large scale Structures in the universe* eds Ardouze, J and Szalay, A.S. (Reidel). p221

Koo, D.C., Dressler A., Windhorst R., 1988, *Observational Cosmology, IAU Symposium 124*, eds. Hewitt et al, D. Reidel Publ. Co., p367.

Kopylov A.I., Kuznatsov D.Y., Fetisova T.S. Shvartzman V.F. 1987 in *Large scale Structures in the universe* eds Ardouze, J and Szalay, A.S. (Reidel). p129

Kron R.G., 1982 *Vistas in Astronomy*, 26,37

Kron R., Koo D.C., Windhorst R.A., 1985 *Astron astrophys* 146 38

Lahav O., 1987 *Mon. Not. R. astr. Soc.* 225,213.

Lahav O., Lyndon-Bell D., Edge A., 1988 *preprint*

Larson,R., Tinsley,B.M., 1978 *Astrophys. J.*,219,46.

Lavery,R.J., Henry,J.P., 1986 *Astrophys. J. Lett.*,304,L5.

Leech K.J., Lawrence A., Rowan-Robinson M., Walker D., Penston M.V., *Mon. Not. R. astr. Soc.*231,977.

Lilly S.S., Longair M.S., 1982 *Mon. Not. R. astr. Soc.* 199,1053.

Lilje P.B., Efstathiou G., 1988 *Mon. Not. R. astr. Soc.* 231,635.

Linde A.D., 1986 *Phys. Lett.*175B,395

Loh, E D and Spillar, E 1986 *Astrophys. J.* 303, 154.

Lucey J.R., Carter D., 1988 *Mon. Not. R. astr. Soc.*235,1177.

Lyndon-Bell D., Faber S.M., Burstein D., Davies R.L., Dressler A., Terelevich R.J., Wegner G., 1988 *Astrophys. J.* 326, 19.

McCall M.L., Rybski P.M., Sheilds G.A., 1985 *Astrophys J. Supp.*,57,1.

Mandelbrot B.B., 1982 *The Fractal Goemetry of Nature* (New York:Freeman)

Mandelbrot, 1986 *Large Scale Structures in the Universe* IAU Symp 130 eds: Audouze J.,Pellenan M., Szalay A. p479

MacLaren, I., Ellis, R.S.,& Couch, W.J., 1988 *Mon. Not. R. astr. Soc.*,230,249.

Metcalfe, N, Shanks, T, Jones, L R, and Fong, R 1987, in *High Redshift and Primeval Galaxies, 3rd IAP Astrophysics Meeting*, eds. Bergeron *et al*, in press.

Miller, G.E., Scalo, J.M., 1979 *Astrophys J. Supp.*,41,513.

Mobasher B., Ellis R.S., Sharples R.M., 1987 *Mon. Not. R. astr. Soc.* bf 223,11.

Moody J.E., Turner E.L., Gott J.R., 1983 *Astrophys. J.* 273, 16.

Morton D.C., Krug P.A., Tritton K.P., 1985 *Mon. Not. R. Astr. Soc.*212,325

Olowin Corwin.,H 1988, Preprint

Oemler A., 1986 *Nearly Normal Galaxies* ed: Faber S.M

Oke J.B., Sandage A., 1968 *Astrophys. J.* 154, 21.

Osmer P., 1981 *Astrophys J.* 247,762

Osterbrock D.E., 1974 *astrophysics of Gaseous Nebulaue* (San Fransisco:Freeman)

Ostriker J.P., 1987 *Large Scale Structures in the Universe* IAU Symp 130 eds: Audouze J.,Pellenan M., Szalay A. p321

Pagel B.E.J. *Phil. Trans. R. Soc. Lond.* 1986 A **320** 557

Peebles P.J.E. 1980 *The large Scale Structure of the Universe* Princeton University Press.

Peebles P.J.E., 1984 *Astrophys. J.* 277, 420.

Peebles P.J.E. 1986 *Phil. Trans. R. Soc. Lond.* A **320** 431

Peebles P.J.E., 1984 *Astrophys. J.* **315**, L73.

Pence, W.D., 1976 *Astrophys. J.* **203**, 39.

Peterson, B.A., Ellis, R.S., Kibblewhite, E.J., Bridgeland, M.T., Hooley T.,& Horne, D., 1979, *Astrophys. J.* **233**, L109.

Peterson, B A, Ellis R S, Bean, A J, Efstathiou, G, Shanks, T, Fong R and Zou Z-L 1986 *Mon. Not. R. astr. Soc.* **221**, 233.

Pietronero L., 1987 *Physica* 144A,257

Phillipps, S., Shanks,T.,1987 *Mon. Not. R. astr. Soc.*,227,115.

Phillipps, S., Disney, M.J., Kibblewhite, E.J., Cawson, M.G.M., 1987 *Mon. Not. R. Astr. Soc.*229,505

Prigogine I, Stengers I., 1984 *Order out of Chaos* (Heinneman:London)

Struck-Marcell C., Scalo J.M., 1987 *Astrophys J. Supp.*,64,39.

Reike G.H., Cutri R.M, Black J.H, Kailey W.F., McAlary, C.W.,Lebofsky,M.J., and Elson R., 1985 *Astrophys. J.* 147,273

Robertson, J.G., 1986 *Publs. Astr. Soc. Pacif.*,98,1220

Rowan-Robinson M., 1987 in *Starburst and Galaxy Evolution*, eds Thuan T.X., Montmerle T., Tran Thahn Van J. (Editions Frontieres), p235.

Rowan-Robinson M., Crawford J., 1989 *Mon. Not. R. astr. Soc.* in Press

Salpeter E.E, 1955 *Astrophys. J.* 121,161

Sandage A., 1961 *Astrophys. J.* 133,355

Scalo J.M., 1987 in *Starburst and Galaxy Evolution*, eds Thuan T.X., Montmerle T., Tran Thahn Van J. (Editions Frontieres), p445.

Schechter,P.L. 1976 *Astrophys. J.* 203,297

Schramm J.M., 1987 in *Starburst and Galaxy Evolution*, eds Thuan T.X. Montmerle T. Tran Thahn Van J. (Editions Frontieres), p593.

Searle L., Sargent W.L.W., Bagnuolo W.G., 1973 *Astrophys. J.* 179,427

Silk J., 1986 in *Spectral Evolution of Galaxies*, eds Chiosi, C and Renzini, A. (Reidel), p419.

Silk J., Szalay A., 1987 *Astrophys. J. Lett.* 323,L107

Shaeffer R., 1986 *Large Scale Structures in the Universe* IAU Symp 130 eds: Audouze J.,Pellenan M., Szalay A. p215

Shanks T., Bean A.J., Efstathiou G., Fong R., Peterson B.A., 1983 *Astrophys. J.* 274,529

Shanks,T., Stevenson,P.R.F., Fong,R., MacGillivray,H.T. 1984 *Mon. Not. R. astr. Soc.* 206,767

Sharples, R M, Ellis, R S, Couch, W J, and Gray, P M 1985 *Mon. Not. R. astr. Soc.*, 212, 687

Stavely-Smith L., Davis R.D., 1987 *Mon. Not. R. astr. Soc.* 224,953

Stevenson,P.R.F., Fong,R., Shanks, T., Fong,R. 1985 in *Spectral Evolution of Galaxies*, eds Chiosi, C and Renzini, A. (Reidel), p419.

Stevenson P.R.F., Ph.D. 1986 *University of Durham*

Struble M.F., Rood M.J., 1987 *Astrophys J. Supp.*,63,555.

Subrahmanya C.R., Kapachi V.K., 1983 *Proc. IAU Symp 104 eds: Abell G., Chincarini* P47

Sutherland W 1988 *Mon. Not. R. astr. Soc.* 234,159

Tinsley, B.M. 1968 *Astrophys.J.*, 151,547

Tinsley, B.M. 1977 *Astrophys.J.*, 211,621

Tinsley, B.M. 1980 *Astrophys.J.*, 241,41

Tinsley, B.M. 1980 *fund. Cosmic Phys.*, 5,287

Tinsley, B.M. 1981 *Mon. Not. R. astr. Soc.*, 194,63

Thuan T.X., Condon J.J., *Astrophys. J. Lett.* 1987 147,L6

Thuan.T.X. 1987 in *Starburst and Galaxy Evolution*, eds Thuan T.X. Montmerle T. Tran Thahn Van J. (Editions Frontieres), p129.

Tonry, J, Davis, M, 1979 *Astron.J.* 84,1511

Tully R.B., 1986 *Astrophys. J.*, 303,25

Tully R.B., 1986 *Astrophys. J.*, 323,25

Turok N., 1987 *Large Scale Structures in the Universe* IAU Symp 130 eds: Audouze J.,Pellenan M., Szalay A. p281

Tyson, J.A. Jarvis, J.F. 1979 *Astrophys.J.Lett.* 230,L153

Tyson, A 1987 *preprint*

Uson J.M., Wilkinson D.T., 1984 *Astrophys. J. Lett.* 277,L1

Weinberg S., 1972 *Gravitation and Cosmology* (New York:Wiley and Sons)

Wilson M.L., Silk J., 1981 *Astrophys.J.*, 243,14

Windhorst R., Ph.D. 1984 Thesis, University of Leiden

White S.D.M, Frenk C.S., Davis M., 1983 *Astrophys. J. Lett* 274,L1

White S.D.M, Frenk C.S., Davis M., Efstathiou G., 1987 *Astrophys. J.* 313,505